The Development and Validation of Novel Biomarkers to Assess the Skin Barrier Function

A thesis submitted in a partial fulfilment of the requirements for the degree of

Doctor of Philosophy

Dilek Guneri

University College London

School of Pharmacy

29-39 Brunswick Square

WC1N 1AX

London

2020

Declaration

I, Dilek Guneri, confirm that the work presented in this thesis is my own. Where information has been derived from other sources, I confirm that this has been indicated in the thesis. Furthermore, I certify that the information that has appeared in publications elsewhere will be cited in suitable sections of the text.

Signature _____   Date _____

Acknowledgement

First of all I would like to express my gratitude to my supervisor Prof. Michael Munday. I am very thankful for the excellent supervision of Dr. Majella Lane, who has been supportive throughout my whole PhD. I would like to thank Prof. Anthony Rawlings for sharing all his knowledge that inspired most of this work during fruitful discussions. Furthermore, I would like to express my special thanks to my industrial supervisor Dr. Rainer Voegeli for his trust and inspiration and the financial support provided by DSM Nutritional Products Inc. My special appreciation goes to Dr. Rebecca Lever who has kindly shared her fluorescence microscope which made most of the work here possible.

I would like to express my special thanks to everyone in UCL School of Pharmacy, especially my group members and everyone in office 308, who contributed to my personal and professional journey. Special Thanks to Rita, Sebastian, Peter, Karolina, and Ines who were there whenever I needed them and for all the laughter and wine.

My family have been greatly supporting me over the distance, especially my brother Ayhan and my father, who made it possible for me to complete my PhD.

Impact statement

The uppermost layer of the skin, the stratum corneum, is an efficient structure to prevent dehydration and limit the entrance of noxious particles. The stratum corneum is built up like a wall with corneocytes as "bricks" and lipid lamellar layers like "mortar" and as it can be appreciated, a strong wall relies on the properties of the bricks. For many years, the pharmaceutical and cosmetic industries have been interested in delivering active compounds via topical applications through the skin which may have an impact on the skin barrier function. For this purpose, the trans epidermal water loss and appearance of the skin were the main indicators of skin health.

This work has been sponsored by DSM Nutritional Products who are interested in sun-exposed skin and how their topical formulations may act on the skin barrier while taking corneocytes into account. Corneocytes are terminally differentiated keratinocytes that further undergo maturation when reaching the stratum corneum. The maturity of corneocytes supports the skin barrier integrity and function. A novel method has been developed that characterises the maturity of corneocytes according to their rigidity, size and hydrophobicity and correlates these traits with the stratum corneum properties. A range of biomarkers were identified to assess the expression pattern of enzymes involved in maturation and structural proteins in photo damaged corneocytes. This allowed a focus on the enzyme 12R-LOX that processes the ceramide precursor as well as transglutaminase that attaches this processed ceramide to the corneocyte. However, the 12R-LOX enzyme has attracted attention only recently thus an activity assay is not yet available and neither are substrates or inhibitors. This project has been conducted with a fluorescence-based activity assay where the activity of 12R-LOX is measured indirectly by detecting reduction by generated reactive oxygen species. DSM Nutritional Products are currently implementing the methods that were developed and validated in this thesis to determine the effect of their formulations on corneocyte maturation. Furthermore, the impact of relative humidity on *ex vivo* corneocyte maturation was examined and linked to a humidity-dependent proteolytic deactivation of transglutaminase. The work should stimulate new research and strategies for development of moisturising formulations that could support the skin barrier function.

Table of contents

List of figures

Figure 3.3. Immunostaining for 12R-LOX (A) is visualised in green and lipids are labelled in red. Scale bar=100 µm. Green pixels in the 12R-LOX (B) are normalised to the protein content to generate the 12R-LOX expression pattern. Mean ± SD, n=14.

Figure 3.4. Immunostaining for eLOX3 (A) is visualised in green and lipids are stained in red. Scale bar=100 µm. Green pixels in the eLOX3 (B) are normalised to the protein content to generate the eLOX3 expression pattern. Mean ± SD, n=14.

Figure 3.5. Expression pattern of CathD on corneocytes is shown in green and lipids in red fluorescence (A). Scale bar=100 µm. Green pixels in the CathD expression is normalised to the protein content (B). Mean ± SD (=14).

Figure 3.6. CathV expression on corneocytes is shown in green and lipids in red fluorescence (A). Scale bar=100 µm. Green pixels are normalised to protein content for CathV expression pattern (D). Mean ± SD (n=14).

Figure 3.7. Expression of INV in CPE is shown in green and the lipids of the CLE are visualised in red fluorescence (A). Scale bar=100 µm. The measured green pixels of INV expression is normalised for the protein content (B). Mean ± SD (n=14).

Figure 3.8. Expression of XP32 is visualised in the CPE in green and lipids of the CLE in red fluorescence (A). Scale bar=100 µm. The measured green pixels of XP32 expression is normalised for the protein content (B). Mean ± SD (n=14).

Figure 3.9. Immunostaining of TG1 in corneocytes visualised in green and the lipids are CLE stained with Nile red (A). Scale bar=100 µm. The measured green pixels for TG1 expression are normalised for the protein content (B). Mean ± SD (n=14).

Figure 4.1. Sonication caused fragile CEs to collapse in a time dependent manner while rigid CEs remain intact. A suitable duration was determined at 10 min. Mean ± SD (n=6).

Figure 4.2. The decrease in CE rigidity depends on the exposure time to sonication. Mean ± SD (n=6).

Figure 4.3. Image analysis with Image J to mark corneocytes to measure fluorescence intensity per unit of surface area.

Figure 4.4. Imaging of PE cheek and PP post auricular CEs. The green and red channels are merged to visualise INV and lipids of CEs. PE1= CEs of cheek, tape strip 1; PE9= CEs of cheek, tape strip 9; PP1= CEs of post auricular, tape strip 1; PP9= CEs of post auricular, tape strip 9. Scale bar=100 µm.

Figure 4.5. Percentage of immature CEs in PE cheek and PP post auricular samples. All data are shown as mean ± SD and compared via one-way ANOVA and post-hoc Sidak-Holm test, (n=14).

Figure 4.6. CE maturity is determined via ratio of lipids (red) and INV expression (green) fluorescence. The ratios are expressed as mean ± SD and compared via the one-way ANOVA, post-hoc Sidak-Holm test (n=14).

Figure 4.7. CE surface area of PE cheek and PP post auricular site. Data are shown as mean ± SD and compared with one-way ANOVA and post-hoc Sidak-Holm test (n=14).

Figure 4.8. The CE maturity determined with the ratio of lipids and INV expression normalized to the CE surface area. Data are represented as mean ± SD and compared with one-way ANOVA, post-hoc Sidak-Holm test (n=14).

Figure 4.9. Fluorescence images of CEs before and after 10 min of sonication of PE cheek and PP post auricular sites. PE1= CEs of cheek, tape strip 1; PE9= CEs of cheek, tape strip 9; PP1= CEs of post auricular, tape strip 1; PP9= CEs of post auricular, tape strip 9. Scale bar=100 µm.

Figure 4.10. CE Rigidity in samples of PE cheek and PP post auricular sites. Data are shown as mean ± SD and differences were determined via one-way ANOVA and post-hoc Sidak-Holm test (n=14).

Figure 4.11. CE Hydrophobicity in non-sonicated samples of PE cheek and PP post auricular sites. Data are shown as mean ± SD and compared with one-way ANOVA, post-hoc Sidak-Holm test (n=14).

Figure 4.12. CE Surface area determined in non-sonicated CEs for both anatomical sites and depths. CE surface area is shown as mean ± SD and compared via one-way ANOVA and post-hoc Sidak-Holm test (n=14).

Figure 4.13. Determination of RCEM based on CE rigidity and hydrophobicity. Data are shown as mean ± SD and compared with one-way ANOVA, post-hoc Sidak-Holm test (n=14).

Figure 5.1. The processing of esterified ω-hydroxyacyl-sphingosine to ω-hydroxyceramides initiated by 12R-LOX.

Figure 5.2. 12R-LOX activity is detected by the reduction of non-fluorescent H_2DCFDA to fluorescent DCF.

Figure 5.3. Determination of Michaelis-Menten kinetics of 12R-LOX activity with ethyl linoleic acid from samples of PE cheek and PP post auricular site (tape 2 and 8). Data are shown as mean ± SD (n=14).

Figure 5.4. A dilution factor of 1:500 was an effective contraction of the 12R-LOX antibody to inhibit the formation of the fluorescence signal in samples of both anatomical sites and depths. Data are shown as mean ± SD and compared with two-way ANOVA, post-hoc Sidak-Holm test (n=14).

Figure 5.5. The eLOX3 antibody showed no influence on the fluorescence signal resulting from the DCF formation. Data are shown as mean ± SD and compared with two-way ANOVA, post-hoc Sidak-Holm test (n=14).

Figure 5.6. The enzyme activity was unaffected by any of the ML351 concentrations which block 5-LOX, 12-LOX and 15-LOX. Results are shown as mean ± SD and compared with two-way ANOVA, post-hoc Sidak-Holm test (n=14).

Figure 5.7. A positive correlation has been demonstrated between high 12R-LOX activity and more mature CEs in the SC surface and deeper SC layers.

Figure 5.8. A negative correlation was shown between low 12R-LOX activity and high TEWL measurements in both anatomical sites.

Figure 6.1. The process of liberating TG1 by CathD in order to attach ω-hydroxyceramides to the INV in the CPE to form the hydrophobic CLE.

Figure 6.2. A range of concentrated salt solution were set up for humidified chambers for *ex vivo* maturation of CEs on first and ninth tape strips.

Figure 6.3. *Ex vivo* CE maturation at low, optimal and high RH after treating CEs on tape strips with protease inhibitor mix or 5% glycerol. *Ex vivo* CE maturation was assessed for the impact of inhibiting TG or 12R-LOX at optimal RH.

Figure 6.4. TG activity was measured after 4 days of *ex vivo* CE maturation at low, optimal and high RH in presence of TG inhibitor or protease inhibitor mix. TG activity was measured after two days of *ex vivo* maturation and compared to four days of incubation. In addition, TG activity was assessed after swapping RH conditions after two days of *ex vivo* maturation.

Figure 6.5. CE rigidity (A), CE hydrophobicity (B) and RCEM (C) was determined in *ex vivo* matured CEs after exposure to a range of RH. Data are shown as mean ± SD and compared via two-way ANOVA and post-hoc Sidak-Holm test, (n=7).

Figure 6.6. Nile Red lipid staining in samples after 10 min of sonication. Visualisation of CE maturity after tape stripping (A). Displaying CE maturity after *ex vivo* maturation without (B) and with TG inhibitor (C). Scale = 100 µm.

Figure 6.7. CE rigidity (A) is reduced while CE hydrophobicity (B) is unchanged in the presence of the TG inhibitor at 70% RH in presence. Inhibition of TG decreases RCEM in both anatomical sites (C). Data are shown as mean ± SD and compared via two-way ANOVA and post-hoc Sidak-Holm test, (n=7).

Figure 6.8. TG activity after tape stripping of PE cheek and PP post auricular sites and after *ex vivo* maturation at 70% RH of respective tapes in the presence of DMSO (vehicle) and in the presence of TG inhibitor (LDN-27219). Data are shown as mean ± SD and compared via two-way ANOVA and post-hoc Sidak-Holm test, (n=14).

Figure 6.9. TG activity in samples from both anatomical sites at baseline and after two and four days of *ex vivo* maturation at 44% RH (A), 70% RH (B) and 100% RH (C). Data are shown as mean ± SD and compared via two-way ANOVA and post-hoc Sidak-Holm test, (n=14).

Figure 6.10. TG activity at baseline and after initial two days of *ex vivo* maturation at 100% RH and further two days at 44% RH (A). TG activity at baseline and after switching from 100% RH to 70% RH (B). Mean ± SD, (n=7).

Figure 6.11. TG activity at baseline and after initial two days of *ex vivo* maturation at 44% RH and two additional days in 100% RH (A). TG activity at baseline and after switching from 70% RH to 100% RH (B). Mean ± SD, (n=7).

Figure 6.12. CE rigidity (A), CE hydrophobicity (B) and RCEM (C) after *ex vivo* maturation at 44% RH (low), 70% RH (optimal RH) and 100% RH (high RH) with and without the PI mix. Data are shown as mean ± SD and compared via two-way ANOVA and post-hoc Sidak-Holm test, (n=7).

Figure 6.13. TG activity after *ex vivo* maturation at low (44% RH), optimal (70% RH) and high RH (100% RH) in the presence and the absence of the PI mixture. Data are shown as mean ± SD and compared via two-way ANOVA and post-hoc Sidak-Holm test, (n=14).

Figure 6.14. CE rigidity (A), CE hydrophobicity (B) and RCEM (C) after *ex vivo* maturation at 70% RH in samples from the PE cheek and PP post auricular with and without exposure to 12R-LOX antibody. Data are shown as mean ± SD and compared via two-way ANOVA and post-hoc Sidak-Holm test, (n=7).

Figure 6.15. 12R-LOX activity was measured in samples at baseline, and after *ex vivo* maturation at 70% RH with and without TG inhibitor, LDN-27219, and 12R-LOX antibody. Data are shown as mean ± SD and compared via two-way ANOVA and post-hoc Sidak-Holm test, (n=14).

List of tables

Abstract

Background: The uppermost skin layer, stratum corneum (SC), is a physical and biochemical barrier against environmental insults. The SC resembles a wall with terminally differentiated keratinocytes, corneocytes, as "bricks" that are embedded in lamellar layers as "mortar". The corneocytes gain in maturity by transglutaminase enhancing rigidity and hydrophobicity. External conditions act on the skin homeostasis and thus understanding these effects on a molecular level might provide new targets for the cosmetic industry.

Objectives: Tape stripping is an established approach to collect successive layers of the SC. These tapes were used to identify biomarkers for the maturation of corneocytes by measuring enzyme activities and protein expression in the photo exposed (PE) cheek and photoprotected (PP) post auricular sites.

Methods: The SC integrity, cohesion and thickness was determined as a reference measurement. Immunostaining of structural proteins and enzymes was used to characterise the corneocyte from the first and ninth tape strip of both anatomical sites. The relative corneocyte envelope maturity assay was developed by determining the rigidity and hydrophobicity of corneocytes that to correlate to the SC properties. In addition, *ex vivo* maturation was tested at a range of relative humidities (RH) to determine the optimal RH. The corneocyte maturation and enzyme activities were investigated at low, optimal and high RH in the presence of protease inhibitors.

Results: The SC of the PE cheek site is thinner with a lower integrity and higher cohesion compared to the PP post auricular site. The corneocytes from the PE cheek site are less mature than from the PP post auricular site. The corneocytes from the PE cheek site were able to increase in rigidity but not in hydrophobicity. Humidity has an impact on proteases which in turn are able to deactivate transglutaminase activity and thus influence corneocyte maturation.

Conclusions: Various methods were tested and correlated with the SC integrity in human subjects. The determination of protein expression was suggested for a set of biomarkers involved in lipid processing enzymes (12R-lipoxygenase and epidermal lipoxygenase 3), structural CE proteins (involucrin and skin-specific protein 32), proteases (cathepsin D and V) and transglutaminase. The impaired *ex vivo* maturation of samples from the PE cheek point towards pre-mature desquamation and thus provide new pharmaceutical targets for moisturising skin care products.

Table of abbreviations

12R-LOX	12R-lipoxygenase
A	α-hydroxyl fatty acid
AB	Antibody
AD	Atopic dermatitis
ANOVA	Analysis of variance
ATP	Adenosine triphosphate
BSA	Bovine serum albumin
CathD	Cathepsin D
CathV	Cathepsin V
CE	Cornified envelope
CEf	Fragile CEs
CEr	Rigid CEs
CLE	Corneocyte lipid envelope
CPE	Corneocyte protein envelope
CV	Coefficient of variation
DS	Dihydrosphingosine
DTT	DL-dithiothreitol
EDC	Epidermal differentiation complex
EDTA	Ethylene diamine tetra acetic acid
eLOX3	Epidermal-type lipoxygenase 3
EO	Esterified ω-hydroxyl fatty acid
EOS	Esterified ω-hydroxyacyl-sphingosine
FITC	Fluorescein isothiocyanate
GTP	Guanosine triphosphate
H	6-hydroxy-sphingosine
INV	Involucrin
KHG	Keratohyalin granules
LB	Lamellar body
LOR	Loricrin
ML351	5-(Methylamino)-2-(1-naphthalenyl)-4-oxazolecarbonitrile
N	Non-hydroxyl fatty acid
NMF	Natural moisturising factor

O	ω-hydroxyl fatty acid
P	Phytosphingosine
PBS	Phosphate-buffered saline
PE	Photo exposed
PP	Photoprotected
RH	Relative humidity
ROS	Reactive oxygen species
S	Sphingosine
SC	Stratum corneum
SD	Standard deviation
SDS	Sodium dodecyl sulfate
SPR	Small proline-rich proteins
TEWL	Trans epidermal water loss
TG	Transglutaminase
TRITC	Tetramethylrhodamine isothiocyanate
UV	Ultraviolet
XP-32	Skin-specific protein 32

CHAPTER 1

Introduction

1. Introduction

1.1 Essential anatomy and functions of the skin

A complex integumentary system is the first line of contact and defence mechanism against the environment and its challenges on the human body. The skin covers the entire body and forms a protective structure. The integumentary system is extended with appendages such as hair, nails, sebaceous and sweat glands as well as feathers, hooves and scales in animals [1]. Each appendage has their own unique function to support the skin in its various responsibilities.

The hair forms a physical barrier to minimise the exposure to the sunlight on the skin. Furthermore, hair insulates the body by trapping air to warm the skin surface. Nails protect the end of the digits while being used in moving small objects from the skin and scraping at the sensation of itch. Sebaceous glands secrete oily sebum to provide water-repellent properties and elasticity to the skin. The sweat glands secrete sweat to prevent hyperthermia in warm environments or during physical exercise. Furthermore, sweat is composed of water, salt and small amounts of waste products that collectively protect the skin of bacterial infection [2].

The skin is considered a large organ considering an average surface area of 1.7 - 2 m^2 and a thickness of 0.2 - 4 mm depending on anatomical site, ethnicity, age and climate conditions. The main function of the skin is to prevent excessive dehydration and external invasion among many other regulatory functions. The skin is distinctively subdivided into the hypodermis, dermis and epidermis (Fig.1.1).
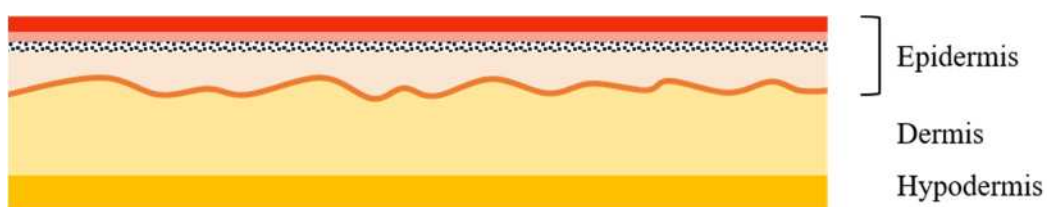
Figure 1.1 Schematic representation of the three basic layers of the skin.

The hypodermis is the deepest layer of the skin and is mainly an insulating adipose tissue [3]. This layer of the skin is less involved in the barrier function but serves as an energy depot and insulator [4]. Adipocytes are embedded as lobules in an extracellular matrix of collagen, elastin and reticulin fibres secreted by fibroblasts [5]. The architecture of the subcutaneous tissue provides insulation of body temperature [6] and cushion functionality [7]. Blood vessels, nerves, glands and the lymphatic system are located in the hypodermis to provide nutrition and oxygen while removing cellular waste products and toxins [5]. The regulation of blood pressure, sensation, pheromone production, vitamin D activation [8], body temperature and immune response are communicated due to the interconnection of the hypodermis to the blood circulation [9], lymphatic [10] and nervous system [11]. These components along with connective matrix fibres reach into the dermis which is a meshwork of capillaries, lymphatics, nerve endings, fibroblasts and immune cells embedded in a matrix of collagen and elastin. Furthermore, the appendages such as the sebaceous and sweat glands as well as hair follicles are located within the dermis [3]. This cellular and biochemical heterogeneity provides the skin with nutrition, oxygen, sensation, immune responses, mechanical resistance and flexibility [8,12].

The dermis contributes to the maintenance of the uppermost skin layer, the epidermis, which is made up of four distinct layers formed of keratinocytes in particular developmental stages derived from tissue homeostasis [13]. The epidermis protects the body from thermal, mechanical and physical stress while forming a physical and chemical barrier to hazardous particles, substances and pathogens. Thus, the skin is part of the innate immune system that recognises components of some pathogens and elicits a rapid immune response, however without generating a lasting response [14]. Keratinocytes form a communication network with the immune cells, Langerhans cells and migrating T lymphocytes, to establish a surveillance system for pathogens and cutaneous neoplasms [15]. The cell-based protection is supported by the acidic mantle of the epidermis [16] with a pH value between 4.2-5.6 [17]. This chemical barrier is generated by the interaction of sebum and sweat [18] which is further supported by fatty acids [19]. This prevents the colonisation of pathogens but also plays a regulatory role in enzyme activities in the epidermis [20].

The epidermis is a complex multi-layered structure populated with keratinocytes [21], however, Langerhans cells [22] are found in the viable epidermis along with Merkel cells. These tactile epithelial cells with mechanoreceptors are connected to nerve endings for touch sensation [23]. The plasticity of the epidermal barrier is crucial for diversity of functions of the skin. However, this plasticity depends highly on maintenance of epidermal hydration and integrity [24].

The integrity of the stratum corneum is referring to the intactness and mechanical stability of the skin surface [25]. This durability depends on the SC coherence between corneocytes as well as to the lamellar layers [26]. The SC cohesion and thickness as well as the composition of the SC lipids determine the SC permeation in which certain compounds may pass deeper into the skin[27]. The epidermal barrier function and its homeostasis is crucial for the water holding capacity of the skin and thus maintain the SC hydration [28].

1.2 Homeostasis of the epidermis

A vertebrate's body is covered with stratified epidermis varying in thickness depending on anatomical site. The thinnest epidermis is found in the eyelids (0.05 mm) while the thickest layer is located on the palms of the hands and the soles of the feet (0.4-0.6 mm) [12]. The epidermis can be distinguished microscopically as four layers; stratum basale, stratum spinosum, stratum granulosum and stratum corneum (SC) (Fig. 1.2) [21]. The layers differ in the stage of keratinocyte differentiation, protein expression as well as the composition of the extracellular matrix and pH value [29]. A specific sequence of developmental stages maintains a constant number of cells in the epidermal layers in order to maintain the epidermal barrier including after injuries [30].

Epidermal stem cells in the stratum basale are anchored to the basement membrane via hemi desmosomes to ensure firm adherence to the extracellular matrix by connecting to the intracellular keratin filaments [31,32]. Asymmetrical cell division results in the original epidermal stem cell remaining attached to the stratum basale while the daughter cell proceeds to differentiate into keratinocytes. These cells are pushed out from the proliferative stratum basale into the stratum spinosum and further into the stratum granulosum while differentiating and changing in cellular properties and extracellular composition. The terminally differentiated keratinocytes undergo a

unique cell death once reaching the uppermost epidermal layer, the SC, where cornification occurs and give rise to corneocytes. Old and brittle corneocytes are shed off the epidermis via desquamation. This is an enzymatic driven process where proteases digest the protein components of the corneodesmosomes causing a loosening of the interconnected corneocytes. Skin homeostasis requires well-regulated proliferation, differentiation, cornification and desquamation (Fig. 1.2).
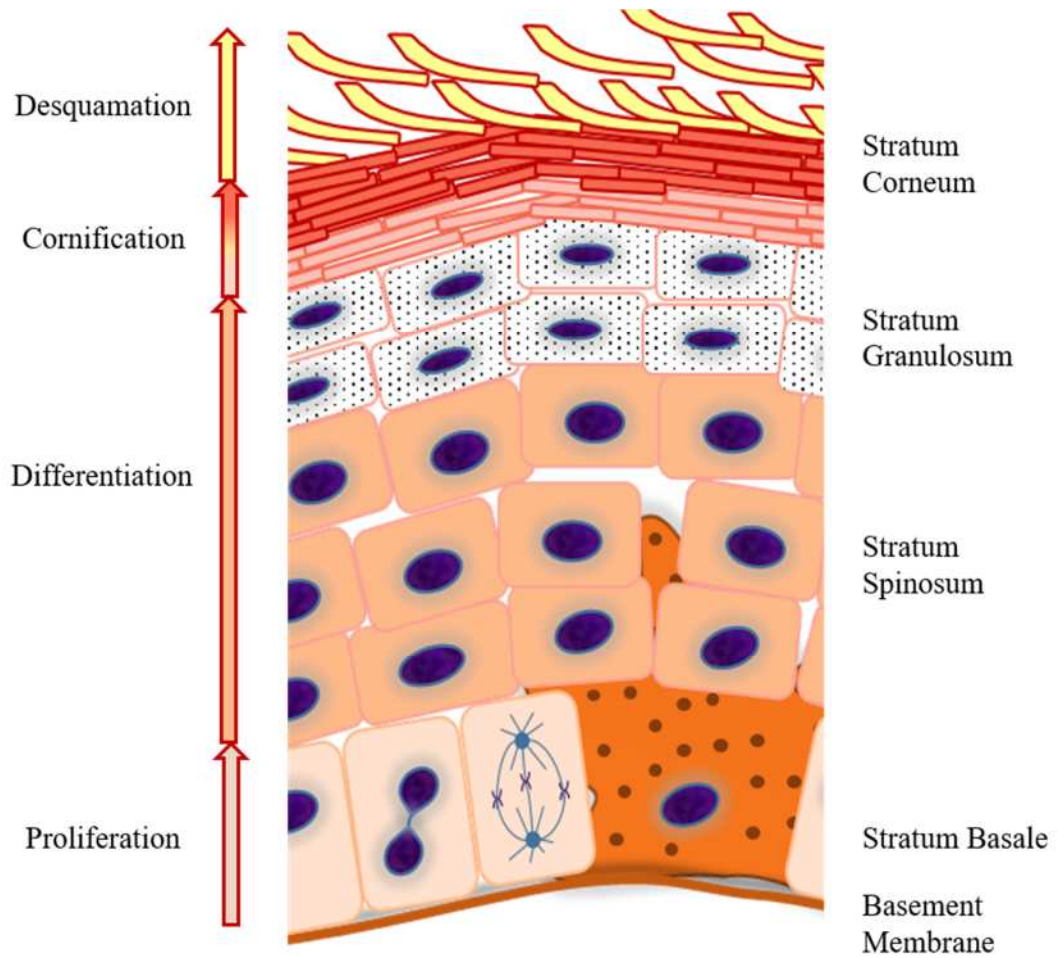
Figure 1.2. The developmental stages to maintain the epidermal layers.

1.2.1 Cellular events in keratinocyte differentiation

The epidermal layers can be characterised according to their altered morphology and biochemical composition at each developmental stage over 28-35 days [29]. Epidermal stem cells are capable of self-renewal, proliferation and differentiation to keratinocytes. These cuboidal/columnar cells are attached to the basement membrane via hemi desmosomes allowing them to receive pro-survival and growth signals to sustain a constant number of mitotic cells in the stratum basale while generating cells for the epidermis [29]. Proliferative stem cells generate one new line of keratinocytes every day aiming to compensate for damage to the skin as well as for natural desquamation [33]. Melanocytes are resident in the stratum basale along with epidermal stem cells (Fig. 1.2), and generate a substantial amount of a photo absorbing pigment, known as melanin. Melanin has been reported to be involved in protection against photo damage (ultraviolet and visible rays) from solar radiation which is also associated with heat damage [34]. Organelles filled with melanin, melanosomes, are transported to adjacent stem cells and keratinocytes to protect against cancer promoting photo damage [35].

The expression pattern of regulatory and structural proteins in proliferating stem cells switches once committed to the keratinocyte differentiation lineage [13]. The main cytoskeletal filament, keratin, is a long and coiled α-helical polymer in epidermal cells. Keratin is subdivided into acidic type I (K1-8) and neutral type II (K9-10; K12-20) keratins which are organised in different arrangements of heterodimers depending on the developmental stage [31]. The epidermal stem cells in the stratum basale express K5/K14 while the late keratinocytes express K1/K10 and K2/K10 [36]. Keratins gain dynamic functions upon post-translational modifications such as phosphorylation [37]. Post-translational modifications are involved in the maintenance of cell integrity by regulating cell growth and apoptosis [38]. Keratinocytes in the stratum spinosum produce mainly desmosomes that interconnect between adjacent cells while being pushed into the stratum granulosum [13]. Keratinocytes in the stratum granulosum accumulate keratin and produce keratohyalin granules (KHG) filled with structural or hydrolytic proteins. Lamellar bodies (LB) are another subtype of granules that are filled with lipids. The high amount of granules result in the grainy appearance in this layer when viewed under a microscope [13,39]. In the final stage of epidermal homeostasis, terminally differentiated keratinocytes undergo a unique

programmed cell death known as cornification. All cell organelles disintegrate and the collapse of the cellular morphology. These keratinocytes are referred to as corneocytes or generically known as dead skin cells. The SC consists of polygonal corneocytes that are interconnected via corneodesmosomes and provide the protective layer of the skin. Desquamation is a process in which proteases degrade the corneodesmosomes which connect neighbouring corneocytes leading to shed of the uppermost SC layers. A controlled desquamation process allows maintenance of a constant number of SC layers with hydrated and robust corneocytes [8,12].

1.3 Stratum corneum – The skin barrier

The external environment presents a variety of threats that may cause serious harm to the body. The skin is a powerful shield against pathogens, irritants and solar radiation while preventing excessive dehydration. Structural and biochemical features of the SC provide these protective characteristics.

The SC is morphologically organised similarly to a shielding wall in which corneocytes (the "bricks") are embedded in lamellar lipids (the "mortar") as depicted in figure 1.3 [27,40]. This physical arrangement of tightly packed and stacked corneocytes surrounded by hydrophobic lipids limits the diffusion pathway of molecules. However, the physicochemical characteristics of molecules determine the permeation rate and efficiency through the epidermis into the dermis and ultimately reach the blood circulation [27,41]. The thickness of the SC varies depending on anatomical site, gender, age and ethnicity. The SC is on average 20 µm thick and is composed of 18 – 21 layers of corneocytes [8]. The efficacy of the skin barrier function has been associated with the SC thickness [24].
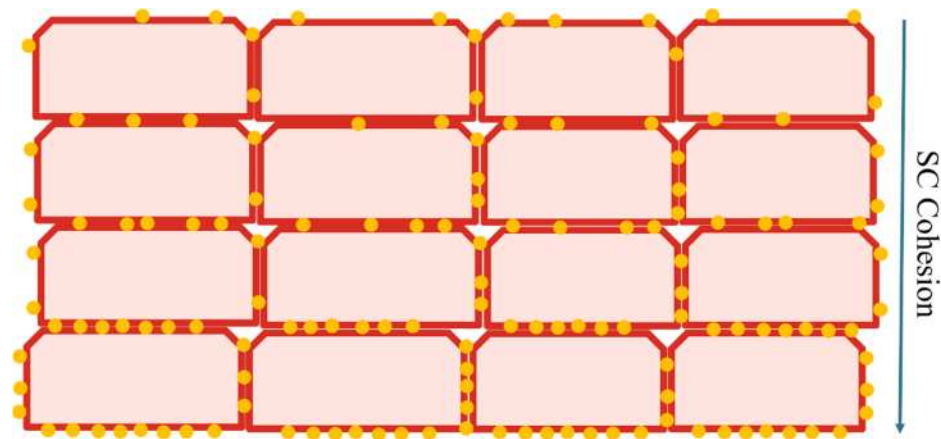
Figure 1.3. The skin is structurally organised with corneocytes interconnected via corneodesmosomes and embedded in intercellular lipid lamellae layers.

Terminally differentiating keratinocytes are pushed towards the SC where they are present as corneocytes with an immature corneocyte protein envelope (CPE) replacing the former cell membrane. Aggregated keratins fill up the intracellular space and replaces the cytoplasmic element of the desmosomes [31]. The structural proteins in the CPE besides keratins are loricrin (LOR), involucrin (INV), trichohyalin, and small proline-rich proteins (SPRs) which account for 7-10% of epidermal total mass.

1.3.1 Structural proteins of the CEs

The main structural protein in the CE is LOR which accounts for 70-85% of SC protein mass [42]. Phosphorylation of KHG is believed to release LOR which is rapidly incorporated into the CPE. However, this theory has not been confirmed, to date, as CPEs are insoluble in physiological solutions which creates a methodological problem to isolate individual protein species [43]. The majority of LORs are cross-linked via isopeptide bonds with each other while a smaller portion are interconnected to SPRs [42].

The classes of SPRs are known for the presence of a head and tail domain rich in glutamine and lysine residues allowing their crosslinking in a bridge-like fashion with other structural proteins [44]. The amount of SPRs within the CPE vary depending on anatomical sites as these cross-bridging proteins influence the flexibility, rigidity and thickness of the CPE [45].

Profilaggrin is a large (about 500 kDa) precursor protein complex stored with LOR in the KHGs [39]. During cornification, profilaggrin is dephosphorylated and catalysed by proteases resulting in individual filaggrin molecules [46]. Filaggrin aggregates keratin fibres into aligned and tight bundles [47] causing the collapse of the cytoskeleton during the early stage of cornification. Filaggrin has a half-life of 6h and is degraded into hydrophilic amino acids, collectively referred to as natural moisturising factor (NMF). These water holding components are essential for osmolality and flexibility of the SC [48]. NMF is a mixture of water soluble compounds with a low molecular weight found in the intracellular space of CEs. These compounds maintain the hydration of CEs and therefore have a major contribution to skin hydration. The combination of corneodesmosomes and the hydrophobic coating of the CE form a strong barrier against dehydration [49]. The hydration of the SC is a crucial aspect of the skin functionalities otherwise the skin becomes brittle, inflexible and ineffective as a barrier [24].

INV is the main structural protein of the CPE that appears in the early stage of CE assembly [38]. INV accumulates close to the former cell membrane and is cross-linked to structural proteins and serves as a protein scaffold for other proteins. Furthermore, INV is believed to be the main protein in the CPE that is covalently linked to the lipids which provides hydrophobicity to the corneocytes [50,51].

1.3.2 The hydrophobic components of the SC

In 1930, linoleic acid was shown to be an essential fatty acid in animals. However, the absence of dietary lipids is known to lead to unhealthy skin [52] and is associated with an increased trans epidermal water loss (TEWL) [53]. Lipids in the SC have been reported to be a crucial compound for the skin barrier function [54]. The water-holding capacity of the SC is provided by NMF. However, this capacity was weakened by the removal of the lipids via solvent extraction which also demonstrated the important function of skin lipids [55].

Free lipids form an arrangement of intercellular lamellae located between CEs giving the layered appearance that has been referred to as the "mortar" of the protective SC [49,56] (Fig. 1.4). These lipids contribute mainly to the skin barrier function by preventing excessive water loss by stacking in a membrane sheet fashion that fill up

the extracellular spaces [57]. The lamellar layer mainly contains ceramides, free fatty acids, and cholesterol accounting for 5-15% of the dry SC weight [58]. These lipids are mixed in an equimolar ratio (1:1:1), however, the composition may vary between individuals and body sites [59].

EOS
Cholesterol
Free fatty acids
Other ceramides
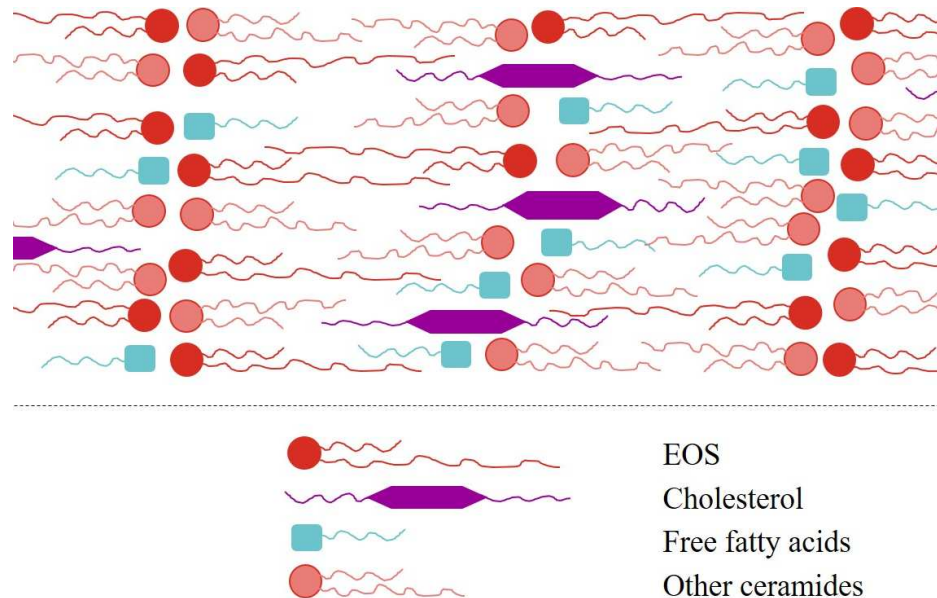
Figure 1.4. SC flexibility and integrity is maintained by lipids arranged in bilayers.

Keratinocytes contain LBs that are filled with polar precursors of the skin lipids, glycosphingolipids, free sterols and phospholipids that are released into the extracellular space via exocytosis [57]. Glycosphingolipids have been identified as precursors for the ceramides, sterols become cholesterol sulfate and phospholipids are converted to free fatty acids and glycerol [60]. The precursor lipids in the LBs are generated by enzymes or derive from the vascular circulation in the stratum basale [61]. The keratinocytes in the stratum basale and spinosum have lipases and phospholipases in order to pre-process lipids [62]. These lipids are further processed by the anabolic reaction of ceramide synthase [63] or cholesterol sulfotransferase [64] which are expressed in keratinocytes in the stratum granulosum. These reactions lead to the final lipids that are packed into the LBs [65]. Keratinocytes transport these vesicles via the Golgi network which allows the vesicles to fuse with the keratinocyte cell membrane in order to release its content to the extracellular space [66]. The release

of LB-content is mediated by the influx of calcium at the interface of the stratum granulosum and stratum corneum [67]. However, the enzymes that metabolise the precursor lipids are co-located in the LBs and are only activated in the intercellular space [65]. Cholesterol is less involved in the barrier function but plays a major role in SC desquamation events [68].

A further requirement for an effective skin barrier is the lipid organisation that is mainly present as two lamellar phases, the more dense orthorhombic packing or less dense hexagonal packing [69]. Free fatty acids and amide-bound fatty acid domains in the ceramides are tightly packed as a gel-phase membrane domain with liquid crystalline domains [70]. Linoleic acid rich phospholipids were considered as the main compounds in the hydrophobic barrier [48] until linoleic acid rich ceramides were discovered [71]. Improvements in methodology resulted in the discovery of many more ceramide classes [72–74]. Fifteen classes of free ceramides have been identified in humans [73] and six have been identified in pigs [58]. Their nomenclature corresponds to their molecular structure with a dihydrosphingosine (DS), sphingosine (S), phytosphingosine (P) or 6-hydroxy-sphingosine (H) as a backbone that is linked to non-hydroxyl fatty acid (N), α-hydroxyl fatty acid (A), ω-hydroxyl fatty acid (O) or esterified ω-hydroxyl fatty acid (EO). The main difference between sphingosine and phytosphingosine as well as 6-hydroxysphingosine is the hydroxyl group on C4 of the sphingosine backbone and C6, respectively, instead of an unsaturated C4 [60]. The hydroxyl group has been shown to increase skin permeability and to decrease orthorhombic packing via its capability to form hydrogen bonds which suggests that the reduction of sphingosine containing ceramides would leave a more permeable and compromised SC barrier [72]. Ceramide 1 also known as esterified ω-hydroxyacyl-sphingosine (EOS) contains linoleic acid that is esterified to the ω-hydroxyl group of the very long chain fatty acid (30-34 carbon atoms) that is linked at the N-acyl moiety to sphingosine [74]. EOS was shown to provide SC flexibility and permeability while preventing the scaling of the skin [75]. Reduced levels of linoleic acid containing ceramides have been linked to skin conditions such as atopic dermatitis [76] and acne [58]. Skin xerosis which is commonly referred to as uncomfortable dry skin where an individual experiences itchy, scaling and cracking skin may occur predominantly in the winter months. Reduced levels of ceramides and cholesterol (up to 40%) as well as fatty acids (about 5%) were demonstrated in human subjects in January compared

to June. Among these changes 25% account for a reduced ceramide 1 level and esterified saturated fatty acids. Topical application of linoleic acid containing triglycerides resulted in a significant improvement in ceramide 1 levels while amounts of other skin lipids were unchanged in human subjects [77]. These studies point to the importance of linoleic acid containing ceramides and their contribution to the SC barrier function. However, the most efficient "mortar" still requires robust and intact "bricks" to form a protective barrier.

1.3.3 Corneocyte envelope maturation

Terminally differentiated keratinocytes undergo cornification in the SC giving rise to corneocytes, the "bricks" of the wall analogy. Corneocytes in the upper stratum granulosum acquire the unique CPE and CLE which is immature in terms of rigidity and hydrophobicity. Cellular metabolism is lost with cornification, however, the SC remains biochemically highly active. All required proteins and lipids are produced in the earlier keratinocyte development. Two events are initiated before CEs can mature; a rise in calcium ions due to controlled cell death of keratinocytes and a decrease in pH. Calcium has a distinct profile across the epidermal layers with a gradual influx via ion pumps into the keratinocytes in the stratum spinosum where differentiating keratinocytes are driven towards the generation of structural proteins such as involucrin [78]. The calcium level reaches a peak in the upper stratum granulosum which initiates the release of the KHGs containing catalytic enzymes and LBs [79]. A rapid efflux of calcium occurs upon keratinocyte death in the lower SC. This crucial event regulates the enzymes that are involved in CE maturation and desquamation [80]. The pH in the viable epidermis is neutral while the non-viable SC is acidic thereby enzyme activities can be regulated [81]. The low pH acts as an antimicrobial defence mechanism [82] while enhancing the activity of proteases. Proteases facilitate desquamation by digesting the corneodesmosomes in the upper SC [83] and enhance the activity of enzymes that initiate cornification in the deeper SC [84].

Cornified corneocyte maturation is facilitated by various enzymes in a cascade-like event. Phospholipases digest the fatty acids of the former keratinocyte cell membrane in order to generate space on the surface of the corneocyte while the free fatty acids contribute to SC acidification [19,85]. EOS and long fatty acids are processed before being linked to the structural proteins of the CPEs. The CEs mature

with the gradual crosslinking of structural proteins in the CPE and the covalent attachment of lipids to the CLE [13]. Studies in humans and mice showed the importance of 12R-lipoxygenase (12R-LOX) and epidermal-type lipoxygenase 3 (eLOX3) in skin physiology [86]. Both enzymes are members of the epidermal subfamily of non-heme iron dioxygenases that process esterified polyunsaturated fatty acids [87]. A functional link has been shown between both lipoxygenases and their involvement in the cornification process of the stratum corneum [86,88]. Mice deficient in 12R-LOX showed an early postnatal death due to severe dehydration [89]. Mice with a deficiency in eLOX3 showed similar impaired barrier function to 12R-LOX deficient mice [86,90]. The analysis of the skin lipids of 12R-LOX and eLOX3 deficient mice has linked the barrier impermanent to a loss in covalently bound ceramides [90]. The linoleate domain of EOS is oxidised by 12R-LOX [91]. eLOX3 has hydroperoxide isomerase activity on processed linoleic acid domain of EOS [87]. Hydrolases cleave the linoleic acid off EOS after being processed by 12R-LOX and eLOX3 [92,93] which produces ω-hydroxyceramide [94].

The ω-hydroxyceramide are covalently attached to the glutamine in structural proteins of the CPE via transglutaminases (TG) [50]. This leads to the formation of the CLE which is associated with the CE maturation by gaining in hydrophobicity. The CLE of the CEs supports the lipid lamellae in hydrophobicity and thus contributes greatly to the skin barrier [26]. However, at the same time, TG catalyses the isopeptide bonds by forming a thiolester acyl-enzyme intermediate to transfer the acyl residue to the primary ε-amine group in lysine. This allows the crosslinking to glutamate thereby forming an insoluble ε-(γ-glutamyl)lysine bond between structural proteins [95].
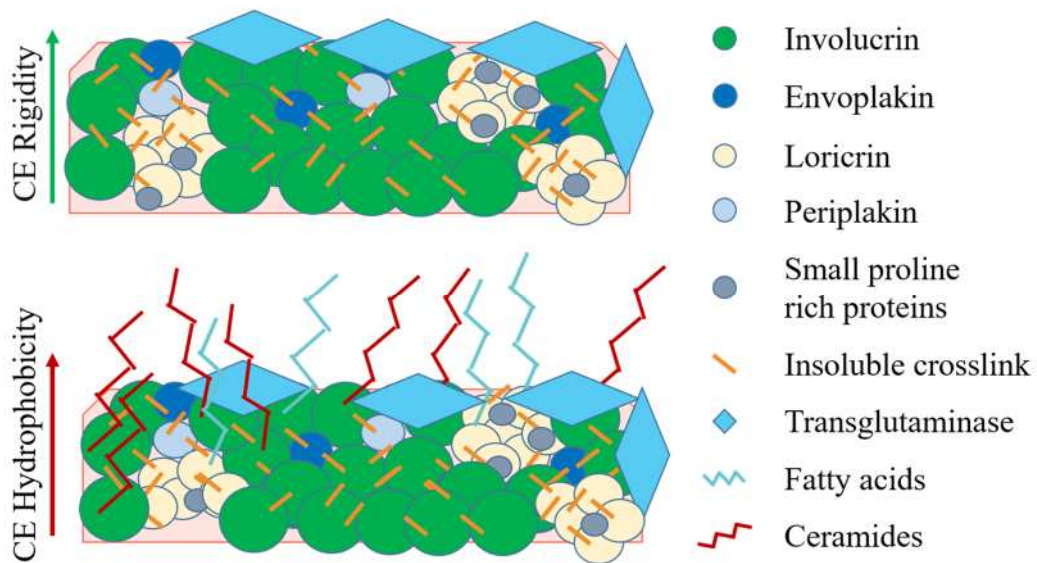
Figure 1.5. Corneocytes mature with the gain in rigidity and hydrophobicity mediated by transglutaminase which supports the SC barrier function.

INVs are located at the surface of the CPE and are mostly interconnected and are thought of as scaffold proteins that ensure the cellular architecture is retained [96]. In a similar fashion TG crosslinks LOR and facilitates the cross-linked bridging to envoplakin, periplakin or SPR proteins [42,84]. The continued cross-linkage of structural proteins increases the rigidity of the CEs. This provides flexibility and mechanical resistance to the SC while the CLE gains in hydrophobicity by the continued attachment of lipids [42,56] (Fig. 1.5). However, it is still to be discovered if CE maturation is arranged in a sequence of events or if the processes are concurrent.

The cohesion between CEs changes during the developmental stage of keratinocytes (Fig. 1.2). The cohesion is strong in the deeper SC layer while decreasing in cohesiveness with desquamation [83,84]. This can be determined by tape stripping where thin layers of the SC can be sampled using adhesive tapes and by measuring protein content via an infrared densitometer [97,98]. The CLE allows hydrophobic interaction with the lamellar layers and creates the "brick and mortar" structure that together protect against external factors [40]. The increase in CE maturity is correlated with SC integrity [99], permeability [100], hydration [101], cohesion [26] and ultimately with the skin barrier function.

1.4 Aims and objectives

The CE maturation is a crucial event for an effective skin barrier function and thus the understanding of the underlying mechanism may provide new targets for skin care products. The skin barrier relies on the rigidity towards mechanical stressors and hydrophobicity terminally differentiated keratinocytes. Two populations of CEs have been identified; immature fragile CEs (CEf) found in the deeper SC and mature rigid CEs (CEr) at the SC surface [102]. The characterisation of CE maturity and epidermal biomarkers should assist the pharmaceutical or cosmetic industry in the development of better topical formulations. New products tend to be tested for permeation in terms of how deep the active compound penetrates through the SC which has been extensively studied [103,104] and reviewed [41]. Studies have shown the efficacy of their products on animal [105] or human *in vivo* studies to characterise the SC cohesion [98,106] and SC integrity [107]. The SC thickness can be estimated via a mathematical approach using the SC integrity and cohesion measurements [108]. The cohesion can be determined via tape stripping and the weight or protein amount of the collected SC sample on the tape strips. Two independent studies correlated the total cumulative protein amount to the SC thickness which has been confirmed with Raman spectroscopy. Both studies reveal that 100 µg cm^{-2} of removed protein corresponds with 1.9 µm of SC [109,110]. Tape stripping was used by some studies to disrupt the barrier function in order to assess the impact before and after any treatment [111,112]. Some products might influence the viable epidermal layers by promoting proliferation or changing gene expression. Others might only act on the SC such as salicylic acid [113], however, this might not reflect the actual impact on the lamellar layer or corneocytes. For many years, CE maturity has been determined via INV/lipid ratio which correlates the INV positive CEs to the fluorescence signal of a lipid staining [114]. This provides a simplified measurement in which immature CEs have more fluorescence signal indicating the expression of INV than the fluorescence signal resulting from the lipid staining. However, there are limitations associated with this standard approach which will be discussed further in Chapter 4.

The structural proteins of the CPE and the enzymes of the SC are suitable biomarkers for CE maturation. Some studies visualise INV or LOR of the SC in histology samples use immunostaining [78] or CEs [106,114,115]. INV and LOR are both encoded in the early cluster of epidermal differentiation complex (EDC) as they

are precursor proteins of the CE. Skin-specific protein 32 (XP32) is a structural protein that is encoded in the late cluster of the EDC[116]. Early and late clusters of the EDC allow a wide variety to regulate proteins crucial to the barrier function. XP32 has been associated to be expressed abundantly in immature CEs in damaged skin barrier such as psoriasis [117]. A recent proteomics work has shown that XP32 expression was significantly higher in the photo-exposed cheek site compared to photoprotected skin [118]. This study also showed an increased expression of two proteases, Cathepsin D and Cathepsin V (CathD and CathV), which are associated with photo damage and desquamation [118–120]. CathD is an aspartic protease which is activated by cysteine proteases such as CathV [121]. CathD and CathV have been shown to degrade corneodesmosomes in photo damaged skin [119,122,123]. CathV aids the antigen presentation of Langerhans cells to facilitate an immune response [124]. CathD has been shown to enhance TG activity which mediates the CE maturation and thus barrier quality [125].

12R-LOX is an enzyme that has just been identified as being involved in the formation of EOS in the human skin [91]. A mouse model has shown that homozygote knockout mice for 12R-LOX died within three hours after birth by dehydration [89]. EOS is first catalysed by 12R-LOX before other enzymes contribute to the preparation of to the substrate preparation for TG [126]. More recently, a study has shown that 12R-LOX was less expressed in photo exposed skin compared to photo protected sites [118] which are associated with decreased CE maturity [92]. The development of the 12R-LOX assay is a challenging task due to the lack of commercially available substrates and inhibitors. However, an assay for 12R-LOX activity still needs to be developed in order to determine if CE maturity in photo exposed skin is decreased due to the lower 12R-LOX expression or activity.

However, the characterisation of the biomarkers might be limited due to the insolubility of the proteins as well as the similarity in peptide sequences within the structural proteins. A combination of methods such as an enzyme assay and the determination of a variety of biomarkers should provide more details about the maturation of corneocytes (Fig. 1.6).
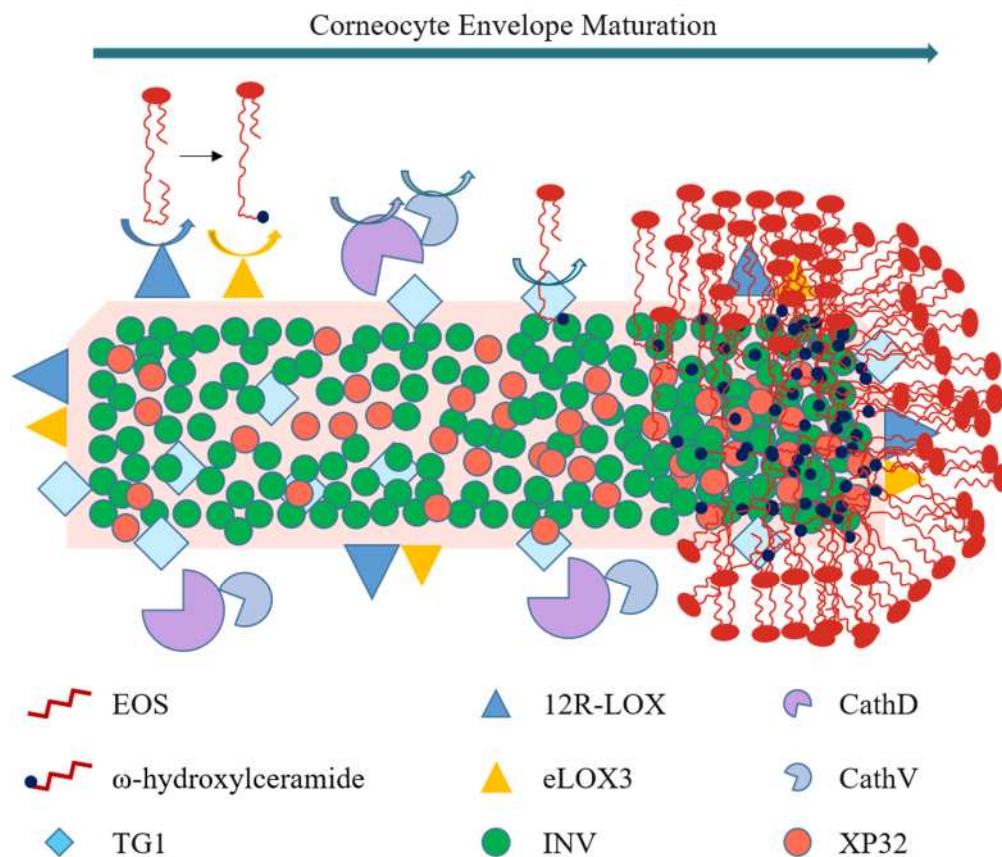
Figure 1.6. Location and interaction of investigated biomarkers of corneocytes: Lipids (EOS and ω-hydroxyceramide), lipid processing enzymes (12R-LOX and eLOX3), proteases (CathD and CathV), CE maturing enzyme (TG1) and structural proteins (INV and XP32).

The primary objective of this project was to develop a robust methodology to characterise and to identify biomarkers of epidermal corneocyte envelope maturation for photo exposed and photo protected skin. The work in this thesis started with assessing basic SC properties between Caucasians and Chinese subjects (Chapter 2). In total 14 participants Caucasians and 14 Chinese participants were recruited to determine the skin barrier integrity, cohesion and thickness. Furthermore, differences between male and female participants were assessed in both ethnic groups. The follow up chapters focus primarily on Chinese participants as their skin has been reported to be more impaired than Caucasian skin [112]. These SC samples collected via tape stripping were used to for the following aspects:

❖ to develop a new and accurate characterisation method for CE maturation that correlates with SC integrity and cohesion

❖ to identify biomarkers for immature and mature CEs

❖ to develop and validate an *in vitro* 12R-LOX activity assay which correlates with CE hydrophobicity and SC integrity

❖ to assess the influence of relative humidity on *ex vivo* CE and on TG, 12R-LOX and cathepsin D activity

❖ to determine the effect of glycerol at low-optimal-high humidity on *ex vivo* CE maturation

CHAPTER 2

Characterisation of the stratum corneum

2. Characterisation of the stratum corneum

2.1 Abstract

Background: The skin barrier function can be characterised by a number of biophysical measurements that determine the SC integrity, cohesion and thickness. These characteristics allow a comparison of SC properties at different anatomical sites, between gender, and in different ethnic groups.

Objectives: The aim of this work is to characterise the SC integrity, cohesion and thickness of photo exposed (PE) cheek and photo protected (PP) post auricular sites in healthy human subjects.

Methods: Nine SC layers were obtained via the minimally-invasive tape stripping approach in healthy Caucasian and Chinese participants. SC integrity was determined via TEWL while SC cohesion was assessed by measuring the protein content on the tape strips with infrared densitometry. The TEWL values and the cumulative protein amounts were used to estimate the SC thickness.

Results: TEWL increased significantly following removal of nine tape strips in the PE cheek site while TEWL in the PP post auricular site remained constant. The SC cohesion in the PE cheek site was stronger than in the PP post auricular site with tape stripping. However, the PE cheek site was determined to be thinner than the PP post auricular site. The TEWL values were comparable between Caucasian and Chinese subjects while the cumulative protein amount removed was higher for both anatomical sites of Caucasians indicating a thicker SC than in Chinese participants. There were no significant differences in cumulative amounts of protein removed via tape stripping and TEWL values between males and females.

Conclusions: The barrier function was reduced in sun-exposed skin in Caucasian and Chinese subjects compared with the sun-protected sites. This study confirms the impact of photo damage on the skin barrier function in Chinese and Caucasian subjects.

Key Words: Tape stripping, TEWL, Cohesion, stratum corneum.

2.2. Introduction

In 1975, a new therapy treatment for psoriasis was developed using UVA light. Some patients showed a 85% clearing of psoriatic plaques while others experienced sunburn-like side effects [127]. The short-term side effects were linked to the pigmentation of the individual's skin and thus that the dosage of the UVA light had to be adjusted in terms of intensity and duration. This led to the concept of classifying six skin types according to skin colour and its response to UV irradiation (Table 1.1) [128].

Table 1.1. The six Fitzpatrick skin typing according to pigmentation and response to UV irradiation.

Type	Skin pigmentation	Response to UV light
I	Very light or pale skin	Always burns and does not tan
II	Light skin	Usually burns and seldom tans
III	Medium to olive skin	Burns moderately and usually tans
IV	Dark olive to light brown skin	Burns mildly and moderate tanning
V	Dark skin	Seldom burns and deeper tanning
VI	Very dark skin	Does not burn and does not tan

The investigation of the upper most skin layers is included in many dermatological studies to establish the SC properties at baseline and after topical application of actives such as salicylic acid [129]. A minimally invasive technique was introduced in 1939 in which adhesive tapes were used to obtain SC layers and examination of the cellular structure on the skin surface [21]. A range of tape brands have been tested since then such as Tesa® and Scotch®. However, D-Squame® tapes

were developed with uniformity in size and adhesiveness to allow comparatively more control in sample collection [130]. Tape stripping is now an established approach to investigate the penetration, distribution profile and the safety of cosmetic products [131], sunscreens [97] and medical application [132].

The amount of collected SC samples may vary with tape strippings. This depends on the corneocyte size which varies between anatomical sites [113,133], age [134], and seasons [135]. Various studies have shown that the number of corneocytes [135], SC layers [136], SC thickness [133,137], lipid amount and composition [138] may vary depending on anatomical site. Variations in amounts of SC collected by tape stripping may also result from the type of tapes [139], application pressure and duration [130] and application of topical preparations [97]. Tape stripping can be used for *in vivo* [107,113,134], *in vitro* [140] and *ex vivo*[141] investigations. The tapes allow controlled disruption of the SC surface which can be used to observe skin barrier recovery [130] and the measurement of the skin barrier function [111,112].

The body loses water through the epidermis at a constant rate via diffusion or evaporation at any given time. This processes is passive and will occur in undamaged skin as well as at low temperature and humidity. However, atmospheric temperature and humidity may affect the rate due to the change in water vapour pressure gradient [142,143]. Measurements of evaporation allow the determination of SC integrity and efficacy of the skin barrier [24,144]. The movement of water through the skin ensures the hydration of the outermost SC layers and thereby provides flexibility to the barrier. In theory, the skin is considered as a dry surface and water is the only permeating molecule reaching the skin surface [108]. The water content in the uppermost skin layer is a crucial element for the activity of enzymes that facilitate SC maturation and desquamation. Trans epidermal waster loss (TEWL) is the measure of water vapour flux density determined as the amount of water evaporating through one square meter of skin per unit of time. This value is assumed to be the same as the steady-state water vapour density flux that passes passively through the intact SC and can be understood using Fick's first law of diffusion [145]:

$$Water\ Flux\ Density\ (g\ m^{-2}\ h^{-1}) = \frac{Amount\ of\ Water\ Vapour}{Area\ x\ Time} \qquad Equation\ 1.$$

The early TEWL measurement devices were designed as open-chamber systems where the upper end exhausts the water vapour that rises from the skin surface. These devices are susceptible to ambient air movements and tend to fluctuate in measurement values [146].

The closed-chamber device has a condenser that creates a constant temperature and Relative Humidity (RH) inside the diffusion zone. This is created by removing and trapping the water vapour in an ice film (Fig. 2.1). This condenser maintains the humidity gradient within the entire chamber by removing the water vapour continuously thereby allowing successive measurements on subjects [145].
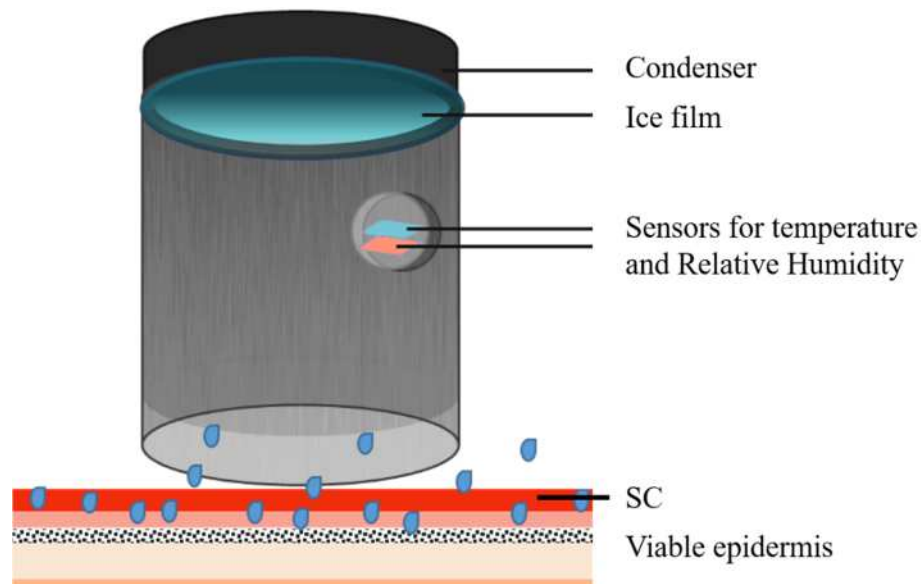
Figure 2.1. TEWL measurement using a closed-chamber device with a condenser to create an ice film from the evaporating water from the SC surface.

The TEWL value depends on anatomical site, age and race. Although gender was considered to have an influence on the skin barrier function this has not been confirmed to date [147,148]. TEWL measurements were also used to demonstrate that compounds such as caffeine can penetrate the forehead to a greater depth than the post auricular site [134]. The forehead, cheek and back of the hand have a higher TEWL than the forearm, elbow, abdomen, buttocks and calf [142]. A higher TEWL was also measured in the cheek compared to the forehead [149]. This was also confirmed in a later study with the mapping of digital images of the face for SC hydration

measurement as well as TEWL [150]. Age is another factor that has an impact on the skin barrier function and it was shown that individuals over 60 tend to have higher TEWL compared to younger participants [151,152]. Race is another aspect that affects the skin barrier function. Interestingly, the baseline TEWL values were shown to be comparable between African and Caucasian subjects. However, the African subjects displayed a higher TEWL following applications of irritants and tape stripping compared to Caucasian subjects [153]. A digital mapping study revealed that black African, Indian and Chinese subjects have a higher TEWL compared to Caucasian subjects upon tape stripping [150]. Variations in the TEWL also indicate differences in SC properties such as number of cell layers [134] and thus SC thickness [154].

The cohesion of the SC is studied to understand the impact of topical application of formulations on desquamation [68] which is a limiting SC thickness [115]. The protein content in the SC accounts for 75 - 80 % of the total SC weight due to the large amount of keratin, corneodesmosomes as well as extracellular and intracellular proteins [155]. The protein content is used to determine the state of the skin health as well as to investigate the effect of topical application of an active compound on the SC [131,156].

There are various approaches to determine the amount of protein on tape strips. The gravimetric method is an established analytical procedure where the tapes are weighed before and after tape stripping. However, the tapes need static discharge before each weighing and topical treatments will also influence the measurements [154]. Alternatives were developed by using the Lowry assay [157] in which sodium hydroxide was used to extract soluble SC protein fractions to determine the protein concentration [158,159]. In principle, the reaction solution containing copper reacts with the nitrogen residues in the amino acids under alkaline conditions that allows the oxidation of the Folin reagent that further reacts with the Ciocalteay reagent. This reaction results in a concentration-dependent colour change of the sample solution which is measured as absorbance via a spectrometer [157]. However, this type of detection is prone to artefacts in measurement depending on the buffers and solvents used for the formulations [97,160].

More recently, the SquameScan 850A® device was introduced which measures the protein amount directly on the D-Square® (Fig. 2.2) tapes via infrared

densitometry [98]. The device has a diode that emits light at a peak wavelength of 850 nm which prevents thermal denaturation of proteins, reduces light scattering of the tapes and diminishes ambient light. In principle, only protein is measured on individual tape strips without detecting any other component of the SC. The SC sample absorbs the light in proportion to its total protein content allowing a reliable and fast approach for measuring the protein concentration indirectly. This method was validated by measuring the protein amount via the SquameScan 850A® and the Micro Bicinchoninic Acid Protein Assay Reagent Kit, a colorimetric approach using a spectrometer. Tape stripping was performed on the ventral forearm of healthy volunteers and a positive correlation was demonstrated between both assays [98]. The infrared densitometry approach has many advantages compared to other techniques and is fast and non-destructive of the sample.

Figure 2.2. The SquameScan 850 measures the absorbance % on D-Square tapes after tape stripping (Modified picture from clinicalandderm.com).

The present study is focused on the impact of sun-exposure on the SC properties of photo exposed (PE) cheek and the photo protected (PP) post auricular sites (Fig. 2.3).
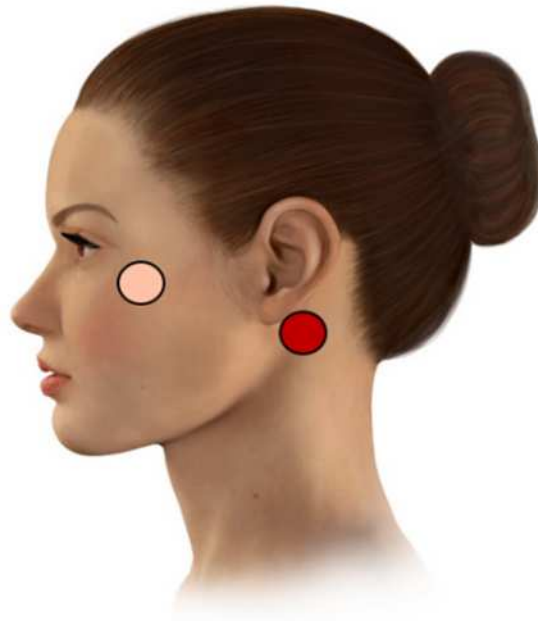
Figure 2.3. The PE cheek and the PP post auricular sites were selected for tape stripping.

UV light is distinguished between type A (320-400 nm) and type B (280-320 nm) radiation. UVB radiation can cause mutations in the DNA of keratinocytes or melanocytes that might trigger cell death or proliferation with the long-term consequence of skin cancer [161]. Direct damage of DNA generates cyclobutane pyrimidine and thymine dimers [162] which may not be repaired because of the corruption in certain genes involved in DNA repair such as p53 [163]. UVA is associated with photo aging which causes visible permanent outcomes such as wrinkles, leathery skin and dark spots [164]. In acute skin damage individuals experience erythema that can lead to delayed tanning [165]. UVA and UVB supress the immune system [166] and cause major skin damage by the generation of reactive oxygen species (ROS) such as hydrogen peroxide which contribute to the long-term effects of sun exposure [167]. Some studies have shown elevated antioxidant levels, as a compensation mechanism for ROS, such as inducible nitric oxide synthase [168,169] and heme oxygenase [170] to UVA, or superoxide dismutase [171] to counteract UVB. These coping mechanisms are overwhelmed or depleted upon repetitive or excessive UV radiation hence various mutations can accumulate and result in tumours or cancer. A recent study demonstrated counteraction to UVB

radiation by introducing superoxide dismutase as a topical application [172]. In fact, sun-damaged skin shares many traits with non-genetic atopic dermatitis (AD) such as decreased degradation of filaggrin to NMF which leads to a decrease in skin hydration [48,92,173]. Furthermore, a decrease in ceramide levels has been demonstrated in sun-damaged skin and AD patients which contributes to the impaired skin barrier function [173,174]. The PE cheek and PP post auricular sites are close in proximity. However, the PP post auricular is a hairless anatomic site that is not being challenged by clothing unlike the buttocks, abdomen, upper thigh or back which are often examined PP anatomical sites [115,137,138]. A previous study showed different protease levels, SC thickness and corneocyte maturity between PE cheek and PP post auricular sites [92]. Furthermore, several variations in proteomics were demonstrated between both anatomical sites such as serine proteases and enzymes involved in CE maturation and lipid procession [118]. The barrier function of cheek and post auricular site most likely do not just differ in enzymology arriving from the epidermis but also from proteases deriving from the skin microbiome amount of sebum and sweat [175–177]. This study will characterise the skin barrier function to assist the understanding of the effects of sun-damage on facial skin barrier function.

2.3 Materials and methods

2.3.1 Materials and equipment

The materials and equipment listed in Table 1.2 were used to determine the SC integrity and CE cohesion of samples collected from participants.

Table 1.2. Materials and equipment used to characterise the SC properties.

Materials	Supplier
Standard D-Squame ® tapes (3.8 cm^2)	CuDerm Corporation, Dallas, Tx, USA
D-Squame tape rack	
D-Squame pressure instrument	
Forceps	VWR international Ltd, Leicestershire, UK
Aquaflux AF103	Biox Systems, London, UK
SquameScan A850 infrared densitometer	Heiland Electronic, Wetzlar, Germany

2.3.2 Methods and study design

2.3.2.1 Participant recruitment

This study was approved by the UCL Research Committee and the NHS London-Bromley Research Committee (Reference: 16/LO/1672) complying with the Declaration of Helsinki. The information participant sheet, questionnaire and written informed consent were adjusted according to the new General Data Protection Regulations of the Data Protection Act 2018. All potential participants were given an information participant sheet and completed a questionnaire to verify if they were suitable candidates. The questionnaire included minimal personal information namely age, gender and ethnicity. Each participant was asked not to use any skincare products for 15 days before the study took place.

Inclusion criteria for potential volunteers:

- must be in good health
- be aged 20-40 years old
- must complete and sign a written informed consent form

Exclusion criteria for potential participants:

- skin variations at the study site such as birthmarks or scars
- current or past history of a skin condition

Suitable participants signed the written informed consent form. There were no drop outs during all conducted samplings.

2.3.2.2 SC sampling via tape stripping

Nine successive tapes were collected from the photo exposed (PE) cheek (3 cm below the eye) and the photoprotected (PP) post auricular (close to the earlobe) sites of healthy participants (Fig. 2.3).

The pressure device provided by CuDerm Cooperation was used to apply 225 g cm^{-2} pressure for 5 s with intervals of 20 ± 5s between each tape stripping [130] while each tape was removed with a single movement. The pressure device allows uniform adherence between the tape strip and the superficial SC layers removed with the removal of the tape [21,178]. The samples were stored at -80 °C until CE isolation. A depth profile of SC properties such as integrity, cohesion and enzyme activities may also be generated from the results [130].

2.3.2.3 SC integrity – Trans epidermal water loss

TEWL was measured prior to every SC sampling to determine the SC integrity. The volunteers were acclimatised for about 20 mins to the temperature and RH of the study area in order to avoid sweat gland activation which would influence the measurements. TEWL was calibrated as recommended by Biox Systems prior to every first measurement of the day. This ensured that the water flux was not influenced by the ambient humidity. Closed-chamber probe devices do not require a "down-time" for TEWL measurements between consecutive tape strippings. The software provided by Biox Systems interpolates the average water flux of 20 measurements once a

constant rate of flux is reached [145]. The TEWL was measured at baseline and after the third, sixth and ninth tape strippings. The baseline measurement is an indicator of the SC integrity while the measurements post-tape stripping provide information about the SC thickness when combined with the measured protein amounts [108].

2.3.2.4 SC cohesion and thickness – Protein amounts

The original protocol to determine the protein content on tape strips was the gravimetric approach which is time consuming, inaccurate, and requires additional discharge of static electricity of the tapes prior to weighing the tape strips [154]. Nevertheless, Mohammed *et al.*, showed that the gravimetric approach can be replaced by infrared densitometry in which the total protein content relates directly to the mass of removed SC [98,109]. Thus, the theoretical amount of removed SC in this present study was determined by plotting the inverse TEWL versus the cumulative protein content. The SC cohesion was determined by measuring the protein content on the individual tape strips using infrared densitometry. Voegeli and colleagues validated a linear relationship between the absorbance (measured in %) and protein content on the tape strip. This resulted in a calibration curve [98] that allows the determination of protein content per tape strip area as shown in Equation 2:

$$\textit{Protein Amount } (\mu g \ cm^{-2}) \ = \textit{1.366 x Absorbance (\%) - 1.557} \qquad \textit{Equation 2.}$$

The resulting protein amount gives information about the SC cohesion while providing a value to normalise protein-based experiments. Tape stripping causes a gradual decrease in the SC thickness leading to an increase in TEWL. This was determined with a modified equation of Fick's First Law of Diffusion (Eq. 1) that considers the SC thickness and the water flux measurement. In the modified equation, the reciprocal value of the water flux diffusing through the remaining SC thickness and the thickness have a linear relationship [108]. The amount of cumulative protein on tape strips reflects the amount of collected SC. The linear graph is extrapolated to the x-axis which gives the estimated total SC protein amount. This value can be used to estimate the SC thickness considering that 100 μg cm^{-2} of protein content on tape strips equals 1.9 μm of SC thickness [109,154].

2.3.2.5 Statistics

The TEWL measurements, CE cohesion and thickness were previously described for the PE cheek and PP post auricular site and thus these values were used to calculate the power and samples size [106,118,150]. The power was analysed to detect the true measurement taking random errors into account. This is ensured by an adequate sample size that is large enough to distinguish the true effect from random variations. The power analysis is the probability of rejecting false Null Hypothesis and thus the probability of a true association. A widely used probability of 80% is used as a desirable power with 95% confidence level from which the sufficient sample size can be calculated. In Equation. 3, the sample size calculation is demonstrated for the standard deviation obtained from TEWL in PE cheek in Caucasian females [112]:

$$Sample\ size = \frac{zsore^2 \times population\ standard\ deviation^2}{margin\ of\ error^2} = \frac{1.96^2 \times 5^2}{5^2}$$
$$= 4 \qquad\qquad\qquad Equation\ 3.$$

Further sample size calculations were computed for both anatomical sites and tested SC parameters which ranged between sample sizes of 3-6. However, sample size of 14 was chosen to increase the statistical power over the obtained results. Microsoft Excel® (Version 2013) was used for data collection. The mean ± standard deviation (SD) and statistical analysis were determined via GraphPad Prism (Version 7). The D'Agostino & Pearson normality test was chosen as the normality test. The data that met the normality test were further analysed for the statistical differences between study groups, site and SC depth. Study site and depths were analysed via the one-way ANOVA multiple comparison test while the two study groups were compared via two-way ANOVA. The Sidak-Holm post-hoc test was applied to assess the variations among and between these groups. The data are shown as mean ± SD (n=14) and statistical significance is represented as followed * $p \leq 0.05$, ** $p \leq 0.001$, *** $p \leq 0.0002$ and **** $p \leq 0.0001$, in addition coefficient of variation (CV %) was determined.

2.4 Results

The first group included 14 Caucasians, seven females (age 28 ± 3) and seven males (age 30 ± 5) participated in the study. The second group consisted of 14 Chinese participants, seven females (age 25 ± 3) and seven males (age 26 ± 1). The samples were collected at a room temperature of 19 ± 2 °C and a Relative Humidity of 44 ± 7% RH. The SC integrity, cohesion and thickness were measured for each participant which allowed comparisons between gender, anatomical site, SC depth and ethnic background.

2.4.1 Stratum corneum integrity

The TEWL was measured to determine the SC integrity at baseline before tape stripping and after the third, sixth and ninth tape stripping.

2.4.1.1 TEWL measurements of PE cheek and PP post auricular sites in Caucasian and Chinese subjects

Caucasians and Chinese subjects displayed the same trend in TEWL for both anatomical sites. The TEWL values increased significantly with tape stripping in the PE cheek site while the TEWL measurements showed no differences in the PP post auricular sites in Caucasian and Chinese (Fig. 2.4) Volunteers. The baseline TEWL of 24.6 ± 7.3 g m^{-2} h^{-1} was measured in the PE cheek in Caucasian subjects which increased to 76.5 ± 23.8 g m^{-2} h^{-1} after nine tape strips ($p \leq 0.0001$). TEWL values were similar with 22.4 ± 2.5 g m^{-2} h^{-1} that increased to 75.7 ± 20.9 g m^{-2} h^{-1} in the PE cheek site of Chinese participants ($p \leq 0.0001$). TEWL measurements in PP post auricular sites in Caucasians were determined as 17.4 ± 2.9 g m^{-2} h^{-1} and increased to 26.1 ± 4.7 g m^{-2} h^{-1} ($p \leq 0.5$). The baseline TEWL in the PP post auricular site of Chinese participants increased from 16.8 ± 2.5 g m^{-2} h^{-1} to 27.3 ± 3.6 g m^{-2} h^{-1} ($p \leq 0.05$) after nine consecutive tape strippings. A significant difference in TEWL measurements was obtained after three tape strippings between the PE cheek and the PP post auricular sites ($p \leq 0.05$). The discrepancy between the two anatomical sites increased with tape stripping ($p \leq 0.0001$). The same differences between anatomical sites were observed in Chinese participants. Baseline TEWL was comparable between PP post auricular and PE cheek sites which increased significantly after the third tape

stripping ($p \leq 0.05$). The difference in TEWL values increased further with the sixth tape stripping ($p \leq 0.0001$) and increased further with the ninth tape stripping ($p \leq 0.0001$).

Furthermore, larger variations in TEWL measurements were observed in the Caucasian PE cheek baseline value (24.6 ± 7.3 g m^{-2} h^{-1}, 29.5% CV), after the third (35.5 ± 13.6 g m^{-2} h^{-1}, 38.4% CV), the sixth (57.3 ± 20.3 g m^{-2} h^{-1}, 35.5% CV) and the ninth tape stripping (76.2 ± 23.8 g m^{-2} h^{-1}, 31.2% CV). The variations in the TEWL values measured in PP post auricular sites are less variable than in the PE cheek site. The TEWL measurements of the PP post auricular site have a variation between 12.5% CV - 17.2% CV. The coefficient of variation was lower for the TEWL values in Chinese participants compared to Caucasian participants.
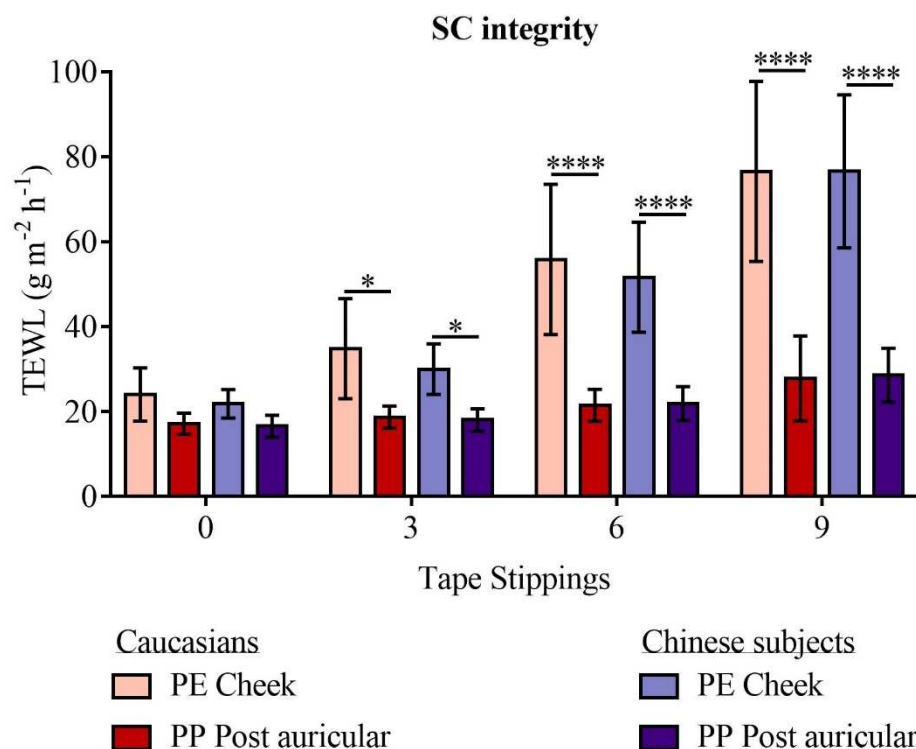
Figure 2.4. TEWL in PE cheek and PP post auricular sites in Caucasians and Chinese subjects. The data are represented as mean $\pm$ SD (n=14).

However, TEWL values in PE cheek sites showed a larger variation compared to PP post auricular sites. The baseline TEWL measurements showed no significant differences between both anatomical sides for Caucasians and Chinese volunteers.

2.4.1.2 The difference of SC integrity between genders

The SC integrity is reflected with the TEWL measurements in the PE cheek and PP post auricular sites of male and female participants of Caucasian and Chinese (Fig. 2.5) ethnic groups. The TEWL indicated no difference in the SC integrity of PE cheek in Caucasian males and females. The increase in TEWL with tape stripping showed the same tendency in both genders and ethnic groups. TEWL values remained constant in the PP post auricular site in Caucasian male and female subjects with tape stripping. The TEWL measurements in Chinese participants showed the same trend in PE cheek and PP post auricular sites in male and female subjects. The data indicates that there are no differences in the SC integrity between genders in Caucasian and Chinese subjects.
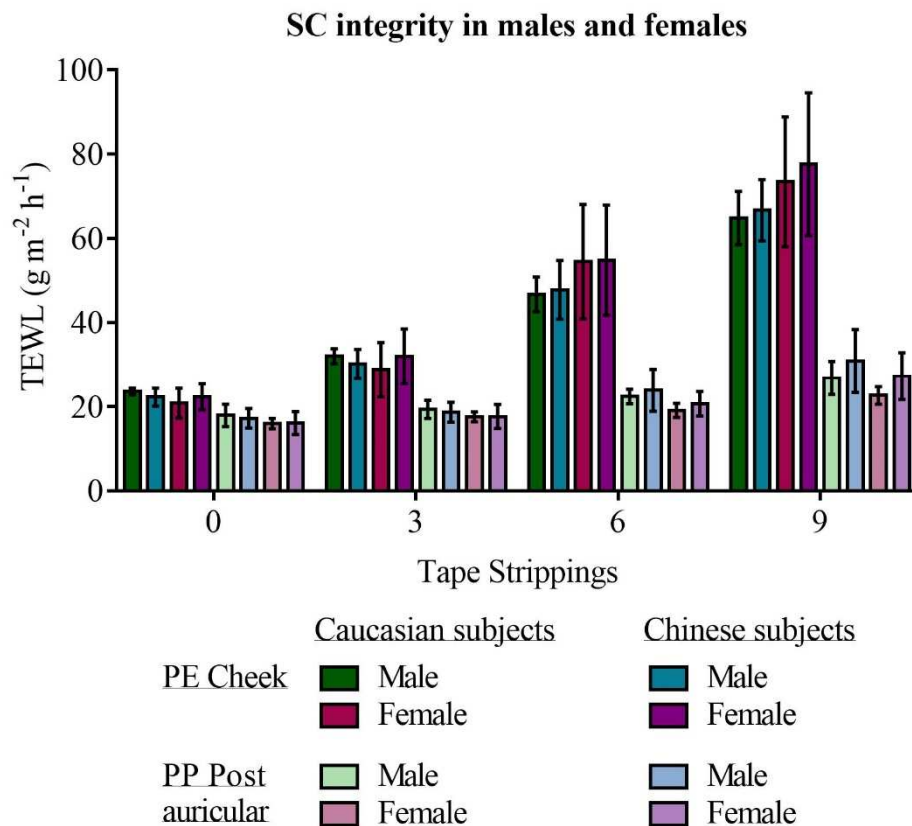
Figure 2.5. SC integrity of PE cheek and PP post auricular sites determined via TEWL measurements in Caucasian and Chinese males and females. The data are represented as mean ± SD (n=7).

2.4.2 SC cohesion

The protein content on the tape strips reflects the cohesion between corneocytes and lamellar layers.

2.4.2.1 Differences in SC cohesion and gender

The protein amount on the tapes was measured via infrared densitometry after tape stripping. The protein content on the tape strips obtained from the PE cheek and PP post auricular sites (Fig. 2.6) showed no difference in male and female Caucasians. Likewise, the protein content on tape strips obtained from Chinese subjects showed no difference in PE cheek and PP post auricular sites between males and females.

The SC cohesion showed no significant difference between genders in Caucasians ($p \leq 0.9$) and Chinese ($p \leq 0.8$) subjects. The following results do not considering the gender but the respective ethnic groups are pooled together to assess differences between ethnicity, SC depth and anatomical sites.
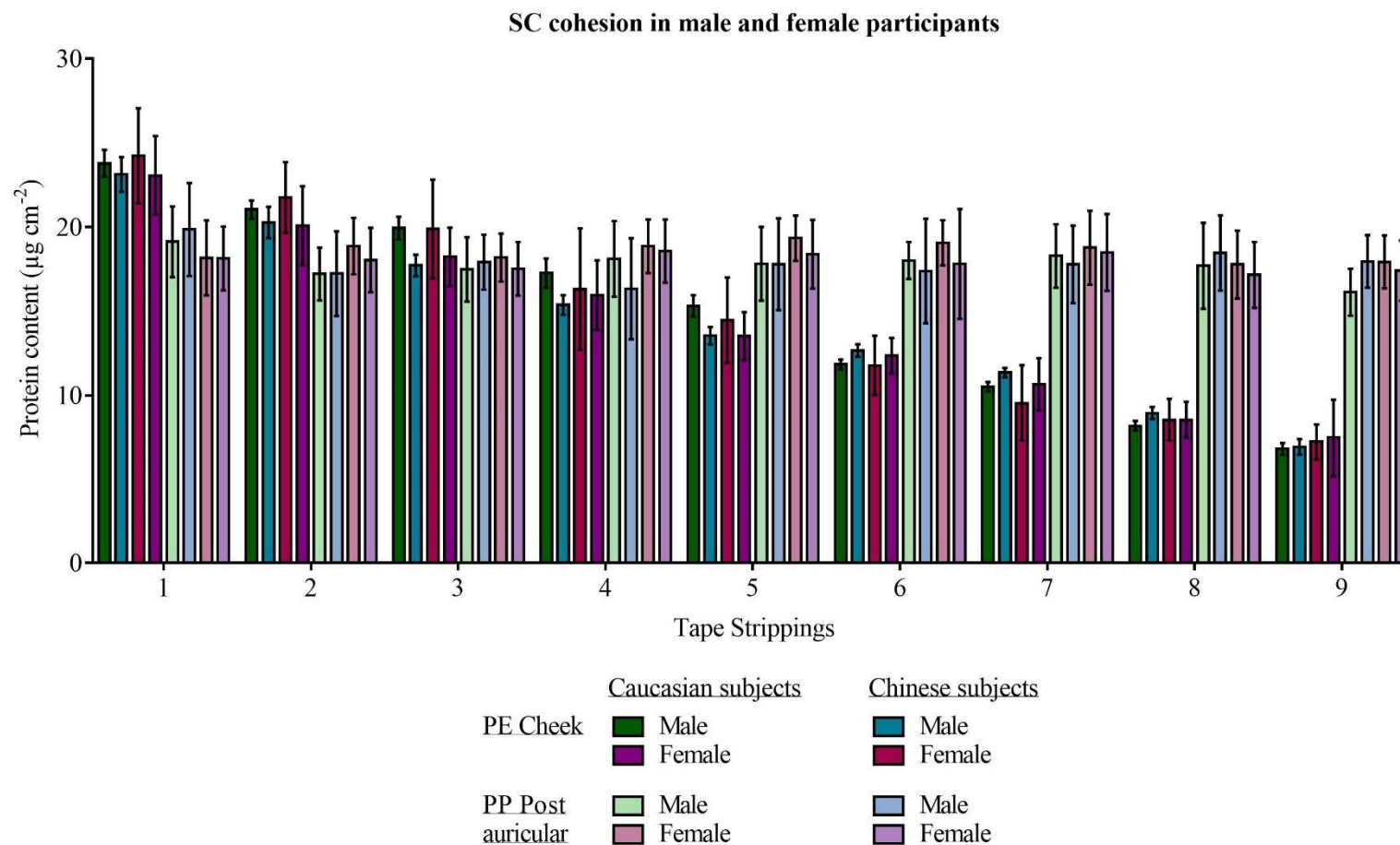
Figure 2.6. SC cohesion represented by collected protein amounts of PE cheek and PP post auricular sites of male and female Caucasian and Chinese subjects. The data are represented as mean ± SD with (n=7).

2.4.2.2 SC cohesion in PE cheek and PP post auricular samples of Chinese and Caucasian subjects

The protein content on the tape strips collected from the PE cheek of Caucasian participants showed no significant difference in protein amounts between the second ($p \leq 0.9$) and the third tape strip ($p \leq 0.2$). The tape strips collected from the PE cheek decrease gradually in the protein content from the fifth tape strip ($14.3 \pm 2.3\ \mu g\ cm^{-2}$) to a protein content of $6.9 \pm 1.1\ \mu g\ cm^{-2}$ on the ninth tape strip ($p \leq 0.0001$). The protein content remained constant on tape strips collected from the PP post auricular site ($p \leq 0.9$). The SC samples collected from the PE cheek ($21.8 \pm 1.4\ \mu g\ cm^{-2}$) and PP post auricular site ($20.5 \pm 1.8\ \mu g\ cm^{-2}$) in the Caucasian subjects showed no difference in the first four tape strips ($p \leq 0.5$). However, the protein content on tape strips collected from the PP post auricular site was significantly higher from the fifth tape strip compared to the protein amounts collected from the PE cheek for Caucasian subjects ($p \leq 0.0002$) (Fig. 2.7).

The SC samples collected from the PE cheek site of Chinese participants showed a gradual decrease in protein content after the second tape strip ($p \leq 0.01$). The protein content decreases steeply between the first ($21.8 \pm 3.0\ \mu g\ cm^{-2}$) and the fifth tape strip ($11.5 \pm 2.0\ \mu g\ cm^{-2}$) from the PE cheek of Chinese subjects ($p \leq 0.0001$). However, the decrease in protein content on the tape strips from the PE cheek site of Chinese participants decrease less markedly from the sixth ($9.5 \pm 1.7\ \mu g\ cm^{-2}$) to the ninth ($6.6 \pm 1.5\ \mu g\ cm^{-2}$) tape strip ($p \leq 0.0002$). Interestingly, the protein content on tape strips from the PP post auricular site of Chinese participants showed no significant difference between tape strippings ($p \leq 0.8$). The protein amount on the first tapes collected from the PE cheek ($21.8 \pm 3.0\ \mu g\ cm^{-2}$) and the PP post auricular sites ($22.5 \pm 1.6\ \mu g\ cm^{-2}$) showed no difference in Chinese participants ($p \leq 0.9$). However, the third tape strip collected more protein from the PP post auricular site than from the PE cheek site ($p \leq 0.05$). The following tape strippings collected more protein ($p \leq 0.0001$) from the SC of the PP post auricular site than the PE cheek site (Fig. 2.7).
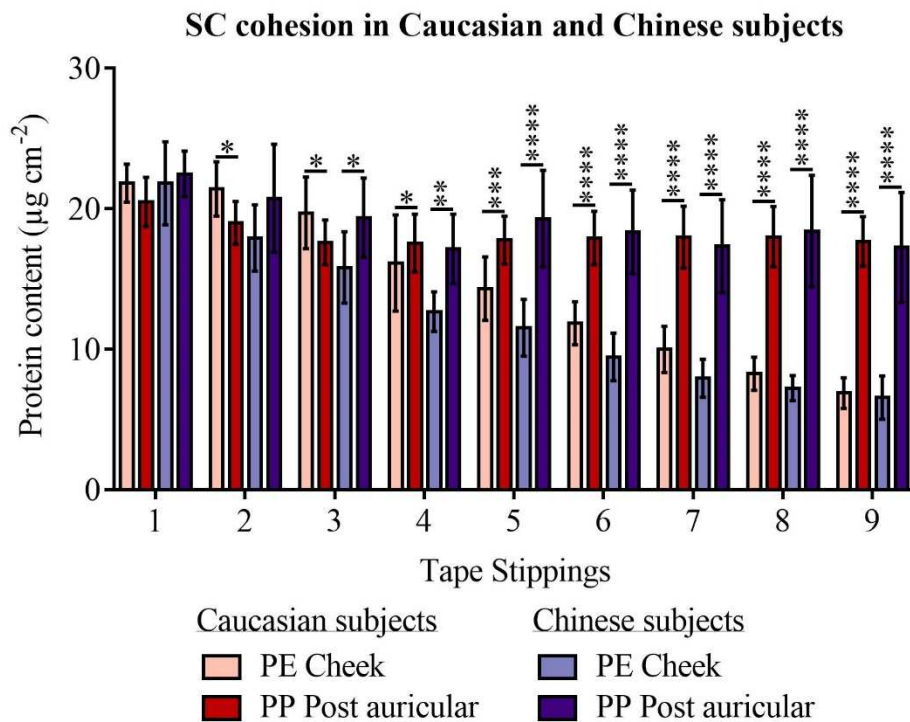
Figure 2.7. Protein content on individual tape strips of PE cheek and PP post auricular sites in Caucasians and Chinese participants. Mean ± SD (n=14).

The protein content on the tape strips collected from the PE cheek and the PP post auricular sites show clear differences in SC cohesion between both anatomical sites in the Caucasian and Chinese subjects. Interestingly, the SC cohesion in the PE cheek of Caucasian and Chinese volunteers show significant differences ($p \leq 0.0001$) from the sixth tape strip on. PE cheek SC samples (6.3-21.2% CV; Median 14.4% CV) showed higher variation in the collected protein amounts in Caucasians than for PP post auricular SC samples (8.0-12.4% CV; Median 9.9% CV). The variation in Caucasian samples was lower compared to Chinese PE cheek samples (11.1-23.4% CV; Median 16.0% CV) and PP post auricular site (7.2-22.6% CV; Median 17.9% CV).

2.4.3 SC thickness

Cumulative values of the collected protein led to the determination of total protein collected from nine tape strippings of both anatomical sites of Caucasian and Chinese subjects (Fig. 2.8). The cumulative protein amount collected from the PE cheek of Caucasian participants increases steeply until the sixth tape strip (slope=16.4 ± 0.8 µg cm^{-2} per tape strip, R^2=0.98, p ≤ 0.0001). The protein content comes to a total amount of 131.8 ± 11.6 µg cm^{-2} from the PE cheek site in Caucasians with a smaller slope from the sixth tape strip (slope=8.6 ± 0.4 µg cm^{-2} per tape strip, R^2=0.99, p ≤ 0.0002). In the PE cheek site of Chinese participants, the cumulative protein amount increases steeply between the first and fourth tape strips (slope=15.9 ± 1.9 µg cm^{-2} per tape strip, R^2=0.97, p ≤ 0.01). The slope between the fourth and ninth tape strip is lower with a slope of 7.3 ± 0.4 µg cm^{-2} per tape strip (R^2=0.99, p ≤ 0.0002). A linear trend was observed between cumulative protein amount and tape stripping in the PP post auricular site in Caucasian (slope=17.8 ± 0.6 µg cm^{-2} per tape strip, R^2=1, p ≤ 0.0001) and Chinese (slope=18.4 ± 0.3 µg cm^{-2} per tape strip, R^2=0.99, p ≤ 0.0001) participants. Cumulative protein amounts on tape strips from the PP post auricular site of Caucasians is 23.0 ± 2.6 µg cm^{-2} on the first tape and cumulates to 160.9 ± 10.4 µg cm^{-2} with nine tape strippings (p ≤ 0.0001). The first tape strip collected 24.4 ± 4.7 µg cm^{-2} for the PP post auricular site of Chinese participants which comes to a total protein content of 172.2 ± 17.7 µg cm^{-2} after nine tape strips (p ≤ 0.0001). A comparison of both anatomical sites shows a significantly higher cumulative protein amount in the PP post auricular site from the seventh tape strip collected from Caucasian subjects (p ≤ 0.01). The cumulative protein amount on tape strips obtained from Chinese participants showed a significantly higher protein amount from the fourth tape strip (p ≤ 0.01). A comparison between both ethnic groups shows that the SC cohesion in Chinese participants is stronger than for the Caucasian subjects (p ≤ 0.0001).
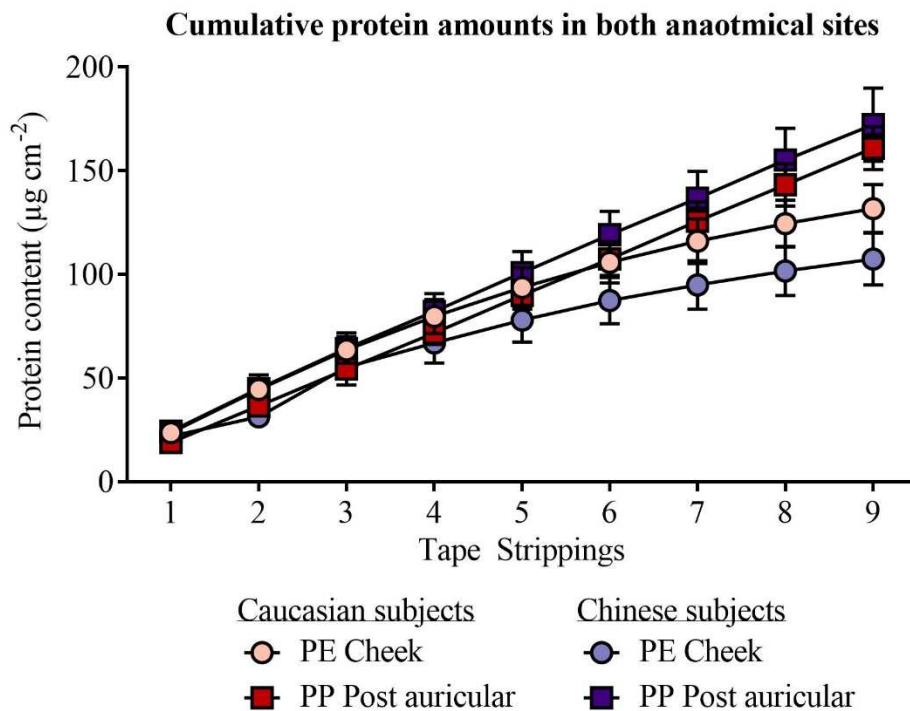
Figure 2.8. Cumulative protein amount of PE cheek and PP post auricular sites in Caucasians (A) and Chinese (B) participants. The data are represented as mean ± SD (n=14).

The total SC protein amount was determined by plotting the reverse TEWL values and the corresponding cumulative protein content. The reverse TEWL and the corresponding cumulative protein amount allow the estimation of the potential total protein amount that may be removed from the SC of Caucasians and Chinese (Fig. 2.9) participants. The dotted line represents the extrapolation to the x-axis and therefore to the total SC protein that could have been collected. This indicated that 193.9 µg cm^{-2} could have been collected from the Caucasian PE cheek and 469 µg cm^{-2} (p ≤ 0.0001) from the PP post auricular site. The total protein amount that could be collected from the Chinse subject was estimated to be 155.4 µg cm^{-2} for the PE cheek and 430.9 µg cm^{-2} (p ≤ 0.0001) for the PP post auricular sites.

Estimation of total protein removal of SC
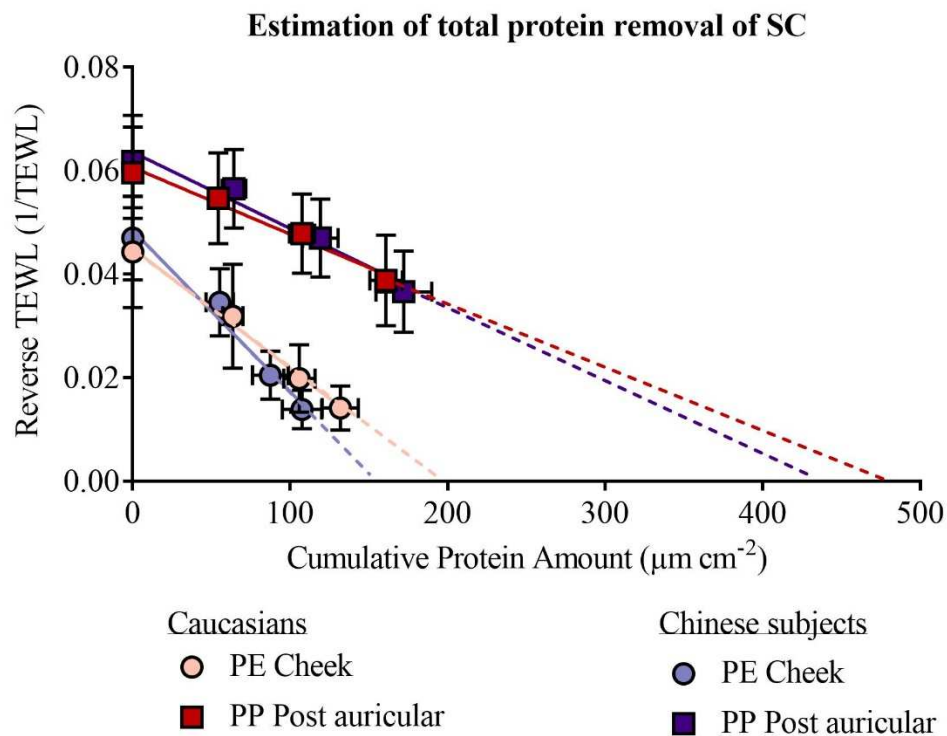
Figure 2.9. Linear plot of cumulative protein amount and reverse TEWL of PE cheek and PP post auricular SC of Caucasian and Chinese participants. The data are represented as mean ± SD (n=14).

The SC thickness was subsequently calculated from the estimated total SC protein and the assumption that 100 µg cm^{-2} of protein on tape strips equals to 1.9 µm of SC thickness (Fig. 2.10). Caucasian participants had a thicker PP post auricular SC (8.9 ± 1.7 µm) than the PE cheek site with 4.7 ± 0.7 µm (p ≤ 0.0001). Chinese volunteers showed a similar trend with a value of PP post auricular SC, of 7.9 ± 1.4 µm and a thinner PE cheek site of 2.9 ± 0.5 µm (p ≤ 0.0001). This demonstrates a clear difference between anatomical sites in both ethnic groups. Caucasians had thicker SC in the PE cheek site (p ≤ 0.0001) than Chinese participants, as well as in the PP post auricular SC sites (p ≤ 0.05). The estimated total protein amount was compared with the actual amount of protein removed which demonstrated that nine tapes removed 67.5 ± 5.9 % of PE cheek SC and 29.0 ± 1.9 % of PP post auricular SC of Caucasians (p ≤ 0.0001). Nine tape strippings removed 71.4 ± 8.3% of PE cheek SC and 39.9 ± 4.1 % of PP post auricular SC in Chinese participants (p ≤ 0.0001).
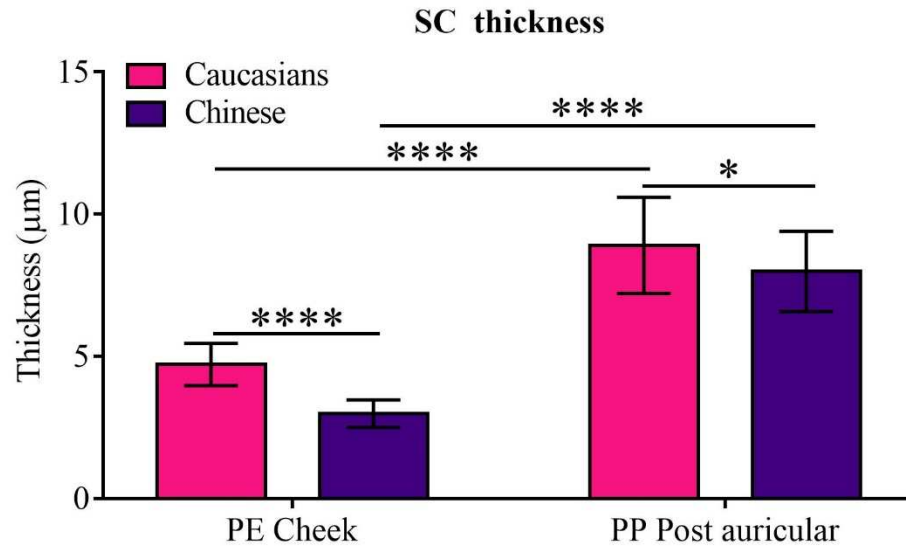
Figure 2.10. Estimated SC thickness of PE Cheek and PP post auricular sites of Caucasian and Chinese participants. The data are represented as mean ± SD (n=14).

2.5 Discussion

One of the most influential features of the environment is the sun which induces photo damage by UV radiation accompanied with heat damage [161]. For a long time, melanin was known as the only defence mechanism against sun light [179]. A recent study links skin pigmentation and photo damage in the face using baseline TEWL as a measurement of skin integrity and recovery. In that study, fair-pigmented individuals had a thicker SC with a lower baseline TEWL and skin hydration [112]. The thicker SC might compensate for the lower melanin levels to protect the deeper layers of the skin from photo damage by absorbing the harming light [35]. In a previous study, four ethnic groups were recruited to map the skin hydration and baseline TEWL in the face [150]. The facial studies revealed a major difference in certain areas independent of ethnicity. The TEWL was found to be highest in the cheek followed by the chin, the forehead and the post auricular site [134]. Another study was conducted on the cheek and post auricular areas of Caucasians, Black Africans and Albino Africans. Interestingly, the melanin-free cheek skin in Albino Africans showed a lower TEWL after tape stripping while Caucasian and Black African skin showed the expected increase in TEWL. Furthermore, the TEWL in the post auricular site was lower compared to the cheek in all three ethnic groups [150]. This is in line with the findings in the present study. The TEWL showed no significant differences in the baseline measurements between PE cheek and PP post auricular sites. Tape stripping induces an artificial thinning of the SC which leads to the increase in TEWL. However, no differences were identified between male and females which is in line with previously reported studies [142,148].

A linear increase in TEWL with SC removal was seen in the PE cheek; interestingly, this trend is missing in the PP post auricular site. The TEWL in both anatomical sites showed no significant differences between Caucasians and Chinese which was conducted in London, United Kingdom. A study in Pretoria, South Africa, compared the TEWL and hydration in Chinese, Caucasian, Indians and Black Africans. These authors reported a significantly higher TEWL in Chinese subjects compared to Caucasians [150]. The contrasting findings between the present study and the reported study [150] may originate from the two major differences, namely the location and the environmental conditions. The earlier study was performed between May and June with an average outdoor temperature of 11 °C and 50-65% RH [150].

The present study was performed between October and December with an average outdoor temperature of about 5-12 °C and 35-40% RH. Although the ambient temperature are comparable, the Relative humidity and the intensity of solar radiation in Pretoria/South Africa is stronger than in Western Europe [180]. Thus it can be assumed that individuals in South Africa are more exposed to the sun in spring than individuals in the UK during autumn and winter [181]. This was supported by another study that measured TEWL at baseline and after challenging the skin barrier function with sorbitol in the summer and the winter season in the same individual. This osmotic stress indicated a stronger skin barrier function during the summer compared to the winter [182]. A comparative study in the leg SC of Caucasian females demonstrated lower ceramide and cholesterol levels in winter compared to summer [77].

Infrared spectrometry has been shown to be an efficient method to quantify the protein content on tape strips [98]. The cumulative protein content indicated that nine tape strips removed different amounts from the SC of both anatomical sites in Caucasian and Chinese participants. However, nine tape strips collected from the PE cheek of Chinese participants obtained less SC than of Caucasians suggesting a stronger SC cohesion in the SC of Chinese subjects. The PE cheek site shows the expected observation with decreasing protein content and increasing SC cohesion in the deeper SC layers [159]. This might be linked to the strength of the corneodesmosomes that are weakened at the surface by enzymes to initiate desquamation. In the deeper SC layers those proteases are less active but also richer in hydration, contributing to strengthening of the CEs and their matrix but decreasing their adhesiveness to the tape strip. Interestingly, the PP post auricular samples remained constant in protein content throughout tape stripping. However, the difference in CE cohesion between PE cheek and PP post auricular sites in this present study is matching previously reported findings [98,109]. The cumulative protein amount shows a linear trend up to the sixth tape strip collected from the PE cheek sites. The protein content on nine consecutive tapes shows an interesting relationship between anatomical sites, removed SC protein, and TEWL measurements. This might be the tipping-point where the desquamation process is reduced. Strong cohesiveness between corneocytes and extracellular matrix results less collectable sample via tape stripping. For the PP post auricular site the TEWL measurement and the protein content on the tape strips remained constant after nine tape strippings. This outcome

strongly suggests that the SC integrity in the PP post auricular skin is stronger than in the PE cheek which continues to match the findings of Voegeli *et al.* in the upper layers of the cheek and post auricular SC [112]. Moreover, the TEWL and protein content results indicate that the SC thickness varies between Chinese and Caucasian subjects in both anatomical sites.

The SC is described as a heterogeneous structure providing a homogeneous barrier to water while the rate of TEWL is determined by the thickness of the SC layers matrix [56]. Fick's Law of Diffusion is used to determine the TEWL as a linear function, however, this is a simplified model [24,108]. In reality, the SC cohesion between the SC layers is irregular thus tape stripping collects irregular amounts of SC leading to a non-linear disruption of the skin barrier by tape stripping [98,159]. A mathematical approach is suggested to provide an estimation for the TEWL rather than absolute numbers [24,108]. The plotting of the reverse values of TEWL and the cumulative amount of SC gives a linear regression line [137]. The extrapolation of this line shows the theoretical total protein mass that could have been sampled from the SC if the tape stripping would have been continued until reaching the stratum granulosum [154].

This study showed no differences in the SC integrity, cohesion and thickness between males and females while the ethnicity and the anatomical site and depth showed significant differences. Chinese subjects have a thinner SC in both anatomical sites compared to Caucasians. Conclusively, the PE cheek sites have a lower SC integrity and increased SC cohesiveness with tape stripping revealing a thinner SC in the PE cheek site than the PP post auricular sites in both ethnic groups. The characterisation of the SC provides a reference point that allows comparison between SC integrity, cohesion and thickness at baseline and after a treatment such as a skin care product [107]. For example, a thicker SC after a treatment indicates an impact on the proliferation of stem cells in the stratum basale or inhibiting effects on the proteases in the stratum corneum. Thus, changes in any of the SC properties can be used to understand events at the molecular level in the epidermis.

CHAPTER 3

Expression profile of corneocyte maturation

3. Expression profile of corneocyte maturation

3.1 Abstract

Background: The "brick" compartment of the skin barrier is comprised of corneocyte envelopes (CE) that are made up of an insoluble protein envelope surrounded by a lipid envelope. These features undergo maturation which supports the skin barrier function by providing mechanical stability and hydrophobic coating.

Objectives: The aim of this chapter is to determine the expression pattern of structural proteins, proteases and lipid processing enzymes.

Methods: Immunostaining was utilised to visualise the expression of ceramide processing enzymes (12R-lipoxygenase and epidermal lipoxygenase 3), proteases (cathepsin D and cathepsin V), structural proteins (involucrin and skin-specific protein 32) and transglutaminase which catalyse CE maturation. The study was conducted on samples collected with the first and ninth tape strips taken from the photo exposed (PE) cheek and photoprotected (PP) post auricular sites of 14 healthy Chinese participants.

Results: The expression of the ceramide processing 12R-lipoxygenase is reduced in PE cheek compared to the PP post auricular site but epidermal lipooxygenase 3 expression is unchanged. Cathepsin D and V are upregulated in PE cheek which indicates photo damage and enhanced desquamation. The expression of the structural proteins was higher in the PE cheek samples compared to PP post auricular samples. The PP post auricular site has a higher transglutaminase expression compared to PE cheek samples.

Conclusions: These biomarkers can indicate the potential for CE maturation and desquamation and may provide evidence for photo damage. The cheek shows signs of photo damage and suboptimal potential for CE maturation due to reduced 12R-lipoxygenase and transglutaminase expression.

Key Words: Protein, Expression, Biomarker, Immunostaining, Sun exposure.

3.2. Introduction

Under the central dogma of molecular biology, the genetic information in DNA is transcribed to mRNA which then is translated into a protein. Some proteins are only expressed at a certain developmental stage or as a response to a trigger which can be used to characterise the cell or an event as well as underlying mechanisms. The gene expression would be determined for the protein of interest which is then compared to the presence of that particular protein. This comparison would either match or reveal a post-transcriptional regulation that could be a target to follow up. The presence of the protein of interest is usually demonstrated via antibody (AB)-based approaches. Immunoglobulins, also known as ABs, are glycoproteins that are naturally produced by plasma cells of the immune system. These structures detect foreign particles with a unique structure. These antigens could be viral or bacterial proteins, sugars or nucleic acids, mammalian hormones or receptors on cells as well as chemical compounds.

ABs can be produced by injecting the antigen, usually into an animal such as a goat, rabbit or cow from which the spleen is isolated containing the B cells [14]. These plasma cell precursors are fused with myeloma tumour cell lines which generate a new cell type, known as a hybridoma. These cells proliferate indefinitely and produce the AB of interest [183]. There are two types of AB commercially available (i) hybridoma-derived monoclonal ABs that detect only one specific epitope and (ii) polyclonal ABs that are obtained from different types of B cells that can collectively recognise different epitopes on the same antigen [14,183]. The antigen-AB binding is usually detected via fluorescence or chemiluminescence either directly or indirectly. However, a secondary AB is usually coupled to a fluorochrom such as fluorescein isothiocyanate (FITC) or an enzyme that cleaves a substrate that results in a luminescence signal. Chemiluminescence is usually used in Western blotting where a protein extract is separated on a sodium dodecyl sulfate gel according to protein sizes. This protein separation is transferred to a membrane and incubation with ABs that detect the particular protein of interest. Sodium dodecyl sulfate gel electrophoresis is a less suitable approach for profiling in this project due to the small amount of samples collected on tape strips and the insolubility of CPEs [42,114]. Nevertheless, ABs can be utilised in immunostaining to visualise the protein of interest.

There is a variety of protocols depending on the specimen and specificity of ABs, however, some steps may vary in incubation time or AB concentration. Immunohistochemistry is the staining procedure in which thin slices of tissue are analysed for morphology and presence of specific proteins. This can be useful to understand the distribution and location of a protein or cell within the whole tissue. Immunostaining has sequential steps that ensure the detection of the protein of interest due to antigen-AB binding. The cells are usually fixed with formaldehyde or methanol which dehydrates and crosslinks the proteins thereby allowing examination of the protein architecture [184]. A buffer solution is used to restore hydration of cells and washout of excessive antibodies. The primary antibody is applied in a blocking solution to challenge the antigen recognition on the cell. The blocking solution provides a more specific antibody-antigen binding, however, a study has shown that some antibodies do not cause unspecific immunostaining [185]. The secondary antibody binds to the constant region of the antibody. The variable region of the antibody is pre-defined by the hybridoma cell while the constant region is determined according to the species of the host where the antibody was generated [183]. Fluorescence microscopy is a popular imaging approach allowing visual evaluation of the resulting AB-antigen binding [186]. Fluorescence is the result of a three-stage process. The fluorescent compound, the fluorochrom, has polyaromatic hydrocarbons or heterocycles that absorb the photon energy from the wavelength of a light source. A specific amount of energy is needed to excite the electrons within the double bonds of the fluorochrom. Once the excited electrons relax to the ground state, the photon energy is emitted at a different wavelength. The emission wavelength has less photon energy and thus a longer wavelength than the excitation wavelength. There are mirrors and filters in fluorescence microscopes to exclude the detection of the excitation wavelength and thereby minimise background fluorescence and increase the resolution of the resulting image [187].

There are various microscopes that have been developed with different capacities, resolutions and contrast to visualise specimens. The most commonly used microscopes are confocal microscopes and optical microscopes that are equipped with fluorescence detectors. The confocal microscope is able to scan the specimen through layers and create a high resolution image; other confocal microscopes are able to generate 3D images. The "simple" fluorescence microscope is the most common imaging technique but has limitations in resolution [187]. Imaging software allows a

digital image to be generated that can be enhanced in terms of contrast and fluorescence intensity. Digital images can be analysed via image processing or analysing software.

Researchers have been using microscopy to analyse the morphology of the skin layers and the expression of certain proteins in the different layers of the skin. Immunohistochemistry in dermatological studies is usually applied to study skin morphology or for diagnostics as reviewed elsewhere [188]. However, this involves rather invasive sample collection via punch biopsy leaving an open wound susceptible to infections [189]. In experimental dermatology, invasive techniques are performed on animal models such as mice but these have limitations as the SC properties and morphology of mice are different from human skin [90,105,190]. New approaches have been developed using skin equivalents to study wound healing, skin barrier function and repair [30] or the effect of topical formulations [191,192]. Immunocytochemistry has been used to analyse protein expression in cell culture lines to localise the protein of interest within the cell [81,193,194]. An early study used immunocytochemistry staining to visualise the structural protein involucrin (INV) in order to determine corneocyte envelope (CE) maturity [114].

The aim of this project is to investigate the expression pattern of some structural proteins and membrane-bound enzymes in CEs of sun-exposed and sun-protected skin (Fig. 1.6). The structural proteins INV and skin-specific protein 32 (XP32) of the corneocyte protein envelope (CPE) should be expressed to a high extent in immature CEs. A number of enzymes will be assessed that are involved in CE maturation and desquamation. Cathepsin D (CathD) is a protease that is responsible for desquamation and the activation of transglutaminases (TG) [125] that are responsible for the CE maturation [84,95]; 12R-lipooxygenase (12R-LOX) and epidermal lipooxygenase 3 (eLOX3) process the precursor ceramide 1 [86,91] which is the main ceramide bound to the corneocyte lipid envelope (CLE). Cathepsin V (CathV) expression will be assessed to determine photo damage [119,123]. The protein expression will be determined in the photo-exposed (PE) cheek and photo protected (PP) post auricular sites of Chinese participants following the tape strippings described in Chapter 2. This expression profile will visualise the differences between both anatomical sites. Furthermore, the effects of sun exposure on CE structural proteins and enzymes will be examined.

3.3 Materials and methods

3.3.1 Materials and equipment

The materials and equipment listed were used for CE extraction, immunostaining and microscopy. The CEs were extracted from the first and ninth tape strip.

Table 3.1. Materials and equipment used to generate expression profiles for CE structural proteins and enzymes by immunostaining.

Materials/Equipment	Supplier
Sodium dodecyl sulfate (SDS)	Sigma Aldrich, Dorset, UK
Ethylene diamine tetra acetic acid (EDTA)	
1M Tris HCl (pH 8)	
DL-dithiothreitol (DTT)	
Nile Red	
Glycerol	
Bovine Serum Albumin (BSA)	
10x Phosphate-buffered saline (PBS), no calcium and magnesium, protease free (pH 7.4)	Thermo Fisher Scientific, Hertfordshire, UK
Polyclonal Rabbit-Anti-human primary 12R-LOX AB (α12R-LOX) Thermo Fisher Scientific Cat# PA5-23608, RRID:AB_2541108	
Super PAP Pen	
Triton X100	
Polysine-coated microscope slides and glass coverslips	VWR international Ltd, Leicestershire, UK
1.5 mL reaction tubes	
Forceps	
Table top centrifuge 5418 R	Eppendorf Ltd, Stevenage, UK

Materials/Equipment	Supplier
Monoclonal Mouse-Anti-human primary CathD AB (αCathD) Santa Cruz Biotechnology Cat# sc-13148, RRID:AB_626808	Santa Cruz Biotechology, Inc., Heidelberg, Germany
Monoclonal Mouse-Anti-human primary CathV AB (αCathV) Santa Cruz Biotechnology Cat# sc-32798, RRID:AB_626812	
Monoclonal Mouse-Anti-human primary TG1 AB (αTG1) Santa Cruz Biotechnology Cat# sc-166467, RRID:AB_2202867	
Polyclonal Rabbit-Anti-human primary eLOX3 AB (αeLOX3) Biorbyt Cat# orb41336, RRID:AB_10998919	Biorbyt Ltd., Cambridgeshire, UK
Polyclonal Mouse-Anti-human primary XP32 AB (αXP32) Novus Cat# NBP1-93557, RRID:AB_11021954	Novus Biologicals, Abingdon, UK
Rabbit-Anti-Mouse-FITC coupled secondary AB (2nd AB (m) Abcam Cat# ab97045, RRID:AB_10687747	ABCAM PLC, Cambridge, UK
Mouse-Anti-Rabbit-FITC coupled secondary AB (2nd AB (rb) Abcam Cat# ab49937, RRID:AB_955159	
Monoclonal Mouse-Anti-human primary INV AB (αINV) Abcam Cat# ab74181, RRID:AB_1269195	

Materials/Equipment	Supplier
Fluorescence microscope and 10x Objective	Nikon, Amsterdam, Netherlands
Super high pressure mercury lamp power supply	
100mm microscope scale	
Monochrome camera	
System for image processing and analysis (Version 4.82)	Lucia Cytogenetics, Praha, Czech Republic
Image J® Version 1.51j8	National Institutes of Health, Bethesda, MD, USA
GraphPad Prism® (Version 7)	GraphPad Software, San Diego, CA, USA

3.3.2 Methods and study design

3.3.2.1 Isolation of CEs

The CEs were isolated from the adhesive tape strips collected from the PE cheek and PP post auricular sites of healthy Chinese volunteers whose SC properties were examined in Chapter 2. The immunostainings were performed on CEs extracted from tape 1 and 9 to determine the expression profiles for both anatomical sites and with depth. Tape strips were exposed for 25 min (shaking 600 rpm) to 750 µL of dissociation buffer containing 20 mM Tris-HCl pH 8.0; 5 mM EDTA; 2% SDS and 10 mM DTT. The insoluble CEs were centrifuged at 5000g for 7 min at room temperature followed by a washing step with PBS and CEs were then re-suspended in 100 µL PBS.

3.3.2.2 Immunostaining

A PAP pen was used on the polysine-coated microscope slide to create water repellent chemical borders. This was used to have eight partitions on one slide which decreases the surface area for the sample application and thus the amount of antibody solution. Squares were drawn with the PAP pen 30 min before sample application. Each antibody was pre-tested at 2 µg mL^{-1}; 4 µg mL^{-1}; 8 µL mL^{-1} and 10 µg mL^{-1}. However, 8 µg mL^{-1} of AB in 1% BSA dissolved in PBS was chosen as the optimal primary AB concentration.

The principle of the immunostaining process is depicted (Fig. 3.1). The isolated CEs were incubated with 0.05% Triton X100 in PBS for 10 min to permeabilise the CEs for better accessibility of the ABs. The primary AB was incubated for 4 h at room temperature in a humidified chamber to prevent dehydration of the CEs. The excess primary AB was washed out three times with 0.05% Triton X100 in PBS for 5 min. The secondary AB was diluted 1:100 in 1% BSA in PBS. The samples were incubated in a humidified chamber for 2 h at room temperature. The excess AB was removed by washing three times with 0.05% Triton X100 in PBS for 5 min. An additional washing step was performed with PBS for 10 min to wash out the Triton X100 which has fluorogenic properties. The lipids of the CEs were stained with 10 µg mL^{-1} Nile red in 75 % glycerol to create a reference staining. A reference staining is a standard addition to an immunostaining to ensure that there are cells or tissue within that sample. In usual immunostaining, the nucleus is stained to show that there is indeed a cell but this organelle is missing in corneocytes and thus the lipids were chosen to be stained.
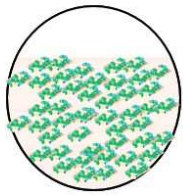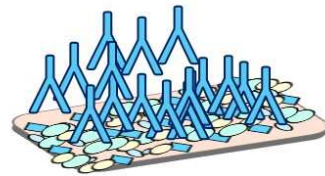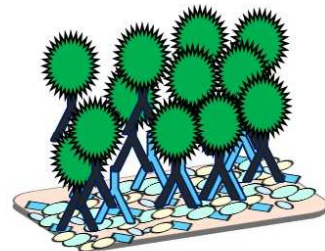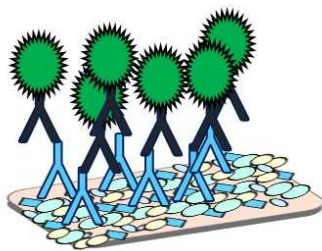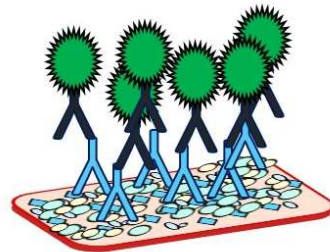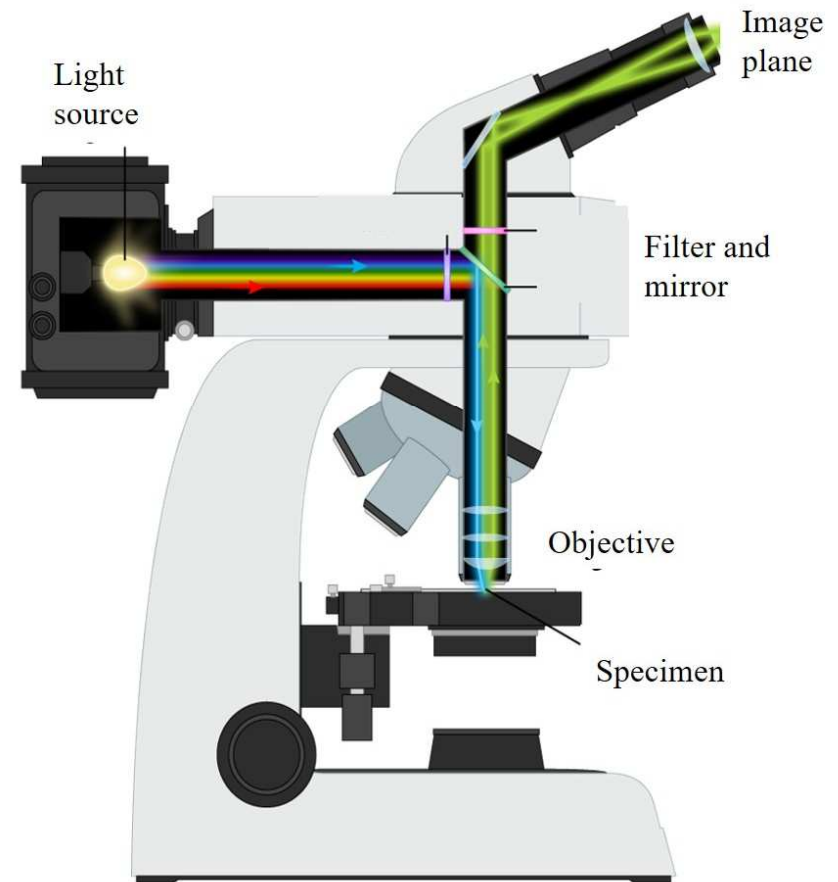
Figure 3.1. Principle of immunostaining to visualise a protein of interest under a fluorescence microscope.

3.3.2.3 Image and data analysis

A fluorescence microscope was used with a filter for green fluorescence to detect FITC (Excitation 495 nm/Emission 519 nm) and a red fluorescence filter to visualise Nile red (Excitation 552 nm/Emission 636 nm). Nine images were taken at comparable regions to ensure good representation of the stained CE population. Image J® was used to measure the green and red fluorescence on individual images and normalised to the protein content on the corresponding tape strips (Chapter 2). The staining was validated for false-positive fluorescence signal due to unspecific binding of primary or secondary AB or Nile red (Fig. 3.2).
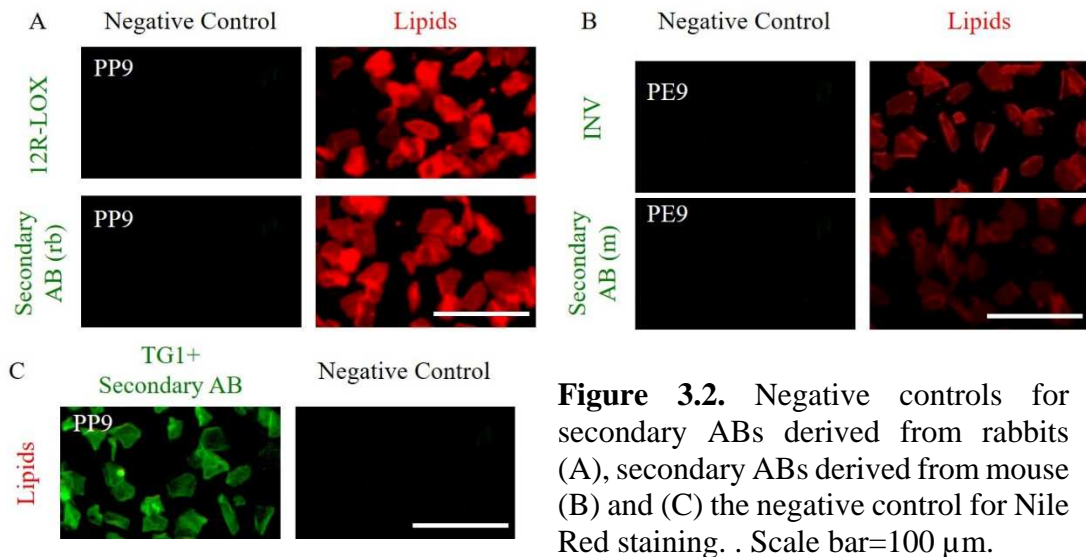
Figure 3.2. Negative controls for secondary ABs derived from rabbits (A), secondary ABs derived from mouse (B) and (C) the negative control for Nile Red staining. . Scale bar=100 µm.

3.3.2.4 Statistics

The fluorescence intensity was determined via the combination of ImageJ and GraphPad Prism. The fluorescence intensities were normalised to the protein content on the individual tape strip that was measured for CE cohesion in Chapter 2. All data points passed the D'Agostino & Pearson normality test and thus the statistical differences were described using the one-way ANOVA followed by the Sidak-Holm post-hoc test. All data are shown as mean ± SD (n=14) and statistical significance is represented as * $p \leq 0.05$, ** $p \leq 0.001$, *** $p \leq 0.0002$ and **** $p \leq 0.0001$; in addition the coefficient of variation (CV %) was determined.

3.3 Results

The immunostaining was performed on CEs obtained from the first and ninth tape strips collected from the PE cheek and PP post auricular sites. Image analysis was performed for the intensity of green pixels that was normalised for the corresponding protein content on the tapes. The qualitative analysis was conducted for different proteins involved in CE maturation or that are indicative of the maturity state of CEs at the time point of sample collection.
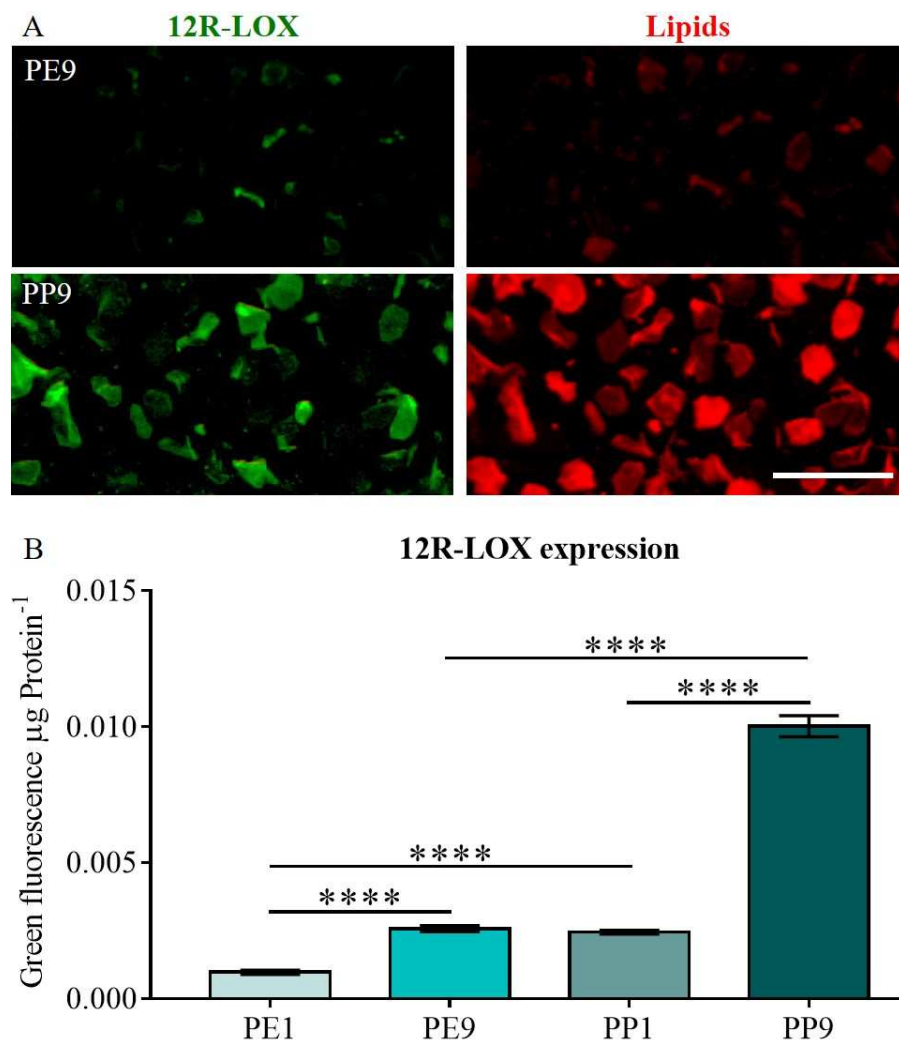
Figure 3.3. Immunostaining for 12R-LOX (A) is visualised in green and lipids are labelled in red. Scale bar=100 μm. Green pixels in the 12R-LOX (B) are normalised to the protein content to generate the 12R-LOX expression pattern. Mean ± SD, n=14.

12R-LOX processes EOS which after further processing is covalent attachment to the CLE in the maturation process. The 12R-LOX was visualised with immunostaining while lipids are labelled via Nile red (Fig. 3.3A). The green fluorescence is normalised with the corresponding protein content (Fig. 3.3B).

The image analysis showed that corneocytes isolated from the ninth tape strip showed a higher 12R-LOX expression than corneocytes from the first tape strip in both anatomical sites ($p \leq 0.0001$). The corneocytes isolated from the first tape strip obtained from the PE cheek site have a lower 12R-LOX expression than corneocytes from the first tape strip of the PP post auricular sites ($p \leq 0.0001$). The 12R-LOX expression is significantly higher in the corneocytes isolated from the ninth tape strip collected from the PP post auricular site ($p \leq 0.0001$). Corneocytes from the ninth tape strip collected from the PE cheek site express 2.5 times more 12R-LOX than corneocytes from the first tape strip ($p \leq 0.0001$). The corneocytes from the ninth tape strip obtained from the PP post auricular express 3.8 times more 12R-LOX than corneocytes from the first tape strip from the PP post auricular site ($p \leq 0.0001$). The corneocytes from the PP post auricular site have a higher 12R-LOX expression than the corneocytes from the PE cheek ($p \leq 0.0001$).

The enzyme eLOX3 follows up on 12R-LOX to process EOS and thus is a crucial enzyme in preparing ceramides for the CLE. The eLOX3 was visualised with immunostaining while lipids are labelled via Nile red (Fig. 3.4A). The total green fluorescence is normalised for the corresponding protein amount on the tape strips (Fig. 3.4B).
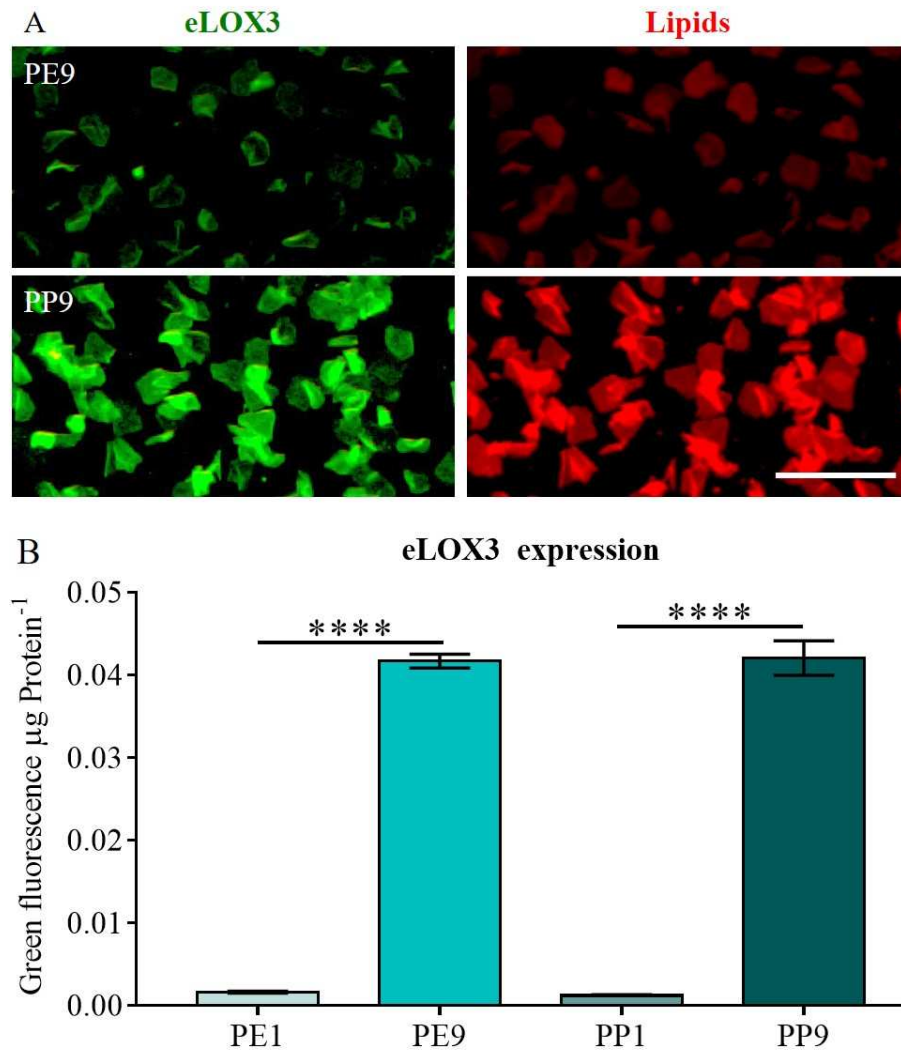
Figure 3.4. Immunostaining for eLOX3 (A) is visualised in green and lipids are stained in red. Scale bar=100 μm. Green pixels in the eLOX3 (B) are normalised to the protein content to generate the eLOX3 expression pattern. Mean ± SD, n=14.

The eLOX3 expression is 4.6 times higher in corneocytes from the first tape strip than in corneocytes from the ninth tape strip collected from the PE cheek ($p \leq 0.0001$). The expression of eLOX3 is 5.5 times higher in corneocytes from the ninth tape strip collected from the PP post auricular site compared to the first tape strip ($p \leq 0.0001$). The PE cheek and the PP post auricular sites showed similar expression levels of eLOX3 in corneocytes isolated from the first tape strip ($p \leq 0.2$) as well as in corneocytes extracted from the ninth tape strip ($p \leq 0.2$).

The protease CathD on corneocytes was visualised via immunostaining and the lipids were stained with Nile red (Fig. 3.5A). The resulting green pixels were measured and normalised to the corresponding protein levels (Fig. 3.5B).
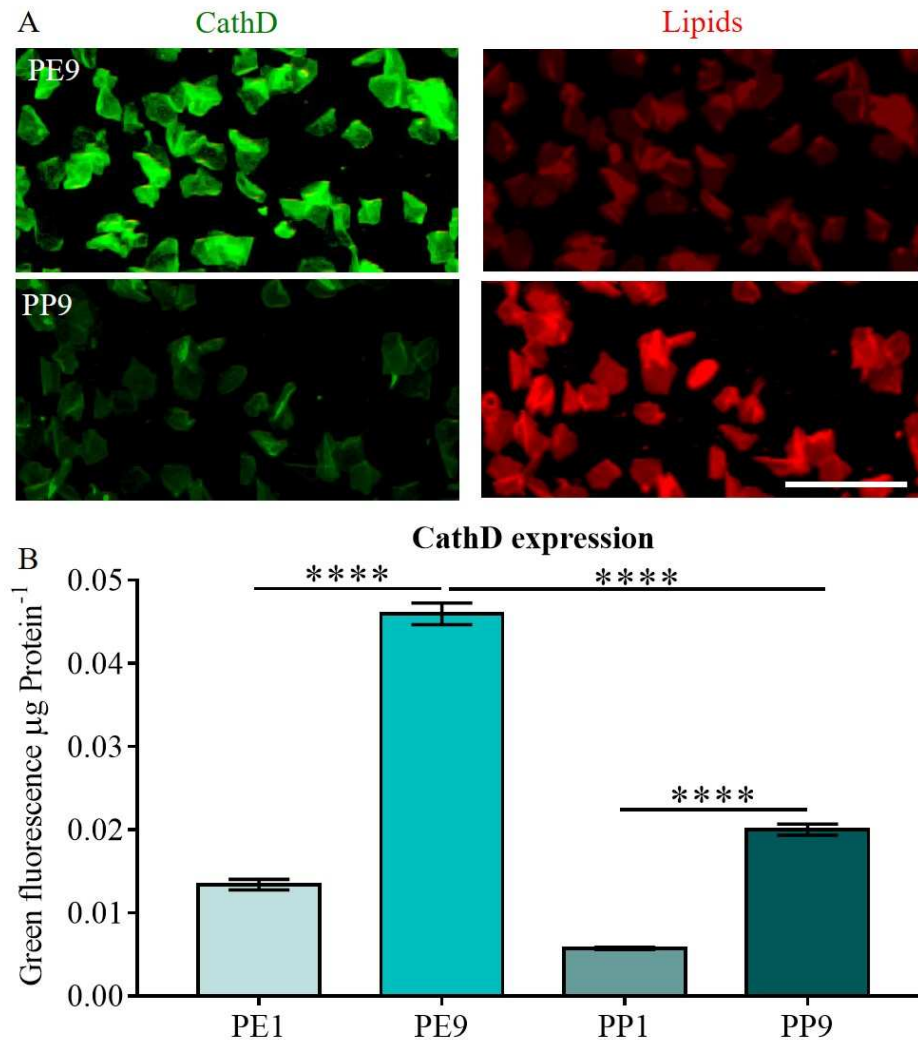
Figure 3.5. Expression pattern of CathD on corneocytes is shown in green and lipids in red fluorescence (A). Scale bar=100 µm. Green pixels in the CathD expression is normalised to the protein content (B). Mean ± SD (=14).

The corneocytes from the first (p ≤ 0.0001) and ninth tape strip (p ≤ 0.0001) obtained from the PE cheek expressed significantly more CathD than corneocytes from the PP post auricular site. Both anatomical sites had a higher population of CathD expressing corneocytes on the ninth tape strip compared to corneocytes from the first tape strip (p ≤ 0.0001).

The protease CathV expression on corneocytes was shown via immunostaining and the lipids were stained with Nile red (Fig. 3.6A). The resulting green pixels were measured and normalised to the corresponding protein levels (Fig. 3.6B).
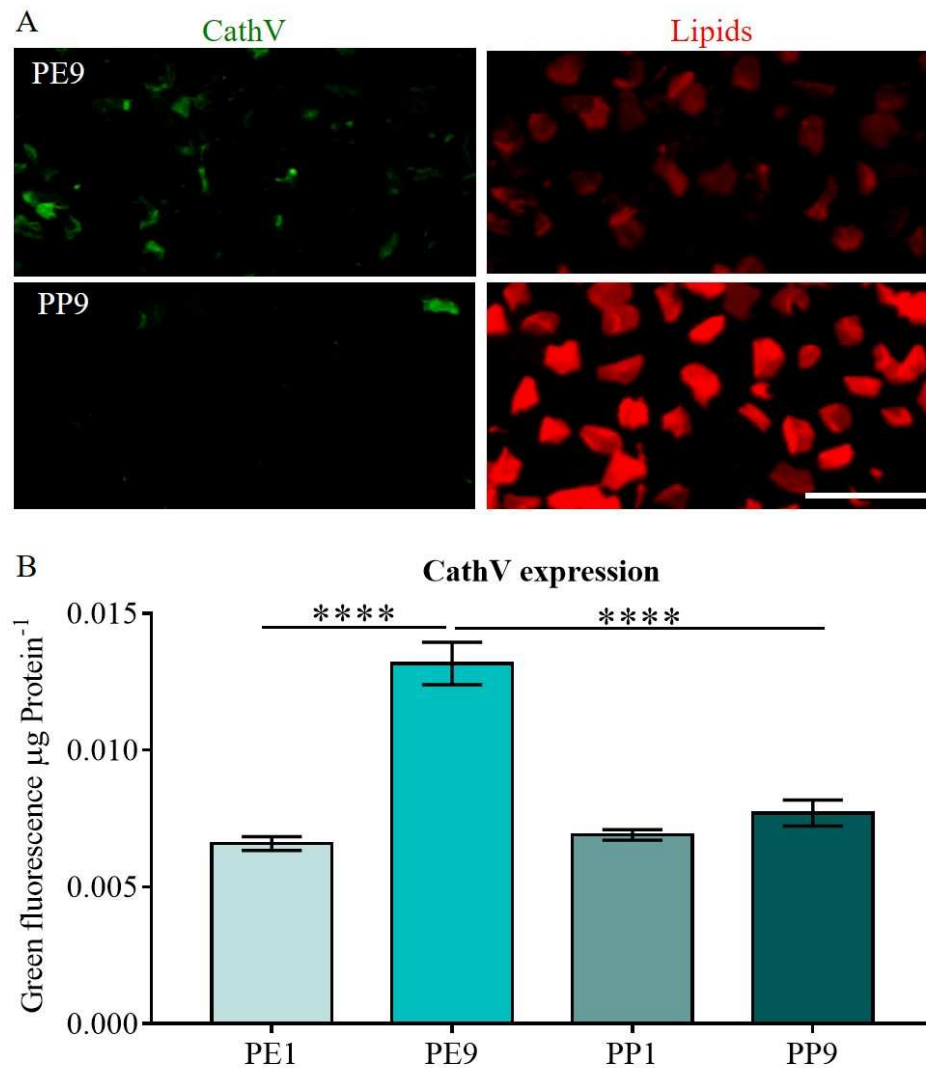
Figure 3.6. CathV expression on corneocytes is shown in green and lipids in red fluorescence (A). Scale bar=100 µm. Green pixels are normalised to protein content for CathV expression pattern (D). Mean ± SD (n=14).

The corneocytes from the ninth tape strip of the PE cheek site showed a significanlty higher CathV expression than the corneocytes from the ninth tape strip collected from the PP post auricular site ($p \leq 0.0001$). Samples collected from the first tape strip of both anatomical sites showed no significant difference in CathV

expression (p ≤ 0.6). Interestingly, the corneocytes from the first and ninth tape strip of the PP post auricular showed no significant difference in Cath D expression (p ≤ 0.5). However, the corneocytes from the ninth tape strip have a significantly higher CathV expression than corneocytes isolated from the first tape strip of the PE cheek site (p ≤ 0.0001).

The structural proteins INV was visualised in corneocytes to investigate the maturity state of the CEs in samples from the PE cheek and PP post auricular sites collected from the first and ninth tape strippings (Fig. 3.7A). The expression profile was determined by the intensity of the green fluorescence signal normalised to the protein content (Fig. 3.7B).

Samples isolated from the first tape strip of the PE cheek site express more INV than the corneocytes from the PP post auricular site (p ≤ 0.05). However, the corneocytes from the PE9 samples express significantly more INV than the corneocytes isolated of PP9 samples (p ≤ 0.0001). Corneocytes from the deeper PE cheek SC express INV to a significantly higher extent than the corneocytes from the superficial layer (p ≤ 0.0001). PP post auricular samples of the deeper SC layer express more INV than PP1 samples (p ≤ 0.01). The PE cheek site has a higher population of corneocytes expressing INV than the PP post auricular site.

Figure 3.7. Expression of INV in CPE is shown in green and the lipids of the CLE are visualised in red fluorescence (A). Scale bar=100 µm. The measured green pixels of INV expression is normalised for the protein content (B). Mean ± SD (n=14).

The structural protein XP32 is visualised in the CPE of corneocytes obtained from the PE cheek and PP post auricular sites (Fig. 3.8A). The expression profile was determined by intensity of the green fluorescence signal normalised to the protein content (Fig. 3.8B).

Corneocytes from the ninth tape strip express significantly more XP32 than samples from the first tape strip (p ≤ 0.0001). Furthermore, the corneocytes from the deeper SC layers of the PP post auricular site have less XP32 expression than

corneocytes from the PE cheek site (p ≤ 0.0001). Corneocytes from the superficial SC layers of the PP post auricular sites express considerably less XP32 than corneocytes from the PE cheek site (p ≤ 0.0001). However, the difference between PP1 and PP9 samples (p ≤ 0.05) are not as marked as for PE1 and PE9 samples (p ≤ 0.0001).
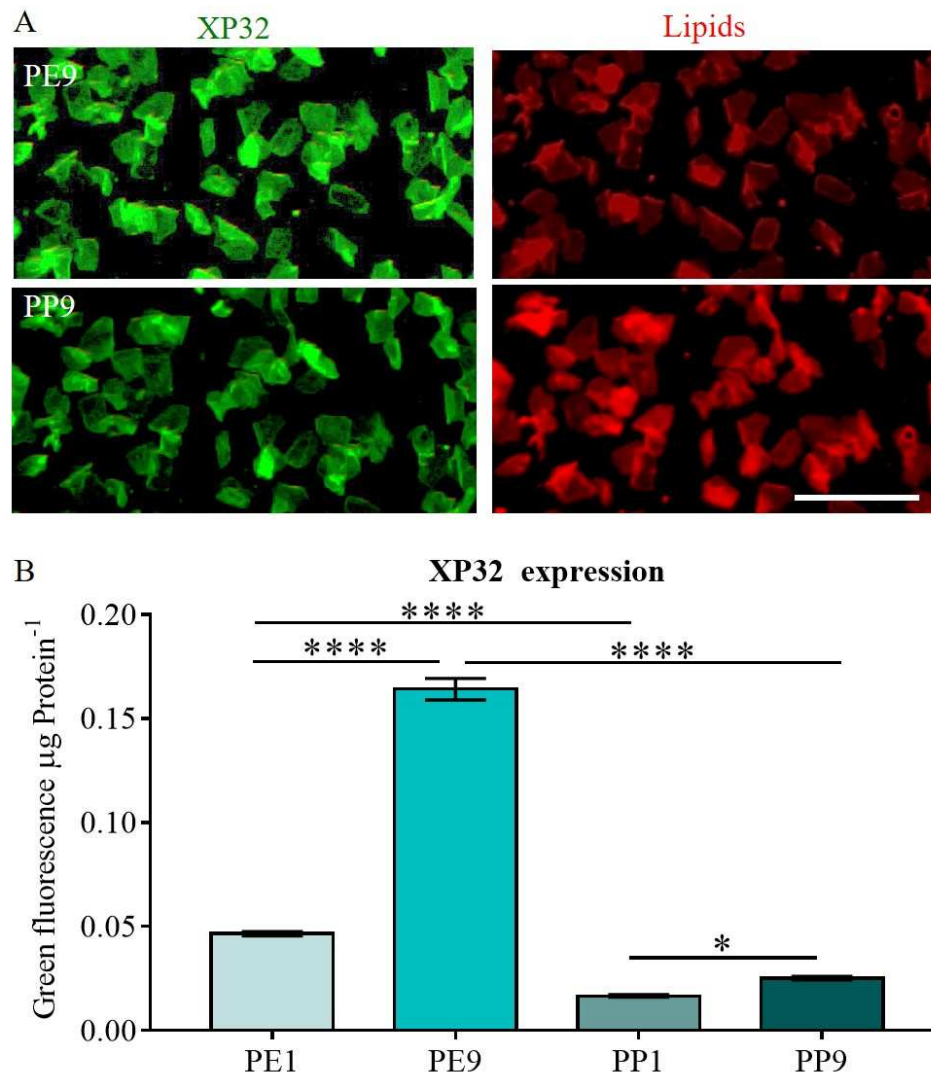
Figure 3.8. Expression of XP32 is visualised in the CPE in green and lipids of the CLE in red fluorescence (A). Scale bar=100 µm. The measured green pixels of XP32 expression is normalised for the protein content (B). Mean ± SD (n=14).

The expression of TG1 in corneocytes from the PE cheek and the PP post auricular sites was shown via immunostaining (Fig. 3.9A). The green fluorescence signal was measured and normalised to the protein level (Fig. 3.9B).
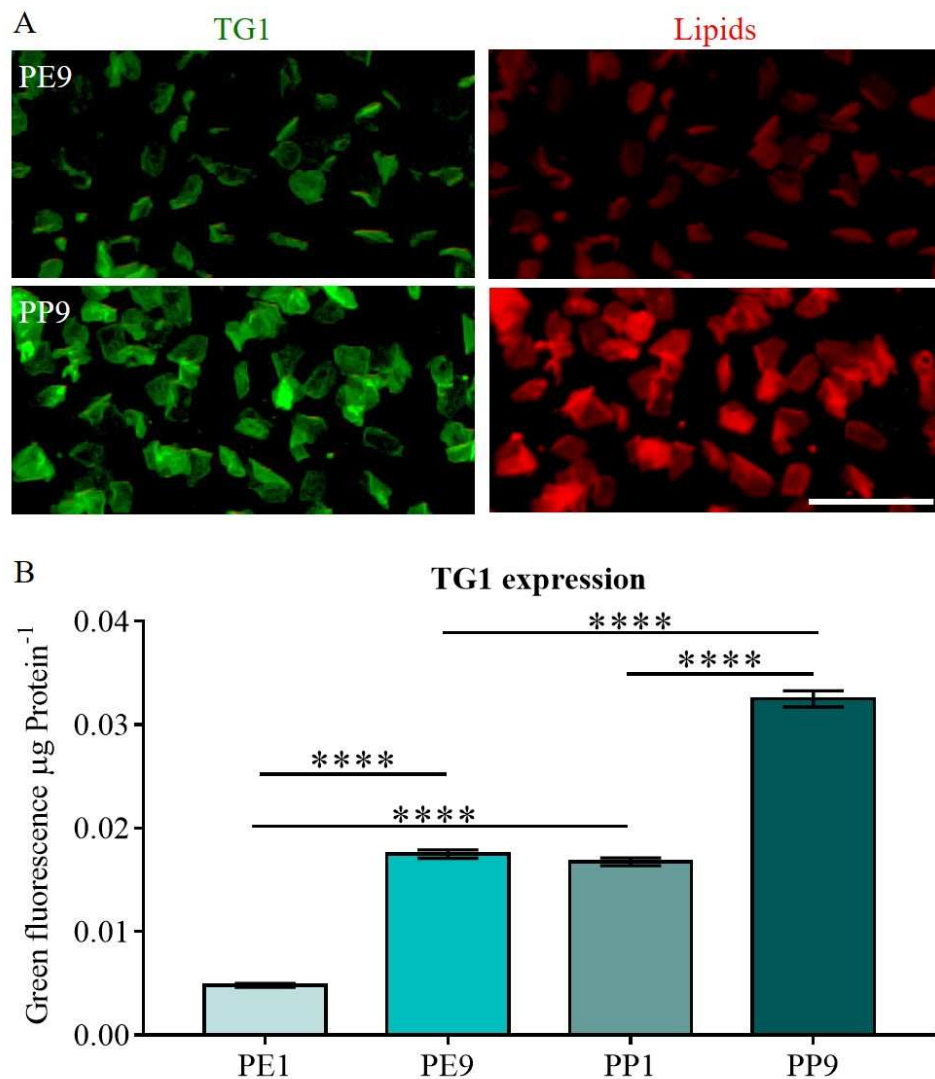
Figure 3.9. Immunostaining of TG1 in corneocytes visualised in green and the lipids are CLE stained with Nile red (A). Scale bar=100 µm. The measured green pixels for TG1 expression are normalised for the protein content (B). Mean ± SD (n=14).

The corneocytes in the deeper SC layers have higher TG1 expression than the superficial SC layers in both anatomical sites (p ≤ 0.0001). However, samples collected from the PP post auricular site express significantly more TG1 than corneocytes from the PE cheek site (p ≤ 0.0001).

3.4 Discussion

The work presented in this chapter aimed to gather more information about the selected study sites. The sun-exposed cheek and the sun-protected post auricular sites showed significant differences as assessed with various biomarkers. As previously reported in other studies [114,195], CEs from the deeper SC layers are more immature than those collected from the superficial SC layers. The Nile red staining showed an intense lipid staining in CEs collected from the PP post auricular site. 12R-LOX and eLOX3 catalyse EOS to ω-hydroxyceramides which are covalently attached to the CLE [91]. The knockout mouse model has shown that 12R-LOX [89] and eLOX3 [90] are crucial enzymes for the skin barrier formation. Neonatal knockout mice that were homozygotically mutant for the 12R-LOX or eLOX3 genes died soon after birth due to excessive dehydration. The absence of 12R-LOX caused a more drastic outcome for the knockout mice with an 8-fold higher trans epidermal water loss (TEWL) that led to a life span of 3 h [89]. The eLOX3 knockout mice survived for 12 h. Hyperproliferative keratinocytes were observed in eLOX3 knockout mice which consequently led to a thicker SC. This might account for a delay in the dehydration, however, it was insufficient to compensate for severe dehydration in that study [90]. In the present work, eLOX3 expression is higher in corneocytes obtained from the deeper SC layers of both anatomical sites but showed no differences between study sites. On the other hand, 12R-LOX showed major differences in expression between PE cheek and PP post auricular sites. The eLOX3 and 12R-LOX findings are in line with mass spectrometry data in a previous study [118]. The Nile red staining which was used as a counterstaining for lipids showed a higher fluorescence intensity in samples from the PP post auricular site compared to those from the PE cheek site. This suggests that corneocytes from the PE cheek site have a reduced amount of ceramides on the CLE. However, this will be discussed in more detail in the following chapters. The low levels of processed ceramides in the PE cheek site seems to originate from the reduced level of 12R-LOX but not eLOX3.

Some cathepsins in the skin have been linked to regulation of desquamation of the upper layer of the SC [122,123,125]. CathD and CathV were suggested as biomarkers for photo damage in the skin. Increased expression of these two cathepsins was observed following UV-radiation [119,123]. Furthermore, UV radiation has been shown to decrease the pH in the SC which in turn enhances proteases in their catalytic

activity [20]. This could be assumed as a compensation mechanism in which photo damaged corneocytes are replaced with intact corneocytes to restore the skin barrier function. Moreover, CathD is a protease that has been shown to activate TG [125] which cross-links the structural proteins such as INV in the CPE [96]. Meanwhile ω-hydroxyceramides are covalently attached to the structural proteins of the CPE to create a hydrophobic CLE [50]. Both processes are mediated by TG hence the presence and activity of TG is crucial for CE maturation. The expression pattern of TG1 was assessed as it was shown to be the main TG involved in CE maturation [50,84,95]. Interestingly, the TG1 and 12R-LOX expression patterns are similar for both anatomical sites and depths. CE samples obtained from the PP post auricular site showed a higher fluorescence signal following immunostaining compared with PE cheek samples. Sun-exposed skin shows a lower potential for CE maturation because of reduced 12R-LOX and TG levels as will be shown in Chapter 5 and Chapter 6, respectively. The increased Cath D expression hints towards a compensatory mechanism in the photo exposed site assuming that all available TG1 is activated to enhance CE maturation. The CathD expression in the deeper SC levels was higher than in samples from the SC surface in both anatomical sites. However, the CathV expression is only increased in CE samples from deeper SC layers of the PE cheek site and is reduced in the superficial SC surface. Increased levels of CathD and CathV confirm that the PE cheek site has been exposed to photo damage.

The structural protein INV is the main structural protein of the CE [96] and has been established as a marker for immature CEs in various studies [114,195,196]. Although, XP32 and INV are both structural components of the CPE, both proteins are expressed at different time points of epidermal differentiation [84]. INV is expressed in the early stages of keratinocyte differentiation while XP32 is expressed at a the later time point of the developmental stages [197]. Corneocytes in the deeper SC layers of both anatomical sites showed higher expression levels of the structural proteins INV and XP32 compared to corneocytes from the superficial SC layers. This confirms that the CEs in the superficial SC layers are less mature than CEs from the deeper SC layers.

Corneocytes from the PE cheek site were demonstrated to be immature and with reduced 12R-LOX and TG1 levels while showing signs of photo damage. The reduced maturity of corneocytes from the PE cheek site contributes to the decreased SC integrity. Furthermore, the increased protease levels might contribute to SC desquamation and thus thinning of the photo damaged SC. This work demonstrated the useful information biomarkers can provide for skin barrier function and integrity.

CHAPTER 4

A novel assay to assess the maturity
of the corneocyte envelopes

4. A novel assay to assess the maturity of the corneocyte envelopes

4.1 Abstract

Background: Corneocytes are enclosed in corneocyte envelopes (CE). This protein-lipid complex supports the barrier functionality of the stratum corneum (SC) by providing mechanical stability and hydrophobicity.

Objectives: The aim of this work was to develop a robust method to characterise CE maturity based on CE rigidity, hydrophobicity and surface area. This offers an alternative to the use of Nile red staining and antigenicity of the structural PE protein, involucrin (INV). The novel and conventional methods are assessed on samples taken from the photo exposed (PE) cheek and photoprotected (PP) post auricular sites.

Methods: Nine consecutive tape strips were obtained from the cheek and post auricular sites of healthy Caucasians. CEs on the first and ninth tape strip were subjected to sonication to assess rigidity and Nile red staining to visualise hydrophobicity per unit surface area. In addition, the presence of INV and lipids was characterised for assessment of CE maturity which was evaluated via the red/green pixel ratio, the percentage of INV positive (+) CEs and the ratio of fluorescence densities.

Results: PP post auricular CEs were more rigid and had a stronger fluorescence signal per unit surface area than PE cheek CEs. The surface area of CEs collected from the deeper SC layers were similar despite the different anatomical sites; interestingly, the CE hydrophobicity and CE rigidity were significantly different. The relative CE maturity (RCEM) summarises the three CE characteristics and provides a higher sensitivity for measurement of CE maturity than the conventional INV and Nile red staining. CEs from the deeper SC layers were less mature than those from the SC surface in both anatomical sites. However, the PP post auricular site had more mature CEs than the PE cheek site.

Conclusions: The combined method allows CE maturity characterisation based on hydrophobicity per unit surface area and rigidity rather than a simple ratio of lipid to INV. A more robust and sensitive measurement has, therefore, been developed addressing the limitations of earlier protocols.

Key Words: Photodamaged skin, Corneocyte envelope maturity, Hydrophobicity, Rigidity.

Declaration

The results of this chapter have been reported in the *International Journal of Cosmetic Science* in March 2018 as "A new approach to assess the effect of photo damage on corneocyte envelope maturity".

4.2. Introduction

The skin has a unique homeostatic mechanism to maintain its integrity and barrier function. Epidermal stem cells in the basal layer differentiate into keratinocytes and migrate upwards towards the stratum corneum (SC) while changing dramatically in morphology and biochemistry. Keratinocytes become corneocytes once the cell nucleus and organelles have disintegrated and lipid-filled lamellar bodies are released into the extracellular matrix [13]. In corneocytes, keratins are stabilised by disulfide bonds [39] and are aggregated with the aid of filaggrin [198] which drives the collapse of the "ghost" cell into a flat polygonal shape [13]. Gradually, various structural proteins such as loricrin and involucrin (INV) are cross-linked by transglutaminases (TG) to provide mechanical strength and replace the plasma cell membrane of keratinocytes with an insoluble corneocyte protein envelope (CPE) [199]. Immature CEs mature with the covalent attachments of ceramides and fatty acids to INV and loricrin, possibly being mediated by TG creating a hydrophobic coating, the corneocyte lipid envelope (CLE). Those bound lipids may stabilise and strengthen the mechanical resistance of the corneocyte envelopes (CEs) [50].

Nomarski contrast microscopy of CEs from different depths of the SC allowed the identification of two populations of CEs. These were characterised as immature "fragile" CEs (CE_f) in the deeper SC layers and mature "rigid" CEs (CE_r) in the superficial SC layers [102]. The CPE gains in rigidity with crosslinking of structural proteins such as INV and loricrin which can be assessed. Tetramethylrhodamine isothiocyanate (TRITC) is a fluorochrom that binds to primary or secondary amines found in proteins and peptides. Combined with the Nomarski contrast microscope TRITC provides a high resolution image of corneocytes. Corneocytes increase in rigidity with maturity and thus a higher TRITC fluorescence intensity is observed in CE_r than in CE_f which are less mature [200]. This finding was confirmed by mechanical micromanipulation experiments where greater force was required to collapse the CEs from the SC surface compared to those from the deeper SC layers.

Furthermore, sun-exposed skin showed a higher population of CE_f in the SC of the cheek [7].

Sonication was developed as an alternative method to micromanipulation in order to investigate the fragility of the CEs in loricrin and 12R-lipoxygenase knock-out mouse models [89,201]. Sonic waves of vibration are created in an ultrasonic bath which transmits the ultrasonic energy through the water into the samples. This method challenges the mechanical resistance of the CEs by shear forces. In theory, this can be used to determine rigidity of CEs and to distinguish CE_f and CE_r in a population of corneocytes. Atomic force microscopy performs imaging at the nano scale in which forces are measured between a sharp probe and the surface of the specimen. The probe is attached to a cantilever which deflects upon force and thereby changes the reflection of the laser beam scanning the surface. Atomic force microscopy allows a determination of mechanical resistance of CEs and simultaneously provides high resolution imaging of the cellular structures [202].

Previous studies have reported INV expression in the upper stratum spinosum and stratum granulosum layers of the epidermis in rats and mice [203] as well as in humans [204]. The INV expression is associated with terminal keratinocyte differentiation [205,206]. In recent years, the standard technique for assessing CE maturity has been based on visualising the CLE with Nile red lipid staining combined with immunostaining for the structural CE protein INV. In the original protocol, CE maturity was expressed as the percentage of INV positive (+) CEs [207] while later studies adapted the measurement of red and green pixels to generate a ratio [195,196]. The immunostaining and image analysis approaches have a number of limitations. For example variation in the INV expression because of skin conditions would influence the resulting CE maturity. Hyperproliferative keratinocytes are typically found in wound healing or skin conditions such as psoriasis where INV expression was observed closer to the basal layer [208–210]. Furthermore, neoplastic keratinocytes found in skin carcinomas have high INV expression [78,204].

Various studies that used solely INV as a biomarker for terminal differentiation are not quantitatively comparable. The authors of the original protocol determined up to 18 ± 5% INV (+) CEs [207] in the cheek site. Following studies from the same anatomical site reported 32 ± 10% INV (+) CEs [141] and 40 ± 30% INV (+) CEs

[211]. Similar observations were found with the ratio of green and red pixels generated by the fluorescence signal of INV (+) CEs and Nile red staining of the CLE. These studies were conducted on the mid-ventral forearm of Caucasians. The CE maturity was determined in samples from the first tape strip with mature CEs with a ratio of 1.4 ± 0.1 [115,195,196] while another study resulted in a red/green ratio of 4.3 ± 1.0 [107,131]. These studies provide a comparison between CE maturities of different body sites, however, CE maturity cannot be compared between studies. The resulting CE maturity based on INV (+) CEs and red/green ratios are highly dependent on the immunostaining for INV. Variations in the methodology might lead to alternations in the outcome. For example, a different batch of antibodies might have a different antigen binding capacity and thus result in different fluorescence intensities. Background staining was observed in all previous studies which cannot be distinguished in the red/green ratio analysis. The studies used a high concentration of the detergent sodium dodecyl sulfate (SDS) which precipitates at low temperatures which has a high potential for background staining and artefacts. Furthermore, the CE morphology might alter due to dehydration during various incubation steps [195,196,207]. However, both analytical methods are associated with high standard errors and coefficients of variation.

The popular term "Golden standard" originates historically from Economics where a different currencies were weigh against gold as a standard allowing the comparison of the payment method. In methodology, the "Golden standard" refers to the best known approach to describe or assess a measurement or test. The particular method that is acknowledged as the "Golden standard" should be used to validate and compare the "Golden standard to the new approaches. However, the term "Golden standard" implies that this method is perfect and thus the standard to which a new approach should be compared and validated to. However, the INV/lipid staining which could be considered the "Golden standard" to determine the CE maturity has been shown with variations in image resolution. The INV/lipid staining provides valuable information for the CPE and CLE, but the different interpretations for maturity makes it challenging to consider it as "Golden standard".

In the present study, CE maturity was investigated in photo exposed (PE) cheek and photo protected (PP) post auricular sites in healthy Caucasians. The conventional method with staining for INV and lipids is compared to a new method. This approach

introduces a new and robust approach based on CE rigidity, hydrophobicity and surface area to characterise the relative CE maturity (RCEM). Sonication was applied to examine the mechanical resistance of CEs and to distinguish between CE_f and CE_r while CE hydrophobicity is assessed via the lipid staining per unit CE surface area. In addition the SC integrity, cohesion and thickness assessed in Chapter 2 is correlated with the CE maturity methods.

4.3 Materials and methods

4.3.1 Materials and equipment

The listed materials and equipment were used for CE extraction, immunostaining, and for the new method characterisation. The CEs were extracted from the first and ninth tape strips of PE cheek and PP post auricular sites of Caucasian participants.

Table 4.1. Materials and equipment used to isolate CEs from tape strips and characterise CE maturity via the conventional and new methods.

Materials/Equipment	Supplier
Sodium dodecyl sulfate (SDS)	Sigma Aldrich, Dorset, UK
Ethylene diaminetetraacetic acid (EDTA)	
1M Tris HCl (pH 8)	
DL-dithiothreitol (DTT)	
Nile Red	
Glycerol	
Bovine Serum Albumin (BSA)	
10x Phosphate-buffered saline (PBS), no calcium and magnesium, protease free (pH 7.4)	Thermo Fisher Scientific, Hertfordshire, UK
Super PAP Pen	
Triton X100	
Polysine-coated microscope slides and glass coverslips	VWR international Ltd, Leicestershire, UK
1.5 mL reaction tubes	
Forceps	
Rabbit-Anti-Mouse- Fluorescein isothiocyanate (FITC) coupled secondary AB Abcam Cat# ab97045, RRID:AB_10687747	ABCAM PLC, Cambridge, UK

Materials/Equipment	Supplier
Monoclonal Mouse-Anti-human primary INV AB Abcam Cat# ab74181, RRID:AB_1269195	ABCAM PLC, Cambridge, UK
Table top centrifuge 5418 R	Eppendorf Ltd, Stevenage, UK
Sonicator (44 Hz)	Grant Instruments Ltd., Cambridgeshire, UK
Fluorescence microscope and 10x Objective	Nikon, Amsterdam, Netherlands
Super high pressure mercury lamp power supply	
100mm microscope scale	
Monochrome camera	
System for image processing and analysis (Version 4.82)	Lucia Cytogenetics, Praha, Czech Republic
Image J® Version 1.51j8	National Institutes of Health, Bethesda, MD, USA
GraphPad Prism® (Version 7)	GraphPad Software, San Diego, CA, USA

4.3.2 Methods and study design

The CE maturity was assessed on samples collected with the first and ninth tape strips taken from healthy Caucasians that were initially collected for SC characterisation as described in Chapter 2.

4.3.2.1 Isolation of CEs

CE maturity was determined from the first and ninth tape strips which are referred to as PE1 and PE9 for the cheek samples and PP1 and PP9 for the post auricular samples. Each tape was cut into halves and isolated according to the original protocol and an alternative protocol.

One of the tape halves was extracted according to the reported protocol with 750 µL of dissociation buffer containing 100 mM Tris-HCl pH 8.0, 5 mM EDTA, 2% SDS, and 20 mM DTT. Tapes were immersed in the dissociation buffer at 75 °C for 10 min, shaken for 3 min at 1000 rpm room temperature and centrifuged for 10 min at 5000 g. The extracted CEs were washed by repeating the procedure three times in dissociation buffer.

The CEs from the other half of the tape were isolated similarly to the procedure above but with less salt and DTT thereby generating a milder dissociation buffer (20 mM Tris-HCl pH 8.0, 5 mM EDTA, 2% SDS, and 10 mM DTT) and a washing buffer containing 20 mM Tris-HCl pH 8.0, 5 mM EDTA, 0.2% SDS, and 10 mM DTT [201].

However, CEs collected from both isolation protocols were suspended in 1x PBS buffer instead of SDS containing buffers to allow a clear fluorescence signal without artefacts or high background noise signals.

4.3.2.2 Immunostaining for involucrin and Nile red staining for lipids

The samples isolated with the higher salt and DTT concentration [195] were placed on polysine-coated microscope slides which was previously marked with a PAP pen. Each sample was applied as 5 µL of CE suspension. The primary monoclonal antibody for INV was diluted to 1:100 in 1% BSA in PBS and incubated overnight at 4 °C in a humidified chamber. The antibody solution was washed off with PBS three times for 5 min before adding the secondary antibody (1:100) in 1% BSA in PBS and incubated for 1 h at room temperature (in the dark) [207]. Slides were washed three times for 5 min with PBS and mounted with 20 µg mL-1 Nile red in 75% glycerol solution.

4.3.2.3 Assessing CE maturity based on rigidity and hydrophobicity per unit of surface area

Extracted CEs collected from the milder dissociation buffer were divided into 20 µL aliquots with one sample being exposed to sonication (44 kHz). The sonication was performed similarly to a previously described protocol which determined 4 °C as an optimal temperature to sonicate CEs (40 kHz) [201]. This temperature might stabilise the structural proteins and prevent heat induced denaturation by the sonication process. Isolated CEs were sonicated at 4 °C between 5-15 min. A duration-dependent decrease is observed in the percentage of intact CEs. CEs collected from the PE cheek site are more susceptible to damage by sonication than those collected from the PP post auricular site. However, at 10 min sonication moderate damage is introduced hence this was chosen as the ideal exposure time (Fig. 4.1).
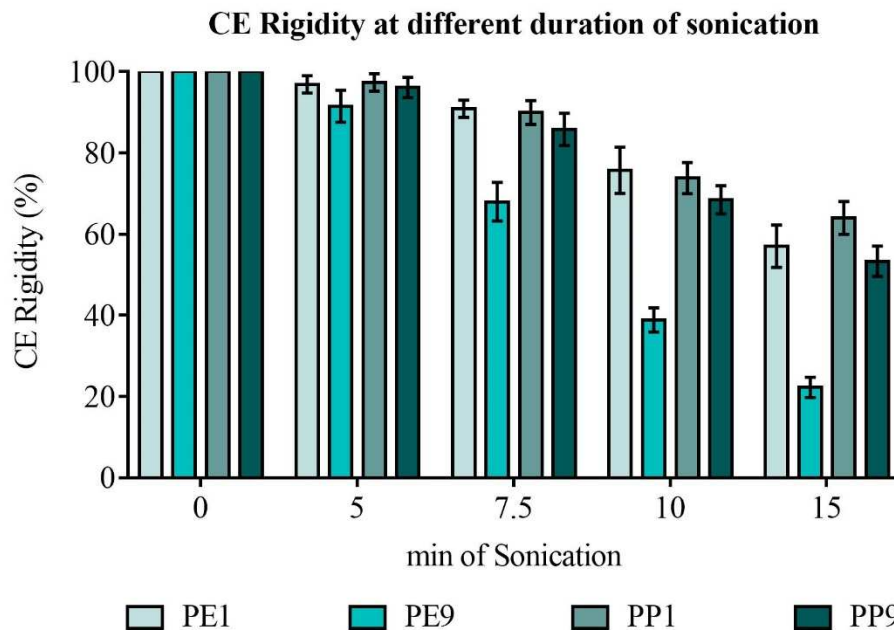
Figure 4.1. Sonication caused fragile CEs to collapse in a time dependent manner while rigid CEs remain intact. A suitable duration was determined at 10 min. Mean ± SD (n=6).

Sonicated and non-sonicated control CEs (three samples of 5 µL) were placed on a polysine-coated microscope slides previously marked with the PAP pen and mounted with 20 µg mL^{-1} Nile red in 75% glycerol solution to stain the lipid coating on CEs.

4.3.3 Image and data analysis

A fluorescence microscope was used with a filter for green fluorescence to detect FITC that is coupled to the secondary antibody (Excitation 495 nm/Emission 519 nm) and a red fluorescence filter to visualise Nile red (Excitation 552 nm/Emission 636 nm). Nine images were taken in total for each CE sample for both maturity assessment protocols with the corresponding fluorescence filter. The fluorescence images were taken at a 10x objective magnification and were analysed via Image J [®], however, the image analysis differs from previous reports [195,196,207] as discussed further below.

The obtained images for the INV immunostaining and the Nile red lipid staining were analysed with three different protocols. The percentage of INV (+) CEs was determined to characterise CE maturity in accordance with the original protocol [207]. The current approach to determine CEs by generating a red/green ratio from the total red and green pixels content. In addition, the average CE surface area was determined from the 8-bit converted images where a threshold was set. Watershed was applied to define CE borders and allow the detection of CEs with a surface area of 300 - 2000 μm^2 [195,196]. Another red/green ratio index was created by measuring the integrated density (fluorescence intensity per surface area) instead of a simple RGB channel measurement.

The images for the new characterisation approach were taken to investigate three different CE parameters. CE rigidity was determined for CE_f and CE_r by counting non-sonicated and sonicated CEs according to their morphological appearance.

$$CE\ Rigidity\ (\%)\ =\ \frac{intact\ CEs\ after\ sonication}{intact\ CEs\ before\ sonication}\ x\ 100 \qquad\qquad Equation\ 4.$$

The actual damage from sonication can be determined using Equation 4 which considers the initial rigidity (Fig. 4.2).

Determination of suitable duration for sonication
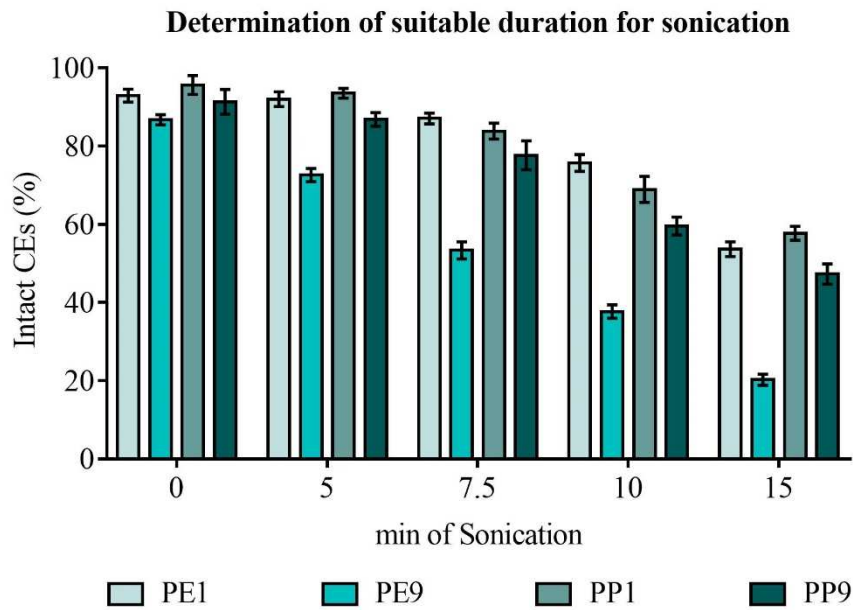
Figure 4.2. The decrease in CE rigidity depends on the exposure time to sonication. Mean ± SD (n=6).

The CE hydrophobicity was measured in non-sonicated CEs and analysed from the red fluorescence per unit of CE surface area. Images were converted into 8-bit and inversion of the image was applied to increase resolution. The thresholding was adjusted by setting up a maximal pixel intensity. Watershed is a function in Image J that allows the separation of particles by predicting the edges. Image J was set up to analyse corneocytes with a surface area of 300 - 1500 μm^2. Recognised CEs that fit into the selected surface area criteria are saved in the region of interest manager. This Image J function results in a black and white image. However, the fluorescence intensity needs to be measured in the original image with red fluorescent CEs, therefore, the original image is reopened. The region of interest manager overlays the marked CEs with the original image. This allows individual selections of CEs in order to exclude any artefacts. The surface area and fluorescence density is measured for selected CE_r. (Fig. 4.3). The fluorescence density expresses the amount of red pixels per unit of surface area of CEs which is equivalent to CE hydrophobicity. This allows a qualitative comparison of CEs from different anatomical sites and depths.
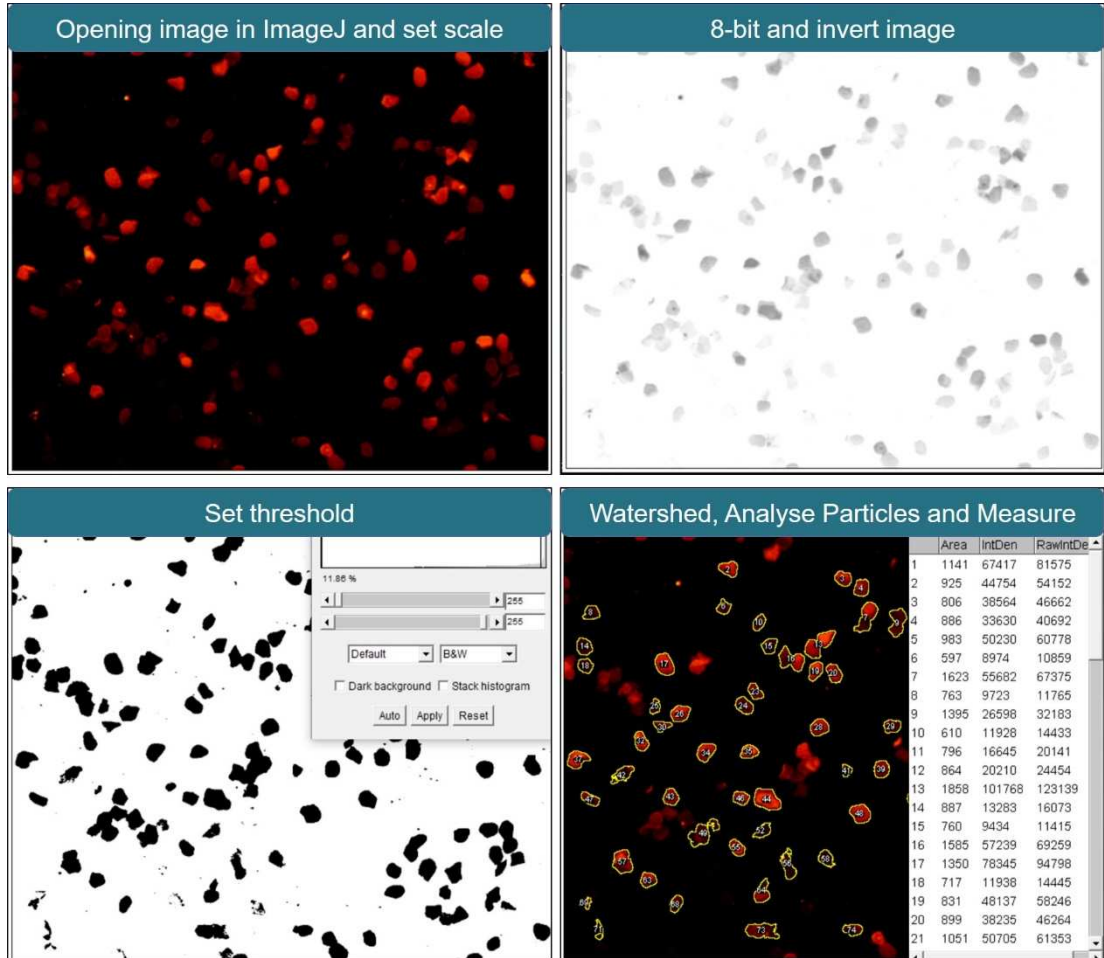
Figure 4.3. Image analysis with Image J to mark corneocytes to measure fluorescence intensity per unit of surface area.

The assessed CE rigidity and CE hydrophobicity represent the relative CE maturity (RCEM). This was expressed as a value by multiplication of the determined CE characteristics. However, CE rigidity is given as a percentage, therefore, the decimal numbers (ex. 0.85 instead of 85%) were multiplied with the fluorescence density (Equation. 5):

$$Relative\ CE\ Maturity\ (AU)\ = Fluorescence\ density\ (\frac{pixels}{\mu m^2})\ x\ Rigidity \qquad Equation\ 5$$

The RCEM is expressed as arbitrary units (AU) to allow the qualitative determination of the CE maturity from corneocytes collected from different anatomical sites and tape strippings.

4.3.2.5 Statistics

All measurements are expressed as mean and standard deviation (SD) and analysed via GraphPad Prism. The CE maturity was determined for the CEs collected from the superficial SC layers (tape 1) and the deeper SC layers (tape 9) of PE cheek and PP post auricular sites. Column statistics were measured for all obtained data which passed the D'Agostino & Pearson normality test. The statistical differences were determined via the One-way ANOVA multiple comparison followed by the Sidak-Holm post-hoc test. * $p \leq 0.05$, ** $p \leq 0.001$, *** $p \leq 0.0002$ and **** $p \leq 0.0001$. The coefficient of variation (CV %) was determined in addition. The Pearson's correlation coefficient was used to analyse SC integrity and cohesion (Chapter 2) and the results of the different CE maturity approaches.

4.3 Results

4.3.1 The conventional and alternative approaches to determine CE maturity via antigenicity of involucrin and lipid staining

The visual comparison of red and green fluorescence shows a clear difference between both anatomical sites. The red fluorescence visualises the lipids attached to the CEs. Samples from the PP post auricular sites have more CEs with a stronger Nile red staining than CEs obtained from the CE cheek sites. However, corneocytes from the deeper SC layers have less lipids than corneocytes from the superficial SC layers in both anatomical sites. The green fluorescence visualises the structural protein INV and is considered as a marker for immature CEs. A higher population of immature CEs were observed in the PE cheek site compared to CEs isolated from tape strips from the PP post auricular samples (Fig. 4.4).
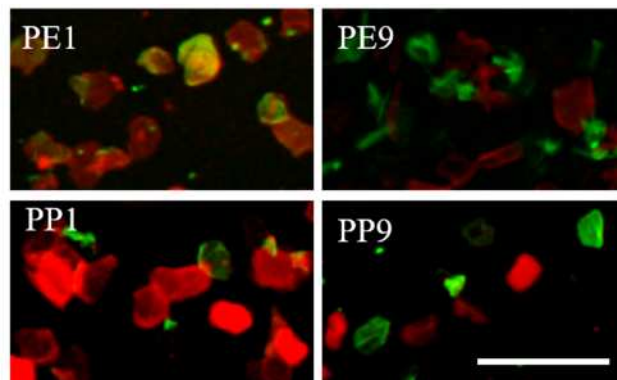
Figure 4.4. Imaging of PE cheek and PP post auricular CEs. The green and red channels are merged to visualise INV and lipids of CEs. PE1= CEs of cheek, tape strip 1; PE9= CEs of cheek, tape strip 9; PP1= CEs of post auricular, tape strip 1; PP9= CEs of post auricular, tape strip 9. Scale bar=100 µm.

The image analysis of the INV and Nile red staining allowed the determination of the percentage of immature CEs in the samples obtained from the two anatomical sites and depths (Fig. 4.5). The PE cheek samples collected from the SC surface have 38.1 ± 20.52 % (CV 53.8 %) immature CEs. The surface of PP post auricular SC has 15.0 ± 8.6 % (CV 54.5 %) immature CEs which is significantly less than in the PE cheek SC (p<0.05). This indicates that the CEs from PP1 are more mature than the

PE1 samples. The deeper SC layers of the PE cheek site has 68.6 ± 15.3 % (CV 22.2 %) immature CEs which is significantly more than samples from PE1 site (p<0.001). Furthermore, CEs from PE9 tapes are more immature than the CEs from PP9 samples (36.4 ± 12.0 %, CV 26.1 %, p<0.05). Interestingly, the obtained CEs from PP9 and PE1 show a similar population in immature CEs (p<0.226).
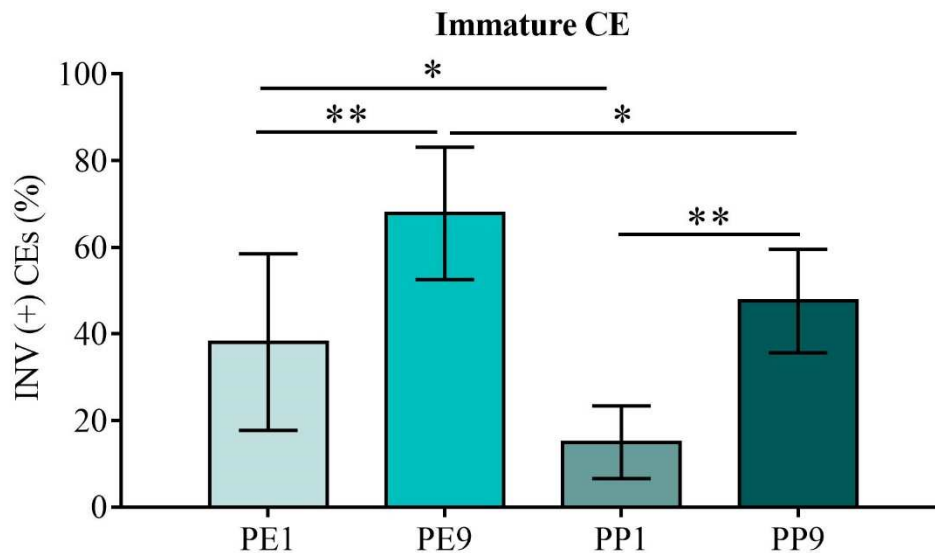
Figure 4.5. Percentage of immature CEs in PE cheek and PP post auricular samples. All data are shown as mean ± SD and compared via one-way ANOVA and post-hoc Sidak-Holm test, (n=14).

Measurements of the red and green channels were used to determine the ratio of red and green pixels which corresponds to the CE maturity (Fig. 4.6). This confirmed that CEs from the superficial SC layers of both anatomical sites are more mature than those from the deeper SC layers. However, CEs collected from the SC surface of the PP post auricular site are significantly more mature (p<0.01), with a red/green ratio of 12.2 ± 4.9 (CV 40.6 %), than CEs from the PE1 site which have a red/green ratio of 5.4 ± 4.4 (CV 81.4 %). The red/green ratio confirmed that CEs from the deeper SC layers of the PE cheek are less mature with a ratio of 1.7 ± 1.6 (CV 97.3 %) than CEs collected from the PE1 site. CEs from the deeper SC of the post auricular site have a significantly lower red/green ratio with a value of 2.2 ± 0.8 (CV 36.9 %) than CEs collected from the surface of PP post auricular SC (p<0.001). However, the

coefficient of variation value for PE9 samples is too large to conclude that there are any significant differences between the deeper SC layers of both anatomical sites.
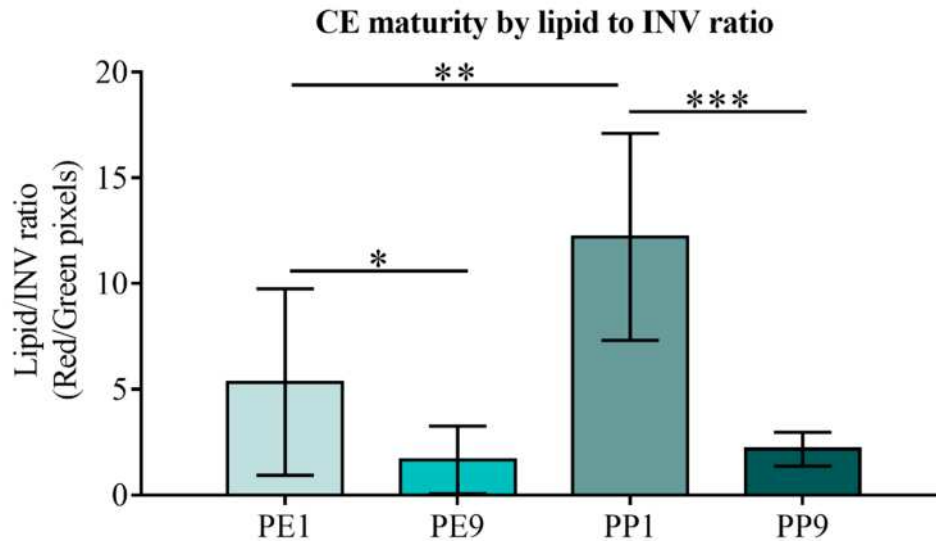
Figure 4.6. CE maturity is determined via ratio of lipids (red) and INV expression (green) fluorescence. The ratios are expressed as mean ± SD and compared via the one-way ANOVA, post-hoc Sidak-Holm test (n=14).

The visual difference in CE populations between the deeper SC layers of both anatomical sites was not reflected in the image analysis of the red/green ratio determined via the RGB channel. Furthermore, the CE surface areas were larger in samples collected from the superficial layers compared to the deeper SC layers in both anatomical sides (p<0.001). Interestingly, the CE surface area showed no difference in samples collected from the SC surface (p<0.14) between PE cheek and PP post auricular sites. Likewise, CE surface area in samples from the deeper SC layers (p<0.13) showed no difference between CEs from the PE cheek and the PP post auricular sites (Fig. 4.7).
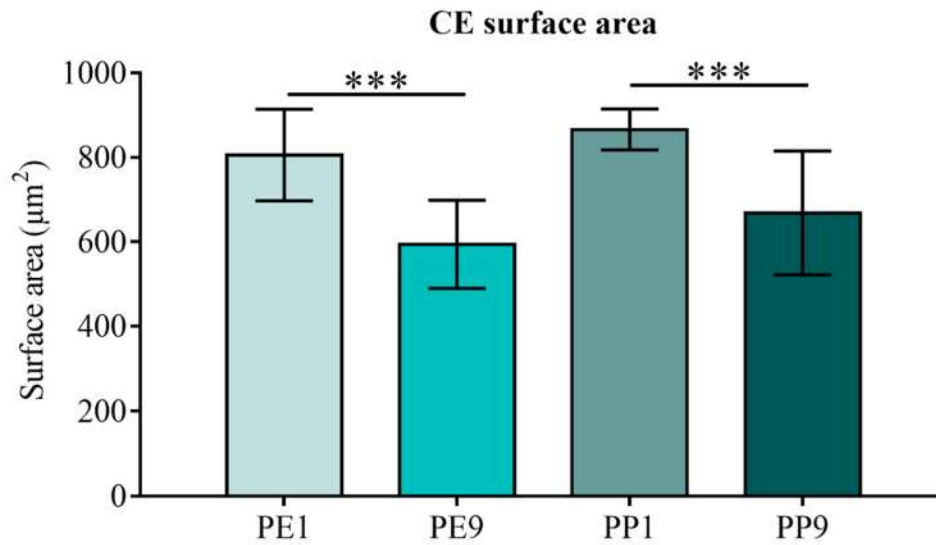
Figure 4.7. CE surface area of PE cheek and PP post auricular site. Data are shown as mean ± SD and compared with one-way ANOVA and post-hoc Sidak-Holm test (n=14).

An alternative image analysis was tested to generate the ratio of the red and green fluorescence intensity which considers the individual CE surface areas (Fig. 4.8).
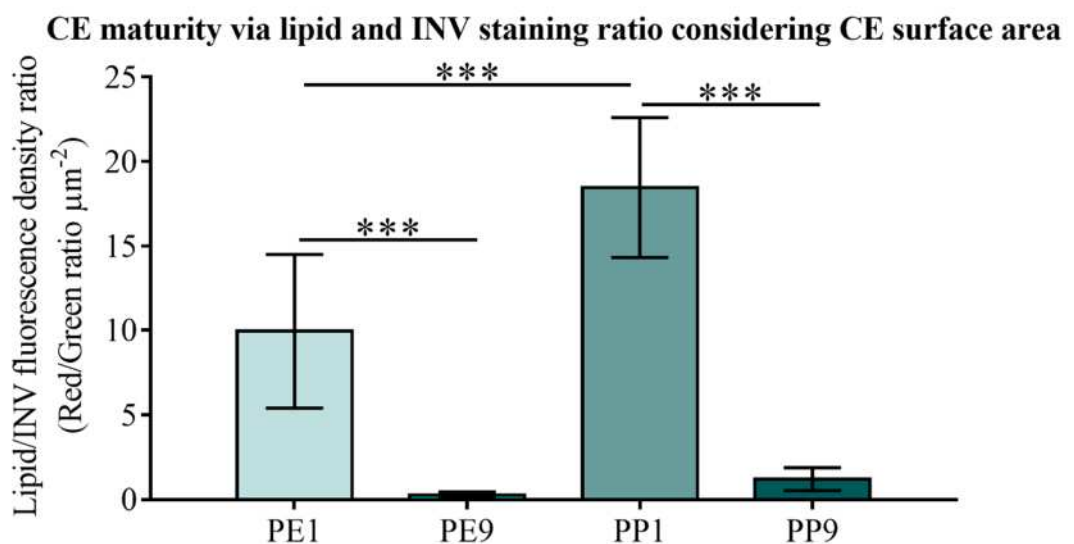
Figure 4.8. The CE maturity determined with the ratio of lipids and INV expression normalized to the CE surface area. Data are represented as mean ± SD and compared with one-way ANOVA, post-hoc Sidak-Holm test (n=14).

The ratio of red and green fluorescence normalised to the CE surface area showed that CEs from the PE1 samples are significantly more mature than those from PE9 samples ($p < 0.001$) and less mature than PP1 samples ($p < 0.001$). The original red/green ratio method showed no significant difference between PE9 and PP9 ($p < 0.69$). The ratio of fluorescence density confirms that there is no difference in CE maturity between PE9 and PP9 samples considering red and green fluorescence ($p < 0.43$). The alternative red/green ratio that considers the CE surface area shows a similar discrimination between sites and depths. However, a clear difference is visible between visual comparison and the image analysis.

4.3.2 The "new" approach to characterise CE rigidity, hydrophobicity and size

The fluorescence signal from Nile Red staining allows the visualisation of the CE lipid coating and CE morphology. CEs from PE1 samples have a higher fluorescence signal than PE9 samples but lesser intensity than PP1 samples. Post auricular CEs from the ninth tape strip have a distinctly higher fluorescence signal than CEs collected for PE9 but lower fluorescence compared to CEs from the SC surface of the PP post auricular site (Fig. 4.9).
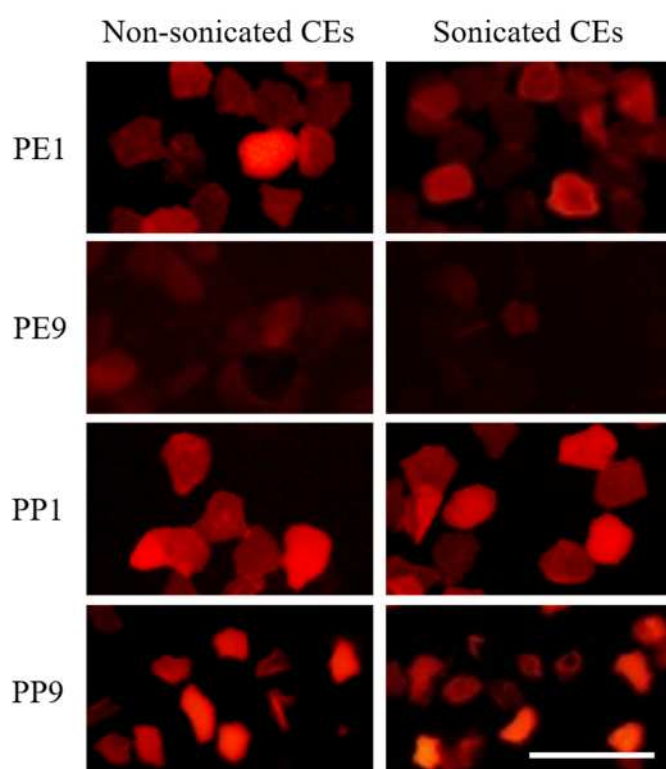
Figure 4.9. Fluorescence images of CEs before and after 10 min of sonication of PE cheek and PP post auricular sites. PE1= CEs of cheek, tape strip 1; PE9= CEs of cheek, tape strip 9; PP1= CEs of post auricular, tape strip 1; PP9= CEs of post auricular, tape strip 9. Scale bar=100 μm.

The rigidity of the collected CEs was determined from images of non-sonicated CEs and sonicated CEs. This allows the determination of the mechanical resistance in CEs obtained from both anatomical sites and depths (Fig. 4.9). The non-sonicated samples are shown as a reference for the initial rigidity before 10 min of sonication. At the SC surface the CEs have higher rigidity with 78.6 ± 8.7 % (CV 11.1 %) intact CEs in PE cheek samples and 85 ± 8.7 % (CV 10.2 %) intact CEs in PP post auricular CEs. For the same vibration force only 43.4 ± 6.5 % (CV 14.9 %) CEs in the deeper SC layers of the PE cheek remain intact while 83.2 ± 8.9 % (CV 10.7 %) of CEs from PP9 were not affected by sonication ($p<0.0001$).
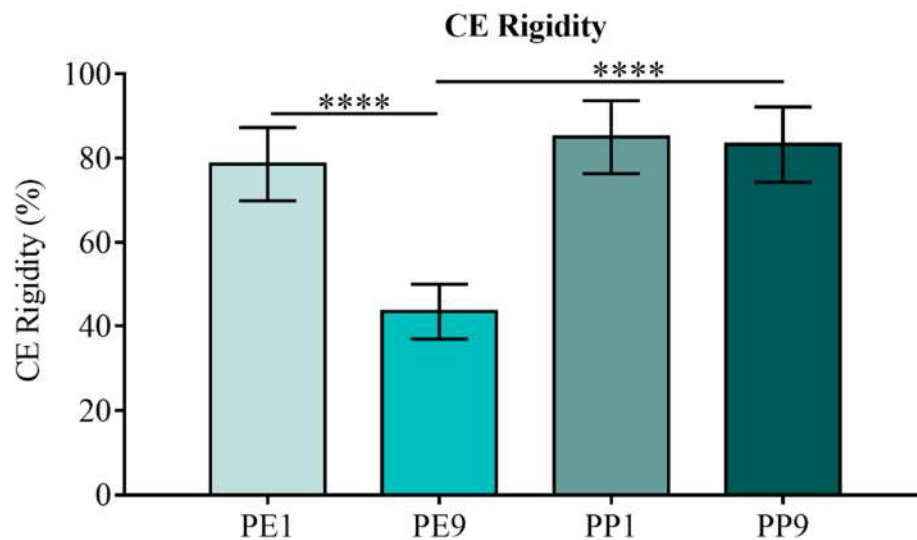
CE Rigidity

Figure 4.10. CE Rigidity in samples of PE cheek and PP post auricular sites. Data are shown as mean $\pm$ SD and differences were determined via one-way ANOVA and post-hoc Sidak-Holm test (n=14).

CE hydrophobicity was evaluated by fluorescence density for red pixels per unit surface area (Fig. 4.10) in the samples without sonication and this confirmed the visual observations (Fig. 4.9). CEs from the SC surface of the PP post auricular site have a CLE with a high lipid content visualised with a red fluorescence density of 28392 ± 5218 red pixels μm^{-2} (CV 18.4 %). The CEs from the SC surface from the PE cheek had less lipid content represented by a value of 16331 ± 3341 red pixels μm^{-2} (CV 20.5 %, $p<0.0001$). CE hydrophobicity was also significantly higher at the SC surface compared to the deeper SC layers in both anatomical sites ($p<0.0001$). The CE

hydrophobicity in CEs from the deeper SC layers of PE cheek have a fluorescence density (p<0.0001) of 9239 ± 1141 red pixels μm^{-2} (CV 12.3 %). The fluorescence density of CEs collected from the PP9 samples had a value of 18134 ± 3276 red pixels μm^{-2} (CV 18.1 %).
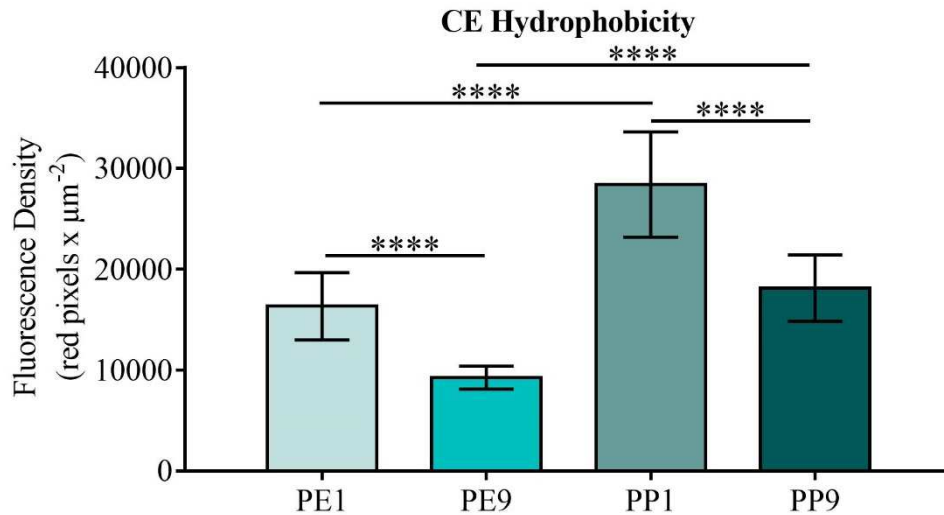
Figure 4.11. CE Hydrophobicity in non-sonicated samples of PE cheek and PP post auricular sites. Data are shown as mean ± SD and compared with one-way ANOVA, post-hoc Sidak-Holm test (n=14).

Surface area was determined for each individual CE from the first and ninth tape strips collected from the PP post auricular and PE cheek SC without sonication (Fig. 4.9). The CEs from the surface of the post auricular site were significantly larger with areas of 1262 ± 96 μm^2 (CV 7.6 %) compared to 1012 ± 116 μm^2 (CV 11.5 %) for CEs collected from the PE cheek SC surface (p<0.0001). CEs obtained from the deeper SC layers of both anatomical sites had comparable surface areas (p<0.2). The conventional (Fig. 4.7) and the novel method (Fig. 4.12) confirmed significantly different CE surface area values (p<0.0001).
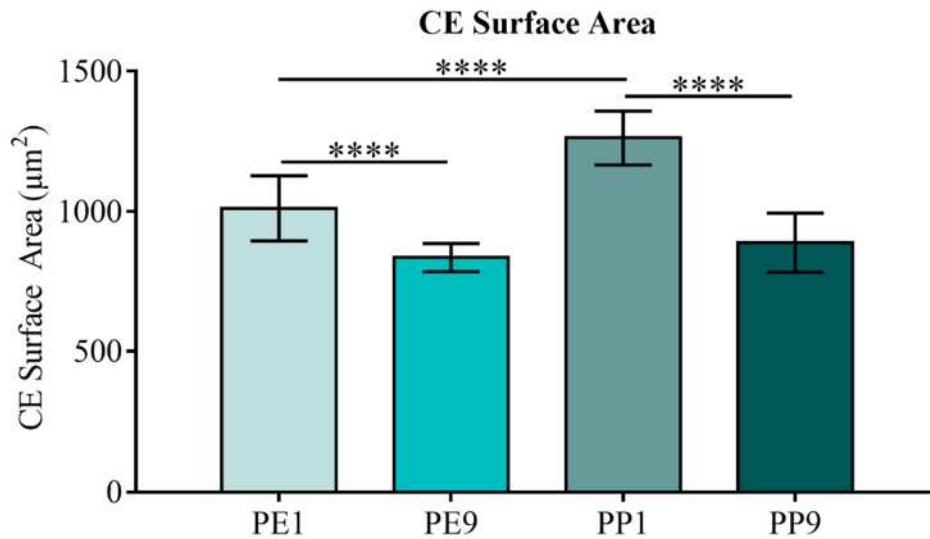
Figure 4.12. CE Surface area determined in non-sonicated CEs for both anatomical sites and depths. CE surface area is shown as mean ± SD and compared via one-way ANOVA and post-hoc Sidak-Holm test (n=14).

The three CE characteristics can be expressed as the RCEM by applying equation 4. This allows a comparison between the two anatomical sites and depths (Fig. 4.13) with a higher sensitivity than the immunostaining approach.
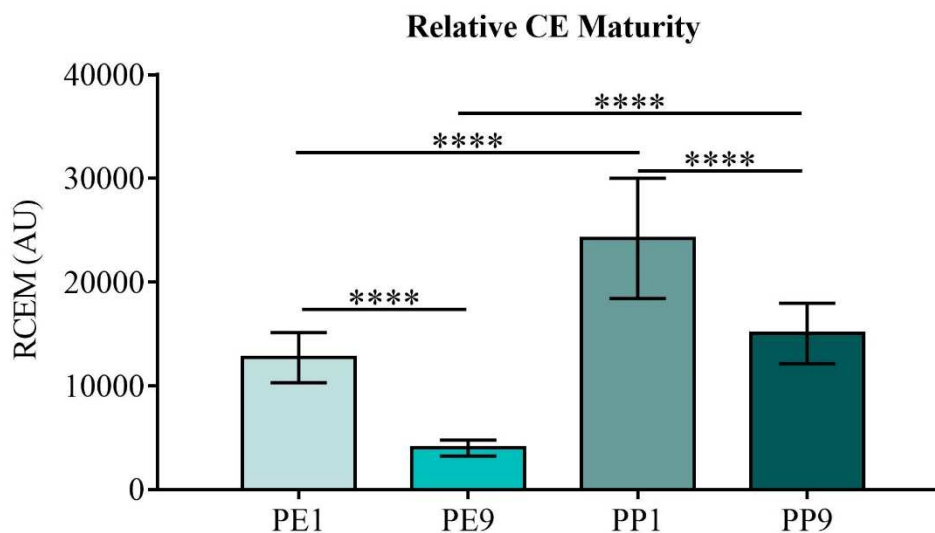
Figure 4.13. Determination of RCEM based on CE rigidity and hydrophobicity. Data are shown as mean ± SD and compared with one-way ANOVA, post-hoc Sidak-Holm test (n=14).

The arbitrary determination of RCEM revealed that samples from the SC surface of the PE cheek site have a larger population of mature CEs (12735 ± 2420 AU, CV 19.1 %) than samples taken from the deeper SC layers (4015 ± 767 AU; CV 19.1 %; p<0.0001). However, the RCEM determination that considers CE rigidity and CE hydrophobicity showed that more mature CEs are located in the SC surface of the PP post auricular site (24214 ± 5796 AU; CV 23.9 %) than the CEs obtained in the deeper SC layers (p<0.0001). This novel determination of CE maturity confirmed that there is indeed a significant difference between both anatomical sites and depths (p<0.0001). Although similar results were obtained compared with the INV (+) staining method the CV's and statistical significance were considerably smaller (p<0.0001).

Pearson's correlation coefficient (r) was analysed for the results for the SC integrity and the SC cohesion (Chapter 2) and the three image analysis approaches for INV/Nile red staining as well as the novel RCEM approach. The outcome of this statistical analysis is summarised in Table 4.2. Interestingly the conventional INV/Nile red staining and the novel RCEM approach showed different correlations to the SC integrity of both anatomical sites.

Table 4.2. Summary of Pearson's correlation coefficients between SC integrity and cohesion versus tested CE maturity approaches. Clear positive correlations are highlighted in green while negative correlations are shown in purple.

Pearson correlation coefficient	INV (+) CEs	R/G ratio	Density ratio	RCEM
PE Cheek SC integrity vs CE maturity	**0.84**	**-0.74**	**-0.88**	**-0.68**
PP Post Auricular SC integrity vs CE maturity	0.15	**0.84**	0.23	**-0.76**
PE Cheek SC cohesion vs CE maturity	**-0.88**	**0.84**	-0.42	**0.89**
PP Post Auricular SC cohesion vs CE maturity	-0.13	0.16	0.11	**0.96**

The INV/Nile red staining was used as the conventional CE maturity assay to determine the population of INV (+) CEs and the correlation to the SC integrity. This resulted in a positive correlation (r=0.84) in the PE cheek site while there was no correlation observed in the PP post auricular site (r=0.15). The same staining was evaluated via the red/green fluorescence ratio and correlated to SC integrity. Interestingly, this showed a negative correlation (r=-0.74) in the PE cheek site and a positive correlation in the PP post auricular site (r=0.84). The SC integrity was correlated with the alternative imaging analysis approach using fluorescence density ratio. The PE cheek site showed a negative correlation for CE maturity and SC integrity (r=-0.88) while there was no correlation in the PP post auricular site (r=0.23). The RCEM approach demonstrated a negative correlation between SC integrity and CE maturity in samples collected from the PE cheek (r=-0.68) site as well as the PP post auricular site (r=-0.76).

The SC cohesion and CE maturity determined via the percentage of INV (+) CEs showed a negative correlation (r=-0.88) for samples taken from the PE cheek. Interestingly, the same samples show a positive correlation between CE cohesion and CE maturity when determined with the red/green ratio (r=0.84) or the RCEM (r=0.89). Moreover, the RCEM in samples obtained from the PP post auricular site showed a clear positive correlation with CE cohesion (r=0.96) which was not detected by the other methods to determine CE maturity. This provides further confidence in the sensitivity of the new approach especially for the CE characterisation in the deeper SC layers of the PE cheek and PP post auricular sites.

4.4 Discussion

CE maturity analysis was originally based on an assessment of the CE morphology and TRITC staining [200]. Hirao and colleagues assessed CE maturity with antigenicity for the structural protein, INV, in parallel with Nile red staining for lipids [207]. The percentage of INV (+) CEs is indicative of CE immaturity in different skin conditions and ethnicities [207]. More recently, an image analysis based method was developed to detect the overall red and green pixels in an image. The RGB channel values were used to generate a descriptive ratio for Nile red stained lipids and INV visualised by FITC which is coupled to the secondary antibody. This approach has been applied to characterise CEs from the PE cheek and the PP post auricular sites of three ethnic groups. Interestingly, no difference in CE maturity was found between both anatomical sites in all tested ethnic groups which included Caucasians, Black Africans and Albino Africans living in Pretoria/South Africa. The published images for this study had a visible high background of green and red fluorescence which was not excluded in the image analysis [92].

In the present study, double staining (Nile red and INV) was evaluated for the two conventional methods and for an alternative approach. The new method determined CE hydrophobicity and mechanical integrity and was compared to the conventional methods for accuracy and sensitivity. The previously reported red/green ratio approach showed a limitation in the discrimination of CE maturity in the deeper SC layers of both anatomical sites. Visual comparison shows a clear difference between CEs collected from PE9 and PP9 sites. However, a ratio of the total red and green pixels of these images failed to detect this difference. The post auricular site had a higher protein content according to the densitometry measurement (Chapter 2). INV is one of the most abundant structural proteins that make up the CPE [96,204]. Therefore, a high protein content suggests a higher probability of detecting more INV than in a sample with less protein content. The difference of protein content in samples might lead to an inaccurate assumption for the CE maturity. The expression of INV has a genetic factor which is influenced by gene transcription and protein translation machinery and thus INV expression may differ from individual to individual [204]. Therefore, the determination of the CE maturity depends highly on INV expression and may weaken the methodology and consequently the outcome [118,212]. Moreover, the INV antibody was reported to be applied in PBS [195,196] instead of

in the presence of a blocking solution as in the original protocol [207]. The blocking solution prevents unspecific binding of the antibodies to proteins other than the protein of interest [185] However, Buchwalow and colleagues have shown that the blocking solution is an optional addition that might not make a dramatic difference to the outcome of the immunostaining [213]. The study here used the previously reported same primary and secondary antibody [195,196] to test the necessity of a blocking solution. Differences were evident in the background fluorescence in the immunostaining without blocking solution. This suggested that the primary or the secondary antibody might bind unspecifically in the absence of blocking solution. Therefore, this present study was conducted in the presence of a blocking solution containing BSA to improve antibody specificity.

The challenges of image analysis have resulted in a wide range of reported values for the red/green ratios and thus high standard errors and high CV's [115,196]. This is also the case when determining the percentage of INV (+) CEs [207,211]. Moreover, comparing results between these two methods showed clear differences. Although the red/green ratio was capable of discriminating between sun-exposed and sun-protected facial sites in tape 1 as reported previously [26], this method indicated no differences in CE maturity for the deeper samples. However, the percentage of INV (+) CEs analysis discriminates the CE maturity at all SC depths. The red/green ratio per unit CE surface area did not show any differences in CE maturity in the deeper SC layers indicating reduced sensitivity of this approach compared to the new RCEM approach. The CE surface area of CEs collected from the SC surface of the cheek has previously been reported to be 500 - 700 μm^2 with no difference compared with the post auricular site for three ethnic groups including Caucasians [92]. In this study, the tape strips were cut into halves in order to compare the conventional method and the new approach. CEs that were processed according to the conventional INV immunostaining and Nile red lipid staining showed similar outcomes for CE surface area as the reported study. Interestingly, the CEs that were processed according to the new procedure demonstrated significant differences in CE surface area for both anatomical sites and depths. The CE surface area was in fact larger in samples collected from the PP post auricular site compared with those from the SC PE cheek.

The novel method is a better choice of characterisation of CE maturity considering that the conventional method seems to influence the CE surface area. The novel approach relies strongly on CE surface area measurement and characterisation of morphology of CEs in terms of their fragile-rigid appearance as well as their hydrophobicity and rigidity hence a milder CE isolation protocol has been applied as described by Koch *et al.* [201]. The dissociation buffer with less salt and reducing agent and the washing buffer with lower detergent allowed a milder isolation process [201]. The original protocol introduced the dissociation buffer with a high salt concentration which results in a higher ionic strength that might have an impact on the resulting CE morphology [207]. The samples were re-suspended in PBS to reduce the background fluorescence observed in previous work [92]. In this present study, overall rigidity was assessed by counting CEs according to their morphological appearance with and without sonication. This mechanical stress revealed differences in the proportion of immature and fragile CEs especially in the deeper SC layers of the PE cheek site. Interestingly, PP post auricular CEs seem to be less affected by the same mechanical forces. The first and ninth tape strips indicate differences in the mechanical resistance probably mediated by crosslinking enzymes such as TG or differences in CE protein composition. A decrease in intact CEs was evident for the PE cheek CEs from the deeper SC due to sonication. CEs from the surface of the PE cheek and both SC depths of the PP post auricular sites were more resistant to sonication. The mechanical behaviour of CEs from the volar forearm has been reported previously [7]. The differences in facial CEs with increasing depth into the SC, using sonication as a mechanical challenge, is reported here for the first time. Indeed the PP9 CEs samples would be reported as immature using conventional methodology but they are clearly not immature in their response neither to mechanical stress nor in terms of their hydrophobicity.

The second assay in our approach was to determine the CE hydrophobicity per unit CE surface area rather than in relation to INV immunostaining. In this study, non-sonicated CEs were assessed to determine CE hydrophobicity. The preliminary observations showed a higher fluorescence signal after sonication which might be the result of lipid rearrangement following sonication [214]. The CEs from the cheek were previously reported to increase in hydrophobicity towards the SC surface [195,207]

which was confirmed in this study. Distinct differences were observed in CE rigidity and hydrophobicity between the PE cheek and PP post auricular sites and depths.

The SC barrier function was assessed via the TEWL measurement which is higher in skin with a lower skin barrier. The maturity of corneocytes supports the barrier function by providing hydrophobicity and mechanical stability. The RCEM approach was shown here to correlate with the barrier function which is supported by a previous study [215]. In this project, the surface areas of the CEs at the SC surface are indeed larger in both anatomical sites. However, the CEs collected from the PP post auricular site are larger than CEs from the PE cheek site. However, the surface areas of CEs from the ninth tape strip of both anatomical sites were comparable. The new approach shows differences between the anatomical sites with reference to CE surface area in the superficial SC layers that were not detectable by the INV and Nile red staining approach.

Following on from this study, the CE maturity should be determined based on CE rigidity and hydrophobicity (Eq. 4). The three parameters allow a more sensitive measurement of CE maturity than the conventional measurement of the red/green ratio and percentage of INV (+) CEs. An earlier study was not able to detect differences in CE surface area between samples collected from the PE cheek and PP post auricular site. [92]. Interestingly, the CEs from the SC surface and the deeper SC layer of the PP site shared similar mechanical characteristics. The CEs from the PE cheek showed major differences in CE rigidity compared with CEs from the superficial SC layer and the deeper SC layers. Furthermore, the red/green ratio failed to discriminate between the maturities of corneocytes from the ninth tape strip collected from the PE cheek and the PP post auricular site.

All four methods showed a correlation between CE maturity and SC integrity in the PE cheek site. However, in the PP post auricular site a negative correlation is observed with the RCEM and TEWL (see Chapter 2) which reflects the increased SC integrity with CE maturity. The INV (+) CE, red/green ratio, and RCEM showed a positive correlation between higher cumulative protein content collected and CE maturity, indicating decreased SC cohesion with CE maturity. Interestingly, the RCEM is the only approach among all tested evaluations that showed a positive correlation between CE maturity and SC cohesion. This is a further confirmation of

the sensitivity of the novel approach, especially for CE characterisation in the deeper SC layers of both anatomical sites.

Nevertheless, PE cheek corneocytes rigidify as they move towards the SC surface but they seem unable to gain increased hydrophobicity to the same extent as PP post auricular corneocytes indicating UV-induced differences in SC enzymology between the facial sites. This is supported by the recent mass-spectrometric protein analysis of PE cheek and PP post auricular SC [118]. In this study, all known proteins were identified and quantified in tape strips collected from the PE cheek and PP post auricular sites. This revealed several targets for understanding the underlying mechanism in photo-damaged skin [118]. A reduced expression of 12R-LOX was discovered in the PE cheek samples compared to the PP post auricular samples [118]. This suggests that the reduced CE hydrophobicity in the PE cheek site is the result of the lower levels of free ω-hydroxyceramides for the TG-mediated attachment to the CLE [118,216]. Equally, reduced levels of loricrin in the CPE may account for the increased CE fragility in corneocytes collected from the PE cheek site [118].

In conclusion, these findings suggest that the PP post auricular SC is thicker and less compromised by tape strippings compared with the PE cheek [112]. However, for the first time differences in CE rigidity between the PE cheek and PP post auricular sites as well as differences in hydrophobicity were demonstrated. The RCEM approach has been shown to be a more robust and sensitive assay for CE maturity than the conventional INV/Nile red staining methodology and thus a challenge to the acknowledged "Golden standard".

CHAPTER 5

Development of the 12R-lipoxygenase assay in photo-damaged skin

5. Development of the 12R-lipoxygenase assay in photo-damaged skin

5.1 Abstract

Background: Corneocytes acquire the corneocyte envelopes (CE), composed of the inner corneocyte protein envelope (CPE) and the outer corneocyte lipid envelope (CLE) during the late stage of keratinocyte differentiation. 12R-lipoxygenase (12R-LOX) pre-processes the esterified ω-hydroxy-linoleoyl-acyl-ceramides before further enzymatic catalysis and their covalent attachment to the CPE surface to form the CLE. The hydrophobicity of the CLE supports the barrier function and integrity of the stratum corneum (SC).

Objectives: The aims of this work were to develop and validate a novel enzyme activity assay for 12R-LOX and to assess 12R-LOX activity in sun-exposed facial skin.

Methods: The 12R-LOX activity was assessed in samples collected on the second and eighth tape strips of photo-exposed (PE) cheek and photo-protected (PP) post auricular SC of healthy Chinese volunteers. A fluorescence based assay was developed with ethyl linoleic acid as the substrate and a polyclonal antibody against 12R-LOX as an inhibitor. The enzyme activity was validated in the presence of a LOX inhibitor (ML351) and an eLOX3 antibody.

Results: Reduced 12R-LOX activity was observed in the samples from the outer SC layers compared to the inner layers. Moreover, markedly lower 12R-LOX activity was shown in the PE vs PP samples. Furthermore, the enzyme activity showed a positive correlation with CE maturity and a negative correlation with transepidermal water loss (TEWL).

Conclusions: A novel enzyme activity assay has been developed and validated and used to demonstrate lower 12R-LOX activity in the PE cheek for the first time. This finding is in line with the presence of less mature CEs and higher TEWL for the PE cheek compared to the PP post auricular site. Therefore this study indicates a strong link between 12R-LOX activity and CE maturation and thus SC integrity and thus the skin barrier function.

Key Words: 12R-lipooxygenase, CLE hydrophobicity, Photo-damaged skin, Corneocyte envelope maturity, skin barrier integrity.

Declaration

The results of this chapter have been reported in the *International Journal of Cosmetic Sciences* in May 2019 under the title "12R-lipoxygenase activity is reduced in photodamaged facial stratum corneum. A novel activity assay indicates a key function in corneocyte maturation".

5.2. Introduction

The stratum corneum (SC) is formed of corneocytes that are embedded in intercellular lipids (Fig. 1.3) and is a barrier to dehydration and environmental impacts [40]. Corneocytes are keratin-filled keratinocytes in which structural proteins are cross-linked and form the insoluble corneocyte protein envelope (CPE) [13]. During the same process, modified ceramide 1 is covalently attached to the CPE surface to generate the corneocyte lipid envelope (CLE). The crosslinking of proteins and attachment of lipids are mediated by transglutaminase (TG) [50] which is referred to as CE maturation [200]. The maturity of corneocytes contributes to the integrity [99] and cohesion [26] of the SC in order to support hydration of this barrier [28]. The CLE and the lamellar lipid layers form an intercellular occlusion to prevent excessive trans epidermal water loss (TEWL) [138]. Dehydration is the consequence of an impaired skin barrier function and is associated with flaky or scaly dry skin that feels rough to touch.

A variety of factors have been identified to increase the probability for dry skin that might lead to further long-term complications or susceptibilities. Frequent use of soaps and synthetic detergents were shown to increase TEWL as a measure of skin irritation [217]. Sodium dodecyl sulfate (SDS) is an anionic surfactant with amphiphilic properties and thus the most common component of detergents and cleaning products. However, low concentrations of SDS are generally found in cosmetic products and soaps. SDS removes sebum and skin lipids [218] leading to a rise in TEWL and lower SC hydration and consequently to dry skin [219]. The barrier function is restored after exposure to detergents by triggering proliferation and differentiation without causing hyper-proliferation and inflammation [220]. However, repetitive exposure to alkaline soaps could cause a long-term barrier defect by increasing the pH in the skin. In early research studies acidic pH of the SC was primarily attributed to its antimicrobial properties [18,221]. However, recent studies

have shown that the increase in skin pH causes a number of skin conditions such as atopic dermatitis [222], psoriasis [223] and autosomal recessive congenital ichthyosis [224].

Severe skin conditions are often multifactorial disorders with an environmental and genetic component. Each mammalian cell has 23 pairs of parental chromosomes in the cell nucleus which contains the genetic inheritance. Mutations in crucial genes that regulate cellular events can have beneficial or harmful consequences. In autosomal recessive conditions both parental chromosomes are faulty for a particular gene. Autosomal recessive congenital ichthyosis is a genetic skin condition with varying severity depending on the particular gene that has a faulty code. The most common genetic cause of a life-threatening skin phenotype of autosomal recessive congenital ichthyosis is associated with variations in the ATP-binding cassette A12 transporter [225]. This protein carries the lamellar granules across the keratinocyte membrane to release the lipids into the intercellular space [226]. Furthermore, mutations in the TG1 encoding gene lead to an impaired skin barrier function due to impaired CE maturation [227]. Another pathogenic trait of autosomal recessive congenital ichthyosis is observed in individuals with mutated 12R-lipoxygenase (12R-LOX) or epidermal lipooxygenase-3 (eLOX3) encoding genes [86].

The above genetic manifestations demonstrate the importance of 12R-LOX and eLOX3 in establishing a functioning epidermal barrier in mammals [86,228]. These two enzymes induce the structural changes in polyunsaturated fatty acids which are esterified in ceramide 1 (Fig. 5.1) [87]. The hydrophobic CLE is mainly composed of ω-hydroxyceramides which are derived from ceramide 1 [229], an esterified ω-hydroxyacyl-sphingosine (EOS) ceramides that is catalysed by 12R-LOX at its linoleic acid moiety [91]. The oxidation of linoleic acid in EOS results in the formation of 9R-hydroperoxide EOS that is subsequently hydrolysed to 9R, 10R epoxy-13R-hydroxy-epoxylalcohol EOS by eLOX3. The final step is the hydrolysis of 9R, 10R epoxy-13R-hydroxy-epoxylalcohol EOS to 9R(10R)-epoxy-13R-hydroxy-octadecanoic acid and the ω-hydroxyceramide [94].

Figure 5.1. The processing of esterified ω-hydroxyacyl-sphingosine to ω-hydroxyceramides initiated by 12R-LOX.

Lipoxygenases are a family of dioxygenases that oxidise polyunsaturated fatty acids such as arachidonic acids or linoleic acids. These fatty acids contain the cis-methylene interrupted by a diene structure and esters [230]. Various isoforms of lipoxygenases were identified according to their stereochemistry and the site of carbon oxidation [231]. Initially, 5(S)-LOX, 8(S)-LOX, 12(S)-LOX and 15(S)-LOX were identified to catalyse arachidonic acid at the respective carbon atom. These lipoxygenase isotypes were found mainly in platelets to form signalling lipid mediators [87]. However, 12R-LOX was found in the epidermis suggesting a local role in lipid metabolism [91]. 12R-LOX activity was tested in primary keratinocytes in a cell

culture model with arachidonic acid [232]. Later studies have shown that arachidonic acid is not a suitable substrate for 12R-LOX [94]. Prior to the development of the assay, reported in this chapter, the 12R-LOX activity was shown indirectly by measuring the formation of 9R-hydroperoxide EOS. The 12(S)-LOX and 12R-LOX were introduced into a cell line via a vector containing either one of the isoforms. Arachidonic acid and linoleic acid were tested as well as methyl esters of both fatty acids. Interestingly, 12R-LOX could only show a signal for of 9R-hydroperoxide EOS formation with the methyl linoleic acid [233]. However, the signal was not strong but significantly higher than in the presence of linoleic acid. This indicates that the enzyme-substrate affinity might depend on the ester in the linoleic acid domain of EOS. Nevertheless, the combination of lipid extraction and high performance liquid chromatography are useful experimental tools which require extensive optimisation. Immunohistochemistry has been used to characterise the expression of LOX enzymes and their distribution in healthy skin and tissue-engineered skin [234]. An artificial full-thickness skin model was used to characterise the relationship between filaggrin and 12R-LOX, eLOX3 and TG1. The knock-down of these three crucial enzymes in the formation of the CLE led to reduced filaggrin levels in the skin model [235]. Filaggrin is a structural protein that is degraded to natural moisturising factors responsible for water retention and maintenance of skin hydration [236]. The reasons for this 12R-LOX-dependent filaggrin processing remain to be further elucidated. One explanation could be that signalling molecules that may arise from processing of EOS to ω-hydroxyceramide control the proteolytic degradation of filaggrin. 12R-LOX deficient mice have shown the complete absence of filaggrin indicating an impairment of the processing of profilaggrin. Furthermore, 12R-LOX homozygous mutant mice had an impaired skin barrier with severe dehydration that led to post-natal death within 5h [89]. More recently, mass spectrometry has demonstrated low 12R-LOX protein levels in photo-damaged facial SC [118] which is associated with a thinner SC and reduced CE maturation as shown in Chapter 4 [133]. The facial SC has reduced acyl-ceramide linoleate levels and thus less ceramides are available for attachment to the CLE [237,238]. A study in non-lesioned and affected skin of patients with atopic dermatitis was compared to individuals with healthy skin. The lipids attached to the CLE were extracted and separated via thin layer chromatography. Interestingly, ω-hydroxyceramide levels were significantly reduced in affected skin and non-lesioned skin areas of patients with atopic dermatitis [239].

The aim of this project was to establish and validate an enzyme assay for 12R-LOX in order to understand its relationship to facial photo-damage. Ethyl linoleic acid was tested to serve as a substrate. Little is known about 12R-LOX as there are no specific inhibitors and only a few antibodies have been described. The enzyme activity was validated using a 12R-LOX antibody while excluding other LOX enzymes via inhibitor or antibody. This would provide a faster and more sensitive approach to assess 12R-LOX activity. Furthermore, the Pearson's correlation coefficient was determined to assess the relationship between 12R-LOX activity and the SC integrity (Chapter 2) as well as Relative CE Maturity (Chapter 4). This is the first time that the 12R-LOX activity was measured in CE samples from tape strippings of PE cheek and PP post auricular sites.

5.3 Materials and methods

5.3.1 Materials and equipment

The materials and equipment used to extract crude protein of CE samples collected via tape stripping of PE cheek and PP post auricular sites and establish the 12R-LOX activity assay are shown in Table 5.1.

Table 5.1. Materials and equipment to obtain protein extracts of tape strips and develop the 12R-LOX assay.

Materials/Equipment	Supplier
Black 96-well plates	Sigma Aldrich, Dorset, UK
Ethylene diaminetetraacetic acid (EDTA)	
Tris	
Calcium chloride	
Ethanol	
Ethyl linoleic acid	
Bovine Serum Albumin (BSA)	
Tergitol^{TM} (NP40)	
Dimethyl sulfoxide (DMSO)	
SpectraMax iD3	Molecular Devices, Berkshire, UK
Polyclonal Rabbit-Anti-human primary 12R-LOX AB (α12R-LOX) Thermo Fisher Scientific Cat# PA5-23608, RRID:AB_2541108	Thermo Fisher Scientific, Hertfordshire, UK
2',7'-dichlorodihydrofluorescein diacetate (H$_2$DCFDA)	
Pierce^{TM} Protease Inhibitor Tablets	
Bio-Pure™ pipetting reservoir	VWR international Ltd, Leicestershire, UK
1.5 mL reaction tubes	
Forceps and small scissors	

Materials/Equipment	Supplier
Polyclonal Rabbit-Anti-human primary eLOX3 AB (αeLOX3) Biorbyt Cat# orb41336, RRID:AB_10998919	Biorbyt Ltd., Cambridgeshire, UK
GraphPad Prism® (Version 7)	GraphPad Software, San Diego, CA, USA
5-(methylamino)-2-(1-naphthalenyl)-4-oxazolecarbonitrile (ML351)	Cayman Chemical, Ann Arbor, Michigan, USA
Pure argon gas	Boc Gas & Gear, Slough, UK
Table top centrifuge 5418 R	Eppendorf Ltd, Stevenage, UK
ThermoMixer F1.5	
12 channel multi-pipette	

5.3.2 Methods and study design

A computer model has studied the docking of EOS and its orientation in the active site of 12R-LOX. This model showed that 12R-LOX activity is 10-times higher when the substrate is non-ionised at pH 6. Furthermore, EOS is recognised at C-12 of the linoleic acid domain. The esterified part of linoleic acid enters the active site of 12R-LOX [240].

The general concept of this assay is to show that ethyl linoleic acid can be used as a substrate of 12R-LOX as EOS is not commercially available. Furthermore, no blocking agent has been commercially released for 12R-LOX to date, thus an antibody against the C-terminus was chosen. As mentioned in Chapter 3, antibodies bind to the recognition site for their antigen thus this could be used in an *in vitro* set up to spatially block the catalytic site of 12R-LOX. The oxidation of ethyl linoleic acid produces reactive oxygen species that reduces 2',7'-dichlorodihydrofluorescein diacetate (H_2DCFDA) to the fluorescent 2′,7′-dichlorofluorescein (DCF) (Fig. 5.2).
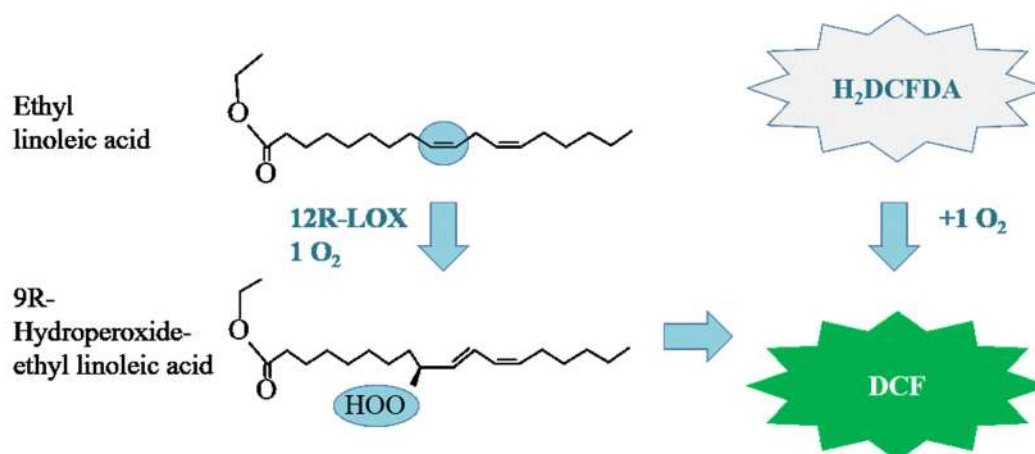
Figure 5.2. 12R-LOX activity is detected by the reduction of non-fluorescent H_2DCFDA to fluorescent DCF.

5.3.2.1 The 12R-LOX activity assay

Crude protein was extracted from the second and eighth tape strip of SC samples of photo-exposed (PE) cheek and photo-protected (PP) post auricular sites of healthy Chinese volunteers (Chapter 2).

Various aspects had to be considered while developing this assay due to the sensitivity of H_2DCFDA. Thus every component of the reaction was purged with pure argon gas to replace oxygen to prevent unspecific oxidation. In theory, an enzyme binds to its substrate and forms an enzyme-substrate complex. The enzyme catalyses the substrate which leads to a chemically changed product and by-product. Michaelis-Menten kinetics are a powerful tool to determine the enzyme activity rate by considering the product formation and substrate concentration. The substrate concentration that leads to the half maximal reaction velocity is termed as the Michaelis constant (K_M) which also describes the affinity of substrate and enzyme. A small K_M value hints towards a high affinity for the enzyme thus a low substrate concentration is enough to reach the maximum velocity [241]. However, this is not only dependent on substrate and enzyme but also on pH and temperature. This has to be considered when developing an enzyme assay.

The 12R-LOX activity assay was adapted from Singh and colleagues' approach to detect 5-LOX, 12-LOX and 15-LOX activities [242]. The crude protein extract was isolated from the tapes using 0.1% Tergitol^{TM} (NP40) in 50 mM Tris (pH 6.5) with Pierce^{TM} Protease Inhibitor Tablets (1 per 10 mL) for 20 min on a shaker with 600 rpm at 4 ℃. The reaction buffer was composed of 50 mM Tris, 4 mM CaCl$_2$, 4 mM EDTA, 0-50 µM ethyl linoleic acid, 5 µM ATP and 5 µM H$_2$DCFDA. The catalytic activity of 12R-LOX is dependent on ATP [243] and calcium [233]. However, the concentration of ATP and calcium in the crude protein mix is unknown as ATP may have degraded [244] while calcium may be depleted. Therefore, ATP and calcium were added into the reaction buffer. The 12R-LOX antibody and the eLOX3 antibody are polyclonal and were pretested in immunostaining which is shown in Chapter 3. This was performed to confirm that the 12R-LOX is blocked antigen specific binding and causes the inhibition of resulting fluorescence signal. The 12R LOX and eLOX3 antibodies were diluted in purged 0.01% BSA and added to the reaction buffer. Furthermore, the blocking agent 5-(Methylamino)-2-(1-naphthalenyl)-4-oxazolecarbonitrile (ML351) was used to block 5-LOX, 12-LOX and 15-LOX activities [245]. This could exclude the appearance of fluorescence from LOX activity therefore (0-400 nM) ML351 in DMSO was added to the reaction buffer. The Michaelis-Menten plot was determined with a range of ethyl linoleic acid concentrations to confirm the K$_M$ and a suitable concentration for the remaining experiments. This assay was conducted with 50 µL crude protein sample and purged 150 µL reaction buffer and measured in a black 96-well plate with a clear flat bottom. The appearance of DCF was measured at Ex/Em: 495/527 nm in a SpectraMax iD3 at an interval of 1 min for 20 mins at 37 ℃. 12R-LOX activity was expressed as U/min normalised to the total SC protein on tape strips.

5.3.2.2 Statistics

The mean and standard deviation (SD) were determined for 14 samples and the D'Agostino & Pearson normality test was applied. The statistical differences were analysed via One-way ANOVA for Michaelis-Menten kinetics. Two-way ANOVA comparison was used to determine the differences between the control and different concentrations of blocking agents. This leads to four groups that are compared for their effects while considering two variables within the measured differences. Both types of ANOVA comparison were corrected with the Sidak-Holm post-hoc test. The statistical differences are expressed as follows: * $p \leq 0.05$, ** $p \leq 0.001$, *** $p \leq 0.0002$ and **** $p \leq 0.0001$. The Pearson's correlations was assessed between 12R-LOX activity and the SC integrity (Chapter 2) and Relative CE Maturity (Chapter 4).

5.3 Results

In principle, this assay detects the reduction of H_2DCFDA to the fluorogenic DCF by the reactive oxygen species created during the enzymatic reaction of LOX enzymes. A crude protein extract was used to determine the 12R-LOX activity in the PE cheek and PP post auricular samples.
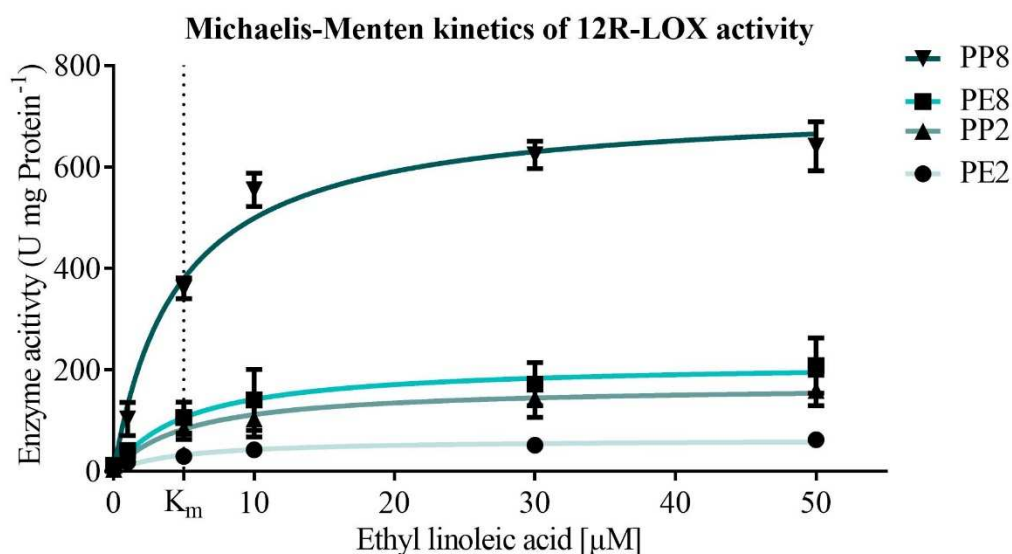
Figure 5.3. Determination of Michaelis-Menten kinetics of 12R-LOX activity with ethyl linoleic acid from samples of PE cheek and PP post auricular site (tape 2 and 8). Data are shown as mean ± SD (n=14).

The Michaelis-Menten kinetics were generated by plotting the enzyme activity at different concentrations of ethyl linoleic acid. All four samples reached their K_M value at $4.91 \pm 0.31\ \mu M$ (Fig. 5.3). The maximal reaction velocity of 12R-LOX in the tested samples showed a 3x higher value (p≤0.0001) in PP post auricular samples compared to PE cheek samples.

The antibody against 12R-LOX was used to demonstrate that the fluorescence arises from 12R-LOX activity thereby excluding unspecific signal detection. A concentration-dependent decrease in 12R-LOX activity was observed in the presence of the 12R-LOX antibody. The fluorescence signal was unchanged in the presence of the control supplemented with 0.01% BSA as well as at the lowest antibody

concentration (1:50000). A significant decrease in enzyme activity was obtained in the samples that were supplemented with 1:5000 12R-LOX antibody diluted in the reaction buffer. Samples collected from the SC surface of the PE cheek ($p \leq 0.05$) and the PP post auricular site ($p \leq 0.0001$) showed a lower fluorescence signal compared to the BSA control and reaction buffer containing diluted 1:50000 12R-LOX antibody. This difference in 1:5000 and the control reactions (BSA as well as baseline) was greater in the deeper SC samples of PE cheek ($p \leq 0.0001$) and PP post auricular sites ($p \leq 0.0001$). Reaction buffer containing diluted 1:500 12R-LOX antibody solution reduced the resulting fluorescence signal to a minimum for samples from both anatomical sites. However, samples from the PP post auricular site show the largest discrepancy between control BSA and enzyme activity in samples from the SC surface ($p < 0.0001$) and deeper SC layers ($p < 0.0001$). These results suggest that the 12R-LOX antibody inhibits the catalytic activity of 12R-LOX (Fig. 5.4). However, this statement needs further validation to exclude other LOX enzymes.
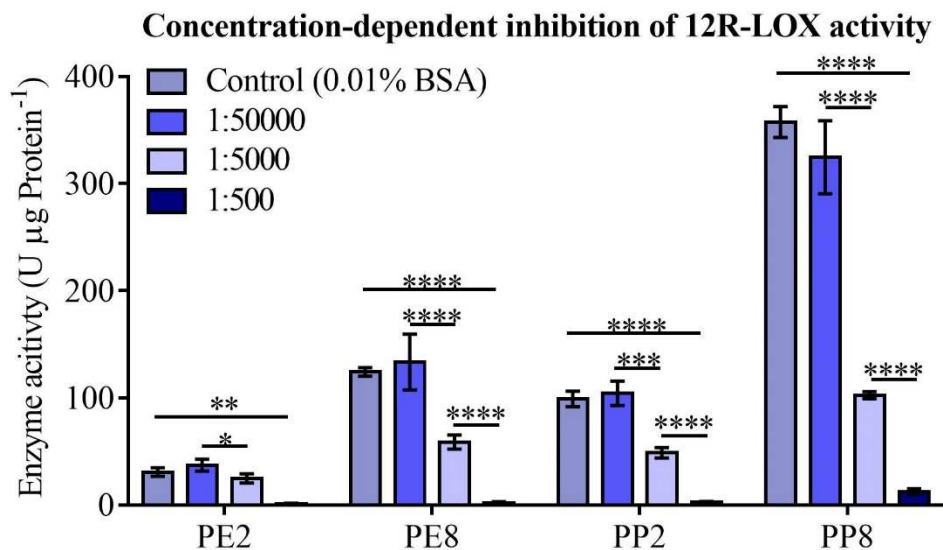
Figure 5.4. A dilution factor of 1:500 was an effective contraction of the 12R-LOX antibody to inhibit the formation of the fluorescence signal in samples of both anatomical sites and depths. Data are shown as mean ± SD and compared with two-way ANOVA, post-hoc Sidak-Holm test (n=14).

The resulting fluorescence signal was validated by excluding eLOX3 activity. The enzyme reaction was performed with the eLOX3 antibody instead of the 12R-

LOX antibody. Interestingly, the fluorescence signal was not influenced in the presence of the eLOX3 antibody at any of the tested concentrations (Fig. 5.5). This confirms that the 12R-LOX antibody blocked the enzyme reaction that generates the reactive oxygen species while processing ethyl linoleic acid.
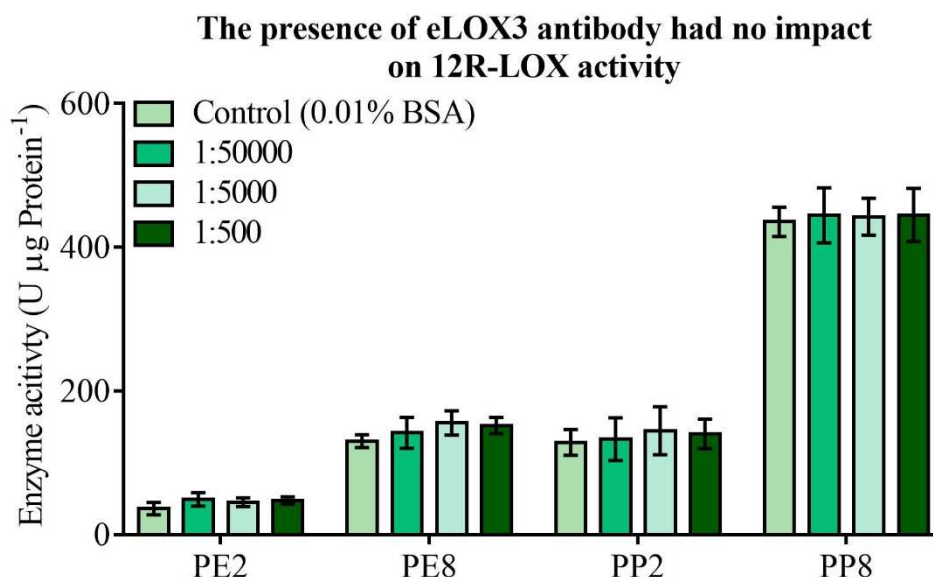
Figure 5.5. The eLOX3 antibody showed no influence on the fluorescence signal resulting from the DCF formation. Data are shown as mean ± SD and compared with two-way ANOVA, post-hoc Sidak-Holm test (n=14).

An additional assay was performed to exclude non-specificity of this enzyme assay and for additional verification that the fluorescence signal is a by-product of 12R-LOX activity. The assay condition remained the same as for the previous experiments, however, ML351 or its vehicle DMSO was added to the reaction buffer. The influence of 5-LOX, 12-LOX and 15-LOX on this enzyme assay was inhibited using ML351. The fluorescence signal showed no difference in the presence of ML351 at any tested concentration to its vehicle DMSO (Fig. 5.6). The reduction of H_2DCFDA was blocked in the presence of the 12R-LOX antibody but not with the eLOX3 antibody nor ML351.
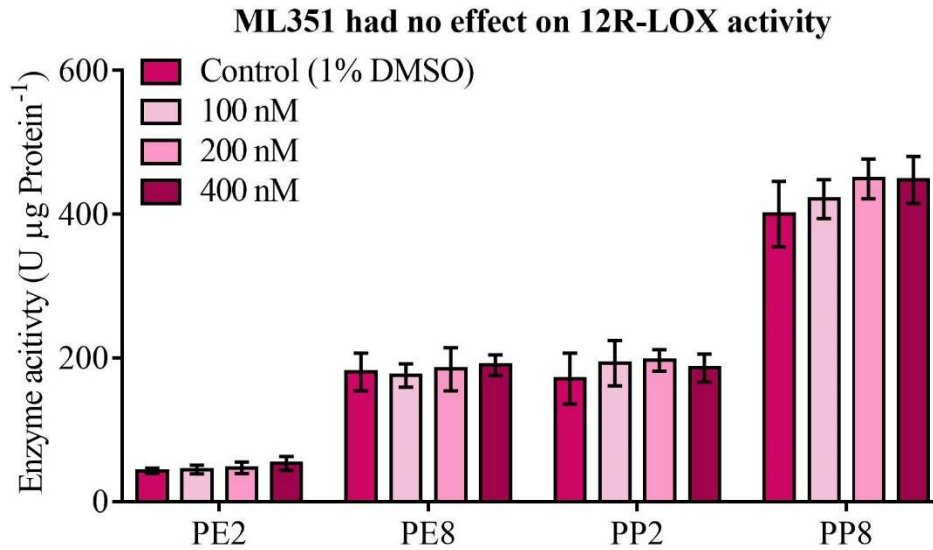
ML351 had no effect on 12R-LOX activity

Figure 5.6. The enzyme activity was unaffected by any of the ML351 concentrations which block 5-LOX, 12-LOX and 15-LOX. Results are shown as mean ± SD and compared with two-way ANOVA, post-hoc Sidak-Holm test (n=14).

This enzyme assay determined the 12R-LOX activity in sun-damaged facial skin samples obtained via tape stripping. The Pearson correlation coefficient was analysed to demonstrate the relationship between maturity of CEs from the first and ninth tapes (Chapter 4) and the 12R-LOX activity on the second and eighth tapes of PE cheek and PP post auricular samples (Tab. 5). The CE rigidity in samples from the PE cheek SC surface (r=0.88) and the deeper SC layer of PE cheek (r=0.91) showed a positive correlation with the 12R-LOX activity in the corresponding layers. The same correlation was observed between 12R-LOX activity and CE rigidity in samples taken from PP post auricular sites at the surface (r=0.94) and in the deeper layers (r=0.97). Moreover, the 12R-LOX activity showed a strong positive correction with CE hydrophobicity in samples from the PE cheek SC surface (r=0.93) and deeper SC layers (r=0.90). The same positive correlations were observed between 12R-LOX activity and CE hydrophobicity in samples from surface of the PP post auricular SC (r=0.97) and the deeper SC layer (0.96). The RCEM depends on the CE rigidity and hydrophobicity and thus the RCEM showed a positive correlation with the 12R-LOX activity in both anatomical sites and depths.

Table 5.2. Summary of Pearson correlation coefficient for 12R-LOX activity and the CE properties.

Pearson correlation coefficient	CE Rigidity	CE Hydrophobicity	RCEM
Surface of PE Cheek SC 12R-LOX activity	0.88	0.93	0.93
Deeper layer of PE Cheek SC 12R-LOX activity	0.91	0.90	0.94
Surface of PP Post auricular SC 12R-LOX activity	0.94	0.97	0.95
Deeper layer of PP Post auricular SC 12R-LOX activity	0.97	0.96	0.98

Collectively, this indicated a strong positive correlation between CE maturity in samples from the SC surface (r=0.98) and deeper SC layers (r=0.98) and the corresponding 12R-LOX activity (Fig. 5.7).
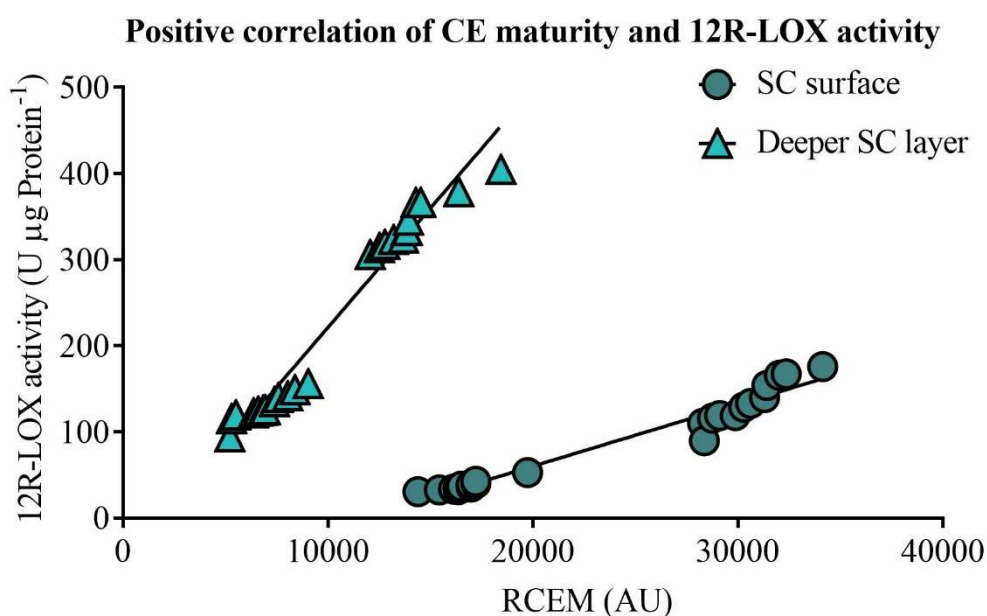
Figure 5.7. A positive correlation has been demonstrated between high 12R-LOX activity and more mature CEs in the SC surface and deeper SC layers.

SC integrity is shown by measuring TEWL before tape stripping (Chapter 2) which is correlated with high 12R-LOX activity. A negative correlation was observed between TEWL measurements and 12R-LOX activity in samples of the PE cheek (r=-0.97) and samples from the PP post auricular sites (r=-0.92) (Fig. 5.8). The Pearson correlation analysis demonstrated a strong negative correlation with high TEWL and low 12R-LOX activity in the corresponding samples (r=-0.95).
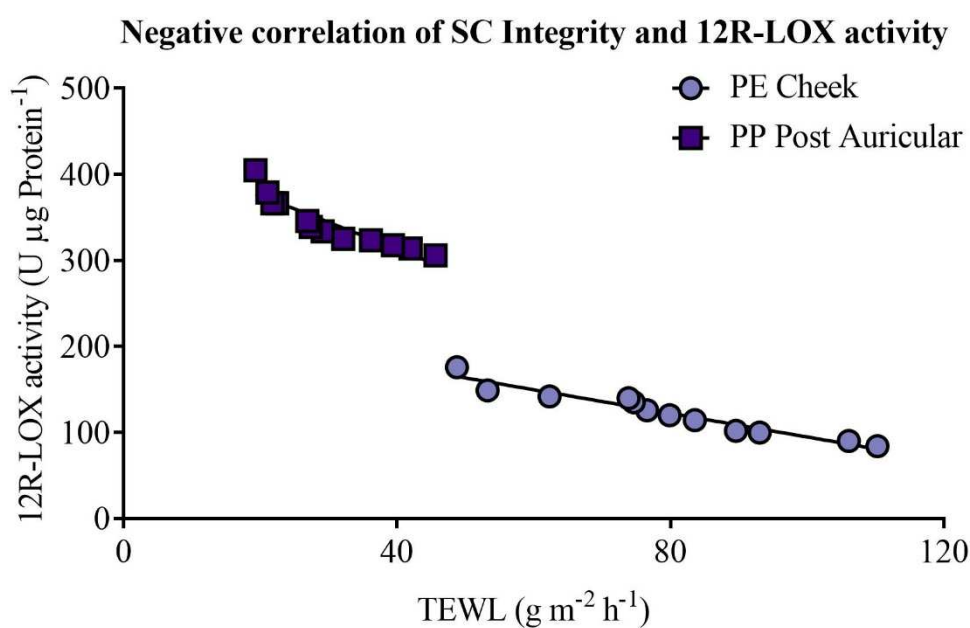
Figure 5.8. A negative correlation was shown between low 12R-LOX activity and high TEWL measurements in both anatomical sites.

This assay was developed to measure the 12R-LOX activity by the resulting fluorescence signal that appears from the reduction of H_2DCFDA to DCF. Ethyl linoleic acid served as a substrate which showed a concentration dependent increase in fluoresence. The lack of specific 12R-LOX inibitor was overcome by using alternatives to validate the fluorescence signal as a result of 12R-LOX activity. The presences of the 12R-LOX antibody reduced the enzyme activity in a concntration-dependent manner while the control with BSA had no impact on the signal. An antibody against eLOX3 had no effect on the enzyme activity and thus the enzyme eLOX3 was excluded to cause the reduction of H_2DCFDA. 5-LOX, 12-LOX and 15-

LOX were excluded collectively by using the ML351 in the reaction buffer. Conclusively, the resulting fluorescence signal is a result of 12R-LOX activity.

A positive correlation was shown between high 12R-LOX activity and mature CEs in both anatomical sites and depths. Furthermore, a negative correlation was demonstrated between low 12R-LOX and elevated TEWL values in PE cheek and PP post auricular sites. This study introduced a new enzyme activity assay for 12R-LOX of samples obtained via tape stripping. A link was shown between 12R-LOX activity and the CE maturity and the SC integrity.

5.4 Discussion

In 1930, the early work of Burr & Burr identified the important role of essential fatty acid-containing lipids in skin physiology [52]. Later studies showed that these lipids are by-products of linoleoyl-acyl-ceramides by lipoxygenases in the skin [71,246]. Brash and collaborators have discovered that 12R-LOX is responsible for the conversion of linoleate-containing EOS ceramides [91,94]. These studies identified 12R-LOX as a crucial enzyme involved in the CLE formation and thus the formation of the epidermal barrier [247,248]. The importance of 12R-LOX has been shown in genetic studies linking 12R-LOX deficiency to autosomal recessive congenital ichthyosis [228]. The formation of the skin barrier has been shown to be impaired in 12R-LOX knockout mice to the extent that the neonates would die of excessive dehydration within hours. Heterogeneous mutation in the 12R-LOX gene led to mice with an impaired skin barrier function but not with lethal consequences. Furthermore, heterogeneous 12R-LOX knockout mice had fragile corneocytes [89]. This chapter focused on sun-damaged facial skin which has been shown to have compromised SC integrity (Chapter 2), less CE maturation (Chapter 4) [92,141,195] and low 12R-LOX protein mass levels [118]. Reduced 12R-LOX mass levels were also observed in Albino Africans who are more susceptible to photo damage compared to Black Africans and Caucasians living in South Africa [249]. Furthermore, an age-related reduction in CLE-bound ceramides has been reported [250]. However, the enzyme activity of 12R-LOX has not been determined in these conditions as no suitable assay was available.

The present work adapted a previously published fluorogenic LOX method [242] and is the first demonstration of the catalytic activity of 12R-LOX in samples collected via tape strippings. 12R-LOX has drawn the attention of skin experts due to its link to the barrier function. However, EOS ceramides as substrates and selective inhibitors are not yet available therefore an alternative approach had to be developed. Ethyl linoleic acid was chosen as the substrate as it resembles the esterified linoleic acid domain in EOS ceramide. The detection agent, H_2DCFDA, is reduced to the fluorescent DCF in the presence of reactive oxygen species. However, the resulting fluorescence signal had to be validated to originate from 12R-LOX activity and not eLOX3, 5-LOX, 12-LOX or 15-LOX.

Antibodies are natural glycoproteins that detect and bind a specific sequence of an antigen. The immunostaining studied, in Chapter 3, demonstrated the affinity and detection of the 12R-LOX and eLOX3 antibody in corneocytes in samples from SC surface and deeper layers of the PE cheek and the PP post auricular sites. In fact, the eLOX3 antibody was ineffective in reducing the detected fluorescence signal. This confirms a specific inhibition by the 12R-LOX antibody and excludes non-specific spatial hindrance. A non-specific LOX inhibitor (ML351) in DMSO was added to the reaction buffer to eliminate 5-LOX, 12-LOX and 15-LOX activities. The presence of DMSO enhanced the fluorescence signal compared to the baseline 12R-LOX activity which is consistent with studies on the LOX enzymes [233,242].

In the late 1980s, the hydroxylated linoleoyl ceramides were identified as important compounds in the epidermis [246]. The enzyme involved in the generation of these ceramides was identified as the 12R-LOX and characterised via cloning and mechanistic studies [91]. Studies demonstrated reduced 12R-LOX mass levels in photodamaged facial skin [118] which guided this 12R-LOX activity-based study. A novel 12R-LOX activity assay was developed using ethyl linoleic acid and inhibition by the 12R-LOX antibody. Interestingly, samples from the photo protected site had a considerably higher 12R-LOX activity compared to samples from the PE cheek site. The high 12R-LOX activity in samples from the post auricular site contributes to the more pronounced CE hydrophobicity. Consequently, the high 12R-LOX activity and enhanced CE maturity support the SC integrity more effectively in the PP post auricular site. This assay provides the activity profile of 12R-LOX activity in the SC and reduced activity in photo-damaged SC which correlates with poor CE maturity and SC integrity. This assay should be of use in studies of SC maturation. The 12R-LOX enzyme could be used as a biomarker for topical treatments aimed at improving CE maturation as well as to probe underlying mechanisms of skin disorders.

CHAPTER 6

The impact of relative humidity on ex vivo corneocyte envelope maturation and their enzymes

6. The impact of relative humidity on *ex vivo* corneocyte envelope maturation and their enzymes

6.1 Abstract

Background: Corneocyte envelopes (CE) are made up of the corneocyte protein envelopes (CPE) surrounded by a corneocyte lipid envelope (CLE). 12R-lipoxygenase (12R-LOX) processes linoleoyl acylceramides followed by other enzymes to form ω-hydroxyceramides. These are attached to the CPE by transglutaminase (TG) while cross-linking the structural proteins. This leads to the gain in hydrophobicity, rigidity and surface area with CE maturation.

Objectives: The primary aim of this work was to demonstrate the impact of relative humidity (RH) on *ex vivo* CE maturation. Low, optimal and high RH were selected to investigate the effect of protease inhibitors (PI) on CE maturation and TG activity; in addition, 12R-LOX and Cathepsin D (CathD) activity were measured at optimal RH. Finally, glycerol was tested at low, optimal and high RH to determine its effect on *ex vivo* CE maturation.

Methods: The first and ninth tape strip of photo-exposed (PE) cheek and photo-protected (PP) post auricular sites were selected to assess CE maturation after *ex vivo* maturation. *Ex vivo* CE maturation was determined for CE rigidity and hydrophobicity in the presence of a TG inhibitor, a 12R-LOX inhibitor or a mixture of PI. The second and eighth tapes from the same healthy volunteers were tested for TG, 12R-LOX and CathD activity.

Results: 70% RH showed the optimal condition for *ex vivo* CE maturation. Irrespective of tape stripping depth, PE samples showed CE rigidity to the same extent as mature CEs from the PP site, but not CE hydrophobicity. The inhibition of 12R-LOX activity resulted in enhanced CE rigidity which was reduced by the TG inhibitor. CE hydrophobicity remained unchanged during *ex vivo* maturation in the presence of TG or 12R-LOX inhibition. CE hydrophobicity was enhanced in the presence of glycerol at 44% RH and 100% RH but not at 70% RH. TG activity was significantly reduced at 100% RH, however, a PI mix reversed this negative effect.

Conclusions: The study adds to the understanding of the roles of 12R-LOX and TG activity in CE maturation, and gives further insight into the effect of glycerol.

Key Words: *Ex vivo* CE maturation, Relative Humidity, Photodamaged skin.

Declaration

The results of this chapter have been reported in the International Journal of Cosmetic Science in August 2019 with the title "The importance of 12R-lipoxygenase and transglutaminase activities in the hydration-dependent *ex vivo* maturation of corneocyte envelopes"

6.2. Introduction

Corneocytes have two structural features, a network of keratin filament bundles stabilised by disulfide bonds. This network is surrounded by covalently cross-linked structural proteins [40] creating an insoluble CPE [13]. The phospholipids of the cell membrane are degraded to generate free fatty acids and this provides space [19] for the covalent attachment of ω-hydroxyceramides to form the CLE [229]. These two processes lead to an increase in rigidity and hydrophobicity of CEs leading to their maturation which continues progressively during cornification [102,200]. The cross-linking of structural proteins in the CPE [95] and the attachment of processed ceramides and fatty acids to the CLE are catalysed by TG [50]. Intermediate thiolester acryl-enzyme complexes are formed with the purpose of transferring the acyl residue to a primary amine [95]. Generally, the amino acceptor is the ε-amino group of a protein-linked lysine to form N^6-(γ-glutamyl)lysine isopeptide bond [95,251]. There are three subtypes of TG expressed in the stratum spinosum of the epidermis, namely TG1 [252], TG3 [253], and TG5 [254]. Interestingly, each of these three subtypes has a role during cornification but at different time points or circumstances. However, TG2 is only expressed under specific circumstances such as wound healing as a support for the other epidermal TGs [255,256]. TG5 was shown to be less expressed than TG1 in healthy skin, however, TG5 is overexpressed in pathological skin conditions. TG5 is commonly associated with hyperkeratotic phenotype such as ichthyosis and psoriasis [257]. TG3 was the first transglutaminase to be characterised [258] which was later on identified to be a soluble proenzyme which is activated upon proteolysis [259]. However, TG3 is considerably less expressed than TG1 which is the main cornifying enzyme [260]. The formation of the CE is ultimately dependent on TG1 activity [261]. This subtype was thought to be preliminary membrane-bound, however, soluble TG1 has been found in the upper SC layers [262]. Two independent studies have shown that in fact, membrane-bound TG1 is the minority TG1 while up to 80% of TG1 was shown to be the soluble type [51,263]. Furthermore, the TG1 activity has been shown to be

enhanced by CathD which exposes further catalytic active sites of the enzyme. However, this study also showed that excessive CathD is gradually reducing TG activity [264]. Interestingly, CathD was shown to be lysosomal aspartyl protease that enhances in activity in the presence of the co-factor ceramide derived from acid sphingomyelinase [265]. Thus, ceramides in the extracellular space activate the protease that enhances the activity of TG1 to build up the CLE [125]. However, CathD has also been shown to be over-expressed in chronically sun-damaged skin which is thought to act as a compensatory mechanism to improve the impaired skin barrier by releasing TG1 and enhancing its activity [119,120]. However, CE maturation by TG1 depends on the availability of ω- hydroxyceramides in order to form the hydrophobic CLE [50]. The generation of this particular ceramide is initiated by 12R-LOX catalysing the precursor linoleoyl acylceramides [89,214]. This is coordinated with CathD liberating the membrane-bound TG1 which enhances the catalytic activity to interconnect INV and the covalent attachment of ω-hydroxyceramides to the CPE to form the CLE resulting in mature CEs (Fig. 6.1). Mature corneocytes subsequently contribute to SC integrity [99] and SC cohesion [26] thus supporting the SC barrier function [28].

The skin physiology has been reported to be affected by environmental changes such as the relative humidity (RH) [49,266]. Murine models demonstrated that the skin barrier is formed more efficiently in mice maintained at conditions of 50-75% RH compared to higher RH levels (above 85%) [267]. A later study demonstrated that hairless mice developed a thicker epidermis with a thicker SC at dry RH (10%) compared to 40-70% RH [268]. These two studies indicate two general factors. Firstly, RH may promote proliferation of epidermal stem cells in the basal layer which has been demonstrated with increased DNA synthesis in mice kept at 10% RH. Furthermore it was hypothesised that low RH leads to increased TEWL which induced epidermal cell proliferation [269]. The second factor is that high humidity has an impact on the protease activity in the SC with consequences for filaggrin degradation [270–272], skin hydration [273,274], skin integrity [268] and desquamation [275]. Aside from these studies, little is known about the effect of RH on corneocyte maturation [49,210,266].
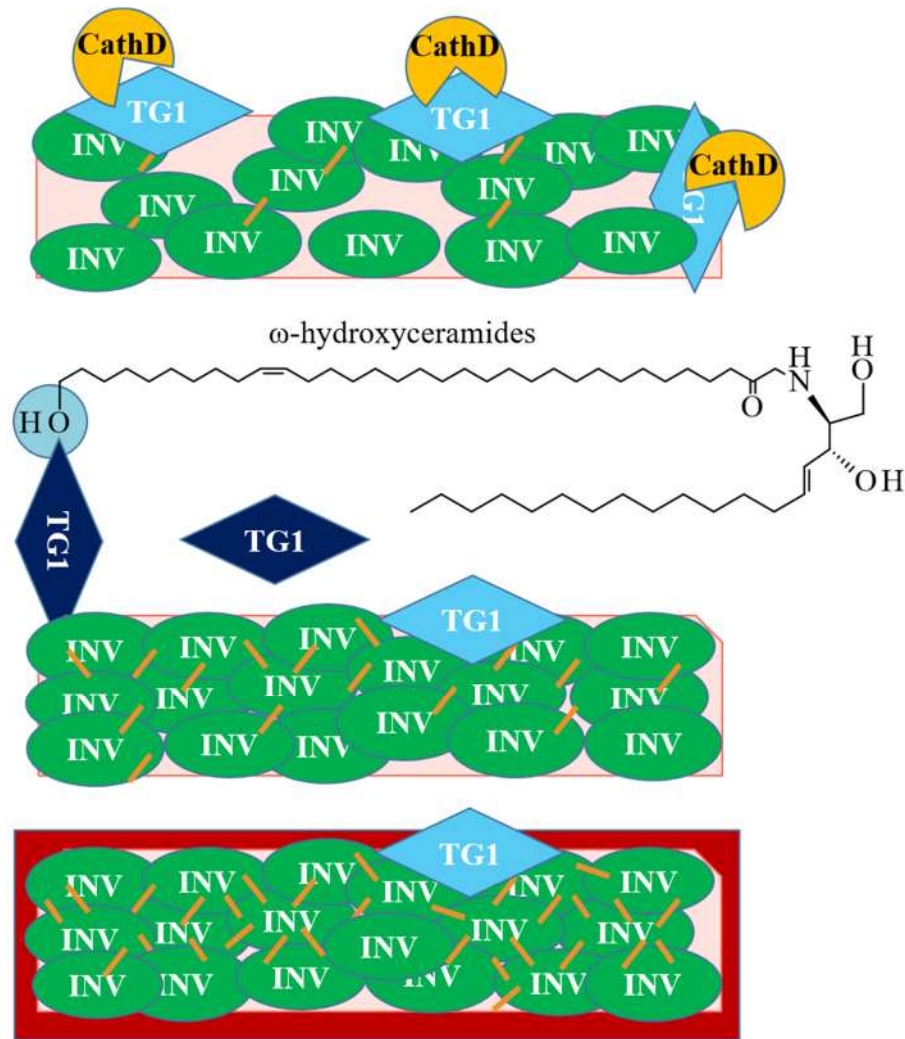
Figure 6.1. The process of liberating TG1 by CathD in order to attach ω-hydroxyceramides to the INV in the CPE to form the hydrophobic CLE.

Keratinocytes at the later developmental stage produce and store a high amount of LBs that are secreted upon terminal differentiation [66]. The LBs contain lipids and enzymes which are necessary for the formation of the SC and ultimately the skin barrier function [65]. Previous work has demonstrated that corneocytes were able to mature *ex vivo* using a test solution containing calcium and dithiothreitol to enhance TG activity. An autofluorogenic exogenous substrate, dansyl cadaverine, was inserted into the CEs by TG. Tape strips from the cheek were immersed in the test solution and exposed to 100% and 70% RH in the presence of glycerol as a humectant. CE maturation was enhanced at 100% RH but suppressed at 70% RH. The diminished CE maturation at 70% RH was enhanced in the presence of glycerol [141,211]. The CE maturity was determined via immunostaining for involucrin and lipid staining [211] an approach that has been recently demonstrated to have methodological limitations

as mentioned in chapter 4 [133]. This may explain why 100% RH was optimal for corneocyte maturation but 70% RH inhibited the maturation process, reversible only in the presence of glycerol [141]. This is surprising as glycerol was observed to improve corneodesmolysis at 80% RH [22] and CE maturation *in vivo* [7] in line with other *in vivo* benefits associated with this humectant [25].

In this current study, the *ex vivo* maturation of corneocytes on SC tape strippings from photo-exposed (PE) cheek and photo-protected (PP) post auricular sites of Chinese subjects was assessed. Inspired by the previous study [141], a range of relative humidity values (44, 55, 70, 80, 90, 95 and 100% RH) were selected in order to identify the optimal humidity for CE maturation. This was followed by investigating the effect of protease inhibition (PI), before *ex vivo* maturation at low, optimal and high RH, on CE maturation. A recent study demonstrated low protein levels of 12R-LOX in photo-damaged facial SC using mass spectrometry [118]. This was shown to be accompanied by a reduced 12R-LOX activity in PE cheek, as shown in chapter 5 [276], along with a lower CE hydrophobicity which was presented in Chapter 4 [133]. Thus, TG and 12R-LOX were blocked to assess the impact on *ex vivo* CE maturation at optimal RH. The enzyme activities of CathD, TG and 12R-LOX were measured with and without inhibition to verify the effect on *ex vivo* CE maturation at optimal RH. Finally, the impact of glycerol on *ex vivo* CE maturation was determined at low, optimal and high RH. In all sets of experiments the changes in CE rigidity and CE hydrophobicity were assessed using the recently published Relative CE Maturity (RCEM) approach reported in Chapter 4 [133].

6.3 Materials and methods

6.3.1 Materials and equipment

The CEs were extracted from the first and ninth tape strips as listed in Chapter 4, Table 4.1, for the determination of RCEM. The crude protein mixture from the second and eighth tape strips were used to measure 12R-LOX activity as described in in chapter 5, table 5.1. The following materials and equipment were used for *ex vivo* CE maturation, the TG activity assay and CathD activity assay (Table. 6.1).

Table 6.1. Materials and equipment for *ex vivo* CE maturation and to measure enzyme activity of TG and CathD.

Materials/Equipment	Supplier
Black 96-well plates	
EDTA	
Tris-HCl (pH 8.5)	
Calcium Chloride	
Potassium carbonate	
Ammonium nitrate	
Bovine Serum Albumin (BSA)	
Ammonium sulfate	Sigma Aldrich,
DMSO	Dorset, UK
DTT	
Potassium sulfate	
Barium chloride	
LDN-27219	
Tritonx100	
skimmed milk powder	
Magnesium Chloride	

Materials/Equipment	Supplier
Alkaline phosphatase streptavidin	GE Healthcare , Little Chalfont, UK
Ultrapure sterile water	Millipore, Watford, UK
Cathepsin D Enzyme Assay	BioVision, Milpitas, CA, USA
SpectraMax iD3	Molecular Devices, Berkshire, UK
Polyclonal Rabbit-Anti-human primary 12R-LOX AB (α12R-LOX) Thermo Fisher Scientific Cat# PA5-23608, RRID:AB_2541108	Thermo Fisher Scientific, Hertfordshire, UK
Invitrogen™ Molecular Probes™ Biotin Cadaverine (N-(5-Aminopentyl) Biotinamide, Trifluoroacetic Acid Salt)	
Nunc-Immuno™ MaxiSorp™ 96 well solid plates	
Pierce™ Protease Inhibitor Tablets	
Bio-Pure™ pipetting reservoir	VWR international Ltd, Leicestershire, UK
1.5 mL reaction tubes	
Para film	
N,N'–Dimethyl casein	
12 well plate	
4-Nitrophenylphosphate (NPP) disodium salt hexahydrate	
Forceps and small scissor	
GraphPad Prism® (Version 7)	GraphPad Software, San Diego, CA, USA
Table top centrifuge 5418 R	Eppendorf Ltd, Stevenage, UK
ThermoMixer F1.5	
Ultracentrifuge 5810 R	

6.3.2 Methods and study design

The insoluble CEs were extracted from the first and ninth tape strips of PE cheek and PP post auricular sites of Chinese subjects. RCEM was determined based on CE rigidity and hydrophobicity as described in Chapter 4. The 12R-LOX activity was determined for samples collected on the second and eighth tape strips of the same participants according to the assay introduced in Chapter 5.

Corneocytes are remnants of keratinocytes that have lost the ability to proliferate and differentiate thus culturing of corneocytes is impossible [277]. *Ex vivo* maturation of corneocytes is an alternative approach to examine CEs after tape stripping. Hirao and colleagues introduced the idea of a humidified chamber as an environment for *ex vivo* maturation, however, a test solution was used on the tape strips before the incubation. This test solution was supplemented with calcium as a co-factor for the calcium-dependent TG1 and exogenous substrate biotinylated cadaverine [141]. Biotinylated cadaverine is a fluorogenic compound that TG recognises as a substrate and is inserted into the CPE. CE maturity was determined using INV-Nile red staining in which the primary antibody INV is visualised with the secondary antibody-coupled to FITC. Cadaverine has the same excitation and emission wavelengths as FITC hence discrimination between both fluorogens is impossible. Nevertheless, the biotinylated cadaverine might increase the CE surface area and thus more lipids may attach during *ex vivo* CE maturation. This would enhance the Nile red lipid staining artificially. The catalysis of biotinylated cadaverine by TG proven the potential to examine CE maturation.

6.3.2.1 *Ex vivo* CE maturation

The tapes were used immediately after tape stripping. Individual 12-well plates were set up with a specific RH value provided by saturated potassium carbonate (44% RH), ammonium nitrate (55% RH), sodium nitrate (70% RH), ammonium sulfate (80% RH), potassium sulfate (90% RH), barium chloride (95% RH) or water (100% RH) (Fig. 6.2) [278]. The tapes were cut into half and incubated at RH conditions in a randomised order and placed with the adhesive side up. The lid was sealed with Parafilm™ to create a humidified chamber. The *ex vivo* maturation was conducted for 4 days at 37 °C.
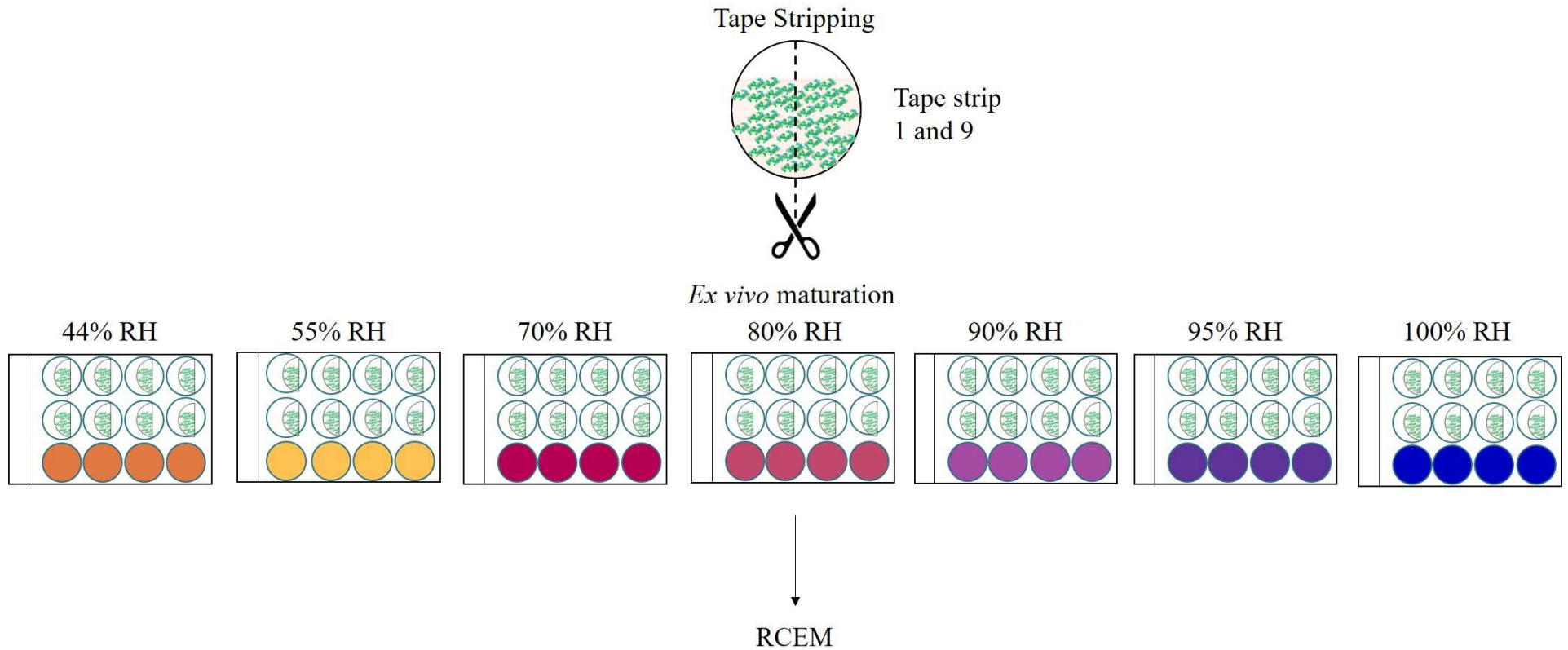
Figure 6.2. A range of concentrated salt solution were set up for humidified chambers for *ex vivo* maturation of CEs on first and ninth tape strips.

The RCEM based on CE rigidity and hydrophobicity was determined in order to identify the optimal RH for the following experiments. Various aspects of *ex vivo* maturation were analysed by treating tape strips prior to incubation. The importance of TG was assessed by using the TG inhibitor 0.5 nM LDN-27219 in DMSO before *ex vivo* maturation at the optimal RH. The effect of protease inhibition was investigated on RCEM at low, optimal and high RH. Furthermore, 12R-LOX activity was blocked using 1:500 anti-12R-LOX antibody before *ex vivo* maturation at the optimal RH. Furthermore, the effect of 5% glycerol was determined on RCEM at low, optimal and high humidity (Fig. 6.3).
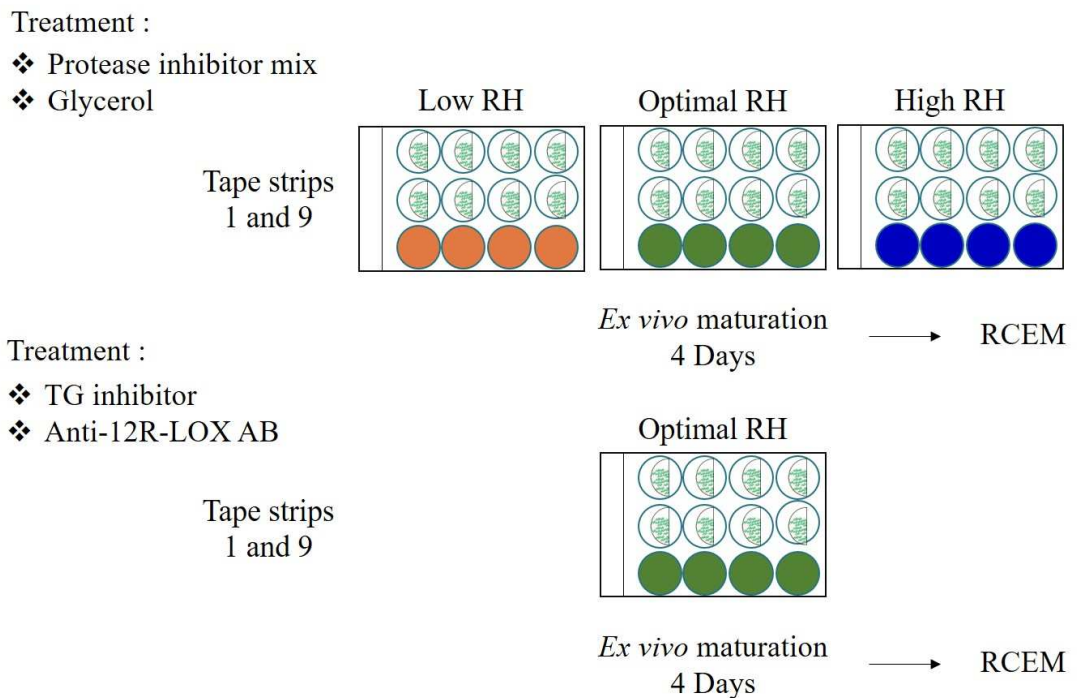
Figure 6.3. *Ex vivo* CE maturation at low, optimal and high RH after treating CEs on tape strips with protease inhibitor mix or 5% glycerol. *Ex vivo* CE maturation was assessed for the impact of inhibiting TG or 12R-LOX at optimal RH.

6.3.2.2 TG activity assay

The enzyme activity assay was adapted from Slaughter *at al.* who designed a solid-phase assay to measure TG activity. Basically, 96-well MaxiSorp plates have a high affinity to molecules with hydrophobic and hydrophilic domains. This chemical property allows the coating of the plate with 20 mg mL^{-1} N,N'–dimethyl casein dissolved in 0.1 M Tris-HCl (pH 8.5) over night at -20 °C. On the day of the assay, the plate was thawed at room temperature. Unbound N,N'–dimethyl casein was discarded. Each well was blocked with 0.5% skimmed milk in 0.1 M Tris-HCl (pH 8.5) for 30 mins at room temperature. The protein in the milk ensures specificity for the binding sites of the enzyme mix. The blocked plate was washed twice with 0.1 M Tris-HCl (pH 8.5) which was discarded at each washing step. The tape strips were incubated in 0.5% TritonX-100 in 0.1 M Tris-HCl (pH 8.5) for 20 mins at room temperature with the thermomixer set to 600 rpm. This extracted the proteins on the tape including soluble and membrane bound proteins. 100 µL of crude protein extract was supplemented and incubated for 30 mins at 37 °C with the substrate solution containing 10 mM calcium chloride, 20 mM DTT and 0.5 mM biotin-cadaverine in 0.1 M Tris-HCl (pH 8.5). In theory, the calcium-dependent TG in the crude protein extract would gain in affinity for biotin-cadaverine in the presence of DTT [141,279]. The substrate biotin-cadaverine is bound to N,N'–dimethyl casein. The unbound reaction solution was discarded and the reaction was stopped with 200 mM EDTA. The streptavidin-alkaline phosphatase was diluted (1:500) in 0.5% skimmed milk and was incubated for 1 h, in the dark at room temperature. Biotin and streptavidin form a strong non-covalently connected complex [280]. The streptavidin-alkaline phosphatase solution was discarded and each well was washed once with 0.01% TritonX-100 in 0.1 M Tris-HCl (pH 8.5) in order to remove remaining proteins from the skimmed milk. The remains of any unbound compound and skimmed milk were washed four times with 0.1 M Tris-HCl (pH 8.5). Fresh 0.1 M Tris-HCl (pH 8.5) was added to each well and supplemented with 1:5 NPP in 0.1 M Tris-HCl (pH 8.5) containing 5 mM magnesium chloride. Alkaline phosphatase is a magnesium dependent enzyme that dephosphorylates NPP to nitrophenol which becomes nitrophenylate under alkaline conditions. Nitrophenylate is a bright yellow compound that can be detected at 405 nm in a plate reader. Slaughter at al., have shown that the alkaline phosphatase activity is proportional to the TG activity with both reaching the maximal velocity of the enzyme

activities. Thus, the increase in absorbance was measured over a period of 1 h with detection intervals of 1 min. TG activity is expressed as the optical density over time normalised to the corresponding protein content on the tape strip determined via densitometry (section 2.3.2.4). Each sample was assayed the three times, furthermore, blanks missing crude protein extract were measured in each assay. A TG inhibitor (LDN-27219) was used to confirm the measured reaction originates due to the TG activity. This reversible allosteric inhibitor binds to the GTP site of TG which leads to a conformational change in the enzyme that prevents the binding of calcium thus leading to the termination of TG activity [281]. A range of concentrations (0.1-1 nM in DMSO) of LDN-27219 were tested for potential TG inhibition and 0.5 nM was chosen as the optimal concentration. However, LDN-27219 had to be tested for any impact on 12R-LOX or CathD activity.

The TG activity was measured at baseline and after *ex vivo* maturation at low, optimal and high RH. In addition samples were also assayed for TG on the second day of *ex vivo* maturation. Furthermore, samples were swapped from low or optimal RH to high RH and vice versa after two days of *ex vivo* maturation. However, the TG activity was measured in *ex vivo* matured CEs at low, optimal and high humidity that were treated with the protease inhibitor mix prior to *ex vivo* maturation.
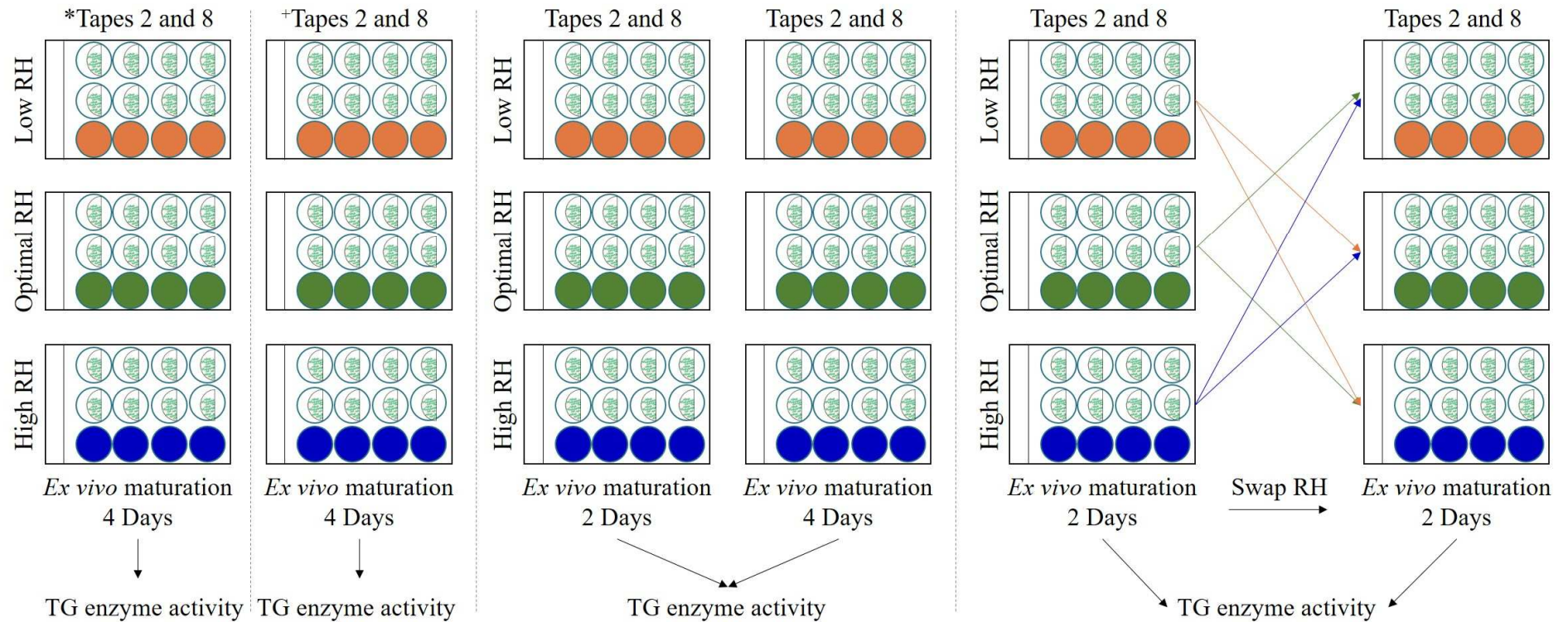
Figure 6.4. TG activity was measured after 4 days of *ex vivo* CE maturation at low, optimal and high RH in presence of TG inhibitor or protease inhibitor mix. TG activity was measured after two days of *ex vivo* maturation and compared to four days of incubation. In addition, TG activity was assessed after swapping RH conditions after two days of *ex vivo* maturation.

6.3.2.3 Cathepsin D activity assay

Cathepsins are lysosomal enzymes that are involved in various physiological processes including photo damage. The assay kit for CathD uses a peptide sequence that has a high affinity for CathD. This peptide is bound to a chromophore (β-(7-methoxy-coumarin-4-yl)-Ala; MCA). The fluorescence signal results when CathD cleaves the peptide from the chromophore [282].

Cathepsin D activity was measured in PE cheek and PP post auricular samples (second and eighth tape) using the fluorometric assay kit. The CathD activity was measured at baseline and for *ex vivo* matured CEs at optimal RH. Samples were lysed in 200 µL of cell lysis buffer, chilled at 4°C on ice for 10 min and centrifuged for 5 min at 13000 rpm. The assay was prepared with 25 µL crude protein extract, 75 µL reaction buffer, and 2 µL substrate solution and the resulting fluorescence was measured in Corning® clear flat bottom black 96-well plates at an interval of 1 min for 1 h at 37 °C with Ex/Em = 328/460 nm in the plate reader. The results are expressed as relative fluorescence unit (RFU) after 10 min of reaction as some samples reached a fluorescence maximum after 15 min; the results were normalised to the total protein amount on the corresponding tape strips.

6.3.2.4 Statistics

The mean and standard deviation (SD) were determined for RCEM (n=7) and for enzyme assays (n=14). The D'Agostino & Pearson normality test was applied to determine the normality of the data in order to choose the appropriate statistical analysis. The statistical differences were analysed via Two-way ANOVA multi-comparison to determine the differences between the control and different conditions or treatments. The statistical differences are corrected via the Sidak-Holm post-hoc test and are expressed as following: * $p \leq 0.05$, ** $p \leq 0.001$, *** $p \leq 0.0002$ and **** $p \leq 0.0001$. The Pearson's correlation coefficient between RH and treatment were assessed at appropriate sections.

6.3 Results

6.3.1 The effect of relative humidity on *ex vivo* CE maturation

The CEs collected at baseline without any treatment show a lower mechanical resistance in the deeper SC layers of the PE cheek ($p \leq 0.0001$) than the CEs in the SC surface of PE cheek. PP post auricular samples from the SC surface are more rigid than CEs from the deeper SC layer of the PP post auricular site ($p \leq 0.001$). CE rigidity values at the SC surface of both anatomical sites are indistinguishable. PP post auricular CEs from the deeper SC layer are more rigid than those obtained from the deeper SC layer of PE cheek ($p \leq 0.0001$). Humidity clearly had an effect on CE rigidity together with hydrophobicity and hence RCEM. A bell-shaped trend was seen in CE rigidity with rising RH, reaching a peak at 70% RH, with a decrease in CE rigidity at 100% RH. Samples from the ninth tape stripping of the PE cheek site showed a stronger response to the tested range of RHs than the other tested samples ($p \leq 0.001$). However, CE rigidity for PE9 samples was maximal following sonication at 70% RH and showed no change at 100% RH compared to the untreated control CEs (Fig. 6.5A). Nile red staining indicated a higher lipid content in CEs from the SC surface compared to those from the deeper SC layers ($p \leq 0.0001$). PP post auricular CEs from the SC surface are more hydrophobic than CEs from the deeper PP post auricular SC layer ($p \leq 0.0001$) while the CE hydrophobicity in PP9 and PE1 samples is similar. The only significant increase in CE hydrophobicity was observed at 70% RH for PP1 ($p \leq 0.001$) and PP9 ($p \leq 0.05$) samples. PE1 and PE9 samples showed an enhancement in CE rigidity while CE hydrophobicity was slightly improved in PE1 ($p \leq 0.05$). There was no change in CE hydrophobicity for PE 9 samples at any RH condition (Fig. 6.5B). More mature CEs were observed in the PP sites compared to PE cheek sites ($p \leq 0.0001$). Corneocytes from the deeper SC layers are less mature than those obtained from the SC surface of respective anatomical site ($p \leq 0.0001$). An overall improvement in RCEM was shown at 70% RH in PP1 ($p \leq 0.01$) and PP9 samples ($p \leq 0.001$) compared to the baseline RCEM. A significant increase in RCEM was obtained in 70% RH in PE1 ($p \leq 0.05$) and PE9 ($p \leq 0.01$) samples compared to baseline RCEM. Corneocytes on tape strips showed no change in RCEM after *ex vivo* CE maturation at 44% RH as well as samples kept at 100% RH. All samples showed an enhancement at 70% RH *ex vivo* maturation (Fig. 6.5C).
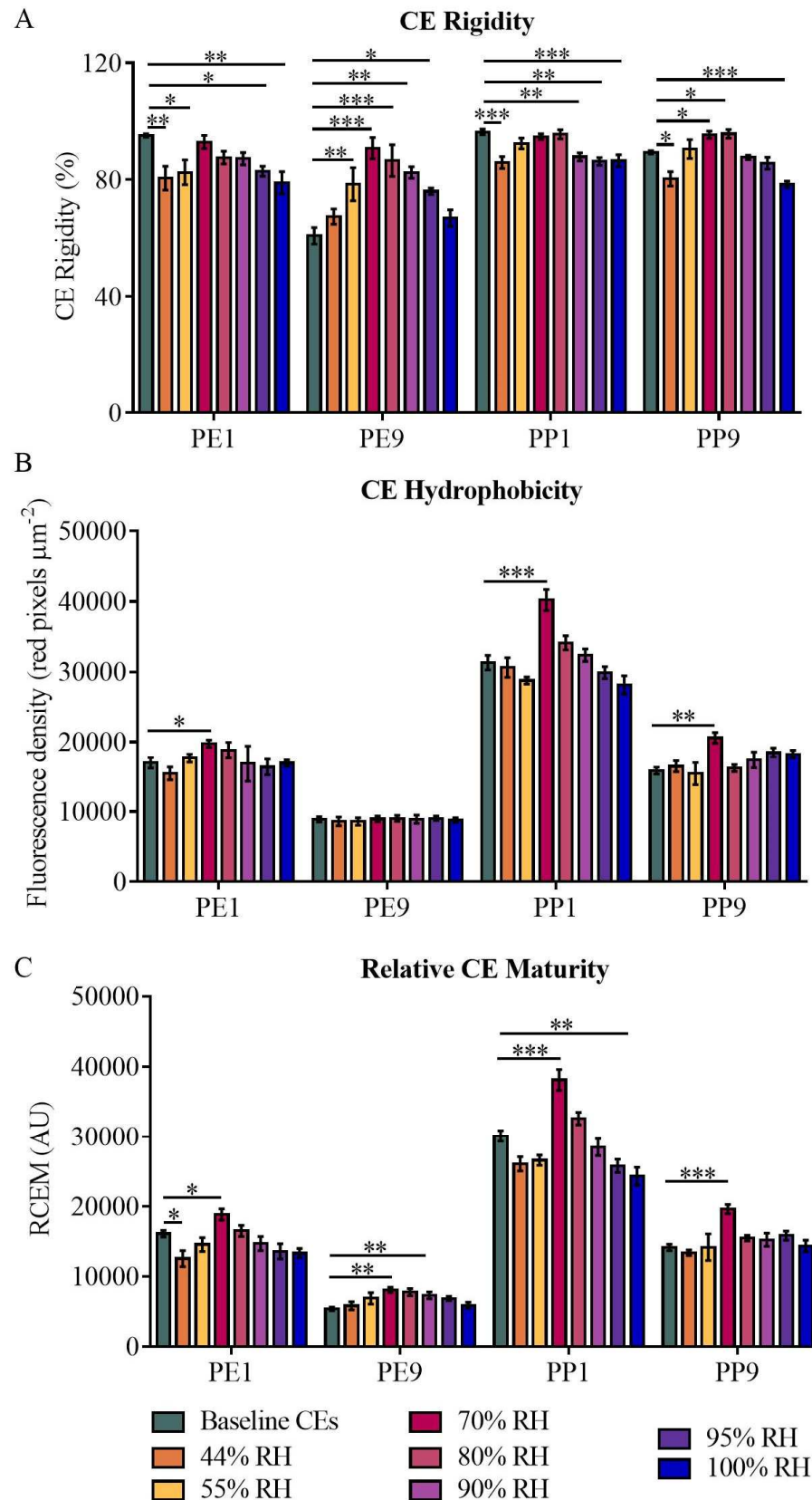
Figure 6.5. CE rigidity (A), CE hydrophobicity (B) and RCEM (C) was determined in *ex vivo* matured CEs after exposure to a range of RH. Data are shown as mean ± SD and compared via two-way ANOVA and post-hoc Sidak-Holm test, (n=7).

6.3.2 The importance of TG in *ex vivo* CE maturation

The TG inhibitor LDN-27219 was applied on to the tape strips prior to *ex vivo* maturation at 70% RH which was selected from the tested RH conditions (Fig. 6.5). Four days of *ex vivo* maturation at optimal RH demonstrated considerably lower Nile red staining in the presence of the TG inhibitor compared to baseline and 70% RH. Interestingly, these visual differences are seen between CEs at baseline and after *ex vivo* maturation with and without TG inhibitor (Fig. 6.6). The visual differences were used to determine CE rigidity CE hydrophobicity and RCEM via image analysis.
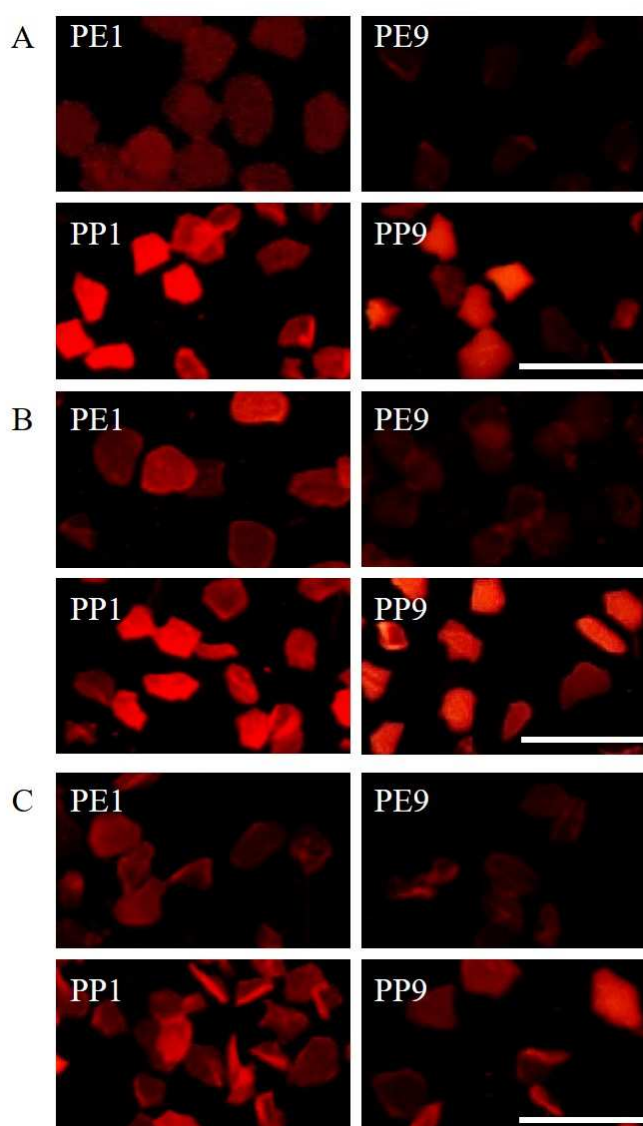
Figure 6.6. Nile Red lipid staining in samples after 10 min of sonication. Visualisation of CE maturity after tape stripping (A). Displaying CE maturity after *ex vivo* maturation without (B) and with TG inhibitor (C). Scale = 100 µm.

Pre-treatment with the TG inhibitor reduced the CE rigidity in all tested samples (p ≤ 0.0001) compared with baseline and *ex vivo* matured CEs at 70% RH. This impact is especially visible in PE9 samples with a baseline CE rigidity value of 60.9 ± 6.9% which then increases to a value of 90.8 ± 8.9% in *ex vivo* matured CEs. Interestingly, *ex vivo* matured PE9 samples had a CE rigidity value of 32.1 ± 3.2% in the presence of TG inhibitor (Fig. 6.7A). CE hydrophobicity is unchanged in the presence of TG inhibitor compared to CEs at baseline (Fig. 6.7B).
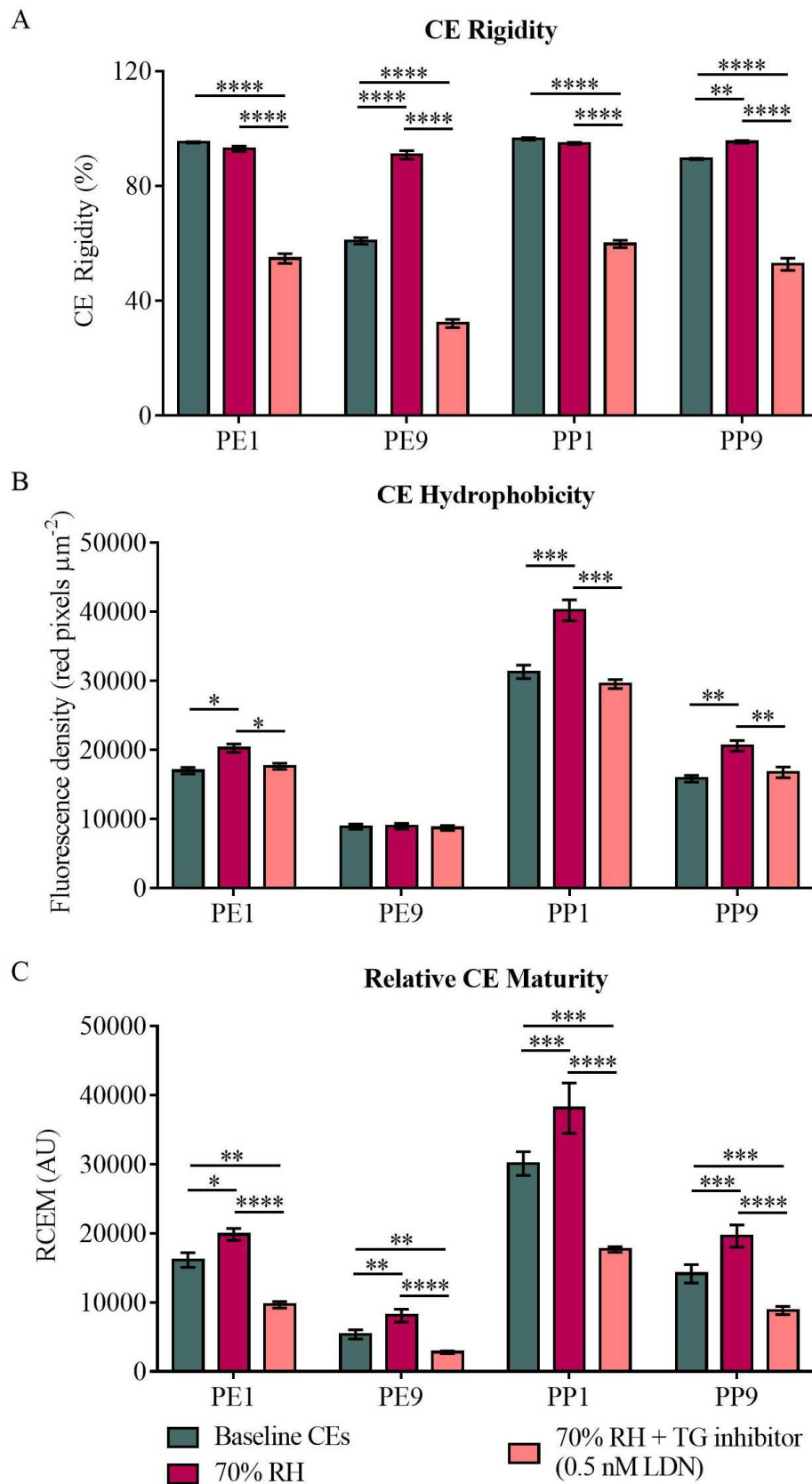
A

B

C

Figure 6.7. CE rigidity (A) is reduced while CE hydrophobicity (B) is unchanged in the presence of the TG inhibitor at 70% RH in presence. Inhibition of TG decreases RCEM in both anatomical sites (C). Data are shown as mean ± SD and compared via two-way ANOVA and post-hoc Sidak-Holm test, (n=7).

The TG inhibitor caused a markedly reduced CE rigidity and no change in CE hydrophobicity resulting in a significant decrease in RCEM. Samples from the PE cheek showed a significant difference to baseline ($p \leq 0.01$) as well as *ex vivo* matured PE cheek samples ($p \leq 0.001$). Samples obtained from the PP post auricular site were significantly lower in the RCEM value in presence of the TG inhibitor compared to the baseline samples ($p \leq 0.001$) and *ex vivo* matured CEs at 70% RH ($p \leq 0.001$) (Fig. 6.7C).

The findings of the *ex vivo* CE maturation (Fig. 6.7) are consistent with the TG enzyme assay (Fig. 6.8). The TG activity is higher in activity in samples obtained from the PP post auricular site compared to the PE cheek site ($p \leq 0.0001$). However, PE9 and PP9 samples have a higher TG activity than the samples from the upper SC layers of respective anatomical site ($p \leq 0.0001$). The TG activity is not affected by *ex vivo* CE maturation at 70% RH ($p \leq 0.5$) nor by the presence of DMSO which is the vehicle used for the TG inhibitor ($p \leq 0.8$). The TG inhibitor, LDN-27219, reduced the TG activity significantly in PE cheek samples obtained from the surface ($p \leq 0.05$) and deeper SC layers ($p \leq 0.0001$). The TG inhibitor reduced considerably the TG activity in the samples collected from the SC surface and deeper SC layer of the PP post auricular site ($p \leq 0.0001$) (Fig. 6.8).
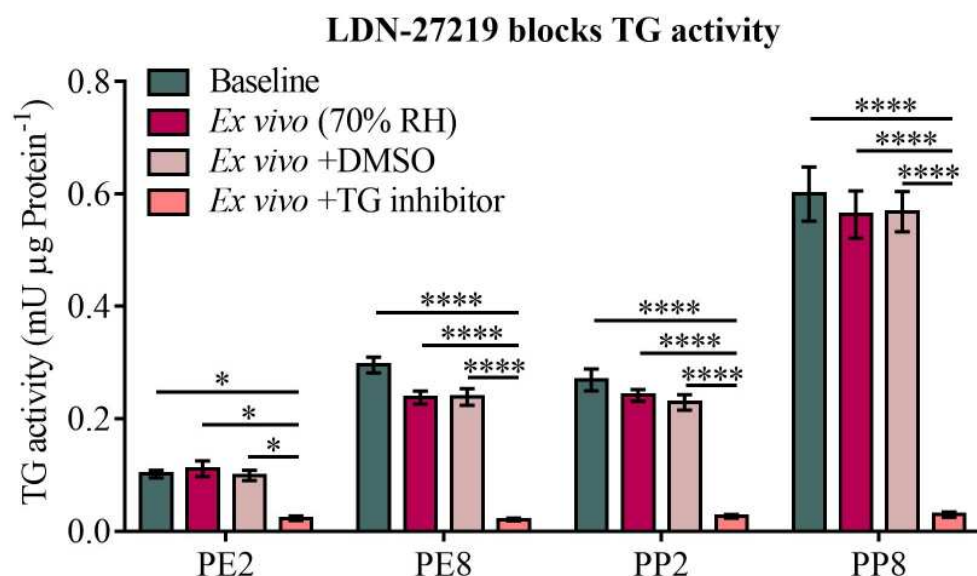
Figure 6.8. TG activity after tape stripping of PE cheek and PP post auricular sites and after *ex vivo* maturation at 70% RH of respective tapes in the presence of DMSO (vehicle) and in the presence of TG inhibitor (LDN-27219). Data are shown as mean ± SD and compared via two-way ANOVA and post-hoc Sidak-Holm test, (n=14).

The TG activity was measured on samples extracted at baseline and corneocytes matured at 44% RH, 70% RH and 100 % RH for two and four days of the *ex vivo* maturation protocol (Fig. 6.9). The enzymatic activity of TG in samples from the SC surface (p ≤ 0.0001) and deeper SC layer (p ≤ 0.0001) of the PP post auricular site is reduced after two days of *ex vivo* maturation at 44% RH. Interestingly, the TG activity remains at the same TG activity level after four days of *ex vivo* maturation at 44% RH in both depths (p ≤ 0.6). The samples from the SC surface of the PE cheek site showed no significant difference between TG activity at baseline and after two days (p ≤ 0.9) or four days (p ≤ 0.8) *ex vivo* maturation at 44% RH. The TG activity in samples from the deeper SC layer of the PE cheek site decreases in TG activity after two days of *ex vivo* maturation at 44% RH (p ≤ 0.0001). This TG activity decreases further for PE8 samples after four days of *ex vivo* maturation at 44% RH (p ≤ 0.05) (Fig. 6.9A).

Samples from the PE cheek and PP post auricular site for both depths showed a significant increase in TG activity after two days at 70% RH (p ≤ 0.0001). The samples kept for four days at 70% RH decreased in TG activity (p ≤ 0.0001) to baseline TG activity level (p ≤ 0.8) (Fig. 6.9B).

However, samples of both anatomical sites and depths showed a dramatic decrease in TG activity after two days of *ex vivo* maturation at 100% RH (p ≤ 0.0001). The TG activity decreased further in all tested samples (p ≤ 0.0001) after four days of *ex vivo* maturation at 100% RH (Fig 6.9C).
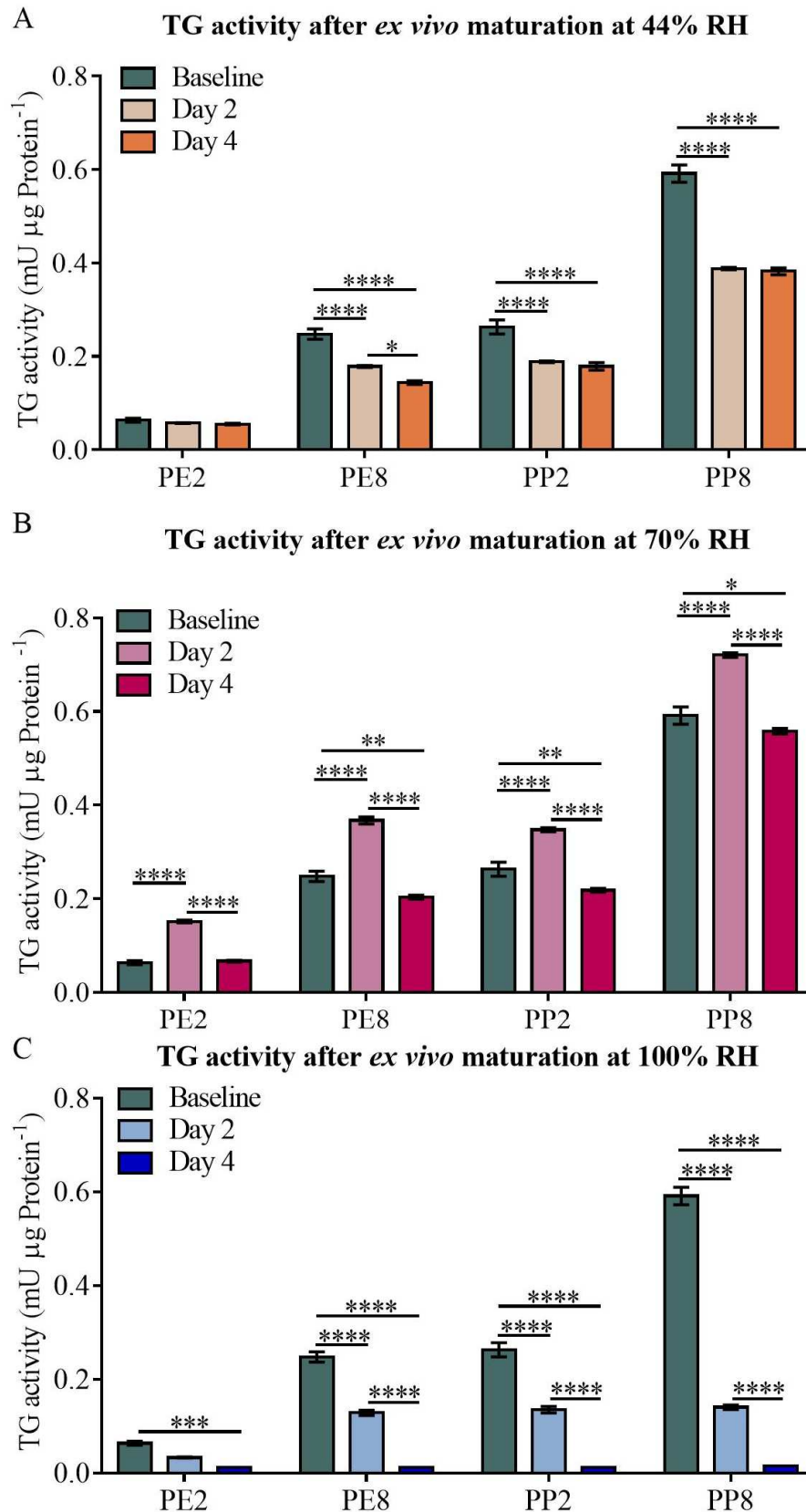
A

TG activity after *ex vivo* maturation at 44% RH

B

TG activity after *ex vivo* maturation at 70% RH

C

TG activity after *ex vivo* maturation at 100% RH

Figure 6.9. TG activity in samples from both anatomical sites at baseline and after two and four days of *ex vivo* maturation at 44% RH (A), 70% RH (B) and 100% RH (C). Data are shown as mean ± SD and compared via two-way ANOVA and post-hoc Sidak-Holm test, (n=14).

The RH conditions were switched after two days of the *ex vivo* maturation protocol from 100% RH to 44% RH or 70% RH for further two days. The changes in TG activity were measured in samples after two days of *ex vivo* maturation at 100% RH and after two days at 44% RH (Fig. 6.10A). TG activity is considerably lower in samples from both anatomical sites after two days of *ex vivo* maturation at 100% RH compared to TG activity at baseline ($p \leq 0.0001$). The samples that were switched from 100% RH to 44% RH showed no change in TG activity ($p \leq 0.09$) in PE cheek samples of both depths. However, samples from the PP post auricular site showed a further decrease when placed in 44% RH for two further days of incubation ($p \leq 0.001$). Interestingly, samples from both anatomical sites and depths showed a marked decrease in TG activity after switching the RH condition from 100% RH to 70% RH ($p \leq 0.0001$) after two days of *ex vivo* maturation (Fig. 6.10B).
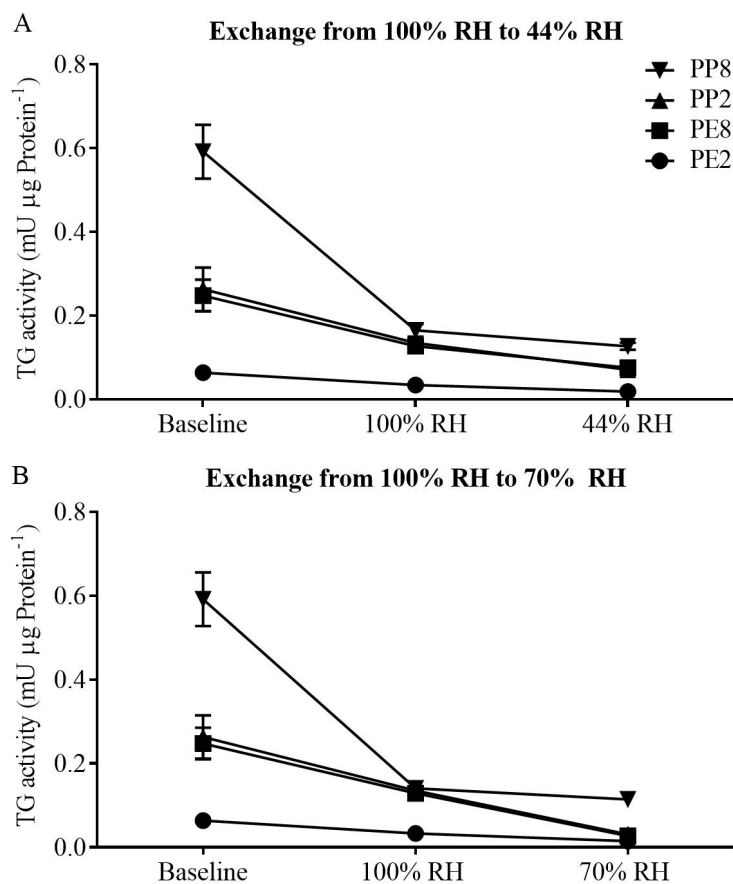
Figure 6.10. TG activity at baseline and after initial two days of *ex vivo* maturation at 100% RH and further two days at 44% RH (A). TG activity at baseline and after switching from 100% RH to 70% RH (B). Mean ± SD, (n=7).

The samples from the PE cheek and PP post auricular site were incubated at 44% RH for two days and were then switched to 100% RH (Fig. 6.11A). The TG activity decreased after two days of *ex vivo* maturation at 44% RH (p ≤ 0.0001) in samples from both anatomical sites and depths. TG activity decreases further when the samples are incubated at 100% RH for two additional days (p ≤ 0.0001). The TG activity increases after two days of *ex vivo* maturation at 70% RH (p ≤ 0.0001) and decreases significantly after two days at 100% RH (p ≤ 0.0001) (Fig. 6.11B).
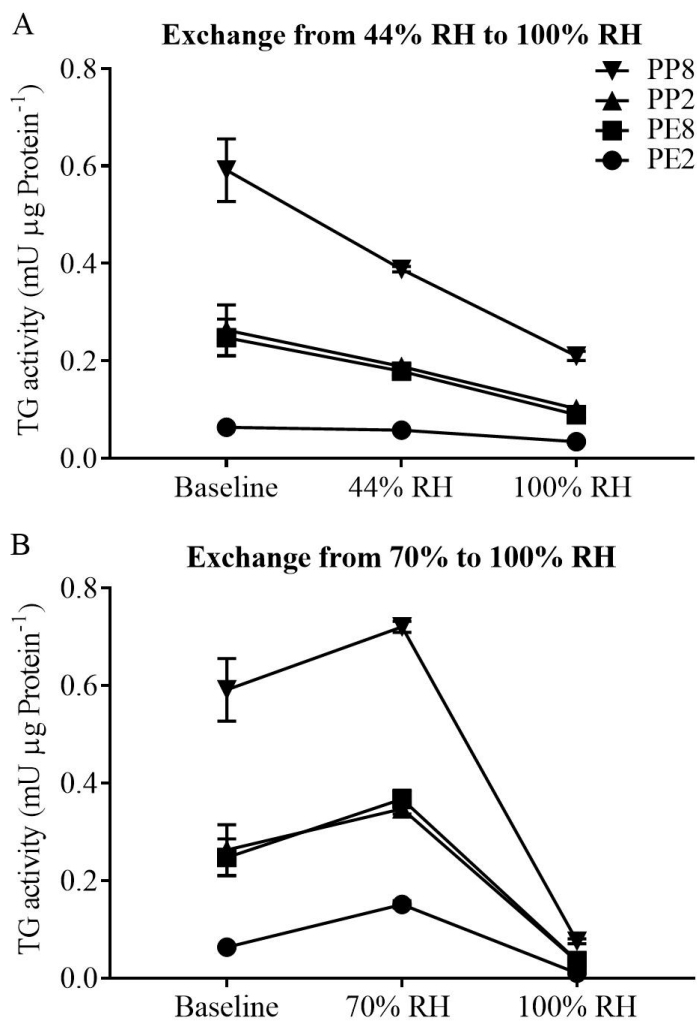
Figure 6.11. TG activity at baseline and after initial two days of *ex vivo* maturation at 44% RH and two additional days in 100% RH (A). TG activity at baseline and after switching from 70% RH to 100% RH (B). Mean ± SD, (n=7).

The Pearson correlations show a clear positive correlation between TG activity and CE rigidity for CEs at baseline (r= 0.91, p ≤ 0.001) and CEs matured *ex vivo* at 44% RH (r= 0.84, p ≤ 0.001), 70% RH (r= 0.93, p ≤ 0.01) and 100% RH (r= 0.67, p ≤ 0.05). Furthermore, a positive correlation was demonstrated between baseline TG

activity and CE hydrophobicity (r= 0.90, p ≤ 0.001) and *ex vivo* CE maturation at 44% RH (r= 0.90, p ≤ 0.001), 70% RH (r= 0.96, p ≤ 0.001) and 100% RH (r= 0.74, p ≤ 0.05). Interestingly, the positive correlation between TG activity at baseline (r=0.89) and 100% RH (r=0.69) was apparent but lower than for those samples *ex vivo* matured at 44% RH (r=0.96) and 70% RH (r=0.95).

6.3.3. The influence of protease inhibition at low, optimal and high RH on *ex vivo* CE maturation and TG activity

The presence of the protease inhibitor mix affected the *ex vivo* CE maturation in both anatomical sites in a humidity-dependent manner. The rigidity of the CEs was not affected by the PI mix at 44% RH or 70% RH while the CE rigidity was restored at samples kept at 100% RH pre-treated with the PI mix. CEs from the superficial and the deeper SC layers become more rigid in the presence of the PI mix at 100% RH compared to *ex vivo* matured CEs at 100% RH without the PI mix (p ≤ 0.0001). Furthermore, CE rigidity of samples from the deeper SC layers of the PP post auricular site gained in mechanical resistance after *ex vivo* maturation in presence of the PI mix at 100% RH (p ≤ 0.6) (Fig. 6.12A).

Samples from the SC surface of both anatomical sites showed an improvement in CE hydrophobicity at 100% RH (p ≤ 0.0001) but no effects were detected in samples *ex vivo* matured at 44% or 70% RH in the presence of the PI mix. The PI mix had no significant impact on CE hydrophobicity in PE9 samples at all RH conditions. Interestingly, the PI mix enhanced CE hydrophobicity in CEs from the deeper SC layers of the PP post auricular site at optimal (p ≤ 0.0001) and high RH (p ≤ 0.0001) but not at low RH (Fig. 6.12B).

The RCEM is determined from the CE rigidity and hydrophobicity thus the changes in those two CE properties altered the RCEM index in the presence of the PI mixture. The RCEM values of samples from both anatomical sites and depths showed an improvement according to the enhanced CE rigidity and CE hydrophobicity at 100% RH with the PI mixture (p ≤ 0.0001). Furthermore, *ex vivo* CE maturation was enhanced in the presence of the PI in CEs from the deeper SC layer of the PP post auricular site at low (p ≤ 0.05), optimal (p ≤ 0.001) and high RH (p ≤ 0.0001) (Fig. 6.12C).
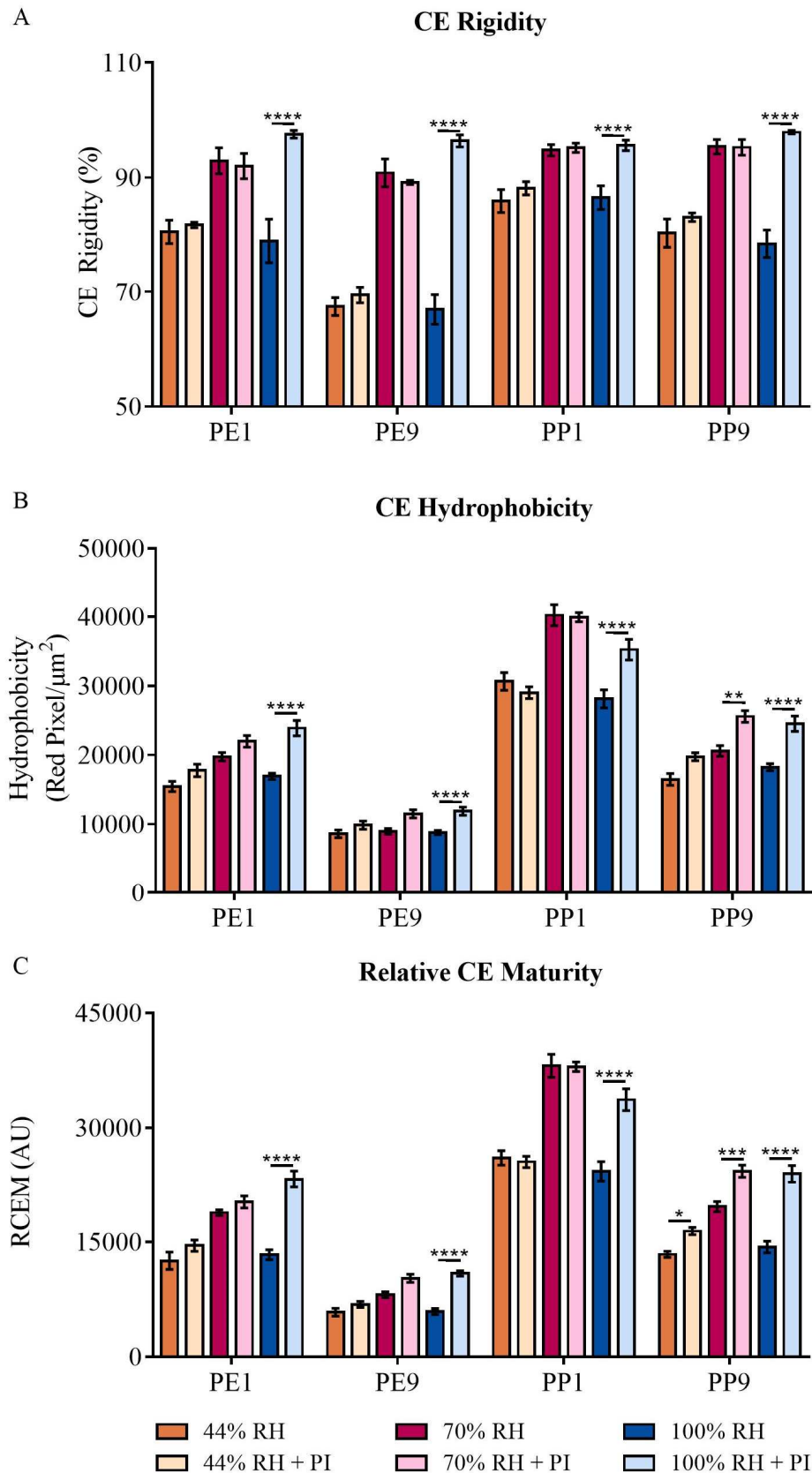
A

CE Rigidity

B

CE Hydrophobicity

C

Relative CE Maturity

Legend: 44% RH, 44% RH + PI, 70% RH, 70% RH + PI, 100% RH, 100% RH + PI

Figure 6.12. CE rigidity (A), CE hydrophobicity (B) and RCEM (C) after *ex vivo* maturation at 44% RH (low), 70% RH (optimal RH) and 100% RH (high RH) with and without the PI mix. Data are shown as mean ± SD and compared via two-way ANOVA and post-hoc Sidak-Holm test, (n=7).

The changes in *ex vivo* maturation in the presence of the PI mixture are consistent with the TG activity in samples kept at the same conditions as those used to assay the CE maturation. Corneocytes exposed to protease inhibitors prior to *ex vivo* CE maturation had a significantly higher TG activity than those matured in the absence of protease inhibitors. However, the effect of protease inhibitors on TG activity shows a hydration dependent tendency where the most notable rise in TG activity is seen in samples kept at 100% RH ($p \leq 0.0001$). The TG activity was significantly increased at 44% RH and 70% RH ($p \leq 0.0001$) (Fig. 6.13).
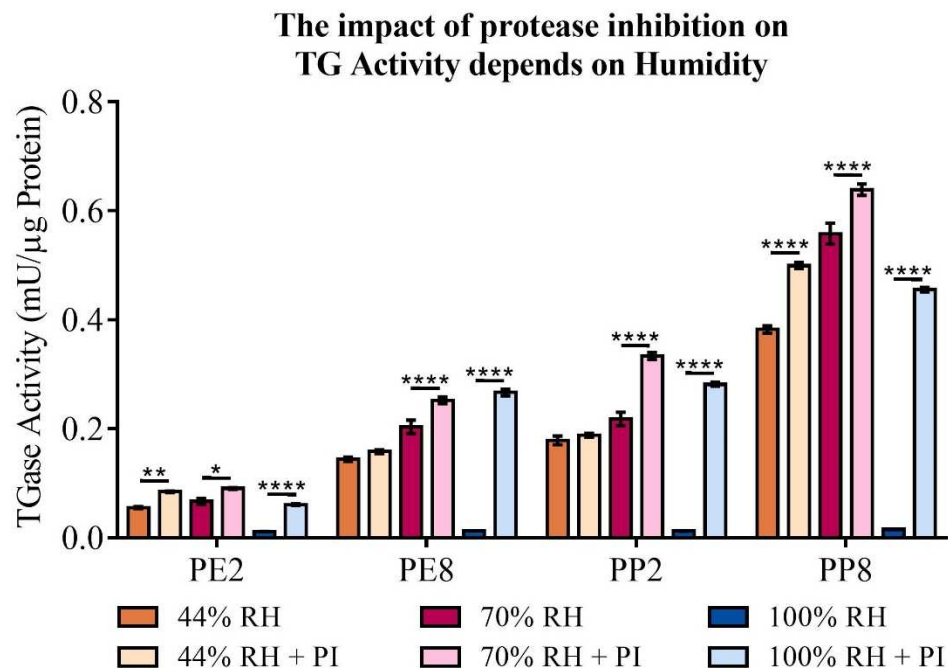
Figure 6.13. TG activity after *ex vivo* maturation at low (44% RH), optimal (70% RH) and high RH (100% RH) in the presence and the absence of the PI mixture. Data are shown as mean ± SD and compared via two-way ANOVA and post-hoc Sidak-Holm test, (n=14).

CEs obtained from the PP post auricular site showed a higher TG activity compared to CEs from the PE cheek site. Interestingly, the TG activity in samples from the superficial SC layer of the PE cheek remains significantly lower than samples from the deeper SC layer of the PE cheek site ($p \leq 0.0001$) for all tested RH conditions regardless of the presence of the PI mixture. Furthermore, samples from tape PE8 had comparable TG activity to samples from tape PP1. However, the TG activity in the

superficial SC layer of the PP post auricular site is lower than TG activity in the deeper SC layer of the PP post auricular site ($p \leq 0.0001$).

6.3.4. The impact of 12R-LOX inhibition at optimal RH on *ex vivo* CE maturation

The CE rigidity was compared between CEs at baseline after tape stripping and CEs *ex vivo* matured at 70% RH with and without the 12R-LOX antibody. The CEs from the PP post auricular of both depths remained rigid after blocking 12R-LOX during *ex vivo* maturation ($p \leq 0.8$). The blocking of 12R-LOX activity had no impact for CEs from the superficial SC layer of the PE cheek site ($p \leq 0.9$). The CE rigidity in PE9 samples reached a comparable percentage as *ex vivo* matured CEs at 70% RH ($p \leq 0.0001$) and samples treated with 12R-LOX antibodies ($p \leq 0.0001$) prior to *ex vivo* maturation (Fig. 6.14A).

The CE hydrophobicity enhanced with *ex vivo* maturation at 70% RH compared to CE hydrophobicity at baseline. This enhancement in CE hydrophobicity was not observed in samples that were treated with the 12R-LOX antibody prior to *ex vivo* maturation ($p \leq 0.8$). In fact, CE hydrophobicity in samples treated with the 12R-LOX antibody remained in the same range as baseline CEs (Fig. 6.14B).

The improved CE rigidity and constant CE hydrophobicity results in an enhanced RCEM in PE9 samples ($p \leq 0.05$) while CE maturity of the PE1 and the PP samples remained at baseline levels (Fig. 6.14C).
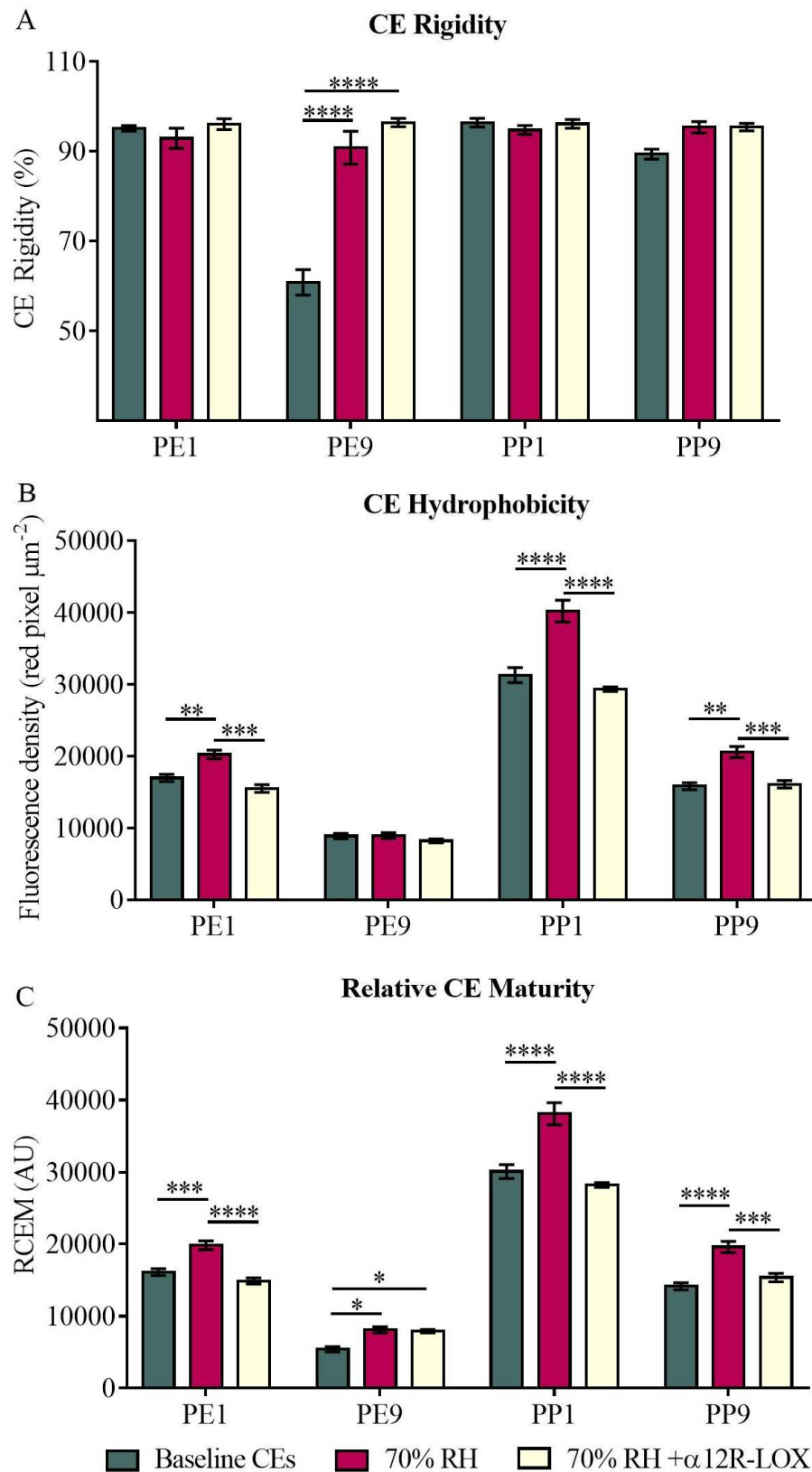
Figure 6.14. CE rigidity (A), CE hydrophobicity (B) and RCEM (C) after *ex vivo* maturation at 70% RH in samples from the PE cheek and PP post auricular with and without exposure to 12R-LOX antibody. Data are shown as mean ± SD and compared via two-way ANOVA and post-hoc Sidak-Holm test, (n=7).

The enzyme activity of 12R-LOX at baseline is higher in samples of the PP post auricular site compared to the PE cheeks site ($p \leq 0.0001$). However, 12R-LOX activity remained low in PE2 samples regardless of *ex vivo* maturation conditions with and without 12R-LOX antibody ($p \leq 0.9$). 12R-LOX activity is significantly higher in samples for the deeper SC layer of the PE cheek site compared to samples from the SC surface of the PE cheek site ($p \leq 0.0001$). Interestingly, 12R-LOX activity was comparable in the PE8 samples and the CEs from the PP2 sample ($p \leq 0.5$). Samples from PE8 tapes and PP post auricular tapes from both depths showed a reduced 12R-LOX activity after *ex vivo* maturation at 70% RH ($p \leq 0.0001$). An additional set up was prepared to test the TG inhibitor, LDN-27219, on 12R-LOX activity. However, the TG inhibitor showed no impact on the 12R-LOX activity in CEs *ex vivo* matured at 70% RH ($p \leq 0.5$). The antibody against 12R-LOX reduced 12R-LOX activity to a minimum compared to samples matured *ex vivo* ($p \leq 0.001$) and baseline ($p \leq 0.0001$) (Fig. 6.15). DMSO, the vehicle for the TG inhibitor, increased 12R-LOX activity compared to 12R-LOX activity in samples at baseline ($p \leq 0.05$) but not in *ex vivo* matured samples ($p \leq 0.8$).
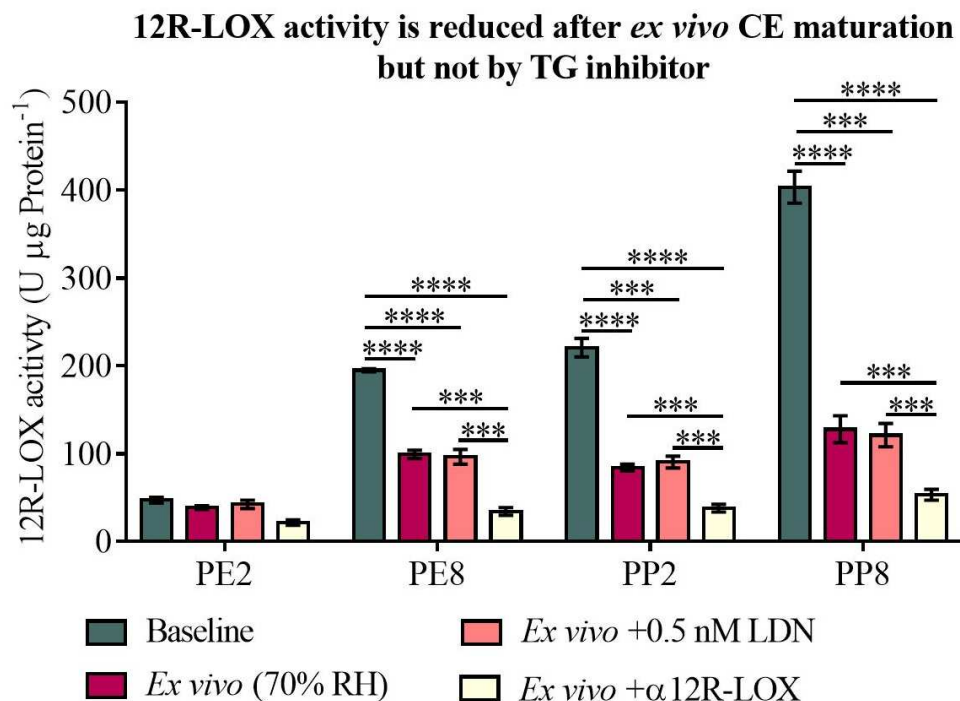
Figure 6.15. 12R-LOX activity was measured in samples at baseline, and after *ex vivo* maturation at 70% RH with and without TG inhibitor, LDN-27219, and 12R-LOX antibody. Data are shown as mean ± SD and compared via two-way ANOVA and post-hoc Sidak-Holm test, (n=14).

6.3.5. The impact of TG inhibitor on CathD activity

The Cath D activity was measured in samples at baseline after tape stripping and in CEs after *ex vivo* maturation at 70% RH (Fig. 6.16). CathD activity remained constant for all tested samples from the PE cheek and PP post auricular sites and depths ($p \leq 0.6$). Furthermore, the TG inhibitor LDN-27219 and its vehicle DMSO had no effect on CathD activity in samples at baseline and in *ex vivo* matured CEs ($p \leq 0.4$). However, the CathD activity is significantly higher in samples from the deeper SC of the PE cheek compared to the SC surface of the PE cheek ($p \leq 0.0001$). The CathD activity is significantly lower in samples from the PP site compared to samples from the PE site ($p \leq 0.0001$). However, PP8 samples have a higher CathD activity than PP2 samples ($p \leq 0.05$).
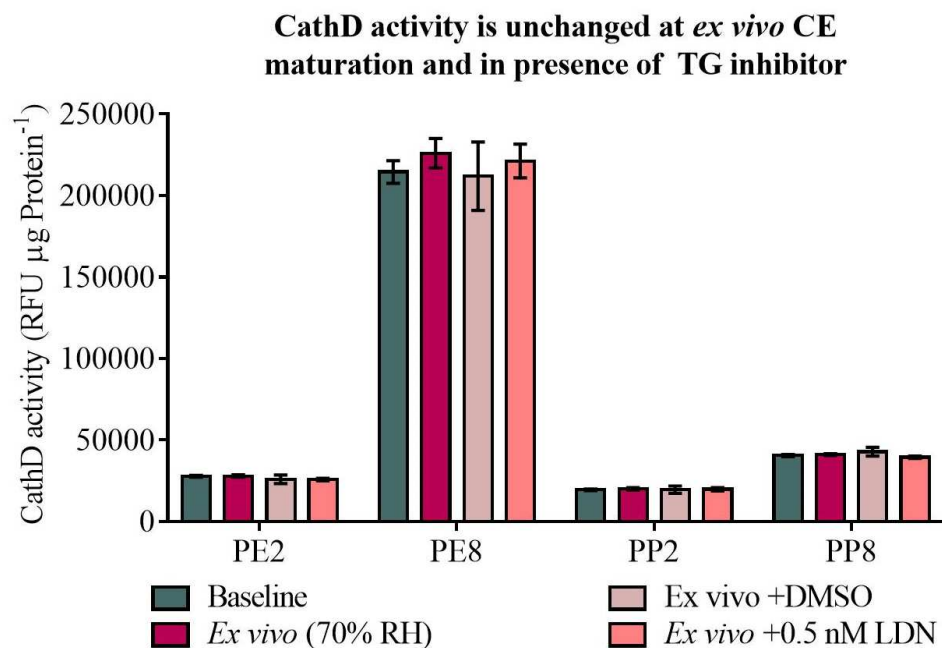
Figure 6.16. CathD activity in samples from the PE cheek and PP post auricular site at baseline and after *ex vivo* maturation at 70% RH with and without TG inhibitor and its vehicle DMSO. Data are shown as mean ± SD and compared via two-way ANOVA and post-hoc Sidak-Holm test, (n=14).

6.3.6. The effect of glycerol on *ex vivo* maturation at low, optimal and high relative humidity

Low relative humidity resulted in a decrease in CE rigidity and had no effect on CE hydrophobicity, but immersing the tapes in glycerol before the *ex vivo* CE maturation at 44 % RH resulted in a clear visual difference (Fig. 6.17).

Figure 6.17. Nile red staining of sonicated CEs after *ex vivo* maturation at 44 % RH and in presence of 5% glycerol. Scale bar=100 µm.

CE rigidity was reduced in PE cheek samples for both depths ($p \leq 0.05$) which were exposed to either water or 5% glycerol before being incubated at 44% RH. Interestingly, CEs from both depths for the PP post auricular site showed no significant difference in CE rigidity in samples kept at 44% RH. However, water significantly reduced the mechanical resistance of CEs from both anatomical sites to sonication compared to 5% glycerol ($p \leq 0.001$) (Fig. 6.18A). CEs from the first ($p \leq 0.0001$) and ninth ($p \leq 0.0001$) tape strips collected from the PE cheek site and treated with glycerol before *ex vivo* maturation showed a significant increase in CE hydrophobicity. Glycerol-treated CEs from the PP post auricular site improved in CE hydrophobicity in PP9 samples ($p \leq 0.0001$) as well as in PP1 samples ($p \leq 0.05$). Corneocytes from PP9 samples showed a comparable CE hydrophobicity to CEs from the PE1 and PP1 site in the presence of glycerol (Fig. 6.18B). Corneocytes matured *ex vivo* at 44% RH and in the presence of glycerol enhanced greatly the RCEM. Samples from the PP1 ($p \leq 0.001$) and PP9 ($p \leq 0.0001$) sites showed an enhanced RCEM compared to baseline CEs and those treated with water. Corneocytes from PE1 samples ($p \leq 0.0001$) and PE9 samples ($p \leq 0.01$) were more mature after *ex vivo* maturation at 44% RH in the presence of glycerol compared to baseline CEs and water treated CEs (Fig. 6.18C).

A

CE Rigidity

B

CE Hydrophobicity

C

Relative CE Maturity

Figure 6.18. CE rigidity (A), CE hydrophobicity (B) and RCEM (C) *ex vivo* maturation at 44 % RH and in the presence of water or 5% glycerol. Data are shown as mean ± SD and compared via two-way ANOVA and post-hoc Sidak-Holm test, (n=7).

The Nile red staining allows visualisation of the CLE which increases in the fluorescence intensity with the amount of lipids. A visual comparison of the CEs shows no distinct difference between glycerol-treated PE cheek CEs matured *ex vivo* at 70% RH and in those *ex vivo* matured at 70% RH without any pre-treatment, for both anatomical sites and depths (Fig. 6.19).
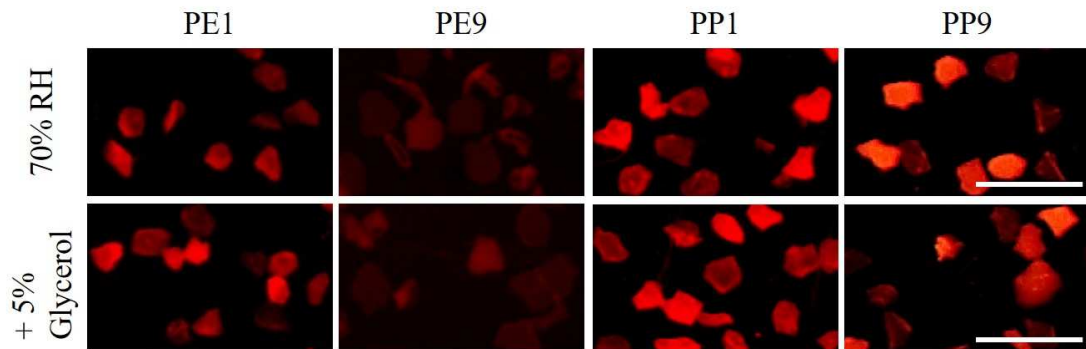
Figure 6.19. Nile red staining of sonicated CEs after *ex vivo* maturation at 70 % RH and in the presence of 5% glycerol. Scale bar=100 µm.

Corneocytes from the ninth tape strips of PE cheek (p ≤ 0.0001) and PP post auricular site (p ≤ 0.001) have a lower CE rigidity in the presence of glycerol compared to *ex vivo* matured CEs solely at 70% RH. Baseline CEs have comparable CE rigidity to glycerol-treated *ex vivo* matured CEs at 70% RH. However, PE cheek samples from the superficial SC (p ≤ 0.0001) and deeper SC layers (p ≤ 0.05) are less rigid after exposure to water and glycerol prior to *ex vivo* maturation (Fig. 6.20A).

CE hydrophobicity enhanced in CEs from the PE1 samples (p ≤ 0.05) and the PE9 sample (p ≤ 0.0001) treated with glycerol compared to those matured at 70% RH. Interestingly, PP samples showed no difference (p ≤ 0.6) with glycerol but showed a significant decrease with water (p ≤ 0.0001) in both depths (Fig. 6.20B).

Corneocytes treated with glycerol before *ex vivo* maturation at 70% RH showed no difference in RCEM values compared to CEs without treatment (p ≤ 0.4). However, water lowered the RCEM value in CEs from the PP sites (p ≤ 0.0001) as well as PE1 (p ≤ 0.0001) and PE9 (p ≤ 0.01) (Fig. 6.20C).

A

CE Rigidity

B

CE Hydrophobicity

C

Relative CE Maturity
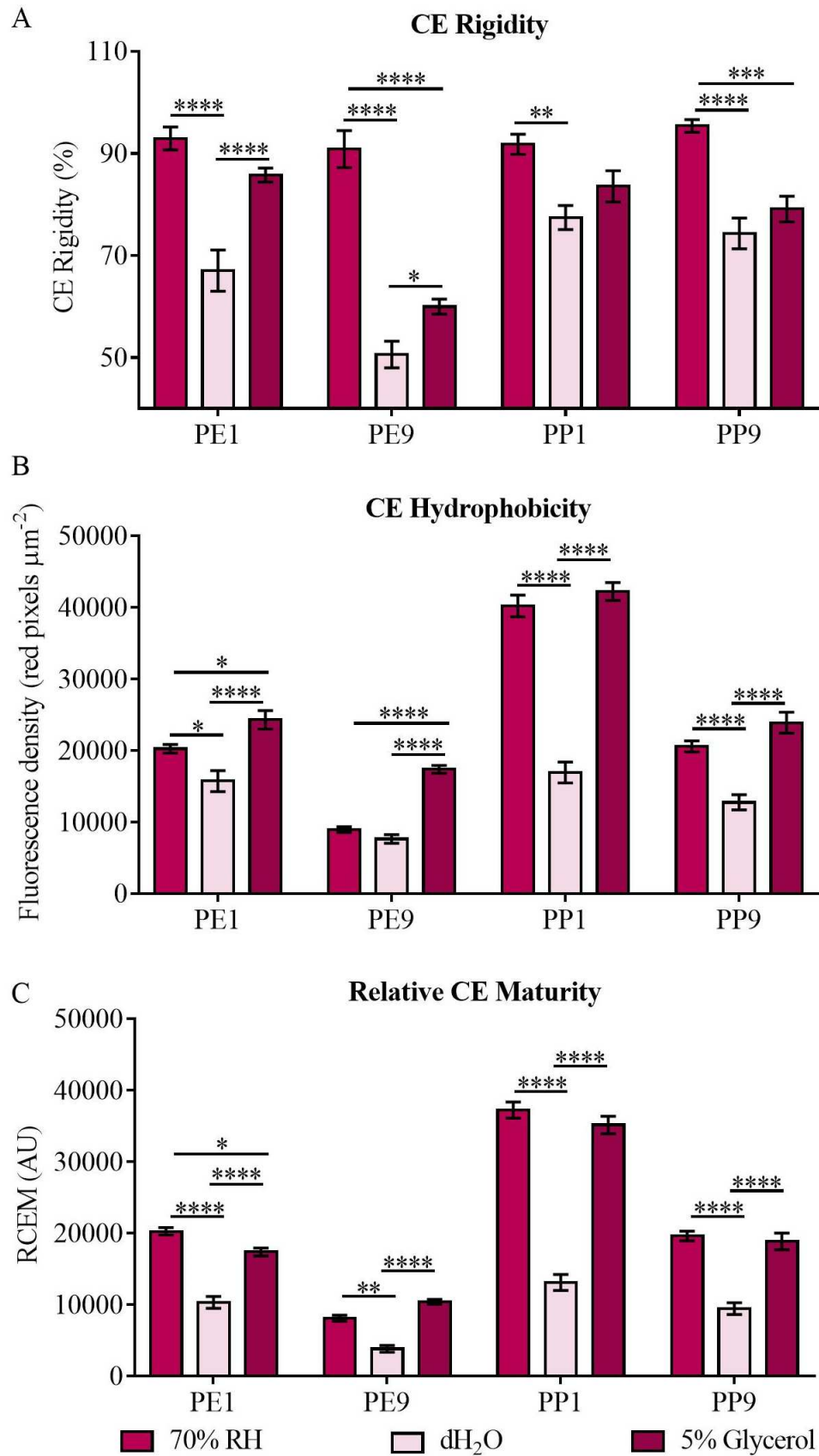
Figure 6.20. CE rigidity (A), CE hydrophobicity (B) and RCEM (C) *ex vivo* maturation at 70 % RH and in presence of water or 5% glycerol. Data are shown as mean ± SD and compared via two-way ANOVA and post-hoc Sidak-Holm test, (n=7).

CEs treated with glycerol prior to *ex vivo* maturation at 100% RH show a lower Nile red staining compared to *ex vivo* matured CEs at 100% RH without any treatment (Fig. 6.21).
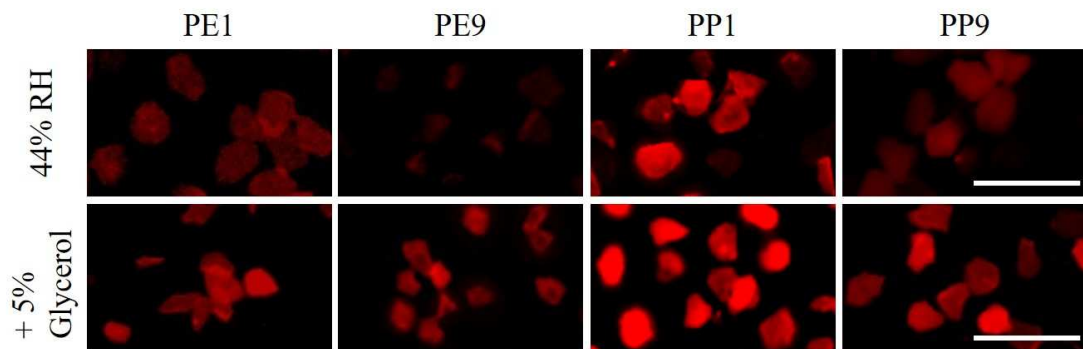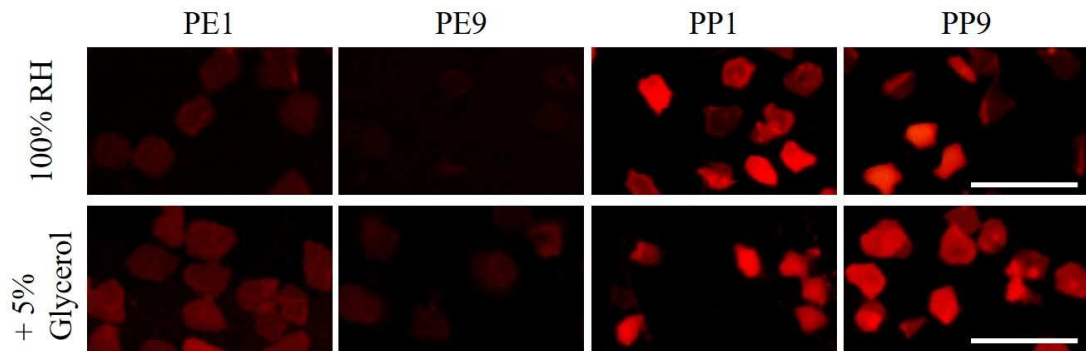

Figure 6.21. Nile red staining of sonicated CEs after *ex vivo* maturation at 100 % RH and in the presence of 5% glycerol. Scale bar=100 µm.

Image analysis of CEs indicate a reduction in CE rigidity in samples from both anatomical sites and depths treated with water instead of glycerol before *ex vivo* maturation at 100% RH (p ≤ 0.0001). Corneocytes exposed to glycerol before *ex vivo* maturation at 100% RH showed no difference in CE rigidity (p ≤ 0.7). However, CEs from PE9 samples showed an increase in CE rigidity in the presence of glycerol and 100% RH (p ≤ 0.01) (Fig. 6.22A). CEs from the SC surface (p ≤ 0.05) and deeper SC layer (p ≤ 0.05) of the PE cheek site enhanced in CE hydrophobicity in CEs treated with glycerol prior to *ex vivo* maturation at 100% RH. However, glycerol enhanced CE hydrophobicity in *ex vivo* maturation at 100% RH in CEs from both depths of the PP post auricular site compared to CEs matured *ex vivo* at 100% RH sites (p ≤ 0.01). Water had no impact on *ex vivo* CE maturation at 100% RH (p ≤ 0.4). However, CE hydrophobicity was significantly lower than in CEs treated with glycerol and 100% RH (p ≤ 0.0001) (Fig. 6.22B). CEs treated with water before *ex vivo* maturation at 100% RH showed a reduced RCEM value compared to CEs *ex vivo* matured at 100% RH with (p ≤ 0.0001) and without glycerol (p ≤ 0.01). RCEM enhanced in CEs from the PE cheek (p ≤ 0.05) and PP post auricular site (p ≤ 0.01) treated with glycerol before exposure to 100% RH compared to CEs matured *ex vivo* at 100% RH (Fig. 6.22C).
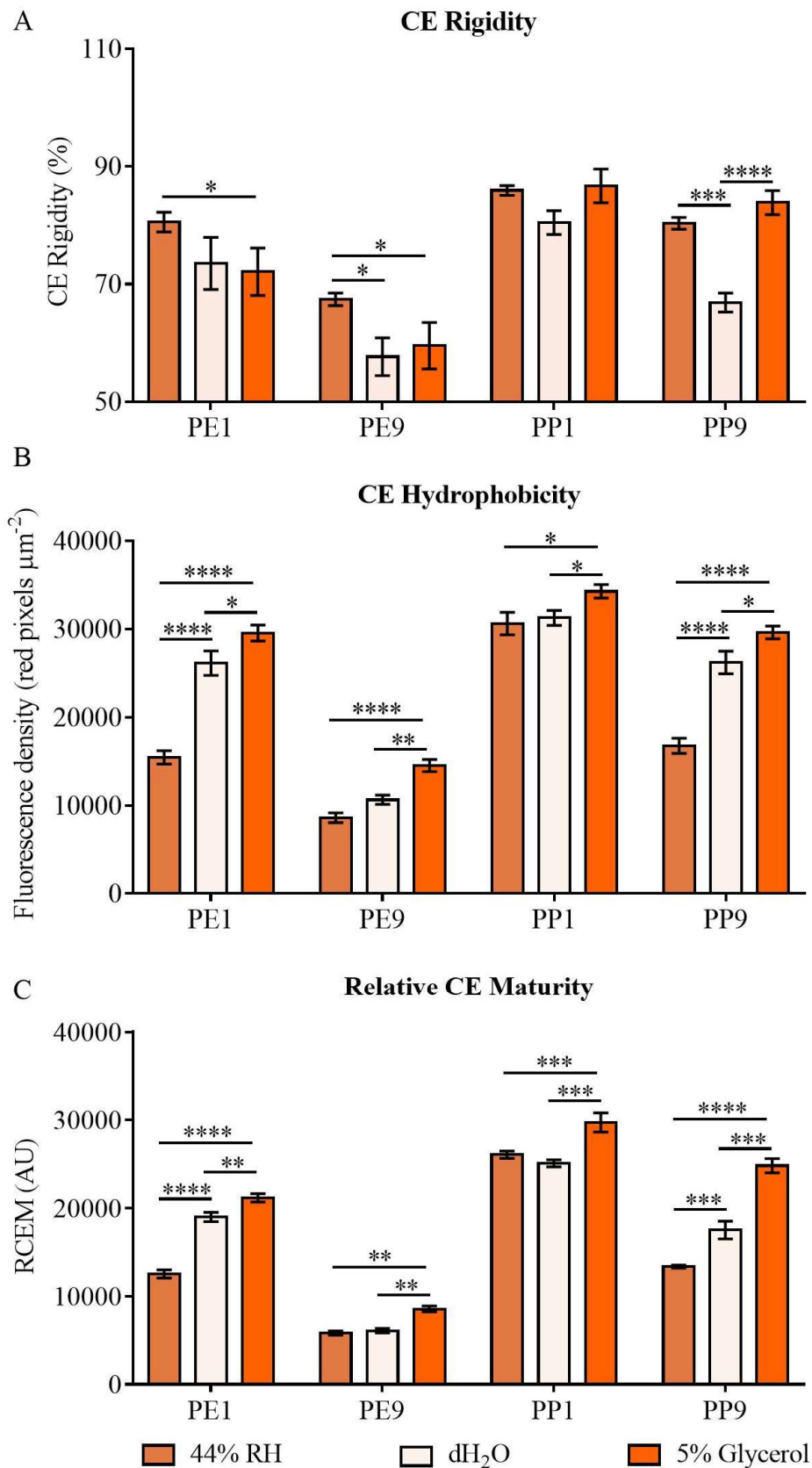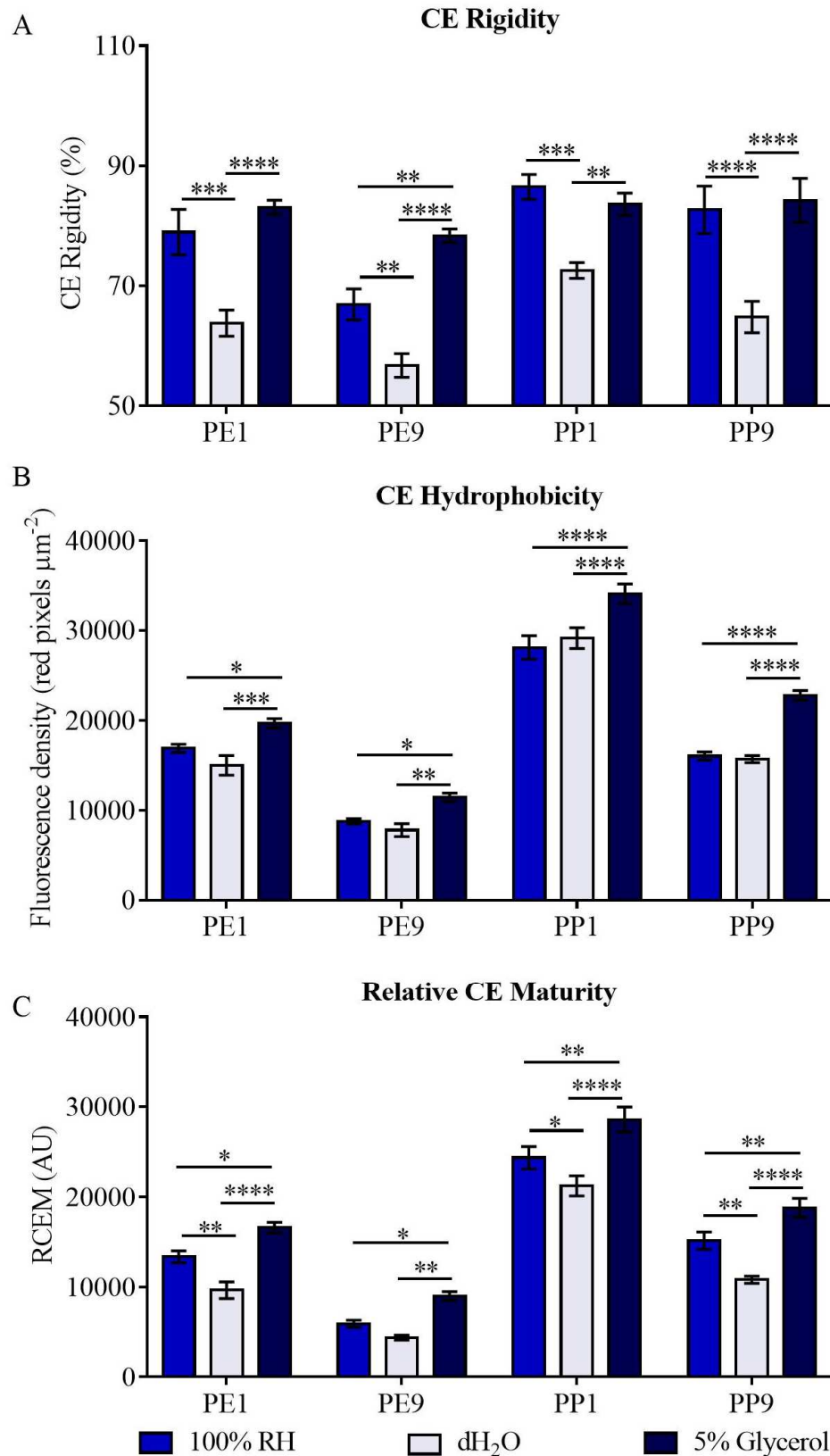
Figure 6.22. CE rigidity (A), CE hydrophobicity (B) and RCEM (C) *ex vivo* maturation at 100 % RH and in the presence of water or 5% glycerol. Data are shown as mean ± SD and compared via two-way ANOVA and post-hoc Sidak-Holm test, (n=7).

6.4 Discussion

The present work investigated facial CE maturation for Chinese subjects using the approach introduced in Chapter 4 and described in a previous study with Caucasians [133]. No differences were found in the SC integrity in Chinese and Caucasian participants in both anatomical sites (Fig. 2.4). The SC cohesiveness was noted to be greater in Chinese participants in both anatomical sites (Fig. 2.7) indicating a thinner SC in Chinese compared to Caucasians (Fig. 2.10). This is consistent with the reported thinner SC in Chinese subjects compared to Caucasians. However, the present data did not indicate a lower barrier function in the Chinese participants [283]. The discrepancy in the barrier function might originate from the environmental and seasonal factors that have an impact on the CE maturation as discussed in Chapter 2 [135,284]. Understanding the underlying mechanisms of CE maturation is essential for the development of new topical formulations that support the skin barrier function.

The skin is under constant exposure to a variety of environmental conditions that can change the physiological properties and architecture of the outermost skin layers. The RH is an environmental feature that changes depending on temperature. The project has shown that RH has a regulatory impact on CE maturation. CE rigidity and CE hydrophobicity improved at 70% RH while no enhancement was observed in CE maturation at 44% RH and at 100% RH (Fig. 6.3). An earlier *ex vivo* study found optimal CE maturation at 100% RH [141]. This controversy in findings may originate from the less sensitive involucrin/Nile red staining that was used to determine the CE maturity as discussed in Chapter 4.
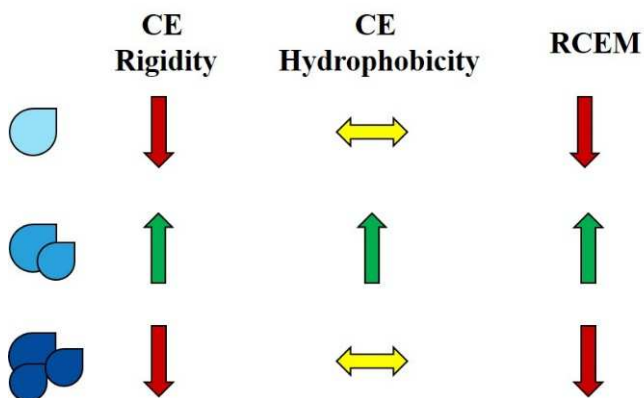
Figure 6.23. Low and high RH are sub-optimal conditions for CE maturation.

Interestingly, PE cheek samples showed no improvement in CE hydrophobicity compared to the enhancement in the PP post auricular samples. This indicates that there is a major difference in the enzymes involved in CE maturation. TG is the enzyme that catalyses the maturation of corneocytes via two major actions during cornification. First, an isopeptide cross-linkage between lysine moieties and glutamine of structural proteins is formed to replace the cell membrane of keratinocytes with a CPE [95]. This processing leads to a progressive increase in CE rigidity [44,285]. Secondly, TG is believed to covalently connect the glutamine residues of CE proteins and the ω-hydroxyl group of ω-hydroxyceramides [50] to enhance the CE hydrophobicity of the CLE [229]. The presence of a TG inhibitor was tested at optimal RH to confirm that CE maturation is dependent on TG activity during *ex vivo* maturation. An unchanged CE hydrophobicity was to be expected, however, CE rigidity decreased considerably in the presence of the TG inhibitor. The CPE is described as an accumulation of insoluble structural proteins hence the decrease in CE rigidity in all samples was unexpected. This decrease in mechanical resistance combined with unchanged CE hydrophobicity was summarised in a reduced RCEM value. There is no existing evidence that explains the decrease in CE rigidity following TG inhibition but this may point to the dissolution of the isopeptide bond. Thus, the importance of TG is not limited to the formation of the CPE but it is also involved in maintenance of the CPE. The TG inhibitor used in the present experiments was shown to decrease TG activity while the TG inhibitor vehicle, DMSO, had no impact on TG activity. DMSO has been shown to have an impact on protein aggregation and stability, however, this effect was seen in higher DMSO concentrations (> 3%) than the amount used in this experiments (1%) [286]. The TG activity after *ex vivo* maturation at 44% RH decreased to half of the baseline enzyme activity after two days and four days of incubation. The optimal RH for *ex vivo* maturation was found to be at 70% RH which is confirmed with the enzyme activity assay. TG activity enhances after two days of incubation at 70% RH and drops to baseline TG activity levels. Interestingly, TG activity fell to half-maximal activity after two days at 100% RH and decreased further with *ex vivo* maturation. In fact, high RH reduced the TG activity more efficiently than the induced TG inhibition by LDN-27219. Furthermore, the decrease in TG activity after two days of *ex vivo* maturation at 100% RH was not restored when samples were maintained at 44% RH or 70% RH for the remaining period of *ex vivo* maturation. The CEs matured *ex vivo* at 44% RH or 70% RH for two days showed a dramatic decrease

in TG activity when maintained at 100% RH for two further days. Thus, humidity has been shown to have an impact on TG activity, however, humidity might not regulate TG activity directly. An overhydrated SC may cause structural changes in the corneocytes such as swelling which could influence the proximity between substrates and enzymes [272,287]. An *in vitro* study has previously characterised the conformational changes in ceramides at different RH conditions via Raman spectroscopy [101]. A clear change in ceramide conformational freedom, weakening of hydrogen bonds and lateral packing was observed at 88% RH [101]. This could limit the accessibility and affinity between TG and ceramides and may explain less improved CE hydrophobicity from 80-100% RH compared to 70% RH for both anatomical sites. The findings in this present work show the detrimental impact of high humidity on CE maturation and skin barrier function.

Other studies have associated high hydration with improved CE maturation [141] but the present study indicates otherwise and supports findings that high humidity enhances corneocyte corneodesmolysis and desquamation [275,288]. Low RH and cold ambient temperature have been shown to cause dry and flaky skin in individuals without a history of skin conditions and worsening of the symptoms of atopic dermatitis patients [222,266]. However, sun-exposed skin has been demonstrated to have markers of mild inflammation [83] with elevated protease expression [118] especially in serine proteases [289]. Proteases have been shown to have high proteolytic activity in an aqueous environment [290] and promote break down of profilaggrin to filaggrin and further into natural moisturising factor (NMF). High and low humidities promote filaggrin degradation [271,274]. Filaggrin may be processed at higher water levels in the SC compared causing structural changes such as swelling [291]. These might seem like contradictory findings, however, the presence of NMF is essential at low RH in order to retain moisture in the skin. This has been interpreted as a compensatory mechanism to normalise the SC hydration as well as to maintain the architecture of the SC and the CEs [270]. A hydration-driven degradation of corneodesmosomes has been suggested with a maximal protease activity at high humidity [22, 26]. The protease inhibition experiments in this study were performed in order to understand if the protease activity was involved in suppressing potential *ex vivo* CE maturation. This involved a mixture of broad spectrum protease inhibitors such as AEBSF which irreversibly inactivates serine proteases such as kallikreins and

plasmin. A previous study has shown that Caucasian subjects have lower SC integrity, increased CE cohesiveness and elevated protease activities and thus a thinner SC in the PE cheek site [290]. Individuals living in humid climates have been reported to have an impaired barrier function [182]. This could be eventually transferable to the findings in this present work with Chinese participants. CE rigidity and hydrophobicity increased significantly in the presence of PIs at 100% RH. This resulted in CEs with similar *ex vivo* maturation as observed for 70% RH. In fact, TG activity was reduced at high humidity levels and recovered in the presence of protease inhibitors. This indicates an insufficiency in naturally produced protease inhibitors which was suggested by reported mass spectrometry data [118].

In this project, the focus was on TG as the enzyme that is responsible for maturing CEs. However, 12R-LOX and CathD are crucial in assisting CE maturation and thus were included in this study. The epidermal lipoxygenase, 12R-LOX, catalyses the dioxygenation of the linoleic acid domain in the acylceramides, in the first step of processing these lipids for their subsequent de-esterification to free the ω-hydroxyceramide, to then be attached to the CLE by TG. Thus, if 12R-LOX is insufficiently expressed or inactive this could result in poor skin barrier function. Autosomal recessive congenital ichthyosis has been linked to loss of function mutation in the 12R-LOX gene with associated changes in CLE composition, however, the condition can vary in severity [86,228]. 12R-LOX knockout mice lacked an appropriate skin barrier that led to excessive dehydration and ultimately postnatal death in mice [89]. Photo-damaged SC has been shown to have reduced 12R-LOX protein mass levels [118] which is consistent with the immunostaining experiments in Chapter 3. Furthermore, the 12R-LOX activity was shown to be reduced in PE cheek sites compared to PP post auricular sites (Chapter 5). TG could be suggested as a compensatory mechanism in impaired barrier integrity in order to support the SC integrity by enhancing CE hydrophobicity [100]. The CEs in knockout mice for 12R-LOX were shown to be fragile [89]. This resembles demonstrated CE rigidity in the present study where samples from the PE cheek site. Furthermore, TG and 12R-LOX activity is reduced compared to samples from the PP post auricular site [276]. Inhibitors for 12R-LOX are still unknown, hence a polyclonal antibody for 12R-LOX was used to block the enzyme activity in these experiments. 12R-LOX activity has been demonstrated to be essential for CLE enhancement in corneocytes. However,

blocking the enzyme activity did not improve CE rigidity compared to the 12R-LOX knockout study in mice [89]. 12R-LOX activity was significantly higher at baseline compared to levels of the enzyme in *ex vivo* matured CEs at 70% RH. The hydrophobicity of the CLE increased, thus, the attached lipids may cause spatial hindrance to the substrate as well as the polyclonal antibody. Moreover, 12R-LOX has the property of suicidal inactivation [292] therefore this may have contributed to an overall lower 12R-LOX activity at the end of the *ex vivo* maturation studies.

Interestingly, CathD activity was higher in PE cheek than PP post auricular sites which is consistent with the increased CathD expression in the mass-spectrometery analysis in photo-damaged facial skin [118] and the immunostaining results in Chapter 3. This suggests a higher potential for TG activation in the PE cheek, however, this study has evidence for limited enhancement in CE maturation in the sun-exposed cheek. In fact, the PP post auricular site has a higher TG activity than the PE cheek site. This would suggest that the CathD activity in the PP post auricular site is sufficient to enhance TG activity. However, other proteases than CathD could act on TG activity which would need further testing in addition to this study. In theory, the TG inhibitor LDN-27219 could have an impact on CathD activity but the experiment set up in this study has demonstrated a TG specific inhibition.

The effect of glycerol was investigated at low, optimal, and high RH during *ex vivo* maturation studies of CEs. Many studies have been conducted with glycerol which is a common component of cosmetic products [293]. A negative impact was observed on CE rigidity in CEs *ex vivo* matured at 44% RH. However, glycerol and water before *ex vivo* CE maturation were beneficial for CE maturation at 44% RH. More interestingly, CE hydrophobicity improved significantly in the presence of glycerol or water for samples matured *ex vivo* at 44% RH from PE cheek and PP9 sites compared to baseline CEs and CEs matured *ex vivo* at 44% RH without any pre-treatment. A previous study has shown that CEs were softer and more prone to fragility after glycerol treatment [266]. This might explain the reduced CE rigidity in samples treated with glycerol before *ex vivo* maturation. This might result in artefactual fragility thereby concealing any possible improvement in CE rigidity. Alternatively, glycerol might promote the lipid attachment due to its influence on lipids [101,214] and TG activity (Fig. 6.24) [48].
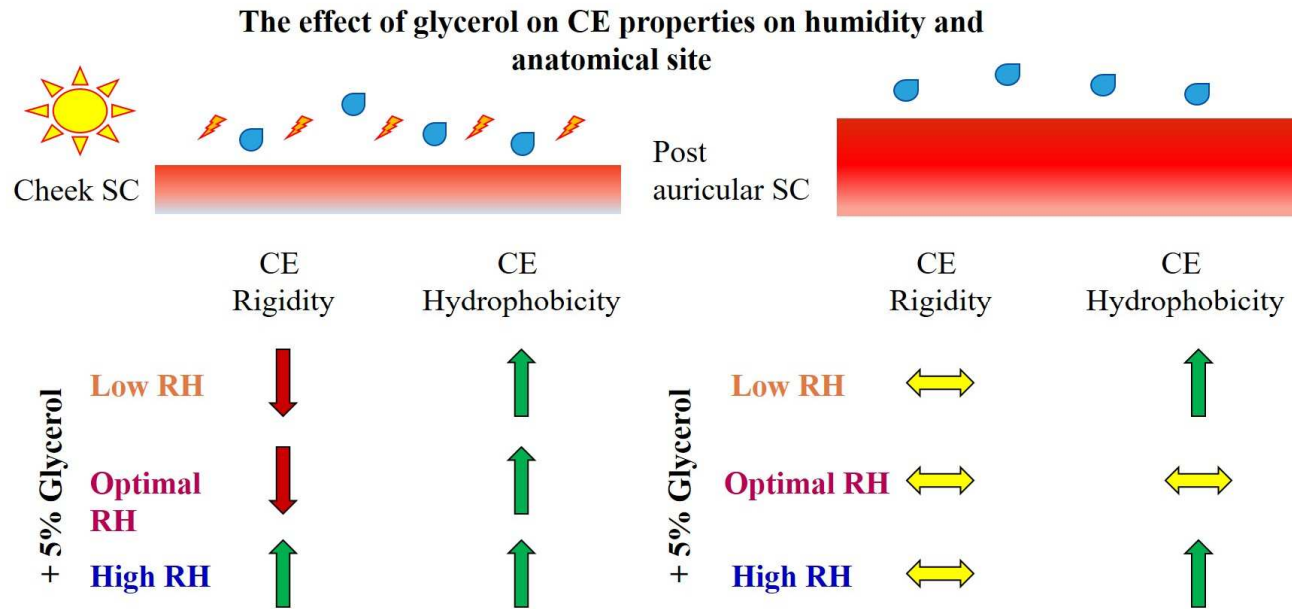
Figure 6.24. Glycerol is more beneficial at low and high RH for CE maturation for the sun-exposed cheek site.

The decreased CE rigidity and enhanced CE hydrophobicity is reflected in a significantly improved RCEM value. Glycerol promoted *ex vivo* maturation at low RH while water was less effective in improving the RCEM which is in line with previously reported differences between water and glycerol for skin hydration [284]. On the other hand, *ex vivo* maturation with hydration, at the optimal RH, resulted in sub-optimal CE maturation in the presence of glycerol or water. Glycerol seems to compensate for the high humidity at 100% RH thereby providing a more beneficial effect than water. Glycerol affects corneocyte maturation positively in terms of CE hydrophobicity especially in the PP post auricular sites and at both tested depths. At high humidity glycerol absorbs moisture while at low humidity it provides hydration for CE maturation [275]. This is in line with the demonstrated findings in the present work where glycerol seems to be more effective at low and high humidity values but not at intermediate humidity levels (Fig. 6.24).

Earlier work [118] revealed differences in proteomics between these two anatomical sites and TG expression is elevated in PE cheek sites compared to the PP post auricular site. Increased TG should overcome and enhance CE maturation in the PE cheek, however, CE rigidity was enhanced only at optimal RH. Samples from the SC surface of the PP post auricular site seem to have reached the potential maximal CE maturation either due to changes in TG activity during *ex vivo* maturation or substrate availability. The mass spectrometry data showed a decreased 12R-LOX protein level in PE cheek samples [118] which was confirmed via immunostaining experiments in this study. However, low 12R-LOX levels hint towards a limitation in CE hydrophobicity which is consistent with findings in this present study. Furthermore, the importance of RH as an environmental factor has been demonstrated to affect CE maturation and has also confirmed the optimal conditions to perform *ex vivo* CE maturation following tape stripping. This has obvious implications for SC maturation *in vivo*. The importance of TG and especially 12R-LOX activities in *ex vivo* CE maturation was also investigated. Furthermore, this work suggests that glycerol as a humectant has limitations at 70% RH but is beneficial at low and high RH, especially for improving CE hydrophobicity. Moreover, the importance of protease inhibition for CE maturation has been identified especially at high humidity. This study provides new insights for CE maturation and demonstrates the effect of 12R-LOX on CE maturation in the SC for the first time.

CHAPTER 7

Conclusions and future works

7. Conclusions and future works

The skin is a powerful barrier against the insults from the environment which can lead to multifactorial consequences. The exposure of the skin to UV radiation has been shown to be beneficial for metabolic functions [294] such as the production of vitamin D [295] which acts on a variety of events such as bone mass formation [296], protection of keratinocytes from apoptosis [297] and regulation of the cardiovascular system [298]. On the other hand, excessive sun exposure is linked to sunburn [299], skin aging [164] and may lead to skin cancer [161]. The benefits and harm depends on the genetic predispositions of every individual and the extent of sun exposure [300]. Another factor is the safety measurements that may be adopted such as the appropriate use of sunscreen [301] as well as the type and duration of UV exposure [302].

The sun may compromise the skin integrity which may lead to a less effective barrier against microbes, viruses and irritants [303]. Recurring damage to the skin may facilitate the formation of wounds and inflammation which might lead to chronic skin conditions. The probability for long-term conditions is increased in individuals with an altered immune system or deficiencies that impair crucial developmental stages of the epidermis. The barrier integrity of the skin can be evaluated via TEWL measurements [24]. This demonstrated that the PE skin indeed had a lower barrier function than the PP site in Caucasians and Chinese participants. An earlier study showed no differences between Caucasian and Chinese populations. The discrepancy in the findings may reflect differences in age and geographical characteristics as well as the subject number [150]. Tape stripping is a useful technique to collect thin layers of the SC; in addition, the adhesive challenges the cohesiveness between the corneocytes. In theory, the cohesiveness originates from the corneodesmosomes which are connected the corneocytes. Corneodesmosomes are degraded during desquamation allowing the shedding of the "old" skin. The amount of collected SC samples reflects the desquamation process which decreases with SC depth. The amount of collected SC can be either expressed in SC weight or in the protein amount on the tape strips. The protein content collected on the tapes showed a major difference between the cheek and the post auricular SC cohesiveness. The cheek decreased in collected protein amounts with tape stripping while the proteins obtained from the post auricular site showed no difference between tape strips. Nine tape strippings collected more compactly connected corneocytes in the cheek while corneocytes in post auricular

site were loosely connected. This reflects a higher SC cohesiveness in the PE cheek than the PP post auricular site. Furthermore, a significant difference was observed between the ethnic groups and between the genders. Tape stripping indicated a higher SC cohesiveness in Chinese participants and in Caucasian subjects in both anatomical sites. A high cohesiveness is the result of a high activity of proteases desquamating the upper most SC layer. A recent study has confirmed that a range of UV radiations intensities induces the degradation of corneodesmosomes resulting in a decreased mechanical stability of the SC [177]. This is in line with other studies showing enhanced desquamation in photo-damaged skin [122]. The SC thickness was estimated from the plot of inverse TEWL measurements and the corresponding cumulative protein amounts via tape stripping. This provides an evaluation of how much protein could have been collected before reaching the stratum granulosum. In fact, the nine tape strips removed up to 70% of the SC from the PE cheek while tape stripping removed up to 40% of the SC from the PP post auricular in this present study. The SC was thinner in both sites for Chinese participants compared to the SC thickness of the Caucasian subjects. The differences in the SC thickness confirms enhanced desquamation in the Chinese subjects in this study suggesting crucial differences between the two ethnic populations living in the same environment. All subjects were asked to refrain from any skin care product to allow measurements of the skin parameters at baseline and without the influence of skin care ingredients. Potentially these subjects may have a higher desquamation rate while having no differences in the SC integrity which might originate from the properties of the corneocytes. Therefore, the Chinese participants were selected for further evaluation for biomarkers of corneocyte maturation.

Corneocytes are composed up of proteins and lipids that may alter in their amounts depending on the genetics of the individual as well as environmental factors. For a number of past years, researchers have been using INV as a biomarker for immaturity of CEs obtained via tape stripping [114,195,196]. The maturity of CEs is a crucial aspect of the skin barrier function. However, relying only on one assessment may lead to missing information that would contribute to the understanding in the corneocyte maturation in different levels. A previous mass spectroscopy study was performed on tape strip samples from the PE cheek and PP post auricular sites in Caucasian females living in Pretoria, South Africa [118]. The analysed samples were

pooled and thus not distinguishing between depths but only anatomical sites. The study identified 204 proteins expressed in the PE cheek site while only 21 proteins were found in PP post auricular sites. Interestingly, comparison of the protein expression revealed 73 proteins are upregulated and 30 proteins are downregulated in PE cheek samples compared to PP post auricular samples. The free EOS ceramide is processed by 12R-LOX and eLOX3 which have been shown to be required to generate the CLE. Both membrane-bound enzymes were assessed as biomarkers to identify differences in ceramide processing enzymes between anatomical sites and depths. The PE cheek and the PP post auricular sites have significant differences in 12R-LOX expression but not eLOX3. This is in line with the down regulated 12R-LOX expression in the previously published mass spectroscopy results [118]. This indicates a lower amount of ceramides that are potentially attached to the CLE. A hydrophobic CLE is a compromising factor for the SC barrier which results in a higher TEWL which was as observed in the PE cheek site.

The proteases including CathD and CathV showed a higher expression in the SC samples from PE cheek site compared to the samples from the PP post auricular site [118]. Corneocytes from the PE cheek have been shown to have a higher protein expression, CathD and CathV, compared to corneocyte from the PP post auricular site. The expression of CathD and CathV seems to decrease towards the surface of the SC with a high population of corneocytes that are prepared for desquamation. The increased proteolytic activity of CathD is confirmed in the samples in the deeper SC layers. The *ex vivo* maturation of corneocytes at 70% RH had no impact on CathD activity. Furthermore, the high fluorescence signal in the PE cheek for CathD and CathV is a confirmation of photo-damage in the PE cheek as described by other researchers [120,122,123]. This provides a further link between photo-damage, proteases and the thinning of the facial SC.

The structural proteins, INV and XP32, in the PE cheek site were shown to be upregulated compared to those in SC samples from the PP post auricular sites [118]. The corneocytes mature on their way to the surface of the SC surface. In the present study, the expression of INV and XP32 are higher in corneocytes from the ninth tape strip compared to CEs from the first tape strip in both anatomical sites. However, the differences between the protein expressions in corneocytes sampled from both

anatomical sites may reflect the fact that nine tape strips reached different depths in the SC.

The primary enzyme responsible for corneocyte maturation is TG which has three subtypes in the epidermis [258]. However, TG1 was identified to be the most abundant variant that cross-links the structural proteins in the CPE [84,95] and attaches the lipids to the CLE [229,261]. The earlier mass spectroscopy study, TG1 was shown to be upregulated with a cheek to post auricular ratio of 1.47 ($p{\leq}0.01$). However, the present study visualised the TG1 expression via immunostaining experiments on corneocytes from the first and ninth tape strip obtained from both anatomical sites. The corneocytes from the PP post auricular site showed higher TG1 expression than corneocytes from the PE cheek site. The immunostaining does not consider unbound TG1 that might be freed from the membrane by CathD. The PE cheek site showed a lower TG1 expression compared to the PP post auricular site in corneocytes from the first and ninth tape strip. Interestingly, 12R-LOX and TG1 have the same protein expression in both anatomical sites. This indicates an impaired CE maturation in the sun-exposed facial skin.

Further investigations should examine localisation of 12R-LOX and TG1 on the corneocytes as well as on keratinocytes. The co-dependency of these two enzymes could be shown in cell culture models by silencing either enzyme and determining the changes in the gene expression profile. This could be combined with a 3D-model and UV radiation as a stress factor to determine its direct influence on the enzymes. This could then be followed by determination of the expression profiles and enzyme activities as well as the change in the barrier functionality. Furthermore, the presented expression profile of a combination of biomarkers could be used as an initial profiling in disease models such as atopic dermatitis or psoriasis.

In 2001, Hirao and colleagues introduced the CE immaturity assay by assessing INV positive CEs via immunostaining and CE hydrophobicity via the Nile red staining [114]. This method was adapted later to generate a green and red pixel ratio of the fluorescence signals in order to save time during the image analysis. However, the obtained ratio was not comparable between studies [115,196]. The ratio does not distinguish between artefacts or background noise which is very likely due to the high level of SDS which precipitates at low temperature. The removal of excessive SDS

and the suspension of CEs in PBS results in a significantly lower background noise and increases the image resolution. However, the INV/Nile red staining was shown to be ineffective to determine CE maturity in the samples collected from the ninth tape strip of both anatomical sites. This confirmed the need for a new characterisation method based on the general understanding that corneocyte maturation leads to rigid and hydrophobic CEs. Sonication was chosen as an appropriate method to challenge the mechanical resistance of CEs and to demonstrate the rigidity of the CEs. Nile red staining was used to visualise the CEs according to their hydrophobicity. The RCEM value is determined according to the CE rigidity and hydrophobicity and provides further insights into the physical and chemical state of the corneocytes. This method showed a clear correlation between RCEM and SC integrity and cohesion in both anatomical sites. The conventional immunostaining approach failed to present correlations between CE and SC properties in the PP post auricular site. Furthermore, variations between subjects were shown to be smaller compared to the conventional INV/Nile red staining analysed via INV (+) CEs and red/green ratio. RCEM assessment confirmed that the corneocytes from the first and ninth tape strip collected from the PE cheek site are less mature than corneocytes from the PP post auricular site. The new method has been shown to be a robust and rapid method to characterise CE maturity.

The CE maturity depends highly on TG activity as well as the enzyme activity of 12R-LOX. However, 12R-LOX has only recently become of interest to skin researchers and thus the substrates and blocking agents are not yet commercially available. A fluorescence based assay for the 12-LOX variant was previously developed with arachidonic acid as a substrate [242]. However, other studies failed to detect any 12R-LOX activity using arachidonic acid as a substrate [87,94]. Ethyl linoleic acid was used as a substrate for 12R-LOX to generate reactive oxygen species which reduce the detection agent, H_2DCFDA. A screening of antibodies for 12R-LOX was performed via immunostaining and the used polyclonal 12R-LOX antibody showed a significant decrease in the fluorescence signal. The antibody for eLOX3 was used as an internal control. However, eLOX3 antibody had no impact on the signal intensity and thus an antigen specific inhibition was confirmed. Furthermore 5-LOX, 12-LOX and 15-LOX activity was excluded, via the inhibitor ML351, to cause the fluorescence signal. The 12R-LOX activity showed a positive correlation with TEWL

measurements as well as the RCEM values. Furthermore, this assay may be a useful method to assess 12R-LOX activity in skin conditions with an impaired barrier function such as xerosis or atopic dermatitis. This is the first reported activity assay for 12R-LOX and thus further analysis will be needed once substrate and selective inhibitors are commercially available.

Blocking 12R-LOX with the polyclonal 12R-LOX antibody resulted in an enhancement in CE rigidity while CE hydrophobicity was unchanged. However, the enzyme activity assay confirmed a decrease in 12R-LOX activity after four days of *ex vivo* maturation of CEs at 70% RH. This indicates a depletion of ω-hydroxyceramides for the CLE for the corneocytes from the PE cheek site.

A recent study has shown that the mechanical flexibility and stability of the SC decreases depending on exposure to UV light of various intensities and RH [177]. A number of studies have demonstrated the adverse effects of high RH on the skin [271,288,304,305]. However, the present study is the first that linked RH and an assay of enzymes in the SC that have an impact on corneocyte maturation. The RCEM approach demonstrated decreasing CE rigidity after *ex vivo* maturation of CEs above 80% RH but no change in CE hydrophobicity. However, samples from the deeper SC layer in both anatomical sites showed a more dramatic change in CE hydrophobicity than corneocytes from the superficial SC layer. This is consistent with most of the enzymes having a higher activity in the deeper SC layers. This ensures appropriate maturation of the CEs reaching the SC surface that provide support for the skin barrier function.

TG is one of the thoroughly characterised enzymes in the skin. TG creates an insoluble CPE by crosslinking the structural proteins [84,95,96] and generates a hydrophobic CLE by attaching ω-hydroxyceramides covalently to the CPE [50,229]. However, blocking TG during *ex vivo* maturation showed a clear decrease in CE rigidity. This finding was unexpected considering that the CPE was reported as an insoluble protein structure. The CPE is constructed and is maintained as a mechanically resistant structure by TG. The TG activity assay confirmed that the TG inhibitor (LDN-27219) blocks TG activity. LDN-27219 has been characterised as a reversible and slow-binding inhibitor that interacts with the guanosine triphosphate (GTP) binding site rather than the catalytic active site of TG [281]. The nucleotide,

GTP, induces conformational changes in TG causing a weakening of the interaction with calcium which is essential for TG activity [306,307]. LDN-27219 did not alter the 12R-LOX and CathD activity in the tested samples while TG activity decreased considerably in the presence of the inhibitor. The TG activity decreased in samples kept at 44% RH for two days, however, after four days TG activity was unchanged. This suggests that low humidity is not beneficial for CE maturation but also not as harmful as high humidity. An additional experiment was performed to understand whether RH can act as a switch for TG activity and if the TG activity could be recovered by changing the RH after two days of *ex vivo* maturation. This meant two days of *ex vivo* maturation at either 44% RH or at 70% RH and then a change to 100% RH for two further days of incubation. Another set of experiments started with two days of *ex vivo* maturation at 100% RH and two more days of incubation at 44% RH or 70% RH. The change in RH had a clear impact on the inactivation of TG activity. The decrease in TG activity was greater in samples *ex vivo* matured at 70% RH that were changed to 100% RH compared to samples that were at 44% RH and then *ex vivo* matured to 100% RH. This could be due to compensatory mechanisms such as the presence of NMF that is capable of binding water to an extent. At 70% RH the water-binding capacity of NMF might be saturated before the samples were placed at 100% RH. However, proteases such as plasmin or desmoglein 1 were shown to be highly active at high humidity [177,288]. In the present study, the broad inhibition of proteases led to an enhancement in CE rigidity and CE hydrophobicity at high humidity. Furthermore, TG activity improved in the presence of the protease inhibitor mixture at all tested humidity values. However, the most remarkable enhancement was observed at 100% RH. This suggests that high humidity has an indirect impact on TG activity by enhancing protease activity.

Natural protease inhibitors might be depleted in the PE cheek site compared to the PP post auricular site. The earlier mass spectroscopy study showed a general downregulation of some protease inhibitors such as serpin A 12 in PE cheek samples [118]. This protease inhibitor binds to the catalytic site of serine proteases and causes an irreversible conformational change [308]. The decrease in protease inhibitors is reflected in the increase of protease expression and activity in the PE cheek site [118,289,290]. The decrease in endogenous protease inhibitors might be related to the impaired and thinner SC with less mature corneocytes in the PE cheek site in the

present study. This needs further investigation in order to identify the proteases with enhanced activity and a selective protease inhibitor to block the protease activity.

The changes in CE maturation at low, optimal and high humidity were altered in the presence of glycerol. The unique feature of either absorbing or releasing humidity depends on the humidity level of the environment. However, glycerol enhanced the CE hydrophobicity at 44% RH and 100% RH but had no effect at 70% RH. Earlier studies have shown that glycerol causes a swelling and softening of corneocytes [309]. Atomic force microscopy could be used for further confirmation of these effects. However, measuring TG and 12R-LOX activity would be a reasonable next step to understand how this moisturising agent acts to enhance *ex vivo* CE maturation. Furthermore, *in vivo* studies would add further understanding concerning the action of glycerol on the corneocyte and on the enzymes involved in CE maturation.

Finally, *in vivo* studies on animal models such as the pig would be the best option to test the effect of moisturisers supplemented with selective protease inhibitor for the hyperactive protease at high humidity. These studies could be followed by the assessment of the skin barrier function, enzyme activities and corneocyte maturation. Biomarkers of the barrier function would provide further validation before applying the product topically on human subjects. A positive outcome could lead towards a patent for commercialisation of the improved moisturiser. In theory, this could prevent development of dry skin after long term moisturisation and should enhance the skin barrier function and integrity.

References

1. Rougier, A., Dupuis, D., Lotte, C., Roguet, R., Wester, R.C., and Maibach, H.I. (1986) Regional variation in percutaneous absorption in man: measurement by the stripping method. *Arch. Dermatol. Res.*, **278** (6), 465–469.

2. Mauldin, E.A., and Peters-Kennedy, J. (2016) Integumentary System, in *Jubb, Kennedy & Palmer's Pathology of Domestic Animals: Volume 1*, Elsevier, pp. 509-736.e1.

3. Markman, B., and Barton, F.E. (1987) Anatomy of the subcutaneous tissue of the trunk and lower extremity. *Plast. Reconstr. Surg.*, **80** (2), 248–254.

4. Alexander, C.M., Kasza, I., Yen, C.-L.E., Reeder, S.B., Hernando, D., Gallo, R.L., Jahoda, C.A.B., Horsley, V., and MacDougald, O.A. (2015) Dermal white adipose tissue: a new component of the thermogenic response. *J. Lipid Res.*, **56** (11), 2061–2069.

5. Lancerotto, L., Stecco, C., Macchi, V., Porzionato, A., Stecco, A., and De Caro, R. (2011) Layers of the abdominal wall: anatomical investigation of subcutaneous tissue and superficial fascia. *Surg. Radiol. Anat.*, **33** (10), 835–842.

6. Hayward, M.G., and Keatinge, W.R. (1981) Roles of subcutaneous fat and thermoregulatory reflexes in determining ability to stabilize body temperature in water. *J. Physiol.*, **320**, 229–251.

7. Reddy, N.P. (1986) Mechanical Stress and Viability of Skin and Subcutaneous Tissue, in *Tissue Nutrition and Viability* (eds.Hargens, A.R.), Springer US, New York, NY, pp. 215–241.

8. Menon, G.K. (2002) New insights into skin structure: scratching the surface. *Adv. Drug Deliv. Rev.*, **54 Suppl 1**, S3-17.

9. Hobson, D.W. (2006) Dermal Absorption Models in Toxicology and Pharmacology. *Int. J. Toxicol.*, **25** (5), 439–441.

10. Salmon, J.K., Armstrong, C.A., and Ansel, J.C. (1994) The skin as an immune organ. *West. J. Med.*, **160** (2), 146–152.

11. Lightwood, R. (1951) Radial nerve palsy associated with localized subcutaneous fat necrosis in the newborn. *Arch. Dis. Child.*, **26** (129), 436–437.

12. Millington, P.F., and Wilkinson, R. (1983) *Skin*, Cambridge University Press, Cambridge [Cambridgeshire] ; New York.

13. Candi, E., Schmidt, R., and Melino, G. (2005) The cornified envelope: a model of cell death in the skin. *Nat. Rev. Mol. Cell Biol.*, **6** (4), 328–340.

14. Murphy, K., Travers, P., Walport, M., and Janeway, C. (2012) *Janeway's immunobiology*, Garland Science, New York.

15. Streilein, J.W. (1983) Skin-associated lymphoid tissues (SALT): origins and functions. *J. Invest. Dermatol.*, **80 Suppl**, 12s–16s.

16. Heuss, E. (1892) Die Reaktion des Schweisses beim gesunden Menschen. *Monatschr Prakt Dermatol*, (14), 341–343.

17. Blank, I.H. (1939) Measurement of pH of the Skin Surface. *J. Invest. Dermatol.*, **2** (5), 231–234.

18. Rippke, F., Schreiner, V., and Schwanitz, H.-J. (2002) The Acidic Milieu of the Horny Layer: New Findings on the Physiology and Pathophysiology of Skin pH. *Am. J. Clin. Dermatol.*, **3** (4), 261–272.

19. Fluhr, J.W., Kao, J., Ahn, S.K., Feingold, K.R., Elias, P.M., and Jain, M. (2001) Generation of free fatty acids from phospholipids regulates stratum corneum acidification and integrity. *J. Invest. Dermatol.*, **117** (1), 44–51.

20. Schmid-Wendtner, M.-H., and Korting, H.C. (2006) The pH of the Skin Surface and Its Impact on the Barrier Function. *Skin Pharmacol. Physiol.*, **19** (6), 296–302.

21. Wolf, J. (1939) Die innere Struktur der Zellen des Stratum desquamans des menschlichen Epidermis. *Z Mikrosk Anat Forsch*, (46), 17–202.

22. Sagebiel, R.W. (1972) In vivo and in vitro uptake of ferritin by Langerhans cells of the epidermis. *J. Invest. Dermatol.*, **58** (2), 47–54.

23. Kurosumi, K., Kurosumi, U., and Suzuki, H. (1969) Fine structures of Merkel cells and associated nerve fibers in the epidermis of certain mammalian species. *Arch. Histol. Jpn. Nihon Soshikigaku Kiroku*, **30** (3), 295–313.

24. Blank, I.H. (1953) Further observations on factors which influence the water content of the stratum corneum. *J. Invest. Dermatol.*, **21** (4), 259–271.

25. Frosch, P.J., Duncan, S., and Kligman, A.M. (1980) Cutaneous biometrics I. The response of human skin to dimethyl sulphoxide. *Br. J. Dermatol.*, **103** (3), 263–274.

26. Wertz, P.W., Swartzendruber, D.C., Kitko, D.J., Madison, K.C., and Downing, D.T. (1989) The role of the corneocyte lipid envelopes in cohesion of the stratum corneum. *J. Invest. Dermatol.*, **93** (1), 169–172.

27. Michaels, A.S., Chandrasekaran, S.K., and Shaw, J.E. (1975) Drug permeation through human skin: Theory and invitro experimental measurement. *AIChE J.*, **21** (5), 985–996.

28. Rawlings, A. (2005) Sources and role of stratum corneum hydration, in *Skin Barrier* (eds.Elias, P., and Feingold, K.), CRC Press, pp. 399–425.

29. Blanpain, C., and Fuchs, E. (2006) Epidermal Stem Cells of the Skin. *Annu. Rev. Cell Dev. Biol.*, **22** (1), 339–373.

30. Lewis, E.E.L., Barrett, M.R.T., Freeman-Parry, L., Bojar, R.A., and Clench, M.R. (2018) Examination of the skin barrier repair/wound healing process using a living skin equivalent model and matrix-assisted laser desorption-ionization-mass spectrometry imaging. *Int. J. Cosmet. Sci.*, **40** (2), 148–156.

31. Fuchs, E., and Weber, K. (1994) Intermediate Filaments: Structure, Dynamics, Function and Disease. *Annu. Rev. Biochem.*, **63** (1), 345–382.

32. Hieda, Y., Nishizawa, Y., Uematsu, J., and Owaribe, K. (1992) Identification of a new hemidesmosomal protein, HD1: a major, high molecular mass component of isolated hemidesmosomes. *J. Cell Biol.*, **116** (6), 1497–1506.

33. Holbrook, K.A., and Odland, G.F. (1974) Regional Differences in the Thickness (Cell Layers) of the Human Stratum Corneum: An Ultrastructural Analysis. *J. Invest. Dermatol.*, **62** (4), 415–422.

34. Thomson, M.L. (1955) Relative efficiency of pigment and horny layer thickness in protecting the skin of Europeans and Africans against solar ultraviolet radiation. *J. Physiol.*, **127** (2), 236–246.

35. Delevoye, C. (2014) Melanin Transfer: The Keratinocytes Are More than Gluttons. *J. Invest. Dermatol.*, **134** (4), 877–879.

36. Tobin, D.J. (2006) Biochemistry of human skin—our brain on the outside. *Chem Soc Rev*, **35** (1), 52–67.

37. Sawant, M.S., and Leube, R.E. (2017) Consequences of Keratin Phosphorylation for Cytoskeletal Organization and Epithelial Functions, in *International Review of Cell and Molecular Biology*, vol. 330, Elsevier, pp. 171–225.

38. Steven, A.C., and Steinert, P.M. (1994) Protein composition of cornified cell envelopes of epidermal keratinocytes. *J. Cell Sci.*, **107 (Pt 2)**, 693–700.

39. Matoltsy, A.G., and Matoltsy, M.N. (1970) The chemical nature of keratohyalin granules of the epidermis. *J. Cell Biol.*, **47** (3), 593–603.

40. Nemes, Z., and Steinert, P.M. (1999) Bricks and mortar of the epidermal barrier. *Exp. Mol. Med.*, **31** (1), 5–19.

41. Brown, M.B., Martin, G.P., Jones, S.A., and Akomeah, F.K. (2006) Dermal and transdermal drug delivery systems: current and future prospects. *Drug Deliv.*, **13** (3), 175–187.

42. Steinert, P.M., and Marekov, L.N. (1995) The Proteins Elafin, Filaggrin, Keratin Intermediate Filaments, Loricrin, and Small Proline-rich Proteins 1 and 2 Are Isodipeptide Cross-linked Components of the Human Epidermal Cornified Cell Envelope. *J. Biol. Chem.*, **270** (30), 17702–17711.

43. Takahashi, M., Tezuka, T., and Katunuma, N. (1992) Phosphorylated cystatin α is a natural substrate of epidermal transglutaminase for formation of skin cornified envelope. *FEBS Lett.*, **308** (1), 79–82.

44. Steinert, P.M., Kartasova, T., and Marekov, L.N. (1998) Biochemical evidence that small proline-rich proteins and trichohyalin function in epithelia by modulation of the biomechanical properties of their cornified cell envelopes. *J. Biol. Chem.*, **273** (19), 11758–11769.

45. Steinert, P.M., Candi, E., Kartasova, T., and Marekov, L. (1998) Small proline-rich proteins are cross-bridging proteins in the cornified cell envelopes of stratified squamous epithelia. *J. Struct. Biol.*, **122** (1–2), 76–85.

46. Resing, K.A., Dale, B.A., and Walsh, K.A. (1985) Multiple copies of phosphorylated filaggrin in epidermal profilaggrin demonstrated by analysis of tryptic peptides. *Biochemistry*, **24** (15), 4167–4175.

47. Steinert, P.M., Cantieri, J.S., Teller, D.C., Lonsdale-Eccles, J.D., and Dale, B.A. (1981) Characterization of a class of cationic proteins that specifically interact with intermediate filaments. *Proc. Natl. Acad. Sci. U. S. A.*, **78** (7), 4097–4101.

48. Rawlings, A.V., Scott, I.R., Harding, C.R., and Bowser, P.A. (1994) Stratum Corneum Moisturization at the Molecular Level. *J. Invest. Dermatol.*, **103** (5), 731–740.

49. Rawlings, A.V., and Voegeli, R. (2013) Stratum corneum proteases and dry skin conditions. *Cell Tissue Res.*, **351** (2), 217–235.

50. Nemes, Z., Marekov, L.N., Fesus, L., and Steinert, P.M. (1999) A novel function for transglutaminase 1: Attachment of long-chain -hydroxyceramides to involucrin by ester bond formation. *Proc. Natl. Acad. Sci.*, **96** (15), 8402–8407.

51. Rice, R.H., and Green, H. (1977) The cornified envelope of terminally differentiated human epidermal keratinocytes consists of cross-linked protein. *Cell*, **11** (2), 417–422.

52. Burr, G.O., and Burr, M.M. (1930) On the nature and role of the fatty acids essential in nutrition. *J. Biol. Chem.*, **86**, 587–621.

53. Prottey, C. (1977) Investigation of functions of essential fatty acids in the skin. *Br. J. Dermatol.*, **97** (1), 29–38.

54. Matoltsy, A.G., Downes, A.M., and Sweeney, T.M. (1968) Studies of the Epidermal Water Barrier. Part II. Investigation of the Chemical Nature of the Water Barrier**From the Department of Dermatology, Boston University School of Medicine, and Evans Memorial Department of Clinical Research, University Hospital, Boston University Medical Center, Boston, Mass. *J. Invest. Dermatol.*, **50** (1), 19–26.

55. Middleton, J.D. (1968) THE MECHANISM OF WATER BINDING IN STRATUM CORNEUM. *Br. J. Dermatol.*, **80** (7), 437–450.

56. Williams, M.L., and Elias, P.M. (1987) The extracellular matrix of stratum corneum: role of lipids in normal and pathological function. *Crit. Rev. Ther. Drug Carrier Syst.*, **3** (2), 95–122.

57. Elias, P.M., Goerke, Jon., and Friend, D.S. (1977) Mammalian Epidermal Barrier Layer Lipids: Composition and Influence on Structure. *J. Invest. Dermatol.*, **69** (6), 535–546.

58. Wertz, P.W., Miethke, M.C., Long, S.A., Strauss, J.S., and Downing, D.T. (1985) The composition of the ceramides from human stratum corneum and from comedones. *J. Invest. Dermatol.*, **84** (5), 410–412.

59. Lampe, M.A., Burlingame, A.L., Whitney, J., Williams, M.L., Brown, B.E., Roitman, E., and Elias, P.M. (1983) Human stratum corneum lipids: characterization and regional variations. *J. Lipid Res.*, **24** (2), 120–130.

60. Bouwstra, J.A., Honeywell-Nguyen, P.L., Gooris, G.S., and Ponec, M. (2003) Structure of the skin barrier and its modulation by vesicular formulations. *Prog. Lipid Res.*, **42** (1), 1–36.

61. Grubauer, G., Feingold, K.R., and Elias, P.M. (1987) Relationship of epidermal lipogenesis to cutaneous barrier function. *J. Lipid Res.*, **28** (6), 746–752.

62. Danso, M., Boiten, W., van Drongelen, V., Gmelig Meijling, K., Gooris, G., El Ghalbzouri, A., Absalah, S., Vreeken, R., Kezic, S., van Smeden, J., Lavrijsen, S., and Bouwstra, J. (2017) Altered expression of epidermal lipid bio-synthesis enzymes in atopic dermatitis skin is accompanied by changes in stratum corneum lipid composition. *J. Dermatol. Sci.*, **88** (1), 57–66.

63. Eckl, K.-M., Tidhar, R., Thiele, H., Oji, V., Hausser, I., Brodesser, S., Preil, M.-L., Onal-Akan, A., Stock, F., Müller, D., Becker, K., Casper, R., Nürnberg, G., Altmüller, J., Nürnberg, P., Traupe, H., Futerman, A.H., and Hennies, H.C. (2013) Impaired epidermal ceramide synthesis causes autosomal recessive congenital ichthyosis and reveals the importance of ceramide acyl chain length. *J. Invest. Dermatol.*, **133** (9), 2202–2211.

64. Kagehara, M., Tachi, M., Harii, K., and Iwamori, M. (1994) Programmed expression of cholesterol sulfotransferase and transglutaminase during epidermal

differentiation of murine skin development. *Biochim. Biophys. Acta*, **1215** (1–2), 183–189.

65. Rassner, U., Feingold, K.R., Crumrine, D.A., and Elias, P.M. (1999) Coordinate assembly of lipids and enzyme proteins into epidermal lamellar bodies. *Tissue Cell*, **31** (5), 489–498.

66. Elias, P.M., Cullander, C., Mauro, T., Rassner, U., Kömüves, L., Brown, B.E., and Menon, G.K. (1998) The secretory granular cell: the outermost granular cell as a specialized secretory cell. *J. Investig. Dermatol. Symp. Proc.*, **3** (2), 87–100.

67. Denda, M., Fuziwara, S., and Inoue, K. (2003) Influx of calcium and chloride ions into epidermal keratinocytes regulates exocytosis of epidermal lamellar bodies and skin permeability barrier homeostasis. *J. Invest. Dermatol.*, **121** (2), 362–367.

68. Sato, J., Denda, M., Nakanishi, J., Nomura, J., and Koyama, J. (1998) Cholesterol Sulfate Inhibits Proteases that are Involved in Desquamation of Stratum Corneum. *J. Invest. Dermatol.*, **111** (2), 189–193.

69. Groen, D., Poole, D.S., Gooris, G.S., and Bouwstra, J.A. (2011) Is an orthorhombic lateral packing and a proper lamellar organization important for the skin barrier function? *Biochim. Biophys. Acta BBA - Biomembr.*, **1808** (6), 1529–1537.

70. Forslind, B. (1994) A domain mosaic model of the skin barrier. *Acta Derm. Venereol.*, **74** (1), 1–6.

71. Bowser, P.A., Nugteren, D.H., White, R.J., Houtsmuller, U.M., and Prottey, C. (1985) Identification, isolation and characterization of epidermal lipids containing linoleic acid. *Biochim. Biophys. Acta*, **834** (3), 419–428.

72. Školová, B., Kováčik, A., Tesař, O., Opálka, L., and Vávrová, K. (2017) Phytosphingosine, sphingosine and dihydrosphingosine ceramides in model skin lipid membranes: permeability and biophysics. *Biochim. Biophys. Acta Biomembr.*, **1859** (5), 824–834.

73. t'Kindt, R., Jorge, L., Dumont, E., Couturon, P., David, F., Sandra, P., and Sandra, K. (2012) Profiling and Characterizing Skin Ceramides Using Reversed-Phase Liquid Chromatography–Quadrupole Time-of-Flight Mass Spectrometry. *Anal. Chem.*, **84** (1), 403–411.

74. Wertz, P.W., and Downing, D.T. (1983) Ceramides of pig epidermis: structure determination. *J. Lipid Res.*, **24** (6), 759–765.

75. Oldroyd, J.R., Critchley, P., Tiddy, G.J.T., Turner, J.E., and Rawlings, A.V. (1994) Specialized role for ceramide one int he stratum corneum water barrier. *J. Invest. Dermatol.*, (102), 525.

76. Yamamoto, A., Serizawa, S., Ito, M., and Sato, Y. (1991) Stratum corneum lipid abnormalities in atopic dermatitis. *Arch. Dermatol. Res.*, **283** (4), 219–223.

77. Conti, A., Rogers, J., Verdejo†, P., Harding, C.R., and Rawlings, A.V. (1996) Seasonal influences on stratum corneum ceramide 1 fatty acids and the influence of topical essential fatty acids. *Int. J. Cosmet. Sci.*, **18** (1), 1–12.

78. Li, E.R., Owens, D.M., Djian, P., and Watt, F.M. (2000) Expression of involucrin in normal, hyperproliferative and neoplastic mouse keratinocytes. *Exp. Dermatol.*, **9** (6), 431–438.

79. Elias, P., Ahn, S., Brown, B., Crumrine, D., and Feingold, K.R. (2002) Origin of the epidermal calcium gradient: regulation by barrier status and role of active vs passive mechanisms. *J. Invest. Dermatol.*, **119** (6), 1269–1274.

80. Celli, A., Mackenzie, D.S., Crumrine, D.S., Tu, C.L., Hupe, M., Bikle, D.D., Elias, P.M., and Mauro, T.M. (2011) Endoplasmic reticulum Ca2+ depletion activates XBP1 and controls terminal differentiation in keratinocytes and epidermis. *Br. J. Dermatol.*, **164** (1), 16–25.

81. Behne, M.J., Meyer, J.W., Hanson, K.M., Barry, N.P., Murata, S., Crumrine, D., Clegg, R.W., Gratton, E., Holleran, W.M., Elias, P.M., and Mauro, T.M. (2002) NHE1 regulates the stratum corneum permeability barrier homeostasis. Microenvironment acidification assessed with fluorescence lifetime imaging. *J. Biol. Chem.*, **277** (49), 47399–47406.

82. Rippke, F., Schreiner, V., Doering, T., and Maibach, H.I. (2004) Stratum corneum pH in atopic dermatitis: impact on skin barrier function and colonization with Staphylococcus Aureus. *Am. J. Clin. Dermatol.*, **5** (4), 217–223.

83. Suzuki, Y., Nomura, J., Koyama, J., and Horii, I. (1994) The role of proteases in stratum corneum: involvement in stratum corneum desquamation. *Arch. Dermatol. Res.*, **286** (5), 249–253.

84. Candi, E., Tarcsa, E., Idler, W.W., Kartasova, T., Marekov, L.N., and Steinert, P.M. (1999) Transglutaminase Cross-linking Properties of the Small Proline-rich 1 Family of Cornified Cell Envelope Proteins: INTEGRATION WITH LORICRIN. *J. Biol. Chem.*, **274** (11), 7226–7237.

85. Freinkel, R.K., and Traczyk, T.N. (1980) The phospholipases A of epidermis. *J. Invest. Dermatol.*, **74** (3), 169–173.

86. Jobard, F. (2002) Lipoxygenase-3 (ALOXE3) and 12(R)-lipoxygenase (ALOX12B) are mutated in non-bullous congenital ichthyosiform erythroderma (NCIE) linked to chromosome 17p13.1. *Hum. Mol. Genet.*, **11** (1), 107–113.

87. Brash, A.R. (1999) Lipoxygenases: Occurrence, Functions, Catalysis, and Acquisition of Substrate. *J. Biol. Chem.*, **274** (34), 23679–23682.

88. Yu, Z., Schneider, C., Boeglin, W.E., Marnett, L.J., and Brash, A.R. (2003) The lipoxygenase gene ALOXE3 implicated in skin differentiation encodes a hydroperoxide isomerase. *Proc. Natl. Acad. Sci.*, **100** (16), 9162–9167.

89. Epp, N., Fürstenberger, G., Müller, K., de Juanes, S., Leitges, M., Hausser, I., Thieme, F., Liebisch, G., Schmitz, G., and Krieg, P. (2007) 12R-lipoxygenase deficiency disrupts epidermal barrier function. *J. Cell Biol.*, **177** (1), 173–182.

90. Krieg, P., Rosenberger, S., de Juanes, S., Latzko, S., Hou, J., Dick, A., Kloz, U., van der Hoeven, F., Hausser, I., Esposito, I., Rauh, M., and Schneider, H. (2013) Aloxe3 Knockout Mice Reveal a Function of Epidermal Lipoxygenase-3 as Hepoxilin Synthase and Its Pivotal Role in Barrier Formation. *J. Invest. Dermatol.*, **133** (1), 172–180.

91. Boeglin, W.E., Kim, R.B., and Brash, A.R. (1998) A 12R-lipoxygenase in human skin: mechanistic evidence, molecular cloning, and expression. *Proc. Natl. Acad. Sci. U. S. A.*, **95** (12), 6744–6749.

92. Raj, N., Voegeli, R., Rawlings, A.V., Summers, B., Munday, M.R., and Lane, M.E. (2016) Variation in the activities of late stage filaggrin processing enzymes, calpain-1 and bleomycin hydrolase, together with pyrrolidone carboxylic acid

levels, corneocyte phenotypes and plasmin activities in non-sun-exposed and sun-exposed facial stratum cor. *Int. J. Cosmet. Sci.*, **38** (6), 567–575.

93. Freinkel, R.K., and Traczyk, T.N. (1985) Lipid composition and acid hydrolase content of lamellar granules of fetal rat epidermis. *J. Invest. Dermatol.*, **85** (4), 295–298.

94. Zheng, Y., Yin, H., Boeglin, W.E., Elias, P.M., Crumrine, D., Beier, D.R., and Brash, A.R. (2011) Lipoxygenases mediate the effect of essential fatty acid in skin barrier formation: A proposed role in releasing omega-hydroxyceramide for construction of the corneocyte lipid envelope. *J. Biol. Chem.*, **286** (27), 24046–24056.

95. Folk, J.E., and Finlayson, J.S. (1977) The ε-(γ-Glutamyl)Lysine Crosslink and the Catalytic Role of Transglutaminases, in *Advances in Protein Chemistry*, vol. 31, Elsevier, pp. 1–133.

96. Steinert, P.M., and Marekov, L.N. (1997) Direct Evidence That Involucrin Is a Major Early Isopeptide Cross-linked Component of the Keratinocyte Cornified Cell Envelope. *J. Biol. Chem.*, **272** (3), 2021–2030.

97. Weigmann, H.-J., Lademann, J., Meffert, H., Schaefer, H., and Sterry, W. (1999) Determination of the Horny Layer Profile by Tape Stripping in Combination with Optical Spectroscopy in the Visible Range as a Prerequisite to Quantify Percutaneous Absorption. *Skin Pharmacol. Physiol.*, **12** (1–2), 34–45.

98. Voegeli, R., Heiland, J., Doppler, S., Rawlings, A.V., and Schreier, T. (2007) Efficient and simple quantification of stratum corneum proteins on tape strippings by infrared densitometry. *Skin Res. Technol.*, **13** (3), 242–251.

99. Meguro, S., Arai, Y., Masukawa, Y., Uie, K., and Tokimitsu, I. (2000) Relationship between covalently bound ceramides and transepidermal water loss (TEWL). *Arch. Dermatol. Res.*, **292** (9), 463–468.

100. Elias, P.M., Schmuth, M., Uchida, Y., Rice, R.H., Behne, M., Crumrine, D., Feingold, K.R., Holleran, W.M., and Pharm, D. (2002) Basis for the permeability barrier abnormality in lamellar ichthyosis. *Exp. Dermatol.*, **11** (3), 248–256.

101. Tfayli, A., Jamal, D., Vyumvuhore, R., Manfait, M., and Baillet-Guffroy, A. (2013) Hydration effects on the barrier function of stratum corneum lipids: Raman analysis of ceramides 2, III and 5. *The Analyst*, **138** (21), 6582.

102. Michel, S., Schmidt, R., Shroot, B., and Reichert, U. (1988) Morphological and biochemical characterization of the cornified envelopes from human epidermal keratinocytes of different origin. *J. Invest. Dermatol.*, **91** (1), 11–15.

103. Luo, L., Patel, A., Sinko, B., Bell, M., Wibawa, J., Hadgraft, J., and Lane, M.E. (2016) A comparative study of the in vitro permeation of ibuprofen in mammalian skin, the PAMPA model and silicone membrane. *Int. J. Pharm.*, **505** (1–2), 14–19.

104. Haque, T., Lane, M.E., Sil, B.C., Crowther, J.M., and Moore, D.J. (2017) In vitro permeation and disposition of niacinamide in silicone and porcine skin of skin barrier-mimetic formulations. *Int. J. Pharm.*, **520** (1–2), 158–162.

105. Jung, E.C., and Maibach, H.I. (2015) Animal models for percutaneous absorption. *J. Appl. Toxicol. JAT*, **35** (1), 1–10.

106. Raj, N., Voegeli, R., Rawlings, A.V., Gibbons, S., Munday, M.R., Summers, B., and Lane, M.E. (2015) Variation in stratum corneum protein content as a function of anatomical site and ethnic group. *Int. J. Cosmet. Sci.*, n/a-n/a.

107.   Mohammed, D., Matts, P.J., Hadgraft, J., and Lane, M.E. (2011) Influence of Aqueous Cream BP on corneocyte size, maturity, skin protease activity, protein content and transepidermal water loss: Influence of Aqueous Cream BP on skin characteristics. *Br. J. Dermatol.*, **164** (6), 1304–1310.

108.   Kalia, Y.N., Pirot, F., and Guy, R.H. (1996) Homogeneous transport in a heterogeneous membrane: water diffusion across human stratum corneum in vivo. *Biophys. J.*, **71** (5), 2692–2700.

109.   Mohammed, D., Yang, Q., Guy, R.H., Matts, P.J., Hadgraft, J., and Lane, M.E. (2012) Comparison of gravimetric and spectroscopic approaches to quantify stratum corneum removed by tape-stripping. *Eur. J. Pharm. Biopharm.*, **82** (1), 171–174.

110.   Boncheva, M., de Sterke, J., Caspers, P.J., and Puppels, G.J. (2009) Depth profiling of *Stratum corneum* hydration *in vivo* : a comparison between conductance and confocal Raman spectroscopic measurements. *Exp. Dermatol.*, **18** (10), 870–876.

111.   Gorcea, M., Hadgraft, J., Moore, D.J., and Lane, M.E. (2013) In Vivo Barrier Challenge and Initial Recovery in Human Facial Skin. *Skin Res. Technol.*, **19** (1), e375–e382.

112.   Voegeli, R., Rawlings, A.V., and Summers, B. (2015) Facial skin pigmentation is not related to stratum corneum cohesion, basal transepidermal water loss, barrier integrity and barrier repair. *Int. J. Cosmet. Sci.*, **37** (2), 241–252.

113.   Schwarb, F.P., Gabard, B., Rufli, T., and Surber, C. (1999) Percutaneous absorption of salicylic acid in man after topical administration of three different formulations. *Dermatol. Basel Switz.*, **198** (1), 44–51.

114.   Hirao, T., Denda, M., and Takahashi, M. (2001) Identification of immature cornified envelopes in the barrier-impaired epidermis by characterization of their hydrophobicity and antigenicities of the components. *Exp. Dermatol.*, **10**, 35–44.

115.   Mohammed, D., Matts, P.J., Hadgraft, J., and Lane, M.E. (2012) Variation of Stratum Corneum Biophysical and Molecular Properties with Anatomic Site. *AAPS J.*, **14** (4), 806–812.

116.   Kypriotou, M., Huber, M., and Hohl, D. (2012) The human epidermal differentiation complex: cornified envelope precursors, S100 proteins and the 'fused genes' family: Human epidermal differentiation complex. *Exp. Dermatol.*, **21** (9), 643–649.

117.   Zhao, X.P., and Elder, J.T. (1997) Positional Cloning of Novel Skin-Specific Genes from the Human Epidermal Differentiation Complex. *Genomics*, **45** (2), 250–258.

118.   Voegeli, R., Monneuse, J.-M., Schoop, R., Summers, B., and Rawlings, A.V. (2017) The effect of photodamage on the female Caucasian facial stratum corneum corneome using mass spectrometry-based proteomics. *Int. J. Cosmet. Sci.*, **39** (6), 637–652.

119.   Zheng, Y., Lai, W., Wan, M., and Maibach, H.I. (2011) Expression of Cathepsins in Human Skin Photoaging. *Skin Pharmacol. Physiol.*, **24** (1), 10–21.

120.   Zheng, Y., Chen, H., Lai, W., Xu, Q., Liu, C., Wu, L., and Maibach, H.I. (2015) Cathepsin D Repairing Role in Photodamaged Skin Barrier. *Skin Pharmacol. Physiol.*, **28** (2), 97–102.

121. Bernard, D., Méhul, B., Thomas-Collignon, A., Simonetti, L., Remy, V., Bernard, M.A., and Schmidt, R. (2003) Analysis of Proteins with Caseinolytic Activity in a Human Stratum Corneum Extract Revealed a Yet Unidentified Cysteine Protease and Identified the So-Called "Stratum Corneum Thiol Protease" as Cathepsin L2. *J. Invest. Dermatol.*, **120** (4), 592–600.

122. Igarashi, S., Takizawa, T., Takizawa, T., Yasuda, Y., Uchiwa, H., Hayashi, S., Brysk, H., Robinson, J.M., Yamamoto, K., Brysk, M.M., and Horikoshi, T. (2004) Cathepsin D, but not cathepsin E, degrades desmosomes during epidermal desquamation. *Br. J. Dermatol.*, **151** (2), 355–361.

123. Sage, J., De Quéral, D., Leblanc-Noblesse, E., Kurfurst, R., Schnebert, S., Perrier, E., Nizard, C., Lalmanach, G., and Lecaille, F. (2014) Differential expression of cathepsins K, S and V between young and aged Caucasian women skin epidermis. *Matrix Biol.*, **33**, 41–46.

124. Brömme, D. (2013) Cathepsin V, in *Handbook of Proteolytic Enzymes*, Elsevier, pp. 1831–1834.

125. Egberts, F. (2004) Cathepsin D is involved in the regulation of transglutaminase 1 and epidermal differentiation. *J. Cell Sci.*, **117** (11), 2295–2307.

126. Krieg, P., Siebert, M., Kinzig, A., Bettenhausen, R., Marks, F., and Fürstenberger, G. (1999) Murine 12(R)-lipoxygenase: functional expression, genomic structure and chromosomal localization. *FEBS Lett.*, **446** (1), 142–148.

127. Fitzpatrick, T.B. (1976) Photochemotherapy for Psoriasis: A Clinical Cooperative Study of PUVA-48 and PUVA-64. *Arch. Dermatol.*, **115** (5), 576.

128. Fitzpatrick, T.B. (1988) The validity and practicality of sun-reactive skin types I through VI. *Arch. Dermatol.*, **124** (6), 869–871.

129. Bashir, S.J., Dreher, F., Chew, A.L., Zhai, H., Levin, C., Stern, R., and Maibach, H.I. (2005) Cutaneous bioassay of salicylic acid as a keratolytic. *Int. J. Pharm.*, **292** (1–2), 187–194.

130. Breternitz, M., Flach, M., Präßler, J., Elsner, P., and Fluhr, J.W. (2007) Acute barrier disruption by adhesive tapes is influenced by pressure, time and anatomical location: integrity and cohesion assessed by sequential tape stripping; a randomized, controlled study. *Br. J. Dermatol.*, **156** (2), 231–240.

131. Mohammed, D., Crowther, J.M., Matts, P.J., Hadgraft, J., and Lane, M.E. (2013) Influence of niacinamide containing formulations on the molecular and biophysical properties of the stratum corneum. *Int. J. Pharm.*, **441** (1–2), 192–201.

132. Pirola, R., Bareggi, S.R., and De Benedittis, G. (1998) Determination of acetylsalicylic acid and salicylic acid in skin and plasma by high-performance liquid chromatography. *J. Chromatogr. B. Biomed. Sci. App.*, **705** (2), 309–315.

133. Guneri, D., Voegeli, R., Gurgul, S.J., Munday, M.R., Lane, M.E., and Rawlings, A.V. (2018) A new approach to assess the effect of photodamage on corneocyte envelope maturity using combined hydrophobicity and mechanical fragility assays. *Int. J. Cosmet. Sci.*

134. Rougier, A., Lotte, C., and Maibach, H.I. (1987) In vivo percutaneous penetration of some organic compounds related to anatomic site in humans: predictive assessment by the stripping method. *J. Pharm. Sci.*, **76** (6), 451–454.

135.   Black, D., Del Pozo, A., Lagarde, J.M., and Gall, Y. (2000) Seasonal variability in the biophysical properties of stratum corneum from different anatomical sites. *Skin Res. Technol. Off. J. Int. Soc. Bioeng. Skin ISBS Int. Soc. Digit. Imaging Skin ISDIS Int. Soc. Skin Imaging ISSI*, **6** (2), 70–76.

136.   Ya-Xian, Z., Suetake, T., and Tagami, H. (1999) Number of cell layers of the stratum corneum in normal skin - relationship to the anatomical location on the body, age, sex and physical parameters. *Arch. Dermatol. Res.*, **291** (10), 555–559.

137.   Schwindt, D.A., Wilhelm, K.P., and Maibach, H.I. (1998) Water Diffusion Characteristics of Human Stratum Corneum at Different Anatomical Sites In Vivo. *J. Invest. Dermatol.*, **111** (3), 385–389.

138.   Greene, R.S., Downing, D.T., Pochi, P.E., and Strauss, J.S. (1970) Anatomical variation in the amount and composition of human skin surface lipid. *J. Invest. Dermatol.*, **54** (3), 240–247.

139.   Jui-Chen, T., Weiner, N.D., Flynn, G.L., and Ferry, J. (1991) Properties of adhesive tapes used for stratum corneum stripping. *Int. J. Pharm.*, **72** (3), 227–231.

140.   Binder, L., Jatschka, J., Kulovits, E.M., Seeböck, S., Kählig, H., and Valenta, C. (2018) Simultaneous penetration monitoring of oil component and active drug from fluorinated nanoemulsions. *Int. J. Pharm.*, **552** (1–2), 312–318.

141.   Hirao, T. (2003) Involvement of transglutaminase in ex vivo maturation of cornified envelopes in the stratum corneum. *Int. J. Cosmet. Sci.*, **25** (5), 245–257.

142.   Machado, M., Salgado, T.M., Hadgraft, J., and Lane, M.E. (2010) The relationship between transepidermal water loss and skin permeability. *Int. J. Pharm.*, **384** (1–2), 73–77.

143.   Hadgraft, J., and Lane, M.E. (2009) Transepidermal water loss and skin site: A hypothesis. *Int. J. Pharm.*, **373** (1–2), 1–3.

144.   Nilsson, G.E. (1977) Measurement of water exchange through skin. *Med. Biol. Eng. Comput.*, **15** (3), 209–218.

145.   Imhof, R.E., De Jesus, M.E.P., Xiao, P., Ciortea, L.I., and Berg, E.P. (2009) Closed-chamber transepidermal water loss measurement: microclimate, calibration and performance. *Int. J. Cosmet. Sci.*, **31** (2), 97–118.

146.   Farahmand, S., Tien, L., Hui, X., and Maibach, H.I. (2009) Measuring transepidermal water loss: a comparative *in vivo* study of condenser-chamber, unventilated-chamber and open-chamber systems. *Skin Res. Technol.*, **15** (4), 392–398.

147.   Reed, J.T., Ghadially, R., and Elias, P.M. (1995) Skin type, but neither race nor gender, influence epidermal permeability barrier function. *Arch. Dermatol.*, **131** (10), 1134–1138.

148.   Oestmann, E., Lavrijsen, A.P.M., Hermans, J., and Ponec, M. (1993) Skin barrier function in healthy volunteers as assessed by transepidermal water loss and vascular response to hexyl nicotinate: intra- and inter-individual variability. *Br. J. Dermatol.*, **128** (2), 130–136.

149.   Fur, I.L., Lopez, S., Morizot, F., Guinot, C., and Tschachler, E. (1999) Comparison of cheek and forehead regions by bioengineering methods in women with different self-reported 'cosmetic skin types'. *Skin Res. Technol.*, **5** (3), 182–188.

150. Voegeli, R., Rawlings, A.V., Seroul, P., and Summers, B. (2015) A novel continuous colour mapping approach for visualization of facial skin hydration and transepidermal water loss for four ethnic groups. *Int. J. Cosmet. Sci.*, **37** (6), 595–605.

151. Conti, A., Schiavi, M.E., and Seidenari, S. (1995) Capacitance, transepidermal water loss and causal level of sebum in healthy subjects in relation to site, sex and age. *Int. J. Cosmet. Sci.*, **17** (2), 77–85.

152. Leveque, J.L., Corcuff, P., de Rigal, J., and Agache, P. (1984) In vivo studies of the evolution of physical properties of the human skin with age. *Int. J. Dermatol.*, **23** (5), 322–329.

153. Berardesca, Pirot, Singh, and Maibach (1998) Differences in stratum corneum pH gradient when comparing white caucasian and black African-American skin. *Br. J. Dermatol.*, **139** (5), 855–857.

154. Russell, L., Wiedersberg, S., and Begonadelgadocharro, M. (2008) The determination of stratum corneum thickness An alternative approach. *Eur. J. Pharm. Biopharm.*, **69** (3), 861–870.

155. Matoltsy, A.G., and Balsamo, C.A. (1955) A study of the components of the cornified epithelium of human skin. *J. Biophys. Biochem. Cytol.*, **1** (4), 339–360.

156. Bornkessel, A., Flach, M., Arens-Corell, M., Elsner, P., and Fluhr, J.W. (2005) Functional assessment of a washing emulsion for sensitive skin: mild impairment of stratum corneum hydration, pH, barrier function, lipid content, integrity and cohesion in a controlled washing test. *Skin Res. Technol.*, **11** (1), 53–60.

157. Lowry, O.H., Rosebrough, N.J., Farr, A.L., and Randall, R.J. (1951) Protein measurement with the Folin phenol reagent. *J. Biol. Chem.*, **193** (1), 265–275.

158. Dreher, F., Arens, A., Hostýnek, J.J., Mudumba, S., Ademola, J., and Maibach, H.I. (1998) Colorimetric method for quantifying human Stratum corneum removed by adhesive-tape stripping. *Acta Derm. Venereol.*, **78** (3), 186–189.

159. Dreher, F., Modjtahedi, B.S., Modjtahedi, S.P., and Maibach, H.I. (2005) Quantification of stratum corneum removal by adhesive tape stripping by total protein assay in 96-well microplates. *Skin Res. Technol.*, **11** (2), 97–101.

160. Weigmann, H.-J., Lindemann, U., Antoniou, C., Tsikrikas, G.N., Stratigos, A.I., Katsambas, A., Sterry, W., and Lademann, J. (2003) UV/VIS Absorbance Allows Rapid, Accurate, and Reproducible Mass Determination of Corneocytes Removed by Tape Stripping. *Skin Pharmacol. Physiol.*, **16** (4), 217–227.

161. Cadet, J., and Douki, T. (2018) Formation of UV-induced DNA damage contributing to skin cancer development. *Photochem. Photobiol. Sci.*, **17** (12), 1816–1841.

162. Tan, E.M., and Stoughton, R.B. (1969) Ultraviolet light induced damage to desoxyribonucleic acid in human skin. *J. Invest. Dermatol.*, **52** (6), 537–542.

163. Lehmann, A.R., Kirk-Bell, S., Arlett, C.F., Harcourt, S.A., de Weerd-Kastelein, E.A., Keijzer, W., and Hall-Smith, P. (1977) Repair of ultraviolet light damage in a variety of human fibroblast cell strains. *Cancer Res.*, **37** (3), 904–910.

164. Kligman, L.H. (1986) Photoaging. Manifestations, prevention, and treatment. *Dermatol. Clin.*, **4** (3), 517–528.

165. Suh, K.-S., Roh, H.-J., Choi, S.-Y., Jeon, Y.-S., Doh, K.-S., Bae, J.-H., and Kim, S.-T. (2007) A long-term evaluation of erythema and pigmentation induced

by ultraviolet radiations of different wavelengths. *Skin Res. Technol.*, **13** (4), 360–368.

166. Clydesdale, G.J., Dandie, G.W., and Muller, H.K. (2001) Ultraviolet light induced injury: Immunological and inflammatory effects. *Immunol. Cell Biol.*, **79** (6), 547–568.

167. Scharffetter-Kochanek, K., Wlaschek, M., Brenneisen, P., Schauen, M., Blaudschun, R., and Wenk, J. (1997) UV-induced reactive oxygen species in photocarcinogenesis and photoaging. *Biol. Chem.*, **378** (11), 1247–1257.

168. Wink, D.A., Miranda, K.M., Espey, M.G., Pluta, R.M., Hewett, S.J., Colton, C., Vitek, M., Feelisch, M., and Grisham, M.B. (2001) Mechanisms of the Antioxidant Effects of Nitric Oxide. *Antioxid. Redox Signal.*, **3** (2), 203–213.

169. Weller, R., Schwentker, A., Billiar, T.R., and Vodovotz, Y. (2003) Autologous nitric oxide protects mouse and human keratinocytes from ultraviolet B radiation-induced apoptosis. *Am. J. Physiol.-Cell Physiol.*, **284** (5), C1140–C1148.

170. Ossola, J.O., and Tomaro, M.L. (1998) Heme oxygenase induction by UVA radiation. A response to oxidative stress in rat liver. *Int. J. Biochem. Cell Biol.*, **30** (2), 285–292.

171. Shindo, Y., Witt, E., Han, D., Epstein, W., and Packer, L. (1994) Enzymic and Non-Enzymic Antioxidants in Epidermis and Dermis of Human Skin. *J. Invest. Dermatol.*, **102** (1), 122–124.

172. Chen, X., Liu, S., Rao, P., Bradshaw, J., and Weller, R. (2016) Topical application of superoxide dismutase mediated by HIV-TAT peptide attenuates UVB-induced damages in human skin. *Eur. J. Pharm. Biopharm.*, **107**, 286–294.

173. Flohr, C., England, K., Radulovic, S., McLean, W.H.I., Campbel, L.E., Barker, J., Perkin, M., and Lack, G. (2010) Filaggrin loss-of-function mutations are associated with early-onset eczema, eczema severity and transepidermal water loss at 3 months of age. *Br. J. Dermatol.*, **163** (6), 1333–1336.

174. Jungersted, J.M., Scheer, H., Mempel, M., Baurecht, H., Cifuentes, L., Høgh, J.K., Hellgren, L.I., Jemec, G.B.E., Agner, T., and Weidinger, S. (2010) Stratum corneum lipids, skin barrier function and filaggrin mutations in patients with atopic eczema: Filaggrin mutations, skin barrier and lipids. *Allergy*, **65** (7), 911–918.

175. Bosko, C.A. (2019) Skin Barrier Insights: From Bricks and Mortar to Molecules and Microbes. *J. Drugs Dermatol. JDD*, **18** (1s), s63-67.

176. Costello, E.K., Lauber, C.L., Hamady, M., Fierer, N., Gordon, J.I., and Knight, R. (2009) Bacterial community variation in human body habitats across space and time. *Science*, **326** (5960), 1694–1697.

177. Lipsky, Z.W., and German, G.K. (2019) Ultraviolet light degrades the mechanical and structural properties of human stratum corneum. *J. Mech. Behav. Biomed. Mater.*, **100**, 103391.

178. Hunter, R., Pinkus, H., and Steele, C.H. (1956) Examination of the Epidermis by the Strip Method. *J. Invest. Dermatol.*, **27** (1), 31–34.

179. Coelho, S.G., Valencia, J.C., Yin, L., Smuda, C., Mahns, A., Kolbe, L., Miller, S.A., Beer, J.Z., Zhang, G., Tuma, P.L., and Hearing, V.J. (2015) UV exposure modulates hemidesmosome plasticity, contributing to long-term pigmentation in human skin: Hemidesmosome plasticity in human skin after UV. *J. Pathol.*, **236** (1), 17–29.

180. Posselt, R., Mueller, R.W., Stöckli, R., and Trentmann, J. (2012) Remote sensing of solar surface radiation for climate monitoring — the CM-SAF retrieval in international comparison. *Remote Sens. Environ.*, **118**, 186–198.

181. Wright, C.Y., Norval, M., Summers, B., Davids, L.M., Coetzee, G., and Oriowo, M. (2012) Solar ultraviolet radiation exposure and human health in South Africa: Finding a balance. *S. Afr. Med. J.*, **102** (8), 665.

182. Muizzuddin, N., Ingrassia, M., Marenus, K.D., Maes, D.H., and Mammone, T. (2013) Effect of seasonal and geographical differences on skin and effect of treatment with an osmoprotectant: Sorbitol. *J. Cosmet. Sci.*, **64** (3), 165–174.

183. Köhler, G., and Milstein, C. (1975) Continuous cultures of fused cells secreting antibody of predefined specificity. *Nature*, **256** (5517), 495–497.

184. Sentein, P. (1976) Methods of fixing, sectioning and staining amphibian eggs for cytological study. *Microsc. Acta*, **78** (5), 427–438.

185. Buchwalow, I., Samoilova, V., Boecker, W., and Tiemann, M. (2011) Non-specific binding of antibodies in immunohistochemistry: fallacies and facts. *Sci. Rep.*, **1** (1), 28.

186. Clauberg, K.W. (1946) Vereinfachte Fluoreszenzmikroskopie mit einer neuen Beleuchtungseinrichtung. *Klin. Prax.*, **1** (8), 138.

187. Sanderson, M.J., Smith, I., Parker, I., and Bootman, M.D. (2014) Fluorescence microscopy. *Cold Spring Harb. Protoc.*, **2014** (10), pdb.top071795.

188. Ferringer, T. (2015) Immunohistochemistry in Dermatopathology. *Arch. Pathol. Lab. Med.*, **139** (1), 83–105.

189. Zuber, T.J. (2002) Punch biopsy of the skin. *Am. Fam. Physician*, **65** (6), 1155–1158, 1161–1162, 1164.

190. Semlin, L., Schäfer-Korting, M., Borelli, C., and Korting, H.C. (2011) In vitro models for human skin disease. *Drug Discov. Today*, **16** (3–4), 132–139.

191. Danso, M.O., Berkers, T., Mieremet, A., Hausil, F., and Bouwstra, J.A. (2015) An ex vivo human skin model for studying skin barrier repair. *Exp. Dermatol.*, **24** (1), 48–54.

192. Sidgwick, G.P., McGeorge, D., and Bayat, A. (2016) Functional testing of topical skin formulations using an optimised ex vivo skin organ culture model. *Arch. Dermatol. Res.*, **308** (5), 297–308.

193. Yoneda, K., Demitsu, T., Manabe, M., Igarashi, J., Kosaka, H., Inagaki, N., Takahashi, H., Kon, A., Kakurai, M., and Kubota, Y. (2010) Expression of wild-type, but not mutant, loricrin causes programmed cell death in HaCaT keratinocytes: WT loricrin induces programmed cell death. *J. Dermatol.*, **37** (11), 956–964.

194. Graczyk, A., and Leśniak, W. (2014) S100A6 expression in keratinocytes and its impact on epidermal differentiation. *Int. J. Biochem. Cell Biol.*, **57**, 135–141.

195. Mohammed, D., Matts, P.J., Hadgraft, J., and Lane, M.E. (2011) Depth profiling of stratum corneum biophysical and molecular properties: Depth profiling of stratum corneum. *Br. J. Dermatol.*, **164** (5), 957–965.

196. Raj, N., Voegeli, R., Rawlings, A.V., Gibbons, S., Munday, M.R., Summers, B., and Lane, M.E. (2016) Variation in stratum corneum protein content as a function of anatomical site and ethnic group. *Int. J. Cosmet. Sci.*, **38** (3), 224–231.

197.   Edqvist, P.-H.D., Fagerberg, L., Hallström, B.M., Danielsson, A., Edlund, K., Uhlén, M., and Pontén, F. (2015) Expression of Human Skin-Specific Genes Defined by Transcriptomics and Antibody-Based Profiling. *J. Histochem. Cytochem.*, **63** (2), 129–141.

198.   Dale, B.A., Resing, K.A., and Lonsdale-Eccles, J.D. (1985) Filaggrin: a keratin filament associated protein. *Ann. N. Y. Acad. Sci.*, **455**, 330–342.

199.   Simon, M., and Green, H. (1985) Enzymatic cross-linking of involucrin and other proteins by keratinocyte particulates in vitro. *Cell*, **40** (3), 677–683.

200.   Harding, C.R., Long, S., Richardson, J., Rogers, J., Zhang, Z., Bush, A., and Rawlings, A.V. (2003) The cornified cell envelope: an important marker of stratum corneum maturation in healthy and dry skin. *Int. J. Cosmet. Sci.*, **25** (4), 157–167.

201.   Koch, P.J., de Viragh, P.A., Scharer, E., Bundman, D., Longley, M.A., Bickenbach, J., Kawachi, Y., Suga, Y., Zhou, Z., Huber, M., Hohl, D., Kartasova, T., Jarnik, M., Steven, A.C., and Roop, D.R. (2000) Lessons from loricrin-deficient mice: compensatory mechanisms maintaining skin barrier function in the absence of a major cornified envelope protein. *J. Cell Biol.*, **151** (2), 389–400.

202.   Fredonnet, J., Gasc, G., Serre, G., Séverac, C., and Simon, M. (2014) Topographical and nano-mechanical characterization of native corneocytes using atomic force microscopy. *J. Dermatol. Sci.*, **75** (1), 63–65.

203.   Djian, P., Phillips, M., Easley, K., Huang, E., Simon, M., Rice, R.H., and Green, H. (1993) The involucrin genes of the mouse and the rat: study of their shared repeats. *Mol. Biol. Evol.*, **10** (6), 1136–1149.

204.   Murphy, G.F., Flynn, T.C., Rice, R.H., and Pinkus, G.S. (1984) Involucrin Expression in Normal and Neoplastic Human Skin: A Marker for Keratinocyte Differentiation. *J. Invest. Dermatol.*, **82** (5), 453–457.

205.   Dover, R., and Watt, F.M. (1987) Measurement of the Rate of Epidermal Terminal Differentiation: Expression of Involucrin by S-Phase Keratinocytes in Culture and in Psoriatic Plaques. *J. Invest. Dermatol.*, **89** (4), 349–352.

206.   Drozdoff, V., and Pledger, W.J. (1993) Commitment to differentiation and expression of early differentiation markers in murine keratinocytes in vitro are regulated independently of extracellular calcium concentrations. *J. Cell Biol.*, **123** (4), 909–919.

207.   Hirao, T., Denda, M., and Takahashi, M. (2001) Identification of immature cornified envelopes in the barrier-impaired epidermis by characterization of their hydrophobicity and antigenicities of the components. *Exp. Dermatol.*, **10** (1), 35–44.

208.   Bernard, B.A., Reano, A., Darmon, Y.M., and Thivolet, J. (1986) Precocious appearance of involucrin and epidermal transglutaminase during differentiation of psoriatic skin. *Br. J. Dermatol.*, **114** (3), 279–283.

209.   Hertle, M.D., Kubler, M.D., Leigh, I.M., and Watt, F.M. (1992) Aberrant integrin expression during epidermal wound healing and in psoriatic epidermis. *J. Clin. Invest.*, **89** (6), 1892–1901.

210.   Hirao, T., Terui, T., Takeuchi, I., Kobayashi, H., Okada, M., Takahashi, M., and Tagami, H. (2003) Ratio of immature cornified envelopes does not correlate

with parakeratosis in inflammatory skin disorders. *Exp. Dermatol.*, **12** (5), 591–601.

211. Hirao, T., Takahashi, M., Kikuchi, K., Terui, T., and Tagami, H. (2003) A novel non-invasive evaluation method of cornified envelope maturation in the stratum corneum provides a new insight for skin care cosmetics. *Int. Fed. Soc. Cosmet. Chem. Mag.*, **6** (2), 103–109.

212. Engelke, M., Jensen, J.M., Ekanayake-Mudiyanselage, S., and Proksch, E. (1997) Effects of xerosis and ageing on epidermal proliferation and differentiation. *Br. J. Dermatol.*, **137** (2), 219–225.

213. Buchwalow, I., Samoilova, V., Boecker, W., and Tiemann, M. (2011) Non-specific binding of antibodies in immunohistochemistry: fallacies and facts. *Sci. Rep.*, **1** (1).

214. Wertz, P.W., and van den Bergh, B. (1998) The physical, chemical and functional properties of lipids in the skin and other biological barriers. *Chem. Phys. Lipids*, **91** (2), 85–96.

215. Gorcea, M., Hadgraft, J., Moore, D.J., and Lane, M.E. (2013) <i>In Vivo<i> Barrier Challenge and Initial Recovery in Human Facial Skin. *Skin Res. Technol.*, **19** (1), e375–e382.

216. Muñoz-Garcia, A., Thomas, C.P., Keeney, D.S., Zheng, Y., and Brash, A.R. (2014) The importance of the lipoxygenase-hepoxilin pathway in the mammalian epidermal barrier. *Biochim. Biophys. Acta BBA - Mol. Cell Biol. Lipids*, **1841** (3), 401–408.

217. Hassing, J.H., Nater, J.P., and Bleumink, E. (1982) Irritancy of Low Concentrations of Soap and Synthetic Detergents as Measured by Skin Water Loss. *Dermatology*, **164** (5), 314–321.

218. Froebe, C.L., Simion, F.A., Rhein, L.D., Cagan, R.H., and Kligman, A. (1990) Stratum corneum lipid removal by surfactants: relation to in vivo irritation. *Dermatologica*, **181** (4), 277–283.

219. Fulmer, A.W., and Kramer, G.J. (1986) Stratum Corneum Lipid Abnormalities in Surfactant-Induced Dry Scaly Skin. *J. Invest. Dermatol.*, **86** (5), 598–602.

220. Le, M., Schalkwijk, J., Siegenthaler, G., van de Kerkhof, P.C.M., Veerkamp, J.H., and van der Valk, P.G.M. (1996) Changes in keratinocyte differentiation following mild irritation by sodium dodecyl sulphate. *Arch. Dermatol. Res.*, **288** (11), 684–690.

221. Schade, H., and Marchionini, A. (1928) Der Säuremantel der Haut (Nach Gaskettenmessungen). *Klin. Wochenschr.*, **7** (1), 12–14.

222. Tsakok, T., Woolf, R., Smith, C.H., Weidinger, S., and Flohr, C. (2019) Atopic dermatitis: the skin barrier and beyond. *Br. J. Dermatol.*, **180** (3), 464–474.

223. Nikam, V., Monteiro, R., Dandakeri, S., and Bhat, R. (2019) Transepidermal water loss in psoriasis: A case-control study. *Indian Dermatol. Online J.*, **10** (3), 267.

224. Richard, G. (2004) Molecular genetics of the ichthyoses. *Am. J. Med. Genet. C Semin. Med. Genet.*, **131C** (1), 32–44.

225. Akiyama, M. (2005) Mutations in lipid transporter ABCA12 in harlequin ichthyosis and functional recovery by corrective gene transfer. *J. Clin. Invest.*, **115** (7), 1777–1784.

226.   Hovnanian, A. (2005) Harlequin ichthyosis unmasked: a defect of lipid transport. *J. Clin. Invest.*, **115** (7), 1708–1710.

227.   Hackett, B.C., Fitzgerald, D., Watson, R.M., Hol, F.A., and Irvine, A.D. (2010) Genotype-phenotype correlations with TGM1: clustering of mutations in the bathing suit ichthyosis and self-healing collodion baby variants of lamellar ichthyosis. *Br. J. Dermatol.*, **162** (2), 448–451.

228.   Eckl, K.-M., Krieg, P., Küster, W., Traupe, H., André, F., Wittstruck, N., Fürstenberger, G., and Hennies, H.C. (2005) Mutation spectrum and functional analysis of epidermis-type lipoxygenases in patients with autosomal recessive congenital ichthyosis. *Hum. Mutat.*, **26** (4), 351–361.

229.   Swartzendruber, D.C., Wertz, P.W., Madison, K.C., and Downing, D.T. (1987) Evidence That the Corneocyte Has a Chemically Bound Lipid Envelope. *J. Invest. Dermatol.*, **88** (6), 709–713.

230.   Bergstrom, S., and Holman, R.T. (1948) Total conjugation of linoleic acid in oxidation with lipoxidase. *Nature*, **161** (4080), 55.

231.   Theorell, H., Holman, R.T., and Akeson, A. (1947) Crystalline lipoxidase. *Acta Chem. Scand.*, **1** (6), 571–576.

232.   Henneicke-von Zepelin, H.H., Schröder, J.M., Smíd, P., Reusch, M.K., and Christophers, E. (1991) Metabolism of arachidonic acid by human epidermal cells depends upon maturational stage. *J. Invest. Dermatol.*, **97** (2), 291–297.

233.   Siebert, M., Krieg, P., Lehmann, W.D., Marks, F., and FüRstenberger, G. (2001) Enzymic characterization of epidermis-derived 12-lipoxygenase isoenzymes. *Biochem. J.*, **355** (1), 97–104.

234.   Simard-Bisson, C., Parent, L.A., Moulin, V.J., and Fruteau de Laclos, B. (2018) Characterization of Epidermal Lipoxygenase Expression in Normal Human Skin and Tissue-Engineered Skin Substitutes. *J. Histochem. Cytochem.*, **66** (11), 813–824.

235.   Eckl, K.-M., Alef, T., Torres, S., and Hennies, H.C. (2011) Full-Thickness Human Skin Models for Congenital Ichthyosis and Related Keratinization Disorders. *J. Invest. Dermatol.*, **131** (9), 1938–1942.

236.   Rawlings, A.V., and Harding, C.R. (2004) Moisturization and skin barrier function. *Dermatol. Ther.*, **17 Suppl 1**, 43–48.

237.   Rogers, J., Harding, C., Mayo, A., Banks, J., and Rawlings, A. (1996) Stratum corneum lipids: the effect of ageing and the seasons. *Arch. Dermatol. Res.*, **288** (12), 765–770.

238.   Ishikawa, J., Yoshida, H., Ito, S., Naoe, A., Fujimura, T., Kitahara, T., Takema, Y., Zerweck, C., and Grove, G.L. (2013) Dry skin in the winter is related to the ceramide profile in the stratum corneum and can be improved by treatment with a *Eucalyptus* extract. *J. Cosmet. Dermatol.*, **12** (1), 3–11.

239.   Macheleidt, O., Sandhoff, K., and Kaiser, H.W. (2002) Deficiency of Epidermal Protein-Bound ω-Hydroxyceramides in Atopic Dermatitis. *J. Invest. Dermatol.*, **119** (1), 166–173.

240.   Aparoy, P., Leela, T., Reddy, R.N., and Reddanna, P. (2009) Computational analysis of R and S isoforms of 12-Lipoxygenases: Homology modeling and docking studies. *J. Mol. Graph. Model.*, **27** (6), 744–750.

241. Michaelis, L., and Menten, M. (1913) Die Kinetik der Invertinwirkung. *Biochem. Ztg.*, (79), 333–369.

242. Singh, R.K., Gupta, S., Tiwari, P., Saini, S., Malik, R., Kant, R., Dastidar, S.G., and Ray, A. (2012) A fluorescent based enzyme assay for recombinant human lipoxygenase enzyme isoforms. *Pharmacologia*, **3** (9), 387–396.

243. Noguchi, M., Miyano, M., and Matsumoto, T. (1996) Physicochemical characterization of ATP binding to human 5-lipoxygenase. *Lipids*, **31** (4), 367–371.

244. Burnstock, G. (2016) Short- and long-term (trophic) purinergic signalling. *Philos. Trans. R. Soc. Lond. B. Biol. Sci.*, **371** (1700).

245. Rai, G., Joshi, N., Perry, S., Yasgar, A., Schultz, L., Jung, J.E., Liu, Y., Terasaki, Y., Diaz, G., Kenyon, V., Jadhav, A., Simeonov, A., van Leyen, K., Holman, T.R., and Maloney, D.J. (2010) Discovery of ML351, a Potent and Selective Inhibitor of Human 15-Lipoxygenase-1, in *Probe Reports from the NIH Molecular Libraries Program*, National Center for Biotechnology Information (US), Bethesda (MD).

246. Nugteren, D.H., Christ-Hazelhof, E., van der Beek, A., and Houtsmuller, U.M. (1985) Metabolism of linoleic acid and other essential fatty acids in the epidermis of the rat. *Biochim. Biophys. Acta*, **834** (3), 429–436.

247. Chiba, T., Thomas, C.P., Calcutt, M.W., Boeglin, W.E., O'Donnell, V.B., and Brash, A.R. (2016) The precise structures and stereochemistry of trihydroxy-linoleates esterified in human and porcine epidermis and their significance in skin barrier function: Implication of a epoxide hydroplase in the transformation of linoleate. *J. Biol. Chem.*, **291** (28), 14540–14554.

248. Zheng, Y., and Brash, A.R. (2010) Formation of a cyclopropyl epoxide via a leukotriene a synthase-related pathway in an anaerobic reaction of soybean lipoxygenase-1 with 15-hydroperoxyeicosatetraenoic acid: evidence that oxygen access is a determinat of secondary reactions with fatty acid hydroperoxides. *J. Biol. Chem.*, **285** (18), 13427–13436.

249. Voegeli, R., Monneuse, J.-M., Klose, C., Schoop, R., Summers, B., Rudolph, T., and Rawlings, A.V. (2018) Phenotypic changes in the corneome and ceramidome of photodamaged dry facial stratum corneum from different ethnic groups. Presented at the International Federation of Societies of Cosmetic Chemists in Munich, Germany.

250. Fujiwara, A., Morifuji, M., Kitade, M., Kawahata, K., Fukasawa, T., Yamaji, T., Itoh, H., and Kawashima, M. (2018) Age-related and seasonal changes in covalently bound ceramide content in forearm stratum corneum of Japanese subjects: determination of molecular species of ceramides. *Arch. Dermatol. Res.*, **310** (9), 729–735.

251. Kubilus, J., and Baden, H.P. (1984) Isopeptide bond formation in epidermis. *Mol. Cell. Biochem.*, **58** (1–2), 129–137.

252. Kim, S.Y., Chung, S.I., Yoneda, K., and Steinert, P.M. (1995) Expression of transglutaminase 1 in human epidermis. *J. Invest. Dermatol.*, **104** (2), 211–217.

253. Kim, I.G., Gorman, J.J., Park, S.C., Chung, S.I., and Steinert, P.M. (1993) The deduced sequence of the novel protransglutaminase E (TGase3) of human and mouse. *J. Biol. Chem.*, **268** (17), 12682–12690.

254. Candi, E., Oddi, S., Terrinoni, A., Paradisi, A., Ranalli, M., Finazzi-Agró, A., and Melino, G. (2001) Transglutaminase 5 Cross-links Loricrin, Involucrin, and Small Proline-rich Proteins *in Vitro*. *J. Biol. Chem.*, **276** (37), 35014–35023.

255. Haroon, Z.A., Hettasch, J.M., Lai, T.S., Dewhirst, M.W., and Greenberg, C.S. (1999) Tissue transglutaminase is expressed, active, and directly involved in rat dermal wound healing and angiogenesis. *FASEB J. Off. Publ. Fed. Am. Soc. Exp. Biol.*, **13** (13), 1787–1795.

256. Zhang, W., Shiraishi, A., Suzuki, A., Zheng, X., Kodama, T., and Ohashi, Y. (2004) Expression and distribution of tissue transglutaminase in normal and injured rat cornea. *Curr. Eye Res.*, **28** (1), 37–45.

257. Candi, E., Oddi, S., Paradisi, A., Terrinoni, A., Ranalli, M., Teofoli, P., Citro, G., Scarpato, S., Puddu, P., and Melino, G. (2002) Expression of Transglutaminase 5 in Normal and Pathologic Human Epidermis. *J. Invest. Dermatol.*, **119** (3), 670–677.

258. Chung, S.I. (1972) Comparative studies on tissue transglutaminase and factor XIII. *Ann. N. Y. Acad. Sci.*, **202**, 240–255.

259. Chung, S.I., Chang, S.K., Cocuzzi, E.T., Folk, J.E., Kim, H.C., Lee, S.Y., Martinet, N., Nigra, T., and Sun, H.S. (1988) Modulation of cellular transglutaminase: protease-induced activation. *Adv. Exp. Med. Biol.*, **231**, 1–13.

260. Negi, M., Matsui, T., and Ogawa, H. (1980) [Activation mechanisms of epidermal transglutaminase, the cross-linking enzyme (author's transl)]. *Nihon Hifuka Gakkai Zasshi Jpn. J. Dermatol.*, **90** (6), 531–533.

261. Kim, S.-Y., Park, W.-M., Jung, S.-W., and Lee, J. (1997) Novel Transglutaminase Inhibitors Reduce the Cornified Cell Envelope Formation. *Biochem. Biophys. Res. Commun.*, **233** (1), 39–44.

262. Kim, S.-Y., Chung, S.-I., and Steinert, P.M. (1995) Highly Active Soluble Processed Forms of the Transglutaminase 1 Enzyme in Epidermal Keratinocytes. *J. Biol. Chem.*, **270** (30), 18026–18035.

263. Rice, R.H., Rong, X.H., and Chakravarty, R. (1990) Proteolytic release of keratinocyte transglutaminase. *Biochem. J.*, **265** (2), 351–357.

264. Negi, M., Matsui, T., and Ogawa, H. (1981) Mechanism of regulation of human epidermal transglutaminase. *J. Invest. Dermatol.*, **77** (5), 389–392.

265. Heinrich, M. (1999) Cathepsin D targeted by acid sphingomyelinase-derived ceramide. *EMBO J.*, **18** (19), 5252–5263.

266. Engebretsen, K.A., Johansen, J.D., Kezic, S., Linneberg, A., and Thyssen, J.P. (2016) The effect of environmental humidity and temperature on skin barrier function and dermatitis. *J. Eur. Acad. Dermatol. Venereol.*, **30** (2), 223–249.

267. Ågren, J., Sjörs, G., and Sedin, G. (2006) Ambient humidity influences the rate of skin barrier maturation in extremely preterm infants. *J. Pediatr.*, **148** (5), 613–617.

268. Denda, M., Sato, J., Masuda, Y., Tsuchiya, T., Koyama, J., Kuramoto, M., Elias, P.M., and Feingold, K.R. (1998) Exposure to a Dry Environment Enhances Epidermal Permeability Barrier Function. *J. Invest. Dermatol.*, **111** (5), 858–863.

269. Sato, J., Denda, M., Ashida, Y., and Koyama, J. (1998) Loss of water from the stratum corneum induces epidermal DNA synthesis in hairless mice. *Arch. Dermatol. Res.*, **290** (11), 634–637.

270. Scott, I.R., and Harding, C.R. (1986) Filaggrin breakdown to water binding compounds during development of the rat stratum corneum is controlled by the water activity of the environment. *Dev. Biol.*, **115** (1), 84–92.

271. Cau, L., Pendaries, V., Lhuillier, E., Thompson, P.R., Serre, G., Takahara, H., Méchin, M.-C., and Simon, M. (2017) Lowering relative humidity level increases epidermal protein deimination and drives human filaggrin breakdown. *J. Dermatol. Sci.*, **86** (2), 106–113.

272. Bouwstra, J.A., Groenink, H.W.W., Kempenaar, J.A., Romeijn, S.G., and Ponec, M. (2008) Water Distribution and Natural Moisturizer Factor Content in Human Skin Equivalents Are Regulated by Environmental Relative Humidity. *J. Invest. Dermatol.*, **128** (2), 378–388.

273. Chou, T.-C., Lin, K.-H., Wang, S.-M., Lee, C.-W., Su, S.-B., Shih, T.-S., and Chang, H.-Y. (2005) Transepidermal water loss and skin capacitance alterations among workers in an ultra-low humidity environment. *Arch. Dermatol. Res.*, **296** (10), 489–495.

274. Katagiri, C., Sato, J., Nomura, J., and Denda, M. (2003) Changes in environmental humidity affect the water-holding property of the stratum corneum and its free amino acid content, and the expression of filaggrin in the epidermis of hairless mice. *J. Dermatol. Sci.*, **31** (1), 29–35.

275. Rawlings, A.V., and Leyden, J.J. (eds.) (2009) *Skin moisturization*, Informa Healthcare, New York.

276. Guneri, D., Voegeli, R., Munday, M.R., Lane, M.E., and Rawlings, A. (2019) 12R-lipoxygenase activity is reduced in photodamaged facial stratum corneum. A novel activity assay indicates a key function in corneocyte maturation. *Int. J. Cosmet. Sci. Submitt.*

277. Eckhart, L., Lippens, S., Tschachler, E., and Declercq, W. (2013) Cell death by cornification. *Biochim. Biophys. Acta BBA - Mol. Cell Res.*, **1833** (12), 3471–3480.

278. Greenspan, L. (1977) Humidity fixed points of binary saturated aqueous solutions. *J. Res. Natl. Bur. Stand. Sect. Phys. Chem.*, **81A** (1), 89.

279. Castorena-Gonzalez, J.A., Staiculescu, M.C., Foote, C.A., Polo-Parada, L., and Martinez-Lemus, L.A. (2014) The obligatory role of the actin cytoskeleton on inward remodeling induced by dithiothreitol activation of endogenous transglutaminase in isolated arterioles. *Am. J. Physiol. Heart Circ. Physiol.*, **306** (4), H485-495.

280. Miller, A.K., and Tausig, F. (1964) Biotin-binding by parenterally-administered streptavidin or avidin. *Biochem. Biophys. Res. Commun.*, **14**, 210–214.

281. Case, A., and Stein, R.L. (2007) Kinetic analysis of the interaction of tissue transglutaminase with a nonpeptidic slow-binding inhibitor. *Biochemistry*, **46** (4), 1106–1115.

282. Ranganathan, R., Lenti, G., Tassone, N.M., Scannell, B.J., Southern, C.A., and Karver, C.E. (2018) Design and application of a fluorogenic assay for monitoring inflammatory caspase activity. *Anal. Biochem.*, **543**, 1–7.

283. Muizzuddin, N., Hellemans, L., Van Overloop, L., Corstjens, H., Declercq, L., and Maes, D. (2010) Structural and functional differences in barrier properties of

African American, Caucasian and East Asian skin. *J. Dermatol. Sci.*, **59** (2), 123–128.

284. Uter, Gefeller, and Schwanitz (1998) An epidemiological study of the influence of season (cold and dry air) on the occurrence of irritant skin changes of the hands. *Br. J. Dermatol.*, **138** (2), 266–272.

285. Simon, M., and Green, H. (1988) The glutamine residues reactive in transglutaminase-catalyzed cross-linking of involucrin. *J. Biol. Chem.*, **263** (34), 18093–18098.

286. Tjernberg, A., Markova, N., Griffiths, W.J., and Hallén, D. (2006) DMSO-Related Effects in Protein Characterization. *J. Biomol. Screen.*, **11** (2), 131–137.

287. Norlén, L., and Al-Amoudi, A. (2004) Stratum Corneum Keratin Structure, Function, and Formation: The Cubic Rod-Packing and Membrane Templating Model. *J. Invest. Dermatol.*, **123** (4), 715–732.

288. Rawlings, A., Harding, C., Watkinson, A., Banks, J., Ackerman, C., and Sabin, R. (1995) The effect of glycerol and humidity on desmosome degradation in stratum corneum. *Arch. Dermatol. Res.*, **287** (5), 457–464.

289. Voegeli, R., Rawlings, A.V., Doppler, S., Heiland, J., and Schreier, T. (2007) Profiling of serine protease activities in human stratum corneum and detection of a stratum corneum tryptase-like enzyme. *Int. J. Cosmet. Sci.*, **29** (3), 191–200.

290. Voegeli, R., Doppler, S., Joller, P., Breternitz, M., Fluhr, J.W., and Rawlings, A.V. (2011) Increased mass levels of certain serine proteases in the stratum corneum in acute eczematous atopic skin: SC serine protease mass levels in atopic skin. *Int. J. Cosmet. Sci.*, **33** (6), 560–565.

291. Rawlings, A.V. (2014) Molecular basis for stratum corneum maturation and moisturization. *Br. J. Dermatol.*, **171**, 19–28.

292. Kuhn, H., Saam, J., Eibach, S., Holzhütter, H.-G., Ivanov, I., and Walther, M. (2005) Structural biology of mammalian lipoxygenases: Enzymatic consequences of targeted alterations of the protein structure. *Biochem. Biophys. Res. Commun.*, **338** (1), 93–101.

293. Fluhr, J.W., Darlenski, R., and Surber, C. (2008) Glycerol and the skin: holistic approach to its origin and functions. *Br. J. Dermatol.*, **159** (1), 23–34.

294. Weller, R.B. (2017) The health benefits of UV radiation exposure through vitamin D production or non-vitamin D pathways. Blood pressure and cardiovascular disease. *Photochem. Photobiol. Sci.*, **16** (3), 374–380.

295. Matsuoka, L.Y., Ide, L., Wortsman, J., MacLaughlin, J.A., and Holick, M.F. (1987) Sunscreens suppress cutaneous vitamin D3 synthesis. *J. Clin. Endocrinol. Metab.*, **64** (6), 1165–1168.

296. Bourdillon, R.B., and Bruce, H.M. (1932) The determination of vitamin D: A comparison of radiography and bone analysis in the estimation of vitamin D. *Biochem. J.*, **26** (2), 506–521.

297. Diker-Cohen, T., Koren, R., Liberman, U.A., and Ravid, A. (2003) Vitamin D Protects Keratinocytes from Apoptosis Induced by Osmotic Shock, Oxidative Stress, and Tumor Necrosis Factor. *Ann. N. Y. Acad. Sci.*, **1010** (1), 350–353.

298. Monaghan, C., McIlvenna, L.C., Liddle, L., Burleigh, M., Weller, R.B., Fernandez, B.O., Feelisch, M., Muggeridge, D.J., and Easton, C. (2018) The effects of two different doses of ultraviolet-A light exposure on nitric oxide

metabolites and cardiorespiratory outcomes. *Eur. J. Appl. Physiol.*, **118** (5), 1043–1052.

299. Luckiesh, M., and Taylor, A.H. (1946) Protective skin coatings for the prevention of sunburn. *J. Am. Med. Assoc.*, **130**, 1–6.

300. Benjamin, C., and Ananthaswamy, H. (2007) p53 and the pathogenesis of skin cancer. *Toxicol. Appl. Pharmacol.*, **224** (3), 241–248.

301. Geller, A.C., Jablonski, N.G., Pagoto, S.L., Hay, J.L., Hillhouse, J., Buller, D.B., Kenney, W.L., Robinson, J.K., Weller, R.B., Moreno, M.A., Gilchrest, B.A., Sinclair, C., Arndt, J., Taber, J.M., Morris, K.L., Dwyer, L.A., Perna, F.M., Klein, W.M.P., and Suls, J. (2018) Interdisciplinary Perspectives on Sun Safety. *JAMA Dermatol.*, **154** (1), 88.

302. Meinhardt, M., Krebs, R., Anders, A., Heinrich, U., and Tronnier, H. (2008) Wavelength-dependent penetration depths of ultraviolet radiation in human skin. *J. Biomed. Opt.*, **13** (4), 044030.

303. Biniek, K., Levi, K., and Dauskardt, R.H. (2012) Solar UV radiation reduces the barrier function of human skin. *Proc. Natl. Acad. Sci.*, **109** (42), 17111–17116.

304. Vyumvuhore, R., Tfayli, A., Duplan, H., Delalleau, A., Manfait, M., and Baillet-Guffroy, A. (2013) Effects of atmospheric relative humidity on Stratum Corneum structure at the molecular level: ex vivo Raman spectroscopy analysis. *The Analyst*, **138** (14), 4103.

305. Wildnauer, R.H., Bothwell, J.W., and Douglass, A.B. (1971) Stratum corneum biomechanical properties. I. Influence of relative humidity on normal and extracted human stratum corneum. *J. Invest. Dermatol.*, **56** (1), 72–78.

306. Bergamini, C.M. (1988) GTP modulates calcium binding and cation-induced conformational changes in erythrocyte transglutaminase. *FEBS Lett.*, **239** (2), 255–258.

307. Di Venere, A., Rossi, A., De Matteis, F., Rosato, N., Agrò, A.F., and Mei, G. (2000) Opposite Effects of Ca $^{2+}$ and GTP Binding on Tissue Transglutaminase Tertiary Structure. *J. Biol. Chem.*, **275** (6), 3915–3921.

308. Hopkins, P.C.R., Crowther, D.C., Carrell, R.W., and Stone, S.R. (1995) Development of a Novel Recombinant Serpin with Potential Antithrombotic Properties. *J. Biol. Chem.*, **270** (20), 11866–11871.

309. Fluhr, J.W., Mao-Qiang, M., Brown, B.E., Wertz, P.W., Crumrine, D., Sundberg, J.P., Feingold, K.R., and Elias, P.M. (2003) Glycerol Regulates Stratum Corneum Hydration in Sebaceous Gland Deficient (Asebia) Mice. *J. Invest. Dermatol.*, **120** (5), 728–737.